Ena/VASP proteins interact directly with the WAVE complex

Xing Chen

University College London

and

Cancer Research UK London Research Institute

PhD Supervisor: Michael Way

A thesis submitted for the degree of

Doctor of Philosophy

University College London

October 2011

Declaration

I, Xing Chen, confirm that the work presented in this thesis is my own. Where information has been derived from other sources, I confirm that this has been indicated in the thesis.

Abstract

Ena/VASP proteins have emerged as key regulators of the actin cytoskeleton during cell migration. They are conserved from flies to mammals, where they consist of three family members: Mena, VASP and Evl. All three proteins localise to sites of cell adhesion and the leading edge of migrating cells, where they play an important role in regulating actin polymerization. Ena/VASP proteins consist of three domains, EVH1 and EVH2 domains, which are separated by a proline rich region. The EVH1 domain mediates the intra-cellular targeting of Ena/VASP proteins by interacting with FPPPP motifs found in proteins such as Zyxin and lamellipodin. The demonstration that Tes, which lacks an FPPPP motif binds to the EVH1 domain of Mena but not VASP and Evl via its LIM3 domain, indicates that EVH1 domains can also bind non-FPPPP containing proteins. My PhD project focused on using biochemical approaches to identify additional non-classical binding partners of the EVH1 domains of Ena/VASP proteins and elucidating their roles during cell migration. I have found that the WAVE complex, which activates Arp2/3 complex-dependent actin nucleation, binds directly to the EVH1 domain of Ena/VASP proteins and that this interaction was mediated by Abi. I identified the EVH1 binding site in both human and *Drosophila* Abi. By expressing Abi mutants deficient in EVH1 binding I was able to demonstrate that Ena/VASP proteins stabilize the WAVE complex the tip of lamellipodia in both Rat-2 cells as well as *Drosophila* S2 and S2R^{+} cells. Moreover, collaborative studies showed VASP could activate the WAVE complex *in vitro* and enhance the effect of Rac on activating the WAVE complex. My work has shown that Ena/VASP proteins are directly coupled to the WAVE complex, suggesting that they may regulate actin dynamics at the plasma membrane in a more coordinated fashion than previously thought.

Acknowledgement

I would like to thank to all the people who helped me during my four years of PhD study in London.

Firstly, I would like to say a big thank you to Michael for providing me this great opportunity to work in his lab, teaching me science and helping me with my scientific English speaking and writing.

I would like to thank Morag for her practical support and encouragement during the beginning of my PhD.

A big thanks to all the past and present lab members. Theresa for organising everything and solving all the problems in the lab. Antonio for asking me great questions about my project and improving my scientific thinking. Yutaka for keeping me company during weekends and late nights in the lab. Jasmine for being confident and making me look forward to the first postdoctoral job. David for his expertise in imaging analysis and teaching me mathematics. Charlotte for her lovely voice and singing in the lab. Ashley for reminding me of the early time of my PhD. Sara for the great time we had in Waterloo. Mark for his wisdom and for discussing my latest results. Amy and Naoko for their lovely smile and loyal friendship. Batiste for his elegant humour. Ina and Joao for showing me how much I have to achieve to get the PhD.

Finally, I would like to thank my family and especially my parents for all their encouragement and support during the past four years.

Table of Contents

Table of figures

List of tables

Abbreviations

Abi	Abl interactor
Abl	Abelson tyrosine
ABP	Actin binding protein
ADP	Adenosine diphosphate
ADP-P_i	Adenosine inorganic phosphate
AI	Auto-inhibitory motifs
AMPK	AMP-activated protein kinase
Arp	Actin-related protein
ARPC	Actin-related protein complex
ATP	Adenosine triphosphate
B	Basic domain
BAR	Bin-Amphiphysin-Rvs
bp	Base pairs
C-terminus	Carboxy terminus
CaCl2	Calcium chloride
CB	Cytoskeletal Buffer
Cc	Critical concentration
CC	Central coiled-coil
Ccdc53	Coiled-coil domain-containing protein 53
cm	Centimetre
CO2	Carbon dioxide
conA	Concanavalin A
CP	Capping protein
CRIB	CDC42 and Rac interactive binding
dAbi	*Drosophila* Abi
dAbl	*Drosophila* Abl
DAPI	4’,6-diamidine-2-phenylidole dihydrochloride
DdVASP	*Dictyostelium* VASP
DMEM	Dulbecco’s modified eagle medium
DMSO	Dimethyl sulfoxide

DNA	Deoxyribonucleic acid
DNase I	Deoxyribonuclease I
dNTP	Deoxynucleoside 5'-triphosphate
dsRNA	Double stranded RNA
ECL	Enhanced chemiluminescence
ECM	Extracellular matrix
EDM	Eucidean Distance Map
Ena	Enabled
EVH	Ena/VASP homology
Evl	Enabled/vasodilator-stimulated phosphoprotein-like protein
F-actin	Polymeric actin filament
FAB	F-actin binding motifs
FACS	Fluorescence activated cell sorting
FH	Formin homology
FITC	Fluorescin isothiocyanate
for	Forward primer
FRAP	FRAP Fluorescence Recovery After Photo -Bleaching
FRET	Fluorescence resonance energy transfer
Fyb	Fyn-binding
G-actin	Globular actin monomer
GAB	G-actin binding motif
GBD	GTPase binding domain
GFP	Green fluorescent protein
hAbi	Human Abi
HRP	Horseradish peroxidase
IF	Immunofluorescence
IP	Immunoprecipitation
IPTG	Isopropyl β-D-1-thiogalactopyranoside

IRSp53	Insulin receptor substrate protein 53
JMY	Junction mediating and regulatory protein
k	Rate constant of recovery
kb	Kilobase
kDa	Kilo Dalton
L	Litre
LacZ	Gene encoding for β-galactosidase
LB	Luria-Bertani
M	Molar
MEM	Minimal Essential Medium
mg	Milligram
min	Minute
ml	Millilitre
mm	Millimetre
mM	Millimolar
MnCl2	Manganese chloride
MOPS	3-(N-morpholino)propanesulfonic acid
ms	Milliseconds
N-Src	Neural Src
N-terminus	Amino terminus
N-WASP	Neuronal Wiskott Aldrich syndrome protein
Nap1	NCK-associated protein 1
NCK	Non-catalytic kinase
NFATc2	Nuclear factor of activated T-cells, cytoplasmic, calcineurin-dependent 2
ng	Nanogram
nm	Nanometre
NPF	Class I Nucleating promoting factors
OD	Optical density

ORF	Open reading frame
PBSA	Phosphate Buffered Saline A
PCR	Polymerase chain reaction
PFA	Paraformaldehyde
PH	Pleckstrin homology
PI3K	Phosphatidylinositol 3-kinase
PIP2	Phosphatidylinositol (4,5)-bisphosphate
PIP3	Phosphatidylinositol (3,4,5)-trisphosphate
PKA	Protein kinase A
PKG	Protein kinase G
PL/L	Plasmid lenti lox
pmol	Picomole
PP1	Type 1 serine/threonine protein phosphatase
PR2	Proline rich 2 (PR2)
PRD	Proline-rich domain
PSB	Protein sample buffer
qRT-PCR	Quantitative real-time polymerase chain reaction
RbCl	Rubidium chloride
rev	Reverse primer
RFP	Red fluorescent protein
RNAi	Ribonucleic acid interference
Robo	Roundabout
rpm	Rounds per minute
RT	Room temperature
SCAR	Suppressor of cyclic AMP repressor
SDS	Sodium dodecyl sulphate
sec	Second
Ser	Serine
SH3	Src homology 3
SHD	SCAR homology domain
siRNA	Small interfering RNA

SLAP	SLP-76 associated protein
Sra1/PIR121	Rac-associated 1
ssRNA	Single stranded RNA
SWIP	Srumpellin and WASH-interacting protein
TBR	Tubulin-binding region
TE	Tris/EDTA
Thr	Threonine
TIRF	Total internal reflection fluorescence microscopy
TOCA1	Transducer of Cdc42-dependent actin assembly 1
Try	Tyrosine
TS	Tris Saline
VASP	Vasodilator-stimulated phosphoprotein
V-ATPase	Vacuolar-type H^+-ATPase
VZ	Ventricular zone
WAHD	WASH homology domain
WASH	WASP and Scar homolog
WAVE	WASP-family verprolin-homologous protein
Wg	Wingless
WH	WASP homology
WHAMM	WASP homolog associated with actin, membranes and microtubules
WIP	WASP interacting protein
WMD	WHAMM membrane-interacting domain
µl	micro litre
µM	micro Molar
µm	Micrometre
5'UTR	5’ untranslated region
3'UTR	3’ untranslated region

Chapter 1. Introduction

1.1 Cell migration is essential for life

Cell migration is a fundamental cellular process that is important for the function and survival of all eukaryotes. In single-celled eukaryotes such as *Dictyostelium*, the ability to migrate enables them to take the advantage of sources of energy over a wider spatial environment. This reduces the level of competition for resources in a population of individuals (Lauffenburger et al., 1982). In higher eukaryotes such as humans, cell migration is required for the normal function of basic cellular processes throughout our whole life span. During development, cell movement is required to create the overall structure of the human body. During gastrulation, for instance, a tubular body plan where a central gut surrounded by three germ layers that are known as the ectoderm, mesoderm, and the endoderm, is formed by a highly coordinated and directed movement of a large number of cells (Narasimha and Leptin, 2000). Following gastrulation, neural crest cells, which are derived from ectoderm, travel long distances from the neural tube to different sites throughout the embryo to form the nervous system (Bronner-Fraser, 1994). In the adult, cell migration is essential for the functioning of the immune system, tissue repair and wound healing. For example, leukocytes leave the bloodstream by crossing the endothelial barrier to reach the affected tissue to defend against foreign invaders and hence serve as a critical part in the innate immune response (Muller, 2011).

Unfortunately, cell migration is not only essential for life, it also plays pathogenic roles in a variety of human diseases including osteoporosis, mental retardation, chronic inflammatory disease and tumour metastasis (Ridley et al., 2003, Insall and Machesky, 2009). Therefore, understanding the molecular basis underling cell migration will not only expand our knowledge of this fundamental cellular process, but may also help us to develop effective therapeutics to treat diseases such as tumour metastasis.

1.2 An overview of cell migration

1.2.1 The classic migration cycle

Michael Abercrombie conceptualised single cell migration *in vitro* as a cyclic process (Abercrombie, 1980). The migration cycle is a four-step process, involving cell protrusion, adhesion, contraction and retraction (Figure 1.1).

In response to external environmental stimuli, a cell first becomes polarised to form distinct anterior and posterior regions in the direction of migration (Lauffenburger and Horwitz, 1996). This results in the re-organisation of the cell shape and leads to the formation of extended protrusions at the anterior of the cell. The protrusions which can be wide, flat-like lamellipodia or elongated, spike-like filopodia, or both are induced by actin polymerisation (Ridley, 2011). In the second step, attachments (termed focal contacts) between the newly formed protrusions and the substrate are formed. These sites of contact are stabilised by integrin-based adhesion complexes, which directly connect the cell actin cytoskeleton to the substrate (Friedland et al., 2009). Following the formation of focal contacts, the intracellular actomyosin network induces the cell body to contract (Chhabra and Higgs, 2007). This serves to pull the cell body forward towards the extended protrusions. In the final step, the anchoring between the posterior of the cell and the substrate is weakened by the disruption of integrin-cytoskeleton interactions via the cleavage of focal adhesion proteins and integrins by calpains, a family of proteases (Franco and Huttenlocher, 2005). This cleavage allows the retraction of the posterior of the cells into the cell body (Figure 1.1).

The four steps described above are closely coordinated to ensure that cells are able to migrate in a directed fashion. Although different cell types are thought to undergo similar steps during cell migration, their morphologies can vary remarkably. For example, little cell shape change is observed during the gliding migration of keratocytes compared with fibroblasts that exhibit distinct alterations in cell morphology during their stop and go based motility (Keren et al., 2008).

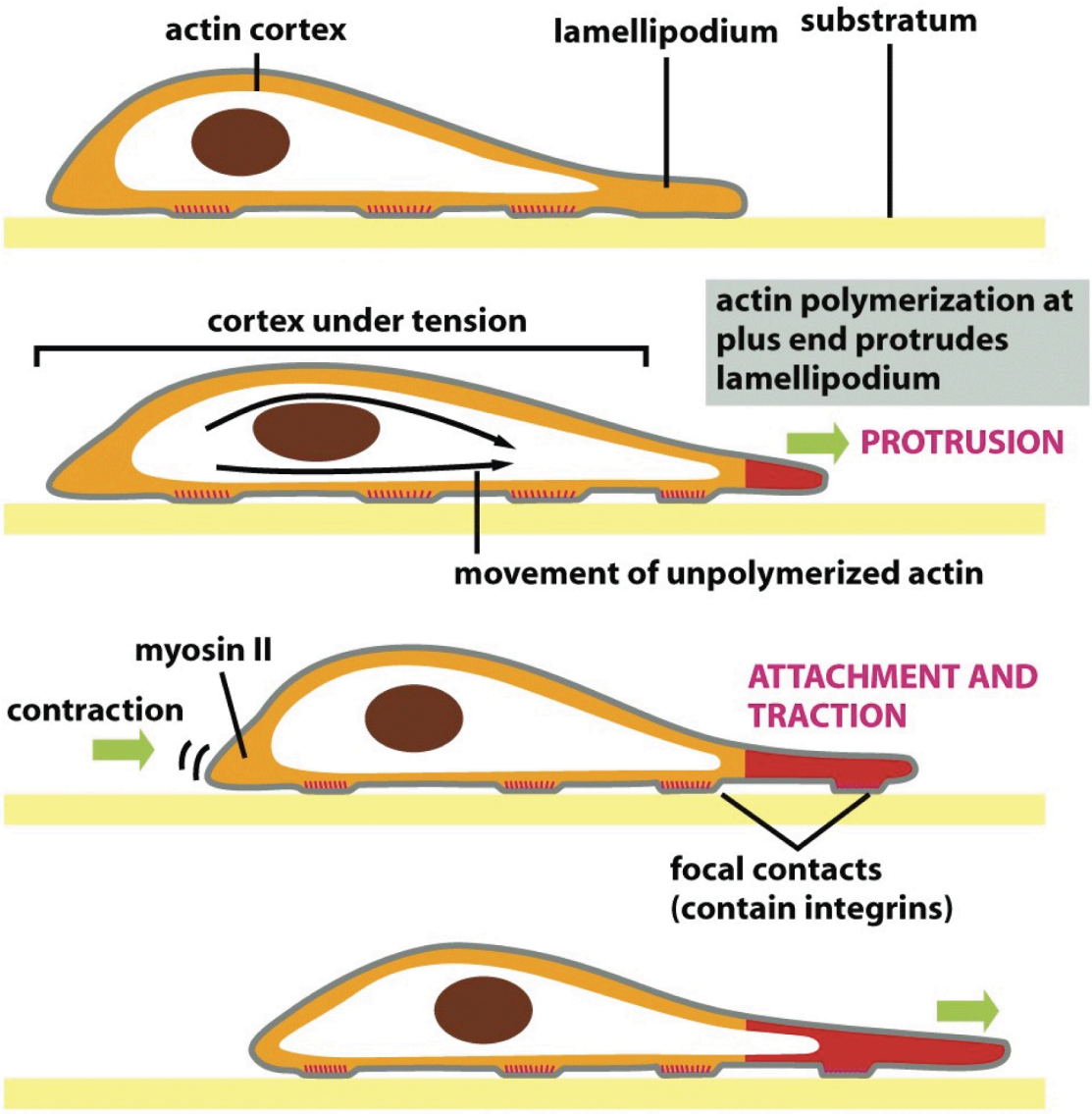

Figure 1.1 The classical migration cycle.
Model of the four steps involved in the migration of a single cell over a substratum. The cell produces actin-based protrusions to extend into new areas of the substrate, where focal adhesions are formed. The rear of the cell then undergoes contraction to move the cell body forward and release focal contacts with the substrate. The same cycle can be repeated, moving the cell forward in a stepwise fashion. Green arrows indicate the direction of movement. The newly formed actin filaments at the leading edge are highlighted in red. Taken from (Alberts et al., 2007). Copyright 2008 from Molecular Biology of the Cell by Alberts et al. Reproduced by permission of Garland Science/Taylor & Francis Books, Inc.

1.2.2 Cell migration *in vivo*

The classical migration cycle that was originally classified based on the morphology of cell migrating *in vitro* is in two dimensions (2D). In the *in vivo* three dimensional (3D) environment, however, different mechanisms and cell morphologies, which reflect their interactions with the surrounding tissue environments, are observed (Figure 1.2).

Fibroblasts and neural crest cells often induce rearrangements of fibrin or collagen in the extracellular matrix (ECM) and use a so-called mesenchymal mode to migrate in 3D (Grinnell, 2008, Tucker, 2004). In contrast, macrophages and some stem cells undergo amoeboid-like migrations by forming bleb-like membrane protrusions at the leading edge in 3D (Blaser et al., 2006, Yoshida and Soldati, 2006). Moreover, leukocytes and *Dictyostelium* also undergo amoeboid migrations, although the migratory process is achieved by forming pseudopodial-like protrusions at the leading edge rather than blebs. Those cells that undergo amoeboid like migrations do not form focal adhesions and migrate at a relatively high speed in either 2D or 3D (Yoshida and Soldati, 2006, Lammermann et al., 2008).

Cells not only migrate individually, they can also move in a collective fashion (Figure 1.2). Groups of migrating cells that are attached to each other to form sheets, strands, tubes and cluster-like structures, have been observed *in vivo* (Friedl and Wolf, 2010, Sahai, 2005). During *Drosophila* oogenesis, for example, a group of six to eight motile cells, named border cells move in a collective fashion from the anterior to the posterior inside the egg chamber to form the micropyle organ (Aman and Piotrowski, 2010). Migration of the lateral line primordium in zebrafish is another example of collective cell migration. During this migratory process, a cluster of about 100 epithelial-like cells move directionally from the anterior head to the posterior of the animal, during which some cells remain at regular spaced intervals to go on to develop into mechano-sensory organs (Weijer, 2009, Friedl and Gilmour, 2009).

It was originally thought that each cell type prefers to use a specific “default” migration mode, such as amoeboid (leukocytes), mesenchymal (stromal cells) or collective migration (epithelial cells) (Friedl, 2004). However, the migratory behaviour of a cell can be influenced by a combination of extra- and intracellular parameters, including cell-cell contact, interactions with the ECM, cytoskeletal polarity, the ability to contract,

protrude and proteolyse the ECM as well as the properties and architecture of the ECM itself. Depending on these multiple parameters, cells can change the nature of their migration mode to adapt themselves to fit the surrounding environment (Friedl and Wolf, 2010). The mesenchymal-to-amoeboid and collective-to-individual transitions are the best studied examples of alterations in cell migration modes during development (Friedl and Wolf, 2010). Moreover, cancer cells are able to alter their migration modes to promote invasion and metastasis, as they are capable of switching their shape and type of migration depending on the context of their surrounding environment (Wolf et al., 2003, Wolf et al., 2007, Hegerfeldt et al., 2002).

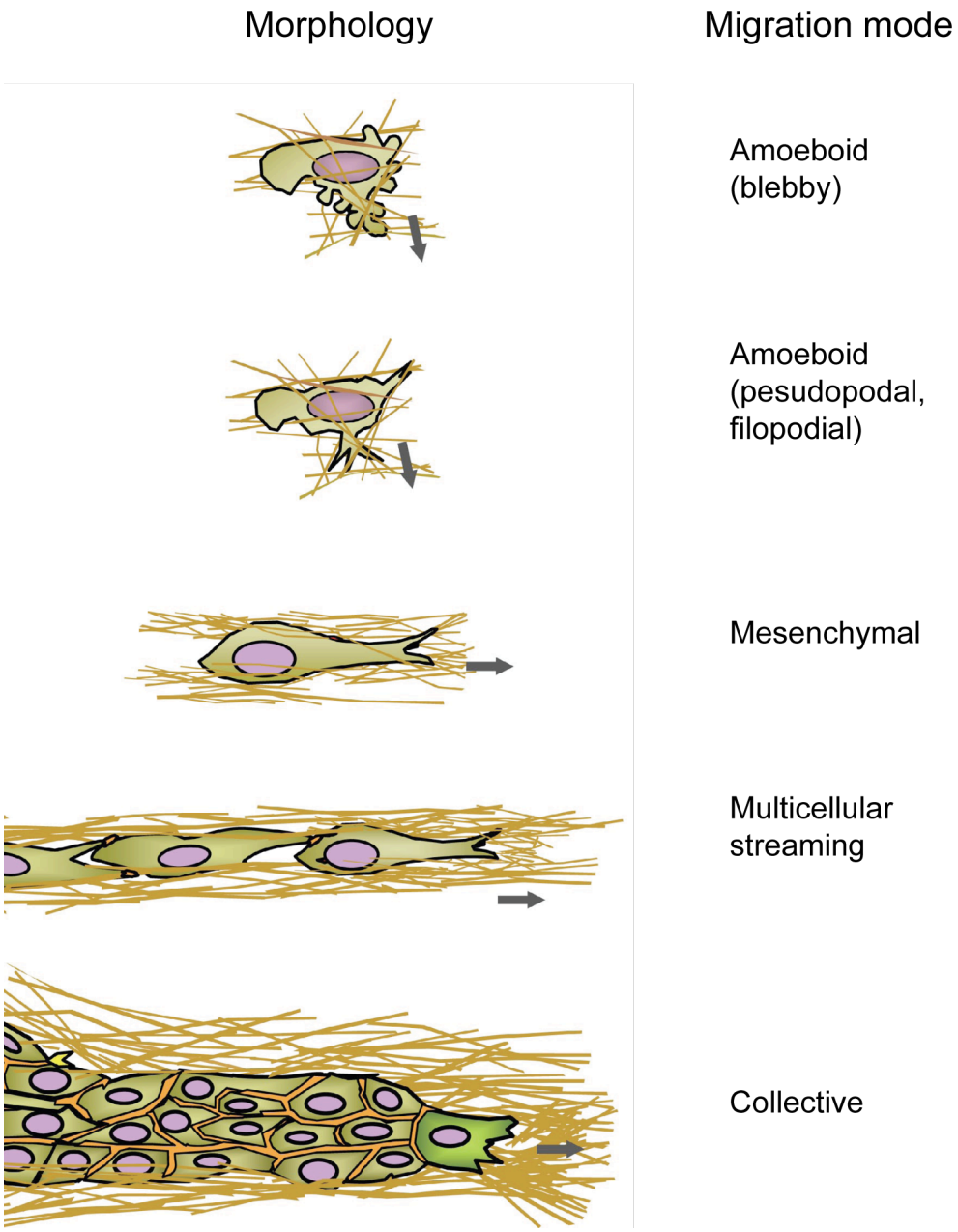

Figure 1.2 Modes of cell migration *in vivo.*
A cartoon illustrating the morphologies of cells in different modes of cell migration *in vivo*. Cells can migrate individually and collectively. A single cell can undergo either amoeboid-like or mesenchymal migrations. Grey arrows indicate the direction of cell migration. Brown lines indicate the ECM. Taken from (Friedl and Wolf, 2010) with permission.

1.3 Actin cytoskeleton

1.3.1 The biochemistry and dynamics of Actin

Actin, which is one of the most abundant proteins of any eukaryotic cell, is central to providing the driving force behind cell migration. There are three actin isoforms in vertebrates. They are the α-, β- and γ-isoforms. α-actin is only found in muscle tissues, where it cooperates with myosin to produce force and cause muscle contraction. By contrast, β-actin and γ-actin, which are the major components of the actin cytoskeleton, can be found in most cell types (Dominguez and Holmes, 2011). Actin (G-actin) is a globular protein with a molecular mass of 42 kDa that interacts with either ATP or ADP-Pi (Pollard and Borisy, 2003). Interestingly, G-actin is also capable of spontaneously self-assembling into a polymeric filament (F-actin) (Figure 1.3).

The process of actin polymerisation occurs in three major steps (dos Remedios et al., 2003) (Figure 1.4A). Firstly, two G-actin monomers associate with each other to form a dimer, which is inherently unstable and likely to dissociate to monomers. If however, the dimer binds another G-actin, it forms a trimer, which is much more stable than the dimer. This trimer is the nucleus for actin filament assembly, a situation, in which actin polymerisation is more likely than depolymerisation. The formation of trimers is therefore the rate-limiting step for actin polymerisation and filament assembly. Once the trimer has been formed, the actin filament rapidly elongates by the addition of actin monomers, if the concentration of G-actin is above the critical concentration (see below).

The arrangement of G-actin subunits in the actin filament is key for the structural and biochemical polarity of F-actin (Rafelski and Theriot, 2004). The structural polarity of F-actin is revealed when the filaments are decorated with the actin-binding domain of myosin (Figure 1.4B). Based on their appearance, the opposite ends of the filament are called the “barbed” and the “pointed” end respectively (Pollard and Borisy, 2003). The asymmetric structure of F-actin leads to a fast growing barbed and a slower growing pointed end through the specific interactions of G-actin at each end (Rafelski and Theriot, 2004). Monomeric G-actin can attach to both ends of F-actin, however, the required amount of free G-actin for addition at the pointed end is seven times higher than that for the addition at the barbed end (Wegner and Isenberg, 1983). This difference explains the unidirectional growth of the actin filament with a consistent flux of G-actin subunits from the fast growing barbed end to the slow growing pointed end

(dos Remedios et al., 2003). Given that the attachment of G-actin to the two ends of F-actin is dependent on the concentration of free actin monomer, the filament growth rate at the two ends of actin filament varies dramatically with the concentration of G-actin (Guo et al., 2010). The concentration of free G-actin, when a dynamic eqilibrium between growth and shrinkage of actin filaments Is reached (no change in net polymer length), is referred to as the critical concentration (Cc) (Guo et al., 2010). Thus, actin filaments undergo polymerisation above the Cc, depolymerise below the Cc and maintain a constant length at the Cc (Sept and McCammon, 2001) (Figure 1.4C).

In vitro, actin filament dynamics are inherently regulated by the structural asymmetry of the filament. The activities of actin assembly and disassembly are also temporally regulated by hydrolysis of the nucleotide that is bound to the actin monomer (Rafelski and Theriot, 2004) (Figure 1.4D). Nucleotides, which bind actin are able to achieve three different nucleotide states corresponding to adenosine triphosphate (ATP), adenosine diphosphate (ADP) and adenosine inorganic phosphate (ADP-Pi) (Korn et al., 1987). Free G-actin preferentially binds ATP to form ATP-G-actin. Soon after the interaction between ATP-G-actin and the barbed end of the actin filament, there is a conversion of the ATP to ADP-Pi. The resulting ADP-Pi-G-actin in the filament is a long-lived intermediate and present in the newly assembled actin filaments. Inorganic phosphate (Pi) is slowly released over time. This leads to the formation of ADP-F-actin, which induces a physical alteration of the actin filament, which promotes the dissociation of ADP-actin monomers from ends of the filaments. This process is called actin depolymerisation, which is not as simple as the opposite of actin polymerisation due to the irreversible property of ATP hydrolysis (dos Remedios et al., 2003). Once ADP-G-actin dissociates from the actin filament, it is rapidly converted to ATP-G-actin by the action of profilin (Perelroizen et al., 1995, Pantaloni and Carlier, 1993, Vinson et al., 1998).

The structural polarity of F-actin together with the irreversible nature of nucleotide hydrolysis regulates actin dynamics spatially and temporally. In addition to the observations on actin dynamics *in vitro*, a number of studies have shown that similar dynamic actin assembly and disassembly also occurs *in vivo* (Wang, 1985, Symons and Mitchison, 1991, Theriot and Mitchison, 1991, Waterman-Storer et al., 1998, Lai et al., 2008). It is the dynamic actin assembly and disassembly that provide the force for cell migration.

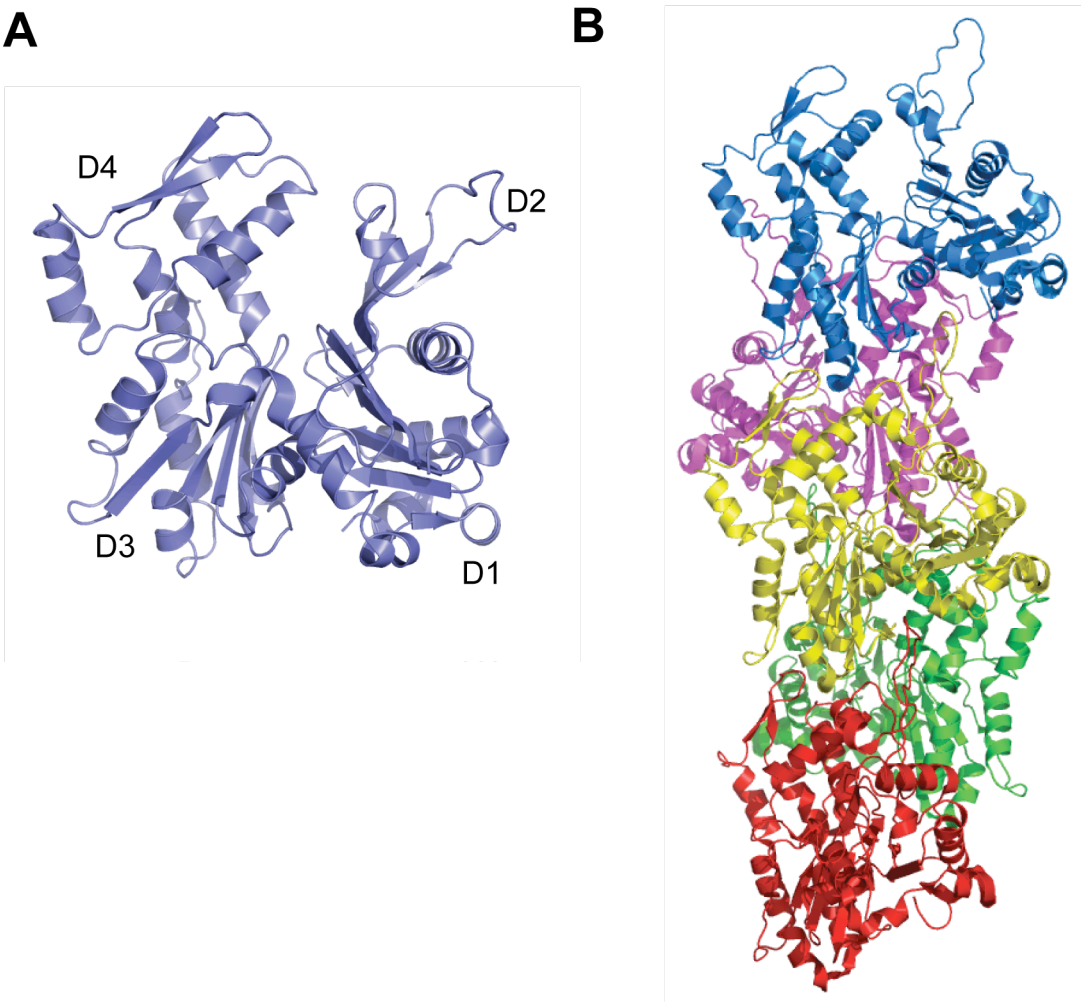

Figure 1.3 Structures of G- and F-actin.
A. Crystal structure of G-actin, which was derived from a complex with profilin (2BTF). Sub-domains are labelled D1-D4. Sub-domain 1 and 2 form the outer domain, whereas sub-domain 3 and 4 form the inner domain. **B.** The helical structure of F-actin that was derived from cryo-electron microscopy (3MFP), in which the structure of G-actin has been fitted. The filament is arranged on a single helix, which consists of five G-actin subunits. Different colours indicate different G-actin subunits in the filament. **A** and **B** were generated using the MacPyMOL Molecular Graphics System, Version 0.99, DeLano Scientific LLC, 2006.

1.3.2 Actin-dependent cell motility

In 1978, actin was first hypothesized to provide the force for cell migration as the fast growing barbed ends of F-actin always pointed towards the direction of membrane protrusions in electron micrographs (Small and Celis, 1978, Small et al., 1978). Subsequent studies supported this hypothesis and demonstrated that microinjected fluorescently labelled G-actin only incorporated into the actin network of lamellipodia (Glacy, 1983, Wang, 1985). Moreover, isolated lamellipodia of keratocytes are able to migrate independently from rest of the cellular components, suggesting the self-organising property of actin alone is capable of driving cell motility (Verkhovsky et al., 1999).

Direct evidence that actin is key for cell migration is based on the experiments using drugs that strongly inhibit actin polymerisation. Cytochalasin D, which is produced by *Helminthosporium*, inhibits actin polymerisation by binding G-actin and the barbed ends of actin filaments (Cooper, 1987). Following treatment with Cytochalasin D, inhibition of actin filament elongation is observed both *in vitro* and *in vivo*. This leads to the termination of protrusions at the leading edge of migrating cells (Sampath and Pollard, 1991, Forscher and Smith, 1988). The observations from these experiments also strongly supported the idea that the driving force for protrusion during cell migration is provided by actin polymerisation.

In addition, evidence also comes from a number of bacterial pathogens such as *Shigella flexneri* and *Listeria monocytogenes*, which can undergo actin-based motility (Pantaloni et al., 2001). Following infection, inside the cytoplasm of the host cell, *Listeria* develops a comet tail, which is made of an oriented, cross-linked network of actin filaments with their barbed ends facing the bacterium (Tilney and Portnoy, 1989). Fluorescently labelled G-actin was only incorporated into the actin tail near the bacterial surface (Sanger et al., 1992). This suggests a role of actin in providing a driving force for motility of *Listeria*. Furthermore, the rate of actin polymerisation is found to be the same as the speed of *Listeria* movement inside the host cell (Theriot et al., 1992). The resulting actin tail not only allows the bacteria to move inside the host cytoplasm, it also plays an important role in the spread of infection (Robbins et al., 1999, Cameron et al., 2000).

Taken together, actin-dependent cell motility is responsible for the formation of cellular protrusions as well as the life cycle of some bacterial pathogens. The underlying mechanism of generating force via actin filament assembly to drive membrane protrusions of the motile cells can be described using the “elastic Brownian ratchet” model. The model suggests that actin monomers are added to the barbed end of the actin filament during thermal fluctuations of the plasma membrane in order to allow membrane protrusions (Mogilner and Oster, 2003).

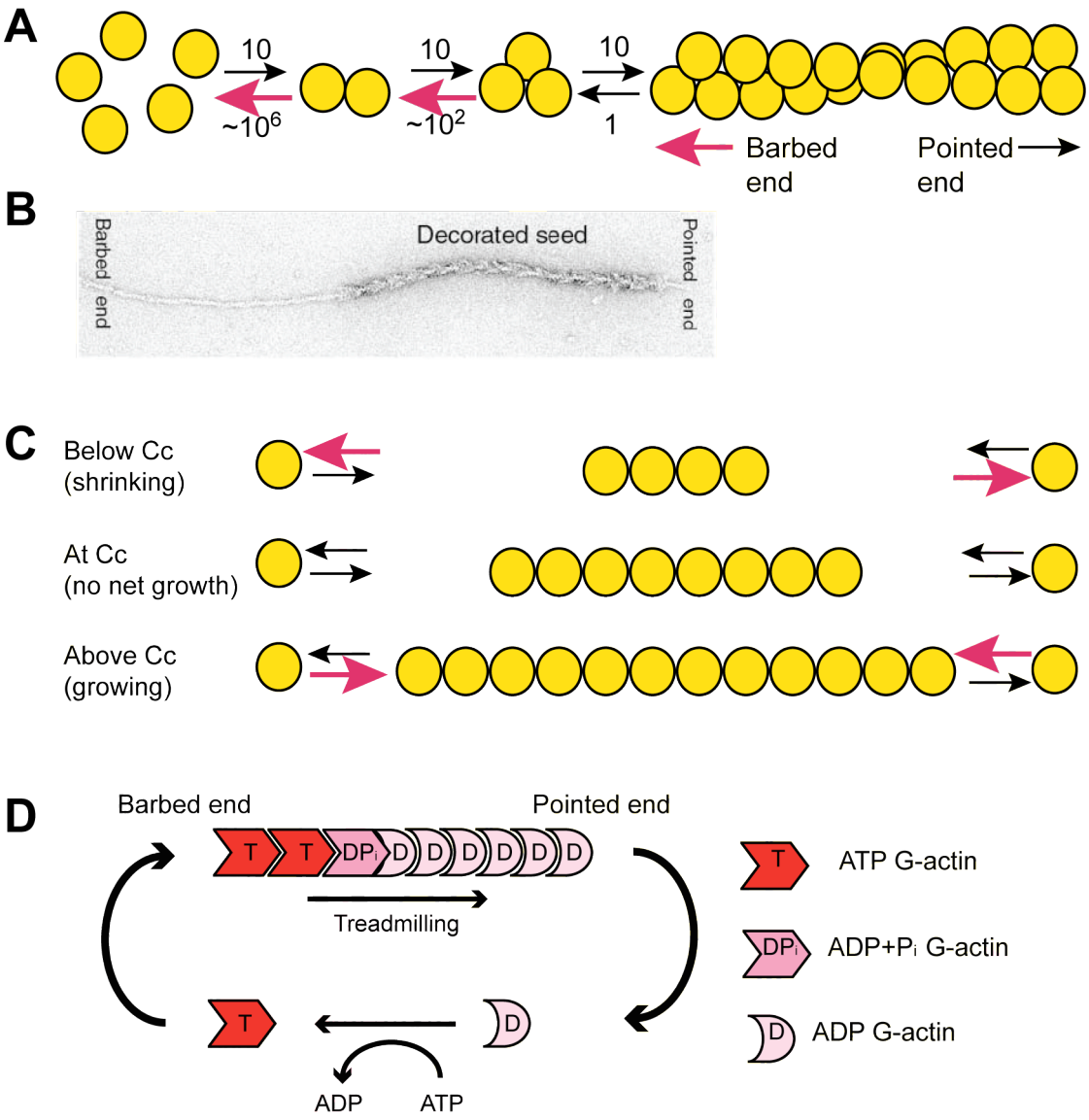

Figure 1.4 The dynamics of actin.
A. The process of spontaneous actin polymerisation. Actin dimers are much more unstable than actin trimers. Following the formation of trimer, rapid polymerisation and elongation of actin filament occurs. Numbers represents the rate constants for adding and removing G-actin. Arrows indicate the fluxes of actin monomers. **B**. An electron micrograph showing an actin filament decorated with the actin binding domain of myosin. The end, which displays the arrowhead appearance, is termed "pointed end". The opposite end is termed the "barbed end". Taken from (Pollard and Borisy, 2003) with permission of Elsevier. **C**. A cartoon showing that the growth and shrinkage of actin filaments is dependent on the free G-actin concentration. Arrows indicate the fluxes of actin monomers. **D**. A cartoon illustrating that ATP hydrolysis cycle during actin filament polymerisation (treadmilling). ATP bound G-actin polymerises at the barbed end of actin filaments, whereas ADP-G-actin dissociates from the pointed end. G-actin monomers are recycled for addition at the barbed end by profilin mediated exchange of ADP to ATP.

1.3.3 *In vivo* actin-based membrane protrusions

In vivo, individual actin filaments are organised into complex macromolecular structures such as web-like structures (networks) and bundles (Insall and Machesky, 2009). These macromolecular actin-based assembles are key in driving membrane protrusions during cell migration. Several distinct actin-based membrane protrusions have been described, including lamellipodia, filopodia, and invadopodia (Figure 1.5).

Lamellipodia, which consist of a two-dimensional cross-linked actin meshwork, have a thin sheet-like structure. They were the first described protrusions at the leading edge of migrating cells (Abercrombie et al., 1970). It is thought that lamellipodia generate the force needed to pull the cell forward during migration (Small et al., 2002). Lamellipodia have been observed in a variety of motile cells, including keratocytes in zebrafish and in epidermal and neural crest cells in both *Xenopus* and zebrafish (Weijer, 2009, Keren et al., 2008).

Filopodia, contain parallel bundled actin filaments and form finger-like protrusions. These protrusive structures can be observed either within the lamellipodia where they are termed microspikes or can be derived from lamellipodia in which case they are called filopodia (Chhabra and Higgs, 2007). Filopodia have been observed in most cell types, including fibroblasts and nerve growth cones, where they act as directional sensors during cell migration (Zheng et al., 1996, Faix and Rottner, 2006).

Cells use both lamellipodia and filopodia during migration in 2D. However, in order to move in 3D, such as during leukocyte transmigration and cancer cell invasion, cells form actin-rich matrix-degrading protrusions that are termed invadopodia (Chen, 1989). The main function of invadopodia is to degrade ECM to facilitate cell invasion (Buccione et al., 2009). These 3D protrusions have been observed in a wide range of cancer cell lines including breast and colon cancer cell lines (Linder et al., 2010)

Each of these protrusive structures contributes to cell migration in both 2D and 3D environments. Their functions correlate with their morphologies, which are highly dependent on the way the underlying actin filaments are organised.

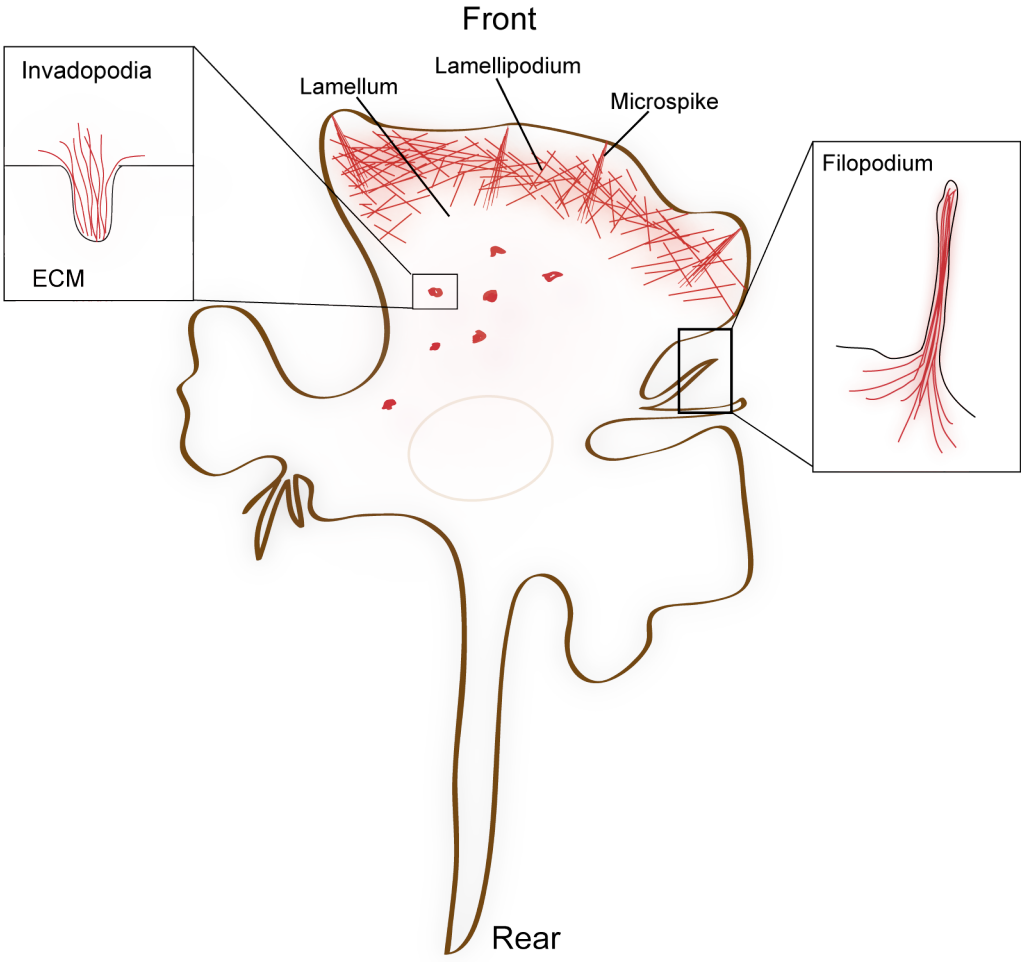

Figure 1.5 Actin-based membrane protrusions.
Schematic representation showing a migrating cell that possesses distinct plasma membrane protrusions. The actin filaments (red) are organised into different structures to provide force to generate these protrusive structures. Adapted from (Ladwein and Rottner, 2008) with permission of Elsevier.

1.3.4 Actin binding proteins (ABPs)

The assembly and organisation of actin filaments *in vivo* is regulated by the interaction with a large number of actin binding proteins (ABPs) (Figure 1.6). Actin binding proteins are part of the actin cytoskeleton. Some ABPs only interact with G-actin (e.g. thymosin) or F-actin (e.g. α-actinin), whereas some ABPs interact with both G-actin and F-actin (e.g. gelsolin). The function of each ABP in modulating the actin cytoskeleton is different. Some ABPs accelerate the disassembly of actin filaments (e.g. cofilin), whereas others prevent the assembly of actin filaments (e.g. capping protein). ABPs also modulate the organisation of F-actin by cross-linking (e.g. filamin), bundling (e.g. fascin) or attaching the filaments to membranes (e.g. spectrin).

Given that the average cell contains more than 100 different ABPs, I will only focus on a number of ABPs that are involved in stimulating the formation of new actin filaments through nucleation. These actin nucleators are the most relevant ABPs for the topic of this thesis.

Although actin can self-assemble by initially forming an actin trimer, this spontaneous nucleation is kinetically unfavourable due to the low stability of the proceeding actin dimer (Goley and Welch, 2006). *De novo* actin filament nucleation is the most important activity enhancing actin polymerisation to generate force for cell migration (Pollard and Borisy, 2003). The nucleators, which are responsible for spontaneous formation of new actin filaments, are classified into three groups. They are the Arp2/3 complex, Spire and formins (Figure 1.7).

Formins and Spire have both been found to nucleate unbranched parallel actin filaments (Goley and Welch, 2006). Formins are very diverse and have a relatively high molecular weight of between 120-220 kDa but share two distinct formin homology-1 (FH1) and forming homology-2 (FH2) domains in their C termini (Chesarone et al., 2010). The FH2 domain alone is capable of mediating actin nucleation through a direct interaction with actin (Pruyne et al., 2002). However, the dimerisation of the FH2 domain is thought to be crucial to stimulate actin filament assembly (Moseley et al., 2004, Xu et al., 2004). Spire was initially identified as an actin nucleator in *Drosophila* (Quinlan et al., 2005). The same study also showed that the tandem WASP-homology-2 (WH2) domains together with an extra G-actin binding linker of Spire are essential to

stimulate actin filament nucleation. Moreover, Spire is found to directly bind and affect the activity of formin in actin filament nucleation, suggesting that Spire may cooperate with formins to regulate un-branched actin filament growth (Quinlan et al., 2007).

In contrast to formin and Spire, the Arp2/3 complex, which has been most extensively studied, is responsible for generating Y-shaped branched actin networks (Campellone and Welch, 2010, Insall and Machesky, 2009, Mullins et al., 1998). The initiation of nascent daughter actin filaments on the side of an existing mother actin filament by the Arp2/3 complex has been visualised *in vitro* (Amann and Pollard, 2001b, Bailly et al., 2001, Rouiller et al., 2008). The resulting branched actin filament networks form the fundamental basis of many membrane protrusions such as lamellipodia and invadopodia (Ridley, 2011).

However, the branched nature of actin filaments has been questioned. It was suggested that the observations of the Y-shaped branches in lamellipodia are due to a fixation artefact, and the actin filaments in lamellipodia are not branched (Koestler et al., 2008, Urban et al., 2010). The data in these studies is controversial and further work is required to settle this dispute.

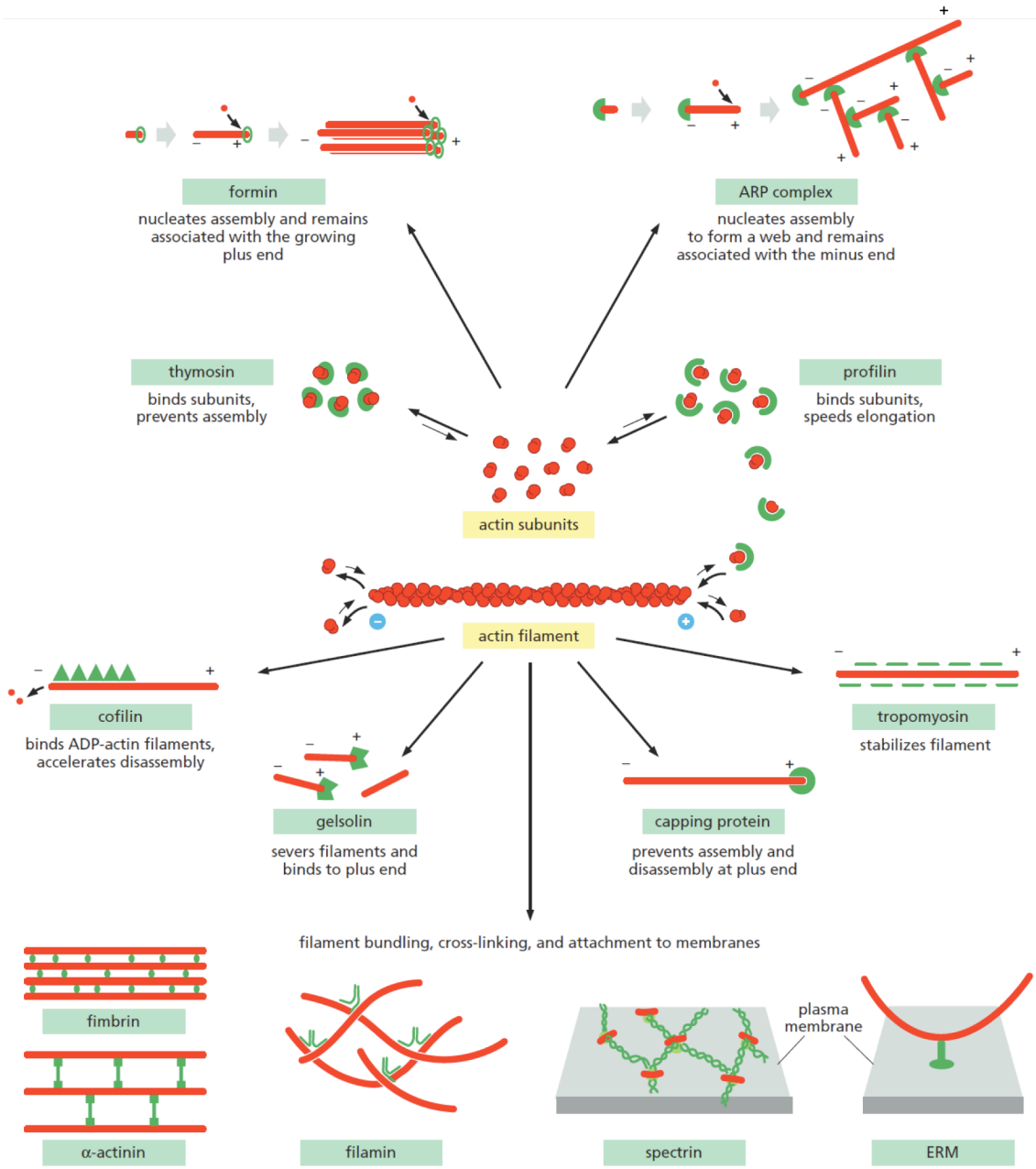

Figure 1.6 Actin binding proteins that regulate the dynamics and organisation of actin cytoskeleton.
Schematic representation of the activity of selected ABPs. More than a hundred different ABPs have been identified so far, although it is likely that many other ABPs that are essential have not been discovered yet. Taken from (Alberts et al., 2007).

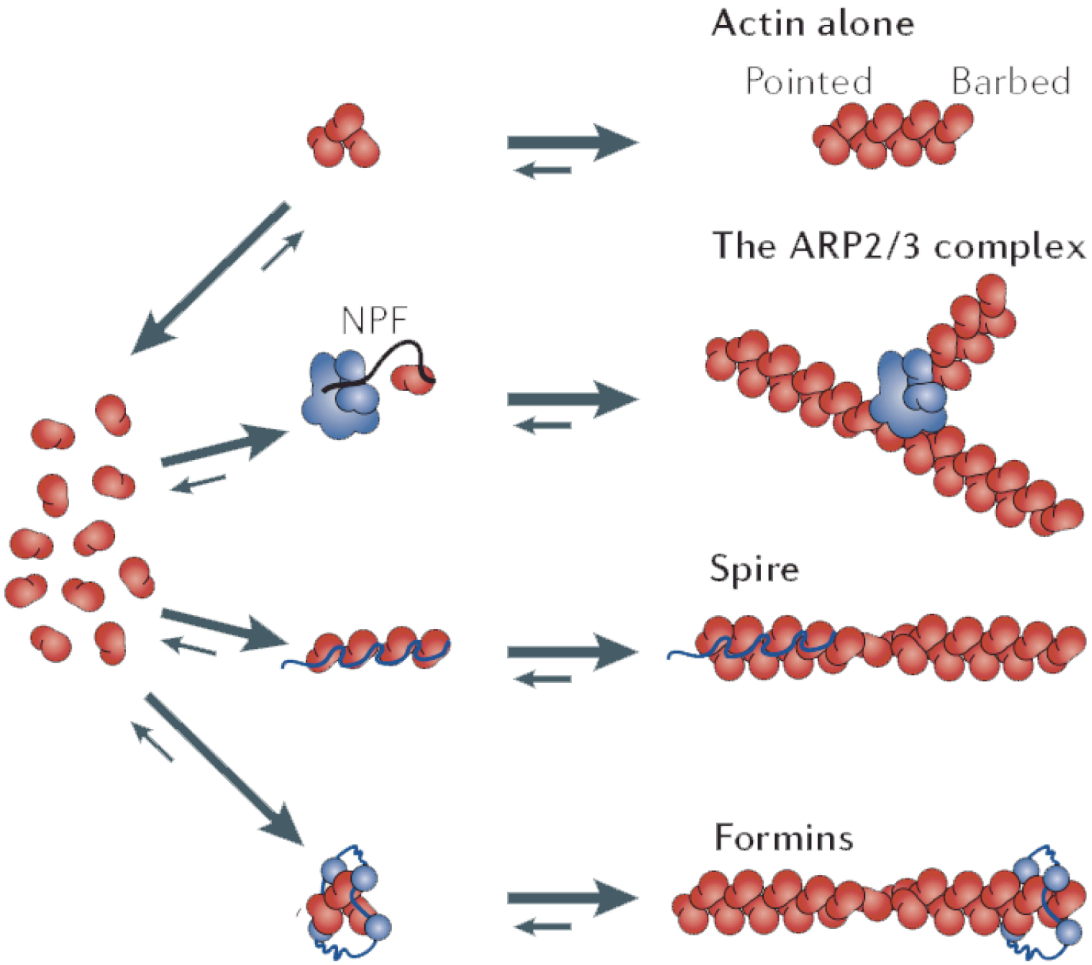

Figure 1.7 Paths to actin nucleation.
Actin is able to self-assemble, although this spontaneous nucleation is kinetically unfavourable, as it requires the formation of a stable trimer. Three classes of actin nucleators are found to promote actin nucleation. They are the Arp2/3 complex, Spire and formins. The Arp2/3 complex is able to generate branched actin networks, whereas Spire and formins are found to promote the nucleation of un-branched parallel actin filaments. The Arp2/3 complex can mimic an actin dimer and acts as a template for the formation of a nascent filament from an existing mother filament. Spire binds actin filaments and acts as a scaffold for actin polymerisation. In contrast to the Arp2/3 complex and Spire, which can dissociate from a growing actin filament after actin nucleation, Formins bind the barbed end of actin filaments and remain associated with the growing barbed end during actin polymerisation. Actin is depicted in red, actin nucleators are shown in blue. Taken from (Goley and Welch, 2006) with the permission of Nature Pulishing Group.

1.4 The Arp2/3 complex

1.4.1 Subunits and branching ability

The actin-related protein 2 (Arp2) was first identified as an actin-like protein in yeast and *Drosophila* (Lees-Miller et al., 1992, Schwob and Martin, 1992, Fyrberg and Fyrberg, 1993). The intact Arp2/3 complex was first isolated from *Acanthamoeba castellanii* extracts using a profilin affinity column (Machesky et al., 1994). This biochemical analysis revealed that the complex comprises seven stably associated subunits: Arp2, Arp3 and five smaller subunits. The five smaller subunits were originally named based on their molecular weight, but are now referred to as actin-related protein complex-1 (ARPC1), ARPC2, ARPC3, ARPC4 and ARPC5 respectively (Goley and Welch, 2006). Following the purification of the Arp2/3 complex from *A. castellanii,* the whole complex was successfully identified and isolated from other organisms such as yeast, *Xenopus* and human (Welch et al., 1997, Winter et al., 1997, Ma et al., 1998).

The nucleating and branching properties make the Arp2/3 complex a unique regulator of the actin cytoskeleton. The Arp2/3 complex has been shown to act as a template for the nucleation of Y-shaped branched actin filaments both *in vitro* and *in vivo* (Blanchoin et al., 2000, Pantaloni et al., 2000, Mullins et al., 1998, Bailly et al., 2001, Amann and Pollard, 2001b, Amann and Pollard, 2001a, Svitkina et al., 1997, Svitkina and Borisy, 1999). Two models were initially proposed to describe the underlying mechanism of actin branch formation by the Arp2/3 complex. In the barbed end branching model, it is suggested that the Arp2/3 complex binds the barbed end of a pre-existing filament to allow the elongation of the mother filament into two nascent daughter filaments (Pantaloni et al., 2000). By contrast, the side branching model suggests that the Arp2/3 complex binds to the side of a mother filament to initiate the nucleation of a new daughter filament that grows away from the mother filament (Rouiller et al., 2008, Blanchoin et al., 2000). The latter model is strongly supported by structural observations and is therefore the favoured model.

1.4.2 Structure of the branch junction

The crystal structure of the Arp2/3 complex was solved in either the presence or absence of bound nucleotide (Robinson et al., 2001, Nolen et al., 2004, Nolen and Pollard, 2007). The Arp2/3 complex structure observed in the crystal is thought to be

the inactive state due to the spatial arrangements of Arp2 and Arp3 within the complex. Arp2 and Arp3 are thought to act as a heterodimer to mimic an actin dimer in order to initiate actin nucleation. However, according to the crystal structure, Arp2 and Arp3 are not closely linked to each other and are therefore unlikely to form a nucleating trimeric complex with G-actin. Thus, it hypothesised that the Arp2/3 complex undergoes a conformational change when it is activated (Robinson et al., 2001) (Figure 1.8A). However, in the absence of a high-resolution structure of the activated Arp2/3 complex, the integration of the complex into actin filaments is a matter of speculation (Pollard, 2007).

Given a high-resolution structure of the activated Arp2/3 complex is currently unavailable, the conformation of the Arp2/3 complex at Y-braches has been examined using a combination of homology modelling and 3D reconstitution after electron tomography (Rouiller et al., 2008, Beltzner and Pollard, 2004) (Figure 1.8B). Based on these approaches, it is thought that Arp2 and Arp3 are responsible for binding directly to the first two subunits in the daughter filament as they are highly conserved and similar to actin. By contrast, ARPC2 and ARPC4 are essential for mediating the direct interaction between the complex and the existing mother actin filament. Using mutagenesis, a recent study defined key residues of the ARPC2 and ARPC4 subunits within the Arp2/3 complex that play a central role in F-actin binding, actin nucleation as well as Y-branch stability (Goley et al., 2010).

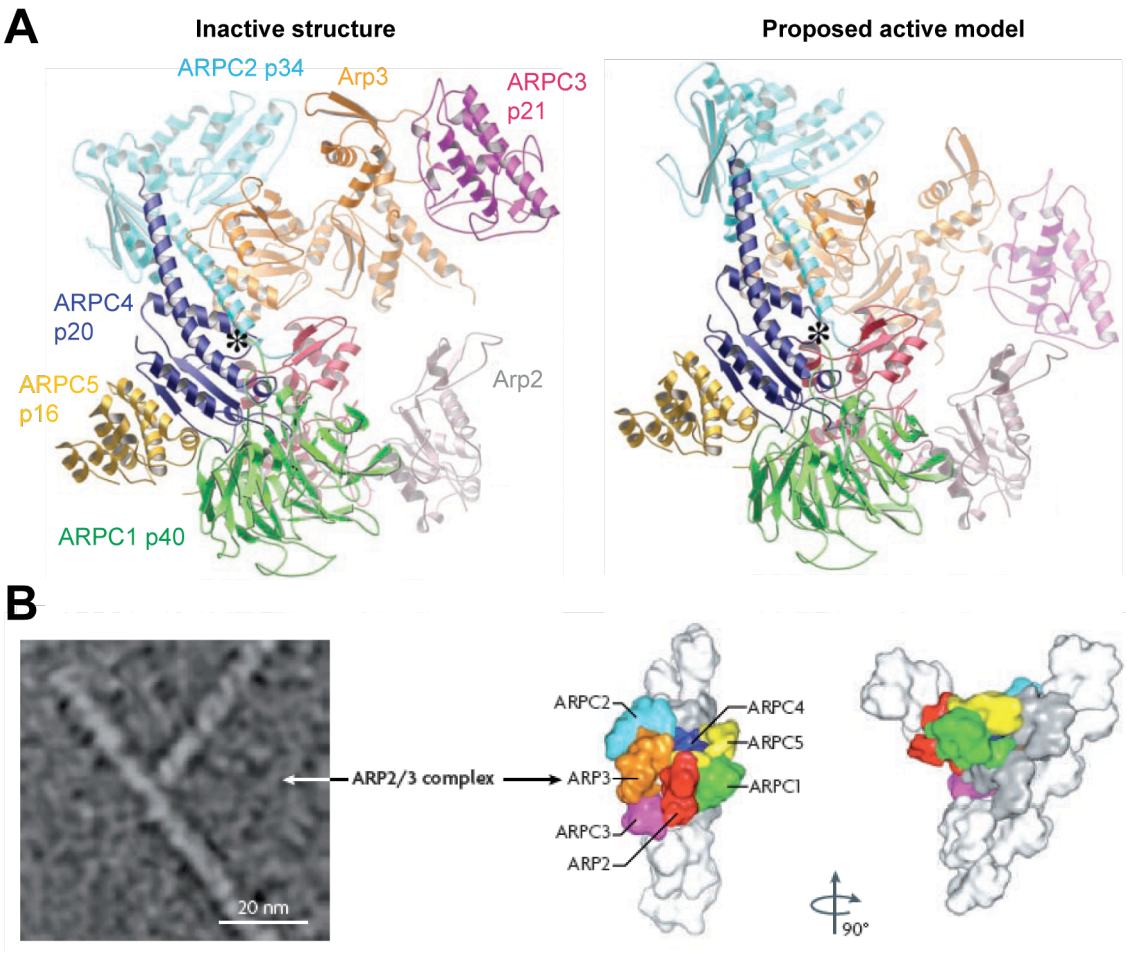

Figure 1.8 The structure of the Arp2/3 complex.
A. Model of Arp2/3 complex activation. Ribbon diagrams of the inactive complex (left) and the proposed active complex (right). Subunits of the Arp2/3 complex are labelled. It is hypothesised that Arp2 and Arp3 are brought into contact through shifting Arp2, ARPC1, ARPC4 and ARPC5. Taken from (Robinson et al., 2001) with permission of The American Association of the Advancement of Science. **B**. The electron micrograph shows the Arp2/3 complex and the morphology of a Y-branched actin filament. The model on the right shows the subunits of the Arp2/3 complex bind the existing mother filament and the newly formed daughter filament. Although all 7 subunits of the Arp2/3 complex contribute to binding of the mother filament, Arp2 and Arp3 act as the first two subunits of the daughter filament. Taken from (Campellone and Welch, 2010) with permission of Nature Publishing Group.

1.4.3 Activation of the Arp2/3 complex

The structure of the Arp2/3 complex showed that Arp2 and Arp3 are not in close proximity suggesting that an inactive form of the complex had been purified and crystallised (Robinson et al., 2001, Nolen et al., 2004, Nolen and Pollard, 2007). Furthermore, *in vitro* experiments revealed that the purified Arp2/3 complex by itself was not very efficient at initiating actin polymerisation (Mullins et al., 1998, Welch et al., 1998, Machesky and Insall, 1998). Based on these observations, it was clear that additional factors are required to achieve a fully activated and functional Arp2/3 complex *in vivo*. Although the structure representing the active state of the Arp2/3 complex has not yet been solved, a number of aspects concerning Arp2/3 complex activation have started to emerge.

1.4.3.1 Activation by ATP

ATP has been found to regulate the activity of the Arp2/3 complex (Goley and Welch, 2006). Evidence for this comes from the crystal structure of ATP bound Arp2/3 complex and fluorescence resonance energy transfer (FRET) experiments (Nolen et al., 2004, Goley et al., 2004). These studies demonstrated that binding of ATP to Arp2 and Arp3 leads to conformational changes in the Arp2/3 complex, suggesting an important role for the nucleotide in activating the complex. Interestingly, despite the fact that both Arp2 and Arp3 can interact with ATP, only ATP hydrolysis on Arp2 has been observed (Le Clainche et al., 2003, Dayel et al., 2001, Martin et al., 2006). ATP hydrolysis by Arp2 and/or Arp3 was originally thought to be important for the activation of the Arp2/3 complex, as it is capable of nucleating actin filaments when it interacts with ADP or a non-hydrolysable ATP analogue (Dayel et al., 2001). However, a subsequent study showed that an Arp2 mutant in yeast that cannot undergo nucleotide hydrolysis did not lead to defects in Arp2/3 complex dependent actin filament nucleation. This led the authors to suggest the role of nucleotide hydrolysis is to facilitate de-branching rather than branching of the “dendritic” actin networks that are created by the Arp2/3 complex (Martin et al., 2006). Similar to actin, ATP hydrolysis may regulate the activity of the Arp2/3 complex temporally, for example, Y-branch disassembly and recycling of the Arp2/3 complex (Goley and Welch, 2006). Thus, the interplay between nucleotide hydrolysis and the Arp2/3 complex dependent actin nucleation remains to be determined.

1.4.3.2 Activation of the Arp2/3 complex by nucleating promoting factors (NPFs)

In addition to nucleotide binding and hydrolysis, the activation of the Arp2/3 complex is regulated by a number of nucleating promoting factors (NPFs). Depending on the mechanisms and efficiencies of the NPFs in activating the Arp2/3 complex, they have been grouped into two classes (Goley and Welch, 2006) (Figure 1.9).

The VCA domain, which is only found in class I NFPs, is thought to be the key for Arp2/3 complex activation (Campellone and Welch, 2010, Goley and Welch, 2006). The VCA domain is divided into different regions based on the specific function of the individual region in activating the Arp2/3 complex. These are a verprolin-homology (V) region, which is also called the WASP-homology-2 (WH2 or W) domain, and is responsible for interacting with monomeric G-actin (Chereau et al., 2005); a central cofilin-homology region, which is also called the connecting (C) region, that shares sequence similarity with the V region and can also bind G-actin (Boczkowska et al., 2008, Irobi et al., 2004); and finally a C-terminal acidic (A) region. The C and A regions together bind and regulate the conformation of the Arp2/3 complex to activate its actin nucleating activity (Marchand et al., 2001, Panchal et al., 2003, Goley et al., 2004, Martin et al., 2005, Rodal et al., 2005).

Cross-linking studies have shown that the VCA domain interacts with multiple subunits of the Arp2/3 complex, including Arp2, Arp3, ARPC1, ARPC3 and ARPC5 (Kreishman-Deitrick et al., 2005, Weaver et al., 2002, Zalevsky et al., 2001a, Kelly et al., 2006, Zalevsky et al., 2001b). However, the detailed mechanism of Arp2/3 complex activation upon its binding to the VCA domain remains to be determined. One working hypothesis suggests that the A region mediates the initial contact with the Arp2/3 complex and the C region causes a conformational change within the Arp2/3 complex to bring Arp2 and Arp3 close to each other (Goley and Welch, 2006). The closely positioned Arp2 and Arp3 together with a G-actin that is presented by the V region of the VCA domain form a trimer. The Arp2/3 complex is therefore activated and the assembly of the daughter actin filament is initiated (Goley and Welch, 2006).

A recent study however showed two VCA domains and two actin monomers are required for maximal Arp2/3 complex activation (Padrick et al., 2011). This study identified two distinct VCA binding sites on the Arp2 and Arp3 subunits of the Arp2/3

complex. Upon binding, each VCA brings one G-actin to the Arp2/3 complex. The same study also showed the two VCA binding sites play different roles during Arp2/3 complex activation. It appears that delivery of actin to the VCA binding site on Arp3 is more important for Arp2/3 complex activation although the binding of actin to the VCA bound to Arp2 is also required. This study is consistent with previous work from the same group that demonstrated that dimerised VCA domains have higher affinities than single VCA domains for the Arp2/3 complex and are better at activating it (Padrick et al., 2008). Furthermore, previous biochemical observations also showed that Arp2 and Arp3 are possible acceptors for the first actin monomer that is delivered by the VCA domain (Marchand et al., 2001, Kreishman-Deitrick et al., 2005, Beltzner and Pollard, 2004, Boczkowska et al., 2008). Moreover, another recent study confirmed that the Arp2/3 complex is able to interact with two VCA domains (Ti et al., 2011). The same group also showed that the binding affinities of the VCA domain for the two sites on the Arp2/3 complex are very different. It has been observed that binding of the VCA domain to the high affinity site on the Arp2/3 complex inhibits the interaction between the complex and F-actin. In contrast, the VCA domain binds to the other site on the Arp2/3 complex with much higher affinity when the Arp2/3 complex is associated with F-actin (Ti et al., 2011). Together, these data indicate that the mechanism of maximal Arp2/3 complex activation involves more than one VCA domain. However, how the VCA domain influences the formation of Y-shaped actin branches by binding to different sites on the Arp2/3 complex remains to be determined.

Additionally, the binding of ATP or ADP to Arp2 and Arp3 can increase the affinity of the VCA domain for the Arp2/3 complex, although ATP is more efficient (Dayel et al., 2001, Goley et al., 2004, Le Clainche et al., 2003). Interestingly, it has also been shown that the binding affinity of ATP to both Arp2 and Arp3 increases when the VCA domain interacts with the Arp2/3 complex (Le Clainche et al., 2003, Dayel et al., 2001). However, it is still not clear how the Arp2/3 complex is activated by the VCA domain, and whether the one VCA domain, one G-actin or the two VCA domains, two actins model is correct. Further biochemical and biological studies are necessary to fully understand the significance of the dynamic interactions between the VCA domain, G-actin and the Arp2/3 complex in initiating actin nucleation.

In contrast to class I NPFs, class II NPFs only contain a related acidic region at their N terminus. This acidic region is responsible for binding the Arp2/3 complex

(Campellone and Welch, 2010). However, class II NPFs lack the G-actin binding region. Instead, they have an F-actin binding region, which is responsible for filament binding and activating the Arp2/3 complex (Campellone and Welch, 2010). Class II NPFs are less potent activators of the Arp2/3 complex when compared to class I NPFs. It has been suggested that class II NPFs function as stabilisers of the newly formed Y-branch following the activation of the Arp2/3 complex by class I NPFs (Goley and Welch, 2006). Examples of class II NPFs include cortactin and coronin (Campellone and Welch, 2010). Cortactin-knockout cells display modest defects in membrane ruffling and motility (Lai et al., 2009). In contrast, depletion of Coronin 1B affects barbed end distribution as well as actin filament organisation at the leading edge (Cai et al., 2007). These studies strongly suggest cortactin and coronin 1 B are essential in regulating actin polymerisation possibly by modulating the activity of the Arp2/3 complex.

Class I NPF will be discussed in more detail in the next section, as they are more relevant to my thesis.

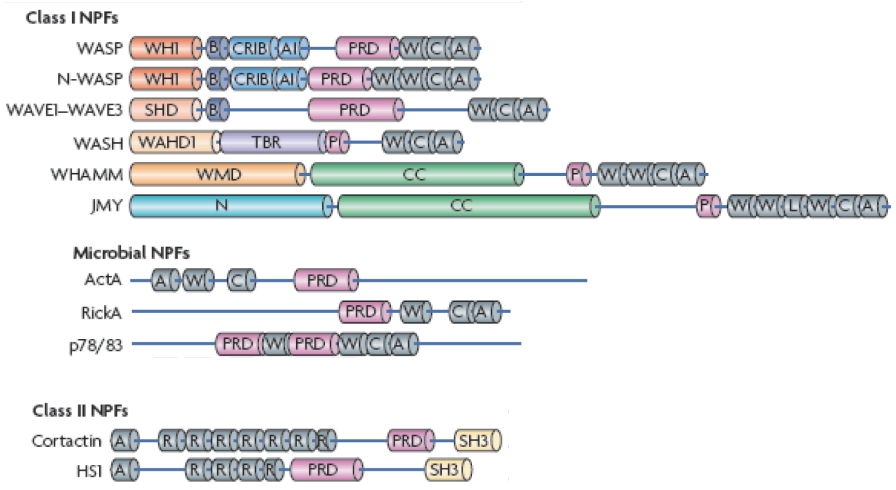

Figure 1.9 Classification Arp2/3 complex NPFs.
NPFs can be divided into two classes. All mammalian class I NPFs consist of variable N-terminal regions and a conserved C-terminal VCA domain. The VCA domain, which binds both G-actin and the Arp2/3 complex, is essential for Arp2/3 complex activation. Class I NPFs are also used by microbial pathogens to induce actin polymerisation. ActA from *Listeria* and RickA from *Rickettsia* are examples of these microbial NPFs. In contrast to class I NPFs, class II NPFs, which lack the VCA domain, bind and activate the Arp2/3 complex via an N-terminal acidic region. In addition, class II NPFs do not interact with G-actin, although they are able to interact with F-actin. Regions of NPFs that are responsible for interacting with actin and the Arp2/3 complex are shown in grey. Taken from (Campellone and Welch, 2010) with the permission of Nature Publishing Group.

1.5 Class I Nucleating Promoting Factors (NPFs)

ActA from *Listeria monocytogenes* was the first class I NPF to be identified that can activate the Arp2/3 complex *in vitro* (Welch et al., 1998). Since then, a number of conserved class I NPFs have been found in metazoans and will be discussed in detail in the following section (Figure 1.9).

1.5.1 WASP and N-WASP

Wiskott-Aldrich Syndrome protein (WASP) and neuronal Wiskott-Aldrich syndrome protein (N-WASP) are the best-characterised class I NPFs. WASP and N-WASP are conserved from fungi to human (Campellone and Welch, 2010, Veltman and Insall, 2010). In contrast to N-WASP, which is ubiquitously expressed, WASP is only found in haematopoietic cells (Molina et al., 1992). In mice, mutations in WASP lead to immunodeficiencies (Molina et al., 1992), whereas deletion of N-WASP is embryonic lethal (Snapper et al., 2001).

WASP and N-WASP proteins share about 50% amino acid sequence identity and have a similar domain organisation (Takenawa and Suetsugu, 2007). Both proteins comprise an N-terminal WASP homology (WH1) domain, which has a similar fold compared to the EVH1 domain of Ena/VASP proteins (Prehoda et al., 1999, Peterson and Volkman, 2009). This WH1 domain is followed by a basic region (B), a Cdc42 and Rac interactive binding region (CRIB), auto-inhibitory motifs (AI), a proline-rich domain (PRD) and a VCA domain (Chapter 1.4.3). The CRIB and AI motifs together are referred to as the GTPase binding domain (GBD). Although WASP and N-WASP have a similar domain organisation, their C-terminal VCA domain differs. The N-VASP VCA domain contains two V regions compared with one in WASP (Figure 1.9)

Each region/domain of WASP and N-WASP interacts with different proteins, some of which regulate their activities (Campellone and Welch, 2010). In their inactive state, the VCA domain is masked due to its interaction with the GBD region (Kim et al., 2000). In this auto-inhibited state, the VCA cannot bind or activate the Arp2/3 complex (Kim et al., 2000). Moreover, WASP interacting protein (WIP), which binds the WH1 domain of WASP and N-WASP, is also thought to stabilise the inactive conformation of the two proteins (Anton et al., 2007). This auto-inhibitory interaction can be released by a variety of signalling pathways that are activated at the plasma membrane in response to extracellular stimuli and transfered to intracellular factors that bind the

GBD or the PRD of WASP/N-WASP (Campellone and Welch, 2010, Moreau et al., 2000, Carlier et al., 2000). For instance, competitive binding of Cdc42 to the GBD causes a conformational change in WASP/N-WASP that leads to the unmasking of the VCA domain (Kim et al., 2000, Prehoda et al., 2000). Src homology 3 (SH3) containing proteins have been found to activate N-WASP by interacting with the PRD. These proteins include non-catalytic kinase 1 (Nck1), Nck2 (Tomasevic et al., 2007, Rivera et al., 2009), transducer of Cdc42-dependent actin assembly 1 (TOCA1) (Ho et al., 2004, Takano et al., 2008) and the Abelson interacting protein 1 (Abi1) (Innocenti et al., 2005). Additionally, phosphorylation of the GBD is thought to not only stabilise the activated WASP/N-WASP but also to enhance the effects of SH2 domain containing proteins on activating WASP/N-WASP family proteins (Torres and Rosen, 2006, Cory et al., 2002, Cory et al., 2003, Blundell et al., 2009, Danson et al., 2007, Pocha and Cory, 2009).

Cells lacking functional N-WASP exhibit defects in the Arp2/3-dependent membrane protrusions, such as impaired dorsal membrane ruffling (Legg et al., 2007), filopodia formation (Snapper et al., 2001, Bu et al., 2009) and membrane invagination (Tsujita et al., 2006). A number of studies have also shown that N-WASP contributes to endocytosis (Innocenti et al., 2005, Bu et al., 2009, Tsujita et al., 2006, Benesch et al., 2005).

1.5.2 WAVE1, WAVE2 and WAVE3

Similarly to WASP and N-WASP, the WASP-family verprolin-homologous protein (WAVE; also referred to as suppressor of cyclic AMP repressor (SCAR)) is also conserved in metazoans (Veltman and Insall, 2010). In mammals, there are 3 WAVE isoforms that are referred to as WAVE 1-3 (Veltman and Insall, 2010). All three mammalian WAVE isoforms are expressed in many cell types, although they are especially enriched in brain tissue. In general, WAVE1 and WAVE2 are expressed more widely than WAVE3 (Campellone and Welch, 2010). In mice, depletion of WAVE1 leads to sensorimotor defects, abnormal behaviour and reduced viability (Dahl et al., 2003, Soderling et al., 2003). In contrast, knockout of WAVE2 is embryonic lethal and results in abnormalities in angiogenesis, in heart and brain development (Yan et al., 2003, Yamazaki et al., 2003).

WAVE1 has about 49% sequence identity compared to WAVE2 and WAVE3, with the C-terminal VCA domain being the most conserved region in all three mammalian isoforms (Suetsugu et al., 1999, Veltman and Insall, 2010). WAVE family proteins consist of an N-terminal SCAR homology domain (SHD) and a basic domain (B) but lack the GBD that is found in WASP and N-WASP (Figure 1.9). Moreover, the PRD of WAVE family proteins, which is next to the C-terminal VCA domain, differs from the PRD of WASP/N-WASP (Figure 1.9). The SHD, which is very distinct from the WH1 domain of WASP/N-WASP, interacts with HSPC300, Abi1, NCK-associated protein 1 (Nap1) and Rac-associated 1 (SRA1; also called PIR121) to form a pentameric complex known as the WAVE complex (Gautreau et al., 2004, Echarri et al., 2004, Innocenti et al., 2004, Leng et al., 2005). Interestingly, depletion of a single component of the WAVE complex significantly reduces the expression of the other subunits in addition to disrupting the stability of the complex itself (Steffen et al., 2004, Innocenti et al., 2004, Rogers et al., 2003, Dubielecka et al., 2011, Kunda et al., 2003). Due to the relevance of the WAVE complex to my study, I will discuss the details of the WAVE complex, such as its cellular function, activation and regulation in section 1.6.

1.5.3 WASH

WASP and Scar homolog (WASH) is a novel class I NFPs that has been identified recently by comparative and phylogenetic analyses (Linardopoulou et al., 2007). WASH is found in many animals and plants, but not yeast (Rottner et al., 2010). In *Drosophila, washout* (WASH ortholog in *Drosophila*) mutant flies display defects in pupal morphology, suggesting that WASH is important during early development (Linardopoulou et al., 2007).

As observed in WASP and WAVE, WASH has a modular domain organization (Figure 1.9). In addition to the C-terminal VCA domain, WASH contains a unique N-terminal WASH homology domain (WAHD, also called WAHD1), which is followed by the tubulin-binding region (TBR; also called WAHD2) (Campellone and Welch, 2010). A proline rich region is also present in WASH, although it is significantly smaller than those found in WASP and WAVE (Figure 1.9).

As seen with WAVE family proteins, WASH seems to function as part of a complex in cells (Campellone and Welch, 2010). These WASH-associated proteins are FAM21, Srumpellin, SWIP (Srumpellin and WASH-interacting protein) and Ccdc53 (coiled-coil

domain-containing protein 53) (Derivery et al., 2009b, Gomez and Billadeau, 2009). Exactly how the WASH-associated complex and the individual components contribute to the assembly and stability of the complex remain to be determined (Campellone and Welch, 2010). However, it has been shown that the WASH-mediated Arp2/3 activity regulates the shape of the membranes of the early and recycling endosomes. This influences recycling of endosomes to the plasma membrane and the trafficking of endosomes to the *trans*-Golgi network (Derivery et al., 2009b, Gomez and Billadeau, 2009, Duleh and Welch, 2010). A recent study also demonstrated a role for WASH in promoting actin polymerization on mature lysosomes in *Dictyostelium* (Carnell et al., 2011). The same study also showed that binding of these newly formed actin filaments on mature lysosomes to the Vacuolar-type H^+-ATPase (V-ATPase) is mediated by WASH. Observations in *Drosophila* suggest that WASH is also able to bundle and crosslink actin filaments and microtubules in response to Rho1 signalling (Liu et al., 2009a). Therefore, WASH not only interacts with actin and the Arp2/3 complex, but can also associate with the microtubule cytoskeleton. WASH may act as a connector to link the actin and microtubule cytoskeletons together.

1.5.4 WHAMM

In addition to WASH, another member of NPF I family: WASP homolog associated with actin, membranes, and microtubules (WHAMM) is also found to associate with both the actin and microtubule cytoskeletons (Campellone et al., 2008, Rottner et al., 2010).

WHAMM was identified during a bioinformatics search of the human proteins that have a VCA motif (Campellone et al., 2008). WHAMM is ubiquitously expressed in vertebrates (Campellone et al., 2008). Using *in vitro* actin-pyrene assays, the same study also demonstrated that like N-WASP there are two V regions in the VCA domain of WHAMM and that this VVCA domain is able to stimulate the actin nucleation activity of the Arp2/3 complex. However, the ability of WHAMM to promote Arp2/3 dependent actin nucleation is less potent than N-WASP. Furthermore it has been reported that the activity of the VVCA domain alone is equal to the activity of the full length WHAMM, suggesting that the protein is not auto-inhibited (Campellone et al., 2008). However, this study was done with pure WHAMM, which might also exist as part of a larger complex that is tightly regulated.

In addition to the C-terminal VVCA domain, WHAMM processes a WHAMM membrane-interacting domain (WMD) at its N-terminus, which has little or no sequence homology to any known protein (Campellone and Welch, 2010). The WMD localises WHAMM to the *cis*-Golgi and tubulovesicular membranes. WHAMM has been found to interact with actin and microtubules and function in ER to Golgi transport (Campellone et al., 2008). The WMD is followed by a central coiled-coil (CC) region and a small proline rich region (Figure 1.9). The binding partners of WHAMM are currently unknown (Campellone and Welch, 2010). Moreover, it is not clear if WHAMM is part of a multi-protein complex like WAVE and WASH (Rottner et al., 2010). Further studies are required to identify proteins that interact with WHAMM to uncover how the activity of WHAMM is regulated.

1.5.5 JMY

Junction mediating and regulatory protein (JMY), which is closely related to WHAMM, is the latest class I NFP to be identified (Campellone and Welch, 2010). Like WHAMM, JMY is confined to vertebrates and is expressed in most mammalian tissues and cell types (Rottner et al., 2010). JMY was originally identified as a cofactor of the transcriptional regulators p300 and p53 (Shikama et al., 1999). JMY was believed to only function with p53 until a recent study demonstrated that JMY has Arp2/3 complex dependent actin nucleation activity (Zuchero et al., 2009).

In addition to a unique N-terminal (N) and a central CC region, which is similar to WHAMM, JMY has an unusual C-terminal VCA domain (Figure 1.9). The C-terminal domain of JMY comprises three V regions and an extra linker sequence that separates the second and third V region (Figure 1.9). Notably, this non-classical VVLVCA domain of JMY can also promote spontaneous actin nucleation in the absence of the Arp2/3 complex (Zuchero et al., 2009). However, the resulting actin networks are unbranched and similar to those induced by formins and spire (Chapter 1.3.4). Moreover, the activity of full-length JMY has not yet been determined. Further studies are required to address whether the Arp2/3 complex and the actin nucleating activities of JMY are coordinated or if one is more dominant than the other (Campellone and Welch, 2010).

In the cell, JMY is able to shuttle between the nucleus and plasma membrane (Zuchero et al., 2009). JMY is enriched in the cell nucleus, where its localisation is correlated

with DNA damage (Coutts et al., 2009). During cell migration, JMY localises to the lamellipodia, where its presence or absence affects the speed of cell migration (Zuchero et al., 2009).

1.6 The WAVE complex

The WAVE1 complex was first purified from bovine brain (Li et al., 2002). Subsequent studies showed that WAVE2 and WAVE3 are also able to associate with the same four subunits as WAVE1 (Innocenti et al., 2004, Gautreau et al., 2004, Suetsugu et al., 2006, Stovold et al., 2005). Although all three WAVE complexes share the same four subunits, they have been found to localise differentially in neuronal growth cones (Nozumi et al., 2003). Moreover, WAVE1-deficient fibroblasts exhibit defects in dorsal ruffling and ECM-degrading MMP-dependent 3D migration, whereas defects in peripheral membrane ruffling at the leading edge were observed in WAVE2-deficient fibroblasts (Suetsugu et al., 2003). These results suggest that each of the WAVE complexes plays a different role in regulating membrane protrusions during cell migration. However, a later study observed the normal production of dorsal ruffles in cells lacking WAVE1 as well as in cells that have reduced levels of WAVE2, whereas cells lacking N-WASP exhibited defects in dorsal ruffles (Legg et al., 2007). It suggests that N-WASP rather than WAVE is essential for Arp2/3-mediated dorsal ruffle formation.

1.6.1 Subunits and structural organisation

The WAVE complex comprises WAVE (68kDa), Abi (55kDa), Nap1 (125kDa), PIR121 (140kDa) and the small HSPC300 (9kDa). All five components of the WAVE complex are evolutionarily conserved (Veltman and Insall, 2010) (Table 1.1). Based on the molecular weight of the individual subunits, a 1:1:1:1 stoichiometry of the WAVE1 complex components is predicted (Eden et al., 2002). By testing all pairwise combinations between the different subunits in a reconstitution system, the molecular architecture of the WAVE complex was predicted to be a stack of HSPC300, WAVE, Abi, Nap1 and PIR121 from top to the bottom (Gautreau et al., 2004). The same study also found that Nap1 and Abi are the most critical components of the WAVE complex by examining the binding ability of the other subunits when one particular subunit is excluded. Moreover, using *in vitro* pull down assays, it has been shown that the interaction between WAVE and Abi involves the N-terminal regions of both proteins (Innocenti et al., 2004). This study also showed Nap1 and PIR121 can be purified as a

subcomplex and that the binding of this subcomplex to WAVE is dependent on Abi. These results pointed to Abi being the most key component for mediating WAVE complex formation. A subsequent study successfully reconstituted the Nap1:PIR121 heterodimer and the WAVE:Abi:HSPC300 heterotrimer *in vitro* using the recombinant proteins (Ismail et al., 2009). Based on the observations from these biochemical studies, a model for the molecular organisation of the WAVE complex was proposed (Figure 1.10A). The interaction between Abi and Nap1 is at the core of the complex. On one side of the core, WAVE interacts with Abi and HSPC300 to form a trimer. On the other side of the core, Nap1 binds PIR121 to form a dimer (Derivery and Gautreau, 2010).

Table 1.1 WAVE complex homologs and nomenclature in various species
Different isoforms of the proteins are spaced by ",". Different names of the same proteins are spaced by "/". Adapted from (Weiner et al., 2006) with permission.

Species	140-kDa Subunit	125-kDa Subunit	68-kDa Subunit	49- to 55-kDa Subunit	9-kDa Subunit
Human, ubiquitous	CYFIP1/ PIR121/Sra1, CYFIP2	Hem-2/ Nap125/ Nap1	WAVE1, WAVE2, WAVE3	Abi1/ E3B1, Abi2, Abi3	HSPC300
Human, hematopoietic-specific		Hem-1			
Drosophila	CYFIP/Sra-1	KETTE	SCAR	Abi	HSPC300
C. elegans	GEX-2	GEX-3	Wve1/ GEX-1	B0336.6	
Dictyostelium	PIR121	NAP1	SCAR	Q55FT9	Q54X65
Arabidopsis	PIRP/ KLUNKER	GRL/NAP P/PIR121	DIS3/ SCAR2		BRK1

More recently, the structure of the WAVE complex has been solved (Chen et al., 2010). Consistent with previous suggestions, the structure of the WAVE complex can be described as two subcomplexes: a Nap1:PIR121 dimer and a WAVE:Abi:HSPC300

trimer (Figure 1.10B). Nap1 and PIR121 form homologous structures and bind to each other extensively to form an elongated pseudo-symmetric dimer. This elongated structure is thought to act as a platform for the rest of the complex. In contrast to Nap1, which only binds Abi, all three subunits in the WAVE:Abi:HSPC300 subcomplex were found to interact directly with the N-terminal region of PIR121. However, the most extensive contact between the two subcomplexes is made by HSPC300, which interacts with WAVE, Abi and PIR121, along its full length. Notably, HSPC300 is the only subunit of the WAVE complex that can either exist as a component of the complex or as an isolated HSPC300 trimer in an abundant cytosolic pool (Derivery et al., 2008). Given the ability of trimeric HSPC300 to associate with newly synthesised subunits to generate a functional WAVE complex, it has been suggested that the free HSPC300 trimer acts as the precursor for the assembly of the WAVE complex (Derivery et al., 2008). A more recent study showed the HSPC300 trimer is formed by the interaction of coiled-coil regions in its C-terminus (Linkner et al., 2011). The crystal structure of this parallel triple coiled-coil bundle in HSPC300 trimer is similar to the heterotrimeric α-helix bundle that is observed in the WAVE:Abi:HSPC300 subcomplex (Chen et al., 2010). HSPC300 therefore appears to be the key subunit mediating the interaction between Nap1:PIR121 and WAVE:Abi:HSPC300 subcomplexes during WAVE complex assembly.

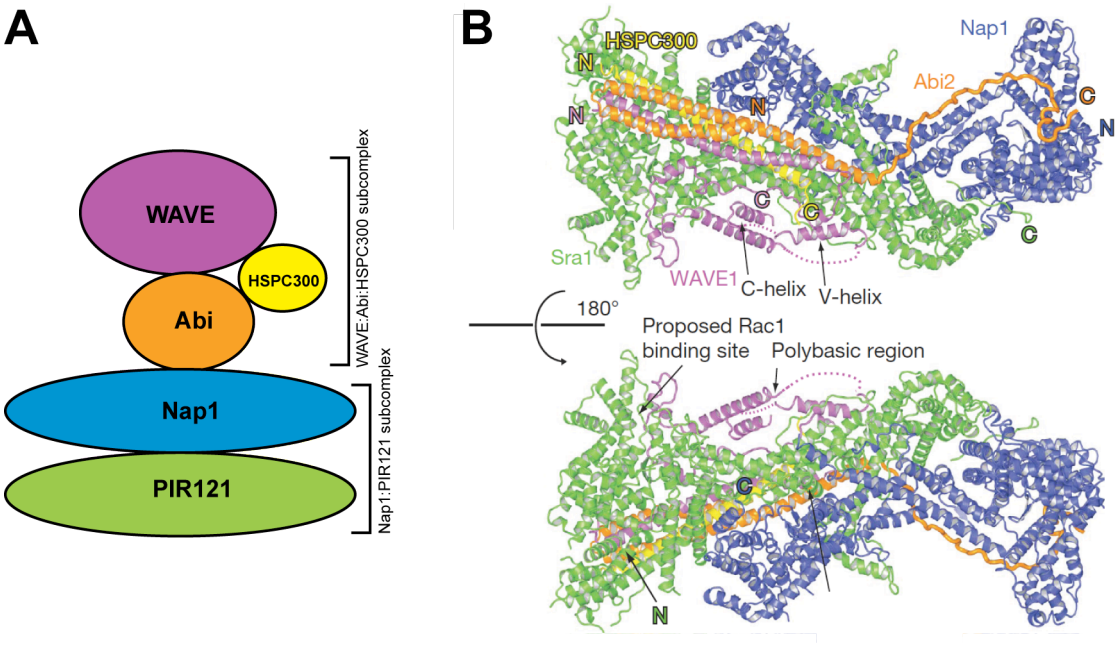

Figure 1.10 Structure of the WAVE complex.
A. The cartoon illustrates the proposed organisation of the WAVE complex. The WAVE complex can be sub-divided into the WAVE:Abi:HSPC300 and Nap1:PIR121 subcomplexes. **B**. The structure of the WAVE complex. Top and bottom structures are related by a 180° rotation around a horizontal axis. Different colours, which are the same as in **A**, indicate the subunits of the WAVE complex. Dashed lines indicate the poly-proline regions of WAVE, which are absent in the structure as they are disordered. **B** was taken from (Chen et al., 2010) with permission of Nature Publishing Group.

1.6.2 Regulation of the WAVE complex

Initial reports suggested that WAVE complex had a basal activity to activate the actin nucleating capacity of the Arp2/3 complex when it was first purified from bovine brain (Li et al., 2002). However, subsequent studies revealed the WAVE complex is inactive using affinity purified WAVE complex from mammalian cell lines or reconstituted recombinant protein complexes from different expression systems (Derivery et al., 2009a, Ismail et al., 2009). Notably, the study using the reconstituted WAVE complex suggested that inhibition of its activity is mediated by an interaction between the VCA domain of WAVE and the Nap1:PIR121 subcomplex (Ismail et al., 2009) (Figure 1.11A). The structure has now shown that the WAVE complex is inhibited through the direct interaction between the C-terminus of WAVE and PIR121 (Chen et al., 2010) (Figure 1.11B). Based on their structural and mutagenic analyses, Chen et al demonstrated that binding of PIR121 to the VCA domain and the adjacent intervening

loops (meander region) of WAVE leads to sequestration of VCA and inhibition of the activity of the WAVE complex towards the Arp2/3 complex (Chen et al., 2010).

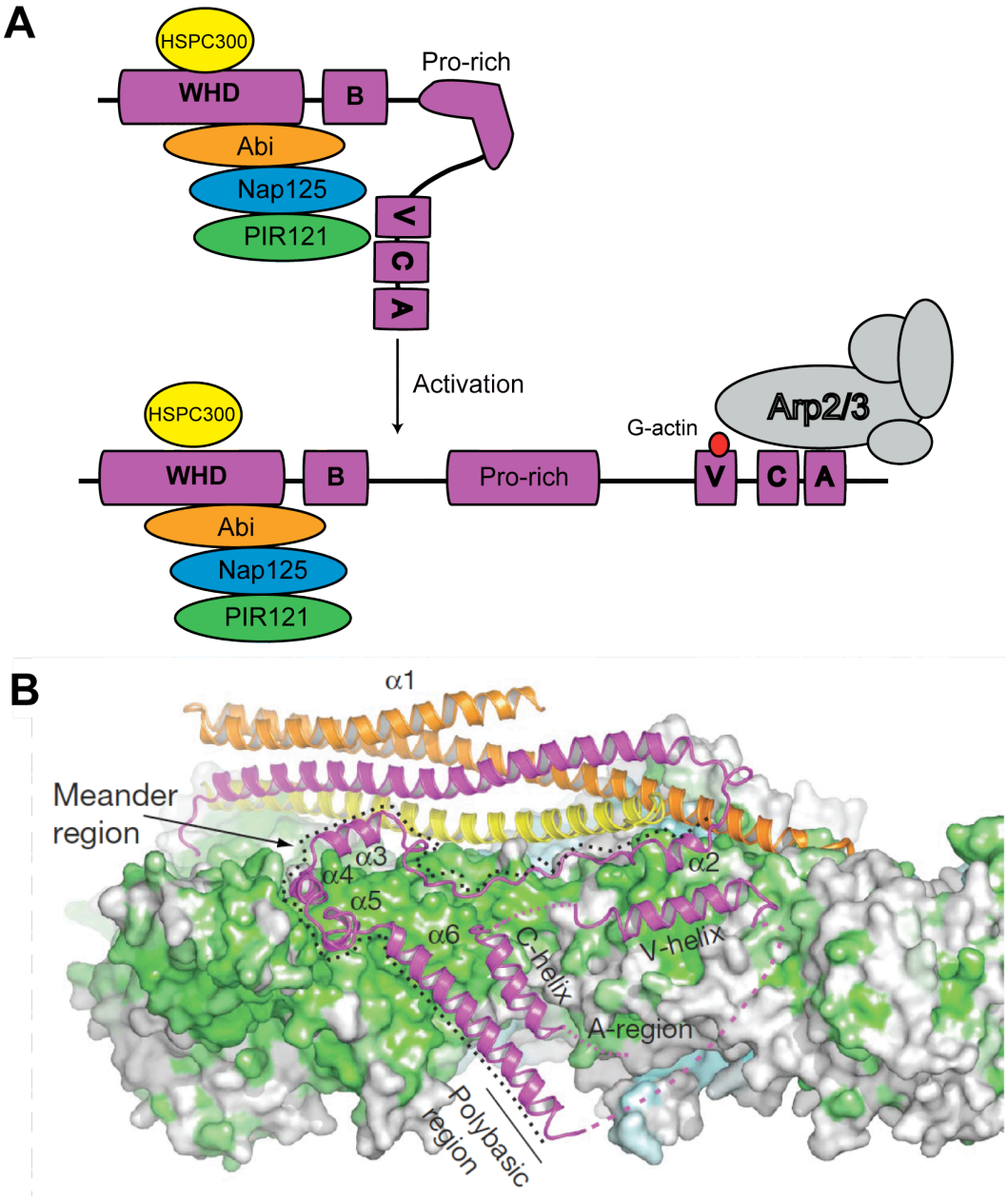

Figure 1.11 WAVE complex regulation.
A. A model for WAVE complex activation. Under resting conditions, the WAVE complex is auto-inhibited by an intermolecular interaction between the VCA domain and the Nap1:PIR121 subcomplex. Activation of the WAVE complex leads to a conformational change within the complex. This results in the exposure of the VCA domain, which subsequently interacts with G-actin and the Arp2/3 complex to initiate actin nucleation. **B**. A close up of the structure of the inhibited WAVE complex. The C terminus of WAVE, which contains a meander region (black dashed line) and the VCA

region, binds directly to PIR121 (green). **B** was taken from (Chen et al., 2010) with permission of Nature Publishing Group.

1.6.2.1 Activation of the WAVE complex by Rac

The best-established activator of the WAVE complex is the small GTPase Rac (Derivery and Gautreau, 2010). Depletion of Abi, Nap1 or PIR121 using RNAi significantly abrogates the formation of Rac dependent lamellipodial protrusions (Innocenti et al., 2004, Steffen et al., 2004). This suggests that Rac plays an essential role in regulating actin-based cell protrusion by activating the WAVE complex. Using pyrene actin assays, subsequent studies demonstrated that Rac is able to active the reconstituted WAVE complex *in vitro* without disrupting the integrity of the complex (Chen et al., 2010, Ismail et al., 2009, Lebensohn and Kirschner, 2009). The data from these *in vitro* biochemical experiments resolved the conflicts in literature that suggested the WAVE complex is disassembled upon addition of active Rac (Eden et al., 2002). Given that WAVE lacks an obvious GBD, it is thought that binding of Rac-GTP to the complex is dependent on PIR121, as it possesses an N-terminal GBD (Kobayashi et al., 1998). Indeed, *in vitro* binding assays revealed that a series of PIR121 mutations severely disrupted the interaction between the WAVE complex and Rac (Chen et al., 2010). The same study also showed that deleting the VCA region from WAVE increases the affinity of the complex for Rac. This suggests that Rac competes with the VCA region of WAVE for interacting with PIR121 in the complex, and that this subsequently leads to activation of the complex (Chen et al., 2010). The recruitment of Rac to the WAVE complex is also thought to be mediated by IRSp53. IRSp53, which was originally identified as an insulin receptor substrate, was subsequently demonstrated to interact directly with Rac-GTP as well as WAVE (Miki et al., 2000). Moreover, IRSp53 RNAi-treated cells exhibit defects in the recruitment and activation of the WAVE complex, leading to decreased lamellipodia formation (Takahashi and Suzuki, 2010, Suetsugu et al., 2006). However, the mechanism by which IRSp53 contributes to Rac mediated activation of the WAVE complex remains to be determined.

1.6.2.2 Activation by membrane clustering

In addition to activation by Rac, the activity of the WAVE complex is also regulated through membrane localisation/clustering (Derivery and Gautreau, 2010). IRSp53 not only acts as a bridge to mediate the interaction between Rac and WAVE, but it appears to play an important role in clustering the WAVE complex at the plasma membrane (Derivery and Gautreau, 2010). IRSp53 possesses a Bin-Amphiphysin-Rvs (BAR)

domain, which is responsible for interacting with Rac as well as phosphatidylinositol (4,5)-bisphosphate (PIP2) at the plasma membrane (Mattila et al., 2007). Cells lacking IRSp53 display defects in the recruitment and activation of the WAVE complex (Takahashi and Suzuki, 2010, Suetsugu et al., 2006). It thus appears that IRSp53 is a central player in recruiting the WAVE complex to the plasma membrane, prior to WAVE complex activation. Furthermore, Phosphatidylinositol (3,4,5)-trisphosphate (PIP3), which is the product of phosphatidylinositol 3-kinase (PI3K), is found to bind directly and recruits WAVE at the plasma membrane (Oikawa et al., 2004). However, a recent study argued that the interaction between the WAVE complex and PIP3 is not direct but is dependent on IRSp53 (Takahashi and Suzuki, 2010). Further studies are required to fully understand how the WAVE complex is regulated through its clustering at the plasma membrane. In particular, the function and relative contribution of various proteins and lipids at the plasma membrane in mediating the activity of the WAVE complex remains to be established.

1.6.2.3 Activation by phosphorylation

Finally, phosphorylation is also emerging as the key mechanism to regulate the activity of the WAVE complex. Tyr150 of WAVE2 (Tyr151 in WAVE1 and WAVE3), which is conserved from plants to humans, can be phosphorylated by Abelson tyrosine (Abl) kinase (Chen et al., 2010). The phosphorylation of WAVE by Abl kinase is key for WAVE complex dependent actin polymerisation and lamellipodia formation (Sossey-Alaoui et al., 2007, Stuart et al., 2006, Leng et al., 2005). The structure of the WAVE complex revealed that Tyr151 localises within the “meander region” at the C terminus of WAVE, which interacts with PIR121 (Chen et al., 2010). WAVE complex containing a Y151E mutation exhibited high activity *in vitro* and *in vivo,* suggesting phosphorylation of Try151 destabilised the inhibited WAVE complex to exposure the VCA region and activate the Arp2/3 complex (Chen et al., 2010). In addition, Src and Cdk5 can phosphorylate Tyr125 and Thr138 in WAVE respectively (Miyamoto et al., 2008, Ardern et al., 2006). As with Tyr151, the location of both Tyr125 and Thr138 are within the “meander region”, suggesting that phosphorylation of these sites will also help activate the WAVE complex (Chen et al., 2010). Furthermore, Casein Kinase 2 and MAP kinases phosphorylate multiple residues within the VCA domain of WAVE (Pocha and Cory, 2009, Mendoza et al., 2011). Phosphorylation of these residues also activates the WAVE complex *in vivo* (Pocha and Cory, 2009, Mendoza et al., 2011). All the residues that can be phosphorylated by a variety of different protein kinases are

found within the “meander region” of WAVE, which plays an important role in regulating the activity of the WAVE complex. Therefore, in addition to the effects of both Rac and membrane clustering, phosphorylation provides an extra layer of regulation of the WAVE complex (Derivery and Gautreau, 2010).

1.6.3 Abl interactor (Abi)

The WAVE component Abi is conserved throughout evolution (Veltman and Insall, 2010) (Table 1.1). Three Abi isoforms exist in mammals including Abi1, Abi2 and Abi3, whereas only one Abi isoform is found in *Drosophila* as well as in *Dictyostelium* (Huang et al., 2007, Pollitt and Insall, 2008, Hirao et al., 2006). Mammalian Abi1 and Abi2, which share the greatest amino acid sequence similarity, were first identified using a yeast two-hybrid screen for potential new binding partners of c-Abl (Shi et al., 1995, Dai and Pendergast, 1995). Mammalian Abi3 (also called NESH), which was identified later when trying to clone p53/73 exon domains, has similar domain organisation to Abi1 and Abi2 but only has amino acid sequence similarity with Abi1 and Abi2 at its N-terminus (Ichigotani et al., 2002, Miyazaki et al., 2000).

All three mammalian Abi isoforms can be incorporated into the WAVE complex (Hirao et al., 2006), although the specific function of each isoform in regulating WAVE complex dependent actin dynamics is currently unknown. However, a recent study using embryonic fibroblasts isolated from a conditional Abi1 knockout mouse showed that loss of Abi1 leads to severe defects in cell motility and that increasing Abi2 expression levels is not sufficient to fully compensate for the loss of Abi1 (Dubielecka et al., 2011). This study for the first time demonstrated that Abi isoforms are not equivalent in their ability to stabilise and/or regulate the WAVE complex.

All mammalian Abi isofoms consist of a N-terminal coil-coiled region, which is followed by several proline rich motifs and a SH3 domain at the very C terminus. Using these domains, Abi can associate with a variety of proteins and participates in different multiprotein complexes to regulate the actin cytoskeleton. Excluding WAVE complex components, the best-characterized binding partner of Abi is Abl (Juang and Hoffmann, 1999, Dai and Pendergast, 1995, Shi et al., 1995). Phosphorylation of Abi by Abl has been observed in *Drosophila* S2 cells and is thought to be essential for lamellipodia formation (Huang et al., 2007). Abi is also capable of interacting with Eps8 and Sos1 to form a trimer, which plays a role in regulating Rho family GTPases (Scita et al.,

1999). The modulation of Rho family GTPases by the Abi:Eps8:Sos1 complex is required for downstream actin polymerisation (Scita et al., 1999). Another study, which showed a direct interaction between Abi and Rac, suggested that this interaction enables Abi to positively regulate cell spreading as well as macropinocytosis in a Rac-dependent manner (Dubielecka et al., 2010). Like PIR121, Abi may be another component of the WAVE complex that is capable of bringing Rac to the complex, leading to the activation of the complex.

Finally, a yeast two-hybrid screen identified Mena as a new binding partner of Abi (Tani et al., 2003). A subsequent study, using a combination of biochemical approaches and mass spectrometry identified VASP as another binding partner of Abi (Dittrich et al., 2010). Both Mena and VASP are members of the Ena/VASP family of proteins, which have emerged as key players in regulating the actin cytoskeleton during cell migration (Bear and Gertler, 2009).

1.7 Ena/VASP proteins

Ena/VASP proteins are highly conserved throughout evolution. They localise to the cell leading edge and focal adhesions, where they play a pivotal role in regulating the actin cytoskeleton during cell migration (Krause et al., 2003). *Drosophila* Enabled (Ena), which was discovered as a dominant suppressor of *Drosophila* Abl (dAbl) is one of the founding member of the Ena/VASP family of proteins (Gertler et al., 1990). Mena, which is the mammalian ortholog of Ena was subsequently identified (Gertler et al., 1996). Vasodilator-stimulated phosphoprotein (VASP), which is another mammalian Ena/VASP protein, was originally identified as a substrate of cyclic nucleotide-dependent kinases such as cAMP and cGMP in platelets (Haffner et al., 1995, Halbrugge and Walter, 1989, Waldmann et al., 1987). In addition to Mena and VASP, mammals have a third Ena/VASP protein called Enabled/vasodilator-stimulated phosphoprotein-like protein (Evl) (Gertler et al., 1996). Evl was identified as an expressed sequence tag with homology to Ena and VASP. Unc-34 and *Dictyostelium* VASP (DdVASP) are the only members of Ena/VASP proteins in *C. elegans* and *Dictyostelium*.

1.7.1 Ena/VASP domain organisation and binding partners

The domain organisation is highly conserved among all members of Ena/VASP family proteins (Krause et al., 2003). Ena/VASP proteins possess N-terminal Ena/VASP homology 1 (EVH1) domain and a C-terminal Ena/VASP homology 2 (EVH2) domain that are separated by a proline rich region (Figure 1.12). Each of these domains has specific binding partners that regulate different aspects of Ena/VASP proteins, namely their localisation, activity and role in controlling the actin cytoskeleton (Krause et al., 2003, Bear and Gertler, 2009).

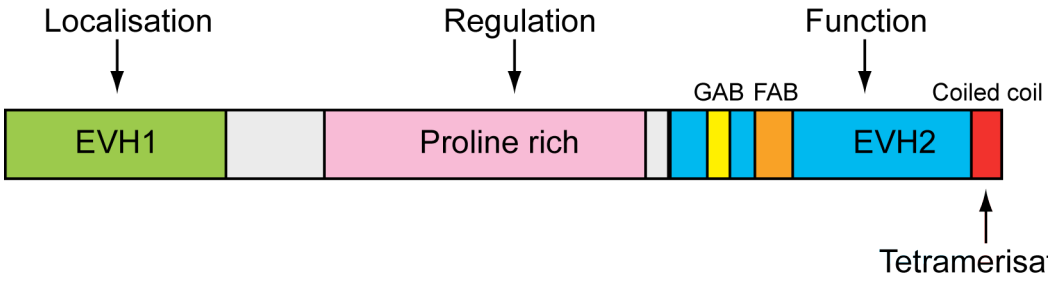

Figure 1.12 Domain organisation of Ena/VASP proteins.
Ena/VASP proteins are highly conserved with the N-terminal EVH1 domain (green) and the C-terminal EVH2 domain (blue) that are separated by a proline rich region (pink). The EVH1 domain is the targeting domain, which drives the intracellular localisation of Ena/VASP proteins. The proline rich region, which harbours binding sites for profilin and a variety of proteins containing either WW or SH3 domains, is thought to be required for regulating the activity of Ena/VASP proteins. The EVH2 domain harbours a G-actin binding motif (GAB) (yellow), and F-actin binding motifs (FAB) (orange). The EVH2 domain is the functional domain of Ena/VASP proteins, which is essential for their ability to regulate the actin cytoskeleton. Ena/VASP proteins can undergo tetramerisation through the coiled coil region at the C terminus (red).

1.7.2 EVH1 domain

Structural studies reveal that the EVH1 domain belongs to the Pleckstrin homology (PH) domain-like superfamily (Ball et al., 2000, Barzik et al., 2001, Beneken et al., 2000, Fedorov et al., 1999, Prehoda et al., 1999). Members of the PH domain superfamily share the PH fold, which consists of two perpendicular β-sheets followed by an α-helix at the C terminus (Peterson and Volkman, 2009). PH domains interact with a variety of ligands including inositol lipids, phosphotyrosines and proline rich sequences (Rebecchi and Scarlata, 1998). The EVH1 domain, however, recognises proline rich sequences through its ligand-binding groove assembled by β-strands 1, 2, 6 and 7 (Peterson and Volkman, 2009, Fedorov et al., 1999, Prehoda et al., 1999).

The EVH1 domain interacts with left-handed polyproline type II rich sequences in a similar fashion to WW or SH3 domains (Prehoda et al., 1999, Fedorov et al., 1999, Ball et al., 2000, Carl et al., 1999, Niebuhr et al., 1997, Peterson et al., 2007, Zarrinpar et al., 2003). The residues flanking the core polyproline type II helix of the ligand define the specificity of interacting with WW, SH3 or EVH1 domains (Krause et al., 2003). Unlike WW and SH3 domains, the EVH1 domain of Ena/VASP proteins only recognises the ligands containing proline rich sequences with the consensus sequence (F/W/Y/L)PPPPX(D/E)(D/E) abbreviated to FPPPP motif (Niebuhr et al., 1997, Ball et al., 2000, Carl et al., 1999, Renfranz and Beckerle, 2002, Peterson and Volkman, 2009). EVH1-like domains have also been found in other protein families such as WASP/N-WASP, Homer/Vesl and some Sprouty-related proteins (SPRED) (Peterson and Volkman, 2009). Although the EVH1 domains of these proteins have strong sequence and structural homology to the EVH1 domains of Ena/VASP proteins, their binding specificities differ. For example, the EVH1 domain of the Homer/Vesl protein family only interact with ligands that have a PPxxF motif (x representing any amino acid) (Beneken et al., 2000, Barzik et al., 2001), whereas a sequence motif in WIP (ISDLPPPEPYVQ) is found to be responsible for binding the EVH1 domain of WASP (Zettl and Way, 2002, Peterson et al., 2007, Volkman et al., 2002).

The EVH1 domain is responsible for the intra-cellular targeting of Ena/VASP proteins through its interaction with a variety of FPPPP motif containing proteins (Ball et al., 2000, Niebuhr et al., 1997, Krause et al., 2003). For example, the localisation of Ena/VASP proteins to focal adhesions is mediated by an interaction with the FPPPP containing protein Zyxin (Drees et al., 2000, Garvalov et al., 2003, Hoffman et al., 2006). In contrast, MRL proteins such as lamellipodin, MIG-10 and RIAM, which also contain multiple FPPPP motifs, recruit Ena/VASP proteins to the leading edge of a migrating cell (Krause et al., 2004, Michael et al., 2010, Lafuente et al., 2004, Quinn et al., 2006). During neural development, Semaphorin 6A-1, another FPPPP containing protein, is thought to recruit Ena/VASP proteins to the plasma membrane by binding their EVH1 domains. The interaction between Semaphorin 6A-1 and Ena/VASP proteins is pivotal in axon guidance (Klostermann et al., 2000). Furthermore, ActA from the intracellular bacterial pathogen *Listeria*, which contains multiple FPPPP motifs, can also recruit Ena/VASP proteins to the bacterial surface by binding directly to the EVH1 domains (Niebuhr et al., 1997). This interaction enhances the ability of *Listeria* to induce actin polymerization to promote their motility inside the host cell

(Cameron et al., 2000, Auerbuch et al., 2003, Geese et al., 2002). Other FPPPP containing proteins that bind directly to the EVH1 domain of Ena/VASP proteins include roundabout (Robo) (Bashaw et al., 2000), Fyn-binding (Fyb)/SLP-76 associated protein (SLAP) (Krause et al., 2000) and Palladin (Mykkanen et al., 2001).

1.7.2.1 Proline rich region

The central proline rich region is the most divergent portion of Ena/VASP proteins. It has been suggested that Ena/VASP proteins interact with different proteins via their proline rich regions in order to be regulated by many different signalling pathways (Krause et al., 2003). The proline rich region of Ena/VASP proteins contains numerous binding sites for proteins containing either SH3 or WW domains (Krause et al., 2003). Given the sequence diversity of this proline rich region, binding specificity for proteins that have SH3 or WW domains to this region is variable among Ena/VASP family proteins. For example, the SH3 domain of Abl and the WW domain of FE65 bind the proline rich region of both Mena and Evl, whereas the SH3-containing protein Neural Src (N-Src) can only interact with Evl (Lambrechts et al., 2000, Gertler et al., 1996, Ermekova et al., 1997). In addition to SH3 and WW-containing proteins, the proline rich region of all Ena/VASP proteins can interact with profilin (Krause et al., 2003). Profilin I and II can bind to the proline rich region of VASP, although the binding affinity of profilin I for VASP is much lower than that of profilin II (Jonckheere et al., 1999).

Profilin, which is one of the most important ABPs, as it plays an essential role in regulating actin dynamics (Bugyi and Carlier, 2010). Profilin binds G-actin and has a higher affinity for ATP-G-actin than for ADP-G-actin (Perelroizen et al., 1995, Pantaloni and Carlier, 1993). Profilin is therefore able to sequester actin monomers to prevent their spontaneous nucleation since profilin bound G-actin can only promote actin polymerisation by being added on to the barbed end of growing actin filaments (Bear and Gertler, 2009, Bugyi and Carlier, 2010). Moreover, upon binding to G-actin, profilin also has the ability to convert the bound ADP to ATP (Vinson et al., 1998). This nucleotide exchange provides a constant pool of ATP-G-actin in order to facilitate efficient actin assembly.

1.7.2.2 EVH2 domain

The C-terminal EVH2 domain has been described as the functional domain (Bachmann et al., 1999). The EVH2 domain contains three sub-domains: an N-terminal G-actin

binding (GAB) site followed by a F-actin binding (FAB) site and a coiled-coil motif at the extreme C terminus. GAB and FAB sites are responsible for interacting with monomeric and filamentous actin respectively (Bachmann et al., 1999, Gertler et al., 1996). The GAB site has strong sequence homologies to the WH2 domains found in many cytoskeletal proteins, including β-thymosin, N-WASP and Spire (Paunola et al., 2002, Dominguez, 2007, Dominguez, 2009). The GAB site is essential for the actin nucleating activity of VASP *in vitro* (Walders-Harbeck et al., 2002). A subsequent study proposed that the GAB site together with the last polyproline segment in the proceeding proline rich region serves as a loading region for binding a profilin:G-actin complex (Ferron et al., 2007). Upon binding to Ena/VASP proteins, the actin in the profilin:G-actin complex is thought to be able to then bind the barbed end of F-actin (Ferron et al., 2007). In contrast to GAB, FAB is found to bind and bundle F-actin (Bachmann et al., 1999, Huttelmaier et al., 1999). Additionally, the C-terminal coiled-coil motif within EVH2 domain is required for the tetramerisation of Ena/VASP proteins (Bachmann et al., 1999, Zimmermann et al., 2002). Homo- and hetrotetramerisation of Ena/VASP family members has been observed *in vivo* (Carl et al., 1999, Ahern-Djamali et al., 1998).

1.7.3 Ena/VASP-mediated cell migration

Ena/VASP proteins have been shown to play a pivotal role in the regulation of the actin cytoskeleton during cell migration (Krause et al., 2003, Bear and Gertler, 2009). However, it is still debated whether Ena/VASP proteins positively or negatively regulate cell migration.

In fibroblasts, the overexpression of Ena/VASP proteins reduces the speed of cell migration in a dose-dependent manner, whereas the depletion of Ena/VASP proteins from focal adhesions and the plasma membrane increases their speed (Bear et al., 2000). Furthermore, complementation of Ena/VASP-deficient cells with Mena leads to a reduction in migration speed (Bear et al., 2002). During corticogenesis, neurons move radially from the germinal areas of ventricular zone (VZ) outward to form the cortical plate (CP) (Rakic, 1978). Inhibition of Ena/VASP function in neurons within the developing neocortex leads to increased neuronal migration towards a more superficial location (Goh et al., 2002). Taken together, these studies support the idea that Ena/VASP proteins act as negative regulators of cell motility.

The first evidence for the positive role of Ena/VASP proteins in regulating actin-dependent cell motility came from analysis of actin-based motility of *Listeria*, which is dependent on ActA (Pistor et al., 1995). Ena/VASP proteins interact with the FPPPP motifs in ActA via their N-terminal EVH1 domains (Niebuhr et al., 1997). Mutation of these EVH1 binding motifs in ActA led to a significant decrease in the intracellular motility of *Listeria*, which suggests that Ena/VASP proteins are positive regulators of actin-dependent motility (Niebuhr et al., 1997, Smith et al., 1996).

Growing evidence suggests that Ena/VASP proteins play a role to promote tumour formation and metastasis (Gertler and Condeelis, 2011). Mena expression is unregulated in invasive tumour cells in rats and mice (Wang et al., 2004, Wang et al., 2007). Furthermore, Mena is able to promote cancer cell motility and invasiveness *in vitro* and *in vivo* (Philippar et al., 2008, Roussos et al., 2011). VASP is also found to contribute to the invasive migration of cancer cells in response to Rac signalling (Han et al., 2008). Overexpression of Evl leads to a significant increase in motility of human cancer breast cells (Hu et al., 2008). These studies suggest that Ena/VASP proteins can act as positive regulators of tumour cell invasion and metastasis.

A positive role of Ena/VASP proteins in controlling actin-dependent cell migration is also supported by recent studies in *Drosophila*. During *Drosophila* oogenesis, border cells migrate from the anterior to the posterior part inside the egg chamber (Montell, 2003). Neutralisation of Ena function in border cells leads to a significant decrease in their migration speed (Gates et al., 2009). This suggests that Ena acts as a positive regulator to promote cell migration *in vivo*. Consistent with this, a new study demonstrated that overexpression of Ena increases the rate of haemocyte migration in the *Drosophila* embryo, whereas depletion of Ena from its normal cellular localisation decreases the rate of cell migration (Tucker et al., 2011).

1.7.4 Molecular functions

Ena/VASP proteins are capable of regulating actin-dependent cell migration in many different types of cells. Different mechanisms have been provided for how Ena/VASP proteins regulate the actin cytoskeleton, such as anti-branching and bundling. However, of all the hypothesised models, the strongest evidence exists for the anti-capping activity of Ena/VASP proteins (Bear and Gertler, 2009). In this model, Ena/VASP proteins bind directly at or near the growing barbed end of actin filaments to inhibit the function of capping proteins that terminate filament growth (Figure 1.13).

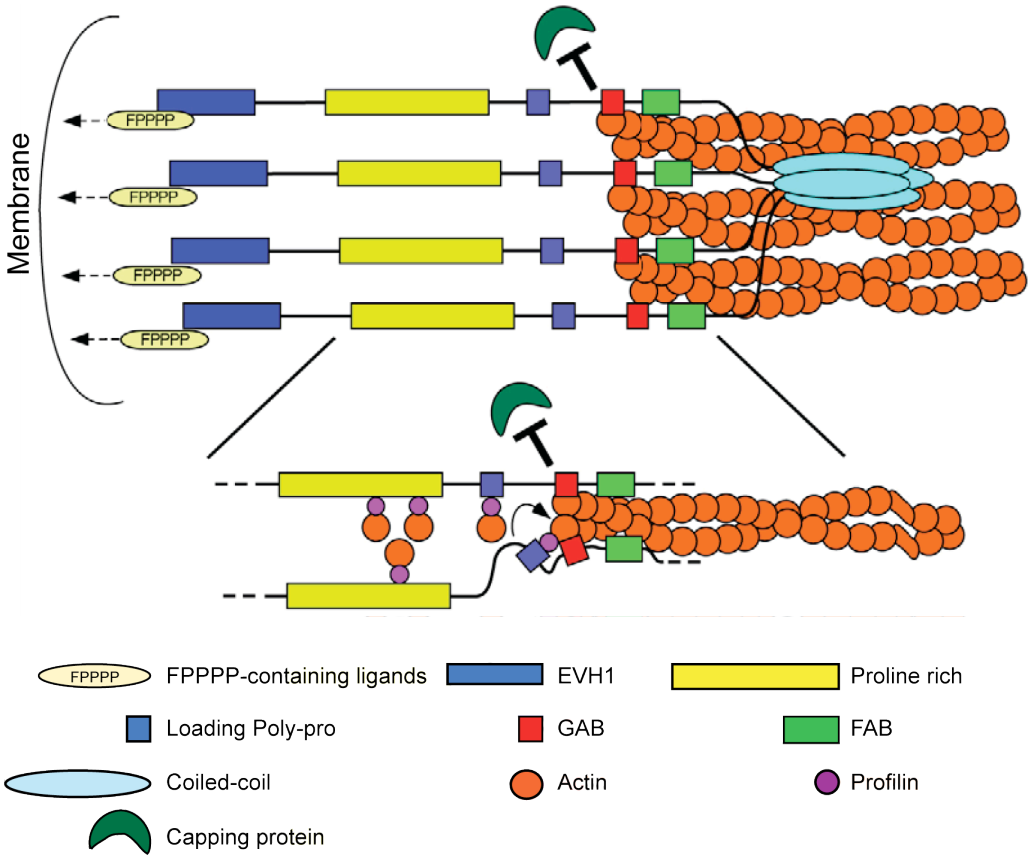

Figure 1.13 Anti-capping activity of Ena/VASP proteins.
Ena/VASP proteins localise to the plasma membrane through the direct interaction with the FPPPP-containing ligands via their N-terminal EVH1 domains (blue). The coiled coil region mediates the tetramerisation of Ena/VASP proteins. Profilin:G-actin complexes are loaded onto the last polyproline segment of Ena/VASP proteins and subsequently added to the barbed end of F-actin. The GAB and FAB motifs within the EVH2 domain are responsible for binding to or near the barbed end of F-actin to block the binding of capping proteins to the barbed end. FPPPP-containing ligands, the structural components of Ena/VASP proteins, actin and actin binding proteins are indicated. Adapted from (Bear and Gertler, 2009) with permission of Company of Biologists Ltd.

1.7.4.1 Anti-capping hypothesis

As its name suggests, capping protein (CP), prevents the addition of G-actin at the barbed end of actin filaments by directly interacting with the barbed end (Pollard and Borisy, 2003). CP is therefore able to tightly regulate actin polymerisation at the leading edge of migrating cells (Pollard and Borisy, 2003).

The anti-capping activity of Ena/VASP proteins was first described in a study where the activity of Ena/VASP proteins was manipulated in fibroblasts (Bear et al., 2002). Electron microscopy showed that actin filaments in lamellipodia of migrating cells were shorter and more branched when Ena/VASP proteins were depleted from the plasma membrane. In contrast, membrane targeted Mena resulted in longer and less branched actin filaments. Subsequently, a direct interaction between Ena/VASP proteins and the barbed end of actin filaments could be verified *in vitro* (Bear et al., 2002). Additionally, *in vitro* polymerisation assays showed that VASP is able to inhibit the capping activity of CP to promote actin filament elongation in a dose-dependent manner. Based on these observations, a functional antagonism between CP and Ena/VASP protein in regulating actin assembly was proposed (Bear et al., 2002). The anti-capping activity of Ena/VASP proteins was also supported by a subsequent study using similar *in vitro* assays (Barzik et al., 2005). This analysis demonstrated that the GAB and FAB motifs as well as the coiled-coil region are all required for the anti-capping activity of Ena/VASP proteins (Barzik et al., 2005).

In addition to indirect *in vitro* pyrene-actin polymerisation assays, total internal reflection fluorescence microscopy (TIRF) assays were used to directly study the function of Ena/VASP proteins in promoting actin assembly (Pasic et al., 2008, Breitsprecher et al., 2008, Breitsprecher et al., 2011, Hansen and Mullins, 2010). The advantage of using TIRF microscopy is that it is possible to monitor the formation of individual actin filaments, to obtain more detailed information including their growth rate. Consistent with previous reports, the elongation of individual actin filaments in the presence of CP and VASP confirmed the anti-capping activity of Ena/VASP proteins (Pasic et al., 2008, Breitsprecher et al., 2008, Breitsprecher et al., 2011, Hansen and Mullins, 2010). Interestingly, one study reported that clustering of VASP on the surface of a bead is able to mediate the elongation of actin filaments even in the presence of high concentrations of CP that would normally inhibit VASP dependent elongation of actin filaments in solution (Breitsprecher et al., 2008). This study suggests that the

clustering of Ena/VASP proteins at cell leading edge is required for their association with the barbed end of actin filaments. However, in order to draw this conclusion, future experiments are required to establish the relationship between the density of Ena/VASP proteins and their anti-capping activity.

The ability of Ena/VASP proteins to interact directly with the barbed end of actin filaments was observed using pyrene and TIRF actin polymerisation assays (Pasic et al., 2008, Bear et al., 2002). A later study using TIRF showed that mutant VASP lacking GAB, FAB or both motifs was still able to capture the barbed end of actin filaments (Pasic et al., 2008). This suggests that although both GAB and FAB motifs are required for the anti-capping activity of Ena/VASP proteins (Barzik et al., 2005), they are dispensable for barbed end binding. Interestingly, a region at the extreme C-terminus of EVH2 domain was found to be required for barbed end capture (Pasic et al., 2008). This C-terminal region contains the coiled-coil region that is responsible for tetramerisation of Ena/VASP proteins (Zimmermann et al., 2002, Bachmann et al., 1999). This suggests that a structural interface that is formed during oligomerisation of Ena/VASP proteins is required for interacting with the barbed end of actin filaments (Bear and Gertler, 2009). However, a more recent study reported that Ena/VASP proteins lack an intrinsic barbed end capture motif and that G-actin binding is required for their interaction with the barbed end of actin filaments (Hansen and Mullins, 2010). Future experiments will be required to resolve these differences and delineate the mechanism by which Ena/VASP proteins bind the barbed end of actin filaments.

Although the studies above all agree that Ena/VASP proteins have an anti-capping activity, there are few issues that remain to be solved. Firstly, it is not clear whether Ena/VASP proteins are potent accelerators of actin filament elongation. One study reported that VASP has only minor effects on the rate of actin filament elongation (Pasic et al., 2008), whereas others concluded that it is actually capable of accelerating elongation (Breitsprecher et al., 2011, Breitsprecher et al., 2008). By replacing the GAB and FAB motifs within the EVH2 domain of mammalian VASP with those of DdVASP, a recent study showed that the rate of actin filament elongation driven by Ena/VASP proteins is dependent on saturation of G-actin on the GAB motif (Breitsprecher et al., 2011). This study suggests that Ena/VASP proteins are fully saturated with G-actin at high actin concentrations and therefore act as potent filament elongators *in vivo*. Moreover, different conclusions regarding the effects of profilin on

the activity of Ena/VASP proteins were drawn from previous studies. Some studies concluded that Ena/VASP proteins accelerate barbed-end actin filament elongation when profilin:actin complexes are present (Barzik et al., 2005, Hansen and Mullins, 2010, Pasic et al., 2008), whereas the other found no effect of profilin on VASP mediated actin assembly (Breitsprecher et al., 2008). These inconsistencies may in part be due to the different techniques used to produce the recombinant Ena/VASP proteins and whether the proteins are in solution or immobilised on beads as well as the ionic strength of the buffers used in the different assays (Hansen and Mullins, 2010, Bear and Gertler, 2009).

1.7.4.2 Additional hypotheses

In addition to their anti-capping activity, other possible roles for Ena/VASP proteins in regulating actin cytoskeleton have been proposed. These additional activities may collaborate with anti-capping to regulate actin dynamics synergistically.

For example, an anti-branching activity of Ena/VASP proteins has been observed in several studies using both light and electron microscopy (Bear and Gertler, 2009, Plastino et al., 2004, Samarin et al., 2003, Skoble et al., 2001). The strongest evidence for this comes from the observation that VASP decreases actin branch formation induced by ActA and the Arp2/3 complex *in vitro* (Skoble et al., 2001). Given CP is not present in these assays, it suggests that the anti-branching activity of Ena/VASP proteins is independent of their anti-capping activity. Moreover, a subsequent study established a link between the anti-branching activity and the anti-capping activity of Ena/VASP proteins in regulating the actin cytoskeleton (Akin and Mullins, 2008). This study showed that the level of G-actin available for polymerisation is elevated by increased filament capping, which leads to more Arp2/3 mediated actin branching. This suggests that Ena/VASP proteins decrease actin filament branching by blocking the function of CP. The effects of Ena/VASP proteins on Arp2/3 complex mediated actin branching need to be examined using more direct assays such as TIRF before a firm mechanistic understanding can be achieved.

Ena/VASP proteins are also involved in bundling (cross-linking) actin filaments in actin based membrane protrusions such as filopodia where large numbers of parallel actin filaments are present (Schirenbeck et al., 2006). Unlike other bundling proteins such as fascin, which are found along the whole length of filopodia, Ena/VASP proteins are

only observed at the distal tips of those actin bundles (Lanier et al., 1999). The EVH2 domain of Ena/VASP proteins is essential for their bundling activity suggesting that the interaction of F-actin and tetramerisation are both required for their bundling activity (Bachmann et al., 1999). A subsequent study suggested that the actin bundling is mediated by the electrostatic interaction between F-actin and Ena/VASP proteins as bundle formation is heavily dependent on the salt concentration that was used in the assay (Barzik et al., 2005).

No evidence has shown that any of the characterised functions of Ena/VASP proteins in regulating actin cytoskeleton is mutually exclusive. It is therefore likely that Ena/VASP proteins coordinate their anti-capping, anti-branching and cross-linking activities to act as multifunctional regulators of actin dynamics.

1.7.5 Regulation of Ena/VASP proteins

It has been shown that all 3 mammalian Ena/VASP proteins are substrates for cAMP- and cGMP- induced protein kinases (PKA and PKG) (Gertler et al., 1996, Lambrechts et al., 2000, Butt et al., 1994). *In vitro* biochemical assays demonstrated that phosphorylation inhibits the ability of Ena/VASP proteins to promote actin polymerisation (Lambrechts et al., 2000, Harbeck et al., 2000). Subsequently, it was shown that the anti-capping and bundling activities of Ena/VASP proteins appear to be inhibited when the proteins are phosphorylated (Barzik et al., 2005). This suggests that the ability of Ena/VASP proteins to regulate actin dynamics is likely to be controlled by phosphorylation, although exactly how phosphorylation modulates the properties of Ena/VASP proteins still remains unclear.

A number of *in vitro* studies have shown that phosphorylation has an effect on the affinities of Ena/VASP proteins for actin and other ligands. However, opposite effects of phosphorylation on the binding of Ena/VASP proteins to actin filaments have also been reported. One group found that phosphorylation of VASP increases its interaction with actin filaments (Laurent et al., 1999), whereas another study reported that phosphorylation of VASP decreases its association with actin filaments (Harbeck et al., 2000). A more recent study supported the latter conclusion, as the co-localisation of VASP and actin filaments in smooth muscle cells is inhibited when VASP is phosphorylated (Defawe et al., 2010). The interaction between VASP and G-actin is also negatively influenced by phosphorylation (Walders-Harbeck et al., 2002). Finally,

phosphorylation affects the interaction between the central proline rich region of the protein and SH3-containing proteins, although the binding of profilin to this region is unaffected (Lambrechts et al., 2000). There is, however, no evidence that phosphorylation of Ena/VASP proteins has any effect on binding FPPPP containing ligands or tetramerisation (Harbeck et al., 2000).

1.7.5.1 Serine/Threonine Phosphorylation

In vitro studies have identified three Serine/Threonine phosphorylation sites (Ser157, Ser239 and Thr278) in VASP (Gertler et al., 1996, Lambrechts et al., 2000, Waldmann et al., 1987). Mena possesses two phosphorylated residues equivalent to VASP Ser157 and Ser239, while Evl only has one phosphorylation site, which corresponds to VASP Ser157 (Gertler et al., 1996, Butt et al., 1994, Lambrechts et al., 2000). In addition to PKA and PKG that phosphorylate Ser157 and Ser239 of VASP, AMP-activated protein kinase (AMPK) was found to phosphorylate VASP on Thr278 (Blume et al., 2007) (Figure 1.14).

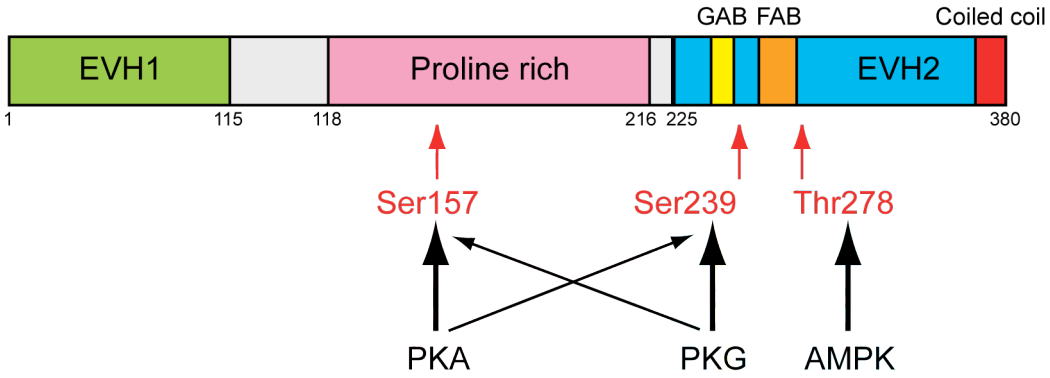

Figure 1.14 Serine/Threonine phosphorylation sites in VASP.
There are three serine/threonine phosphorylation sites in VASP. They are Ser157, Ser239 and Thr278. Red arrows indicate the locations of these phosphorylation sites in VASP. Ser157 and Ser239 can be phosphorylated by both PKA and PKG. However, Ser157 is the primary target for PKA, whereas Ser239 is preferentially phosphorylated by PKG. Thr278 is exclusively phosphorylated by AMPK. The thickness of the black arrows indicates the preferences for each kinase.

Phosphorylation of Ena/VASP proteins has been shown to alter actin based cell adhesion and migration. Howe et al 2002 showed that detachment of fibroblasts from fibronectin lead to rapid PKA dependent phosphorylation of VASP on Ser157 and reattachment of fibroblasts to fibronectin causes the phosphorylation of VASP (Howe et al., 2002). Following cell spreading, VASP becomes phosphorylated again (Howe et al., 2002). Another study demonstrated that a mutant Mena, which cannot be phosphorylated on Ser236 (equivalent of VASP Ser157) by PKA/PKG, is unable to rescue the normal motility of fibroblasts that lack endogenous Ena/VASP proteins (Loureiro et al., 2002). In contrast, a phosphomimetic Ser236 mutant functions as efficient as the wild type protein to fully rescue the motility of MVD7 cells (Loureiro et al., 2002). Taken together, these studies suggest that phosphorylation VASP and Mena at their first conserved Serine phosphorylation site adjacent to the proline rich region affects the ability of Ena/VASP proteins to regulate actin cytoskeleton (Figure 1.14).

Subsequent studies showed that phosphorylation of VASP on Ser239 and Thr278 also regulates the actin cytoskeleton (Benz et al., 2009). Using both *in vitro* and *in vivo* assays Benz et al., showed that phosphorylation of Ser157 leads to translocation of VASP to the cell periphery but there were no major effects on actin filament assembly, whereas phosphorylation of Ser239 and Thr278 induces a significant increase in actin filament assembly (Benz et al., 2009). Similar results were obtained when the sites equivalent to Ser157 in Mena and Evl were phosphorylated (Benz et al., 2009). This study suggests that phosphorylation of VASP on Ser239 and Thr278 enhances actin assembly. However, the results are not consistent with previous work, which demonstrated that phosphorylation of VASP on Thr278 by AMPK inhibits actin filament assembly (Blume et al., 2007). It is not clear why these studies have such different outcomes. It is also difficult to compare the results from the two studies because different cell types and assays were used.

A number of recent studies also suggest VASP phosphorylation on Ser239 is essential in modulating actin based cell motility. Overexpressed VASP containing a phosphomimetic Ser239 mutation leads to significant depletion of VASP at the leading edge of migrating epithelial cells (Lindsay et al., 2007). This leads to a loss of lamellipodial protrusions followed by retraction of the leading edge and cell rounding (Lindsay et al., 2007). A subsequent study demonstrated that co-localisation of VASP

and F-actin is disrupted by phosphorylation of VASP Ser239, suggesting that binding of VASP to F-actin is negatively regulated by phosphorylation of Ser239, which lies within the EVH2 domain (Defawe et al., 2010). The interaction between the EVH2 domain of VASP and F-actin is key for the localisations of Ena/VASP proteins at the lamellipodia tips (Loureiro et al., 2002). Phosphorylation of VASP Ser239 may therefore inhibit lamellipodia protrusions at the leading edge of migrating cells by interfering VASP binding to actin filaments. VASP Ser239 phosphorylation has also been shown to play a role in suppressing cancer cell invasion and metastasis by inhibiting the proteolytic function of invadopodia (Zuzga et al., 2011).

1.7.5.2 Tyrosine phosphorylation

Ena was first identified as a suppressor of *Drosophila* Abl (dAbl) and was subsequently shown to be the substrate of this kinase (Gertler et al., 1995). Six tyrosine phosphorylation sites have been identified in Ena*,* although mutation of all six sites only has a minor effect on the ability of Ena to rescue the phenotype of the *ena* mutant fly (Comer et al., 1998). Abl has however, been shown to regulate the cellular localisation of Ena. One study observed the amount of Ena at the apical cortex of blastoderm cells in the embryo of the *abl* mutant is much higher than the wild type situation (Grevengoed et al., 2003). Moreover, another study found that Abl RNAi-treated D16-C3 cells display higher amount of Ena at the tip of filopodia than control cells (Gates et al., 2009). These studies suggests there is a regulatory role for Abl in controlling the intracellular localisation of Ena, although it is not clear whether this is mediated by phosphorylation of Ena itself. Given phosphorylation Ena by Abl has been shown to disrupt the interaction between Ena and its SH3-containing ligands (Comer et al., 1998), it is likely that phosphorylation events interfere with the ability of its binding partners to tether it to sites of action (Bradley and Koleske, 2009).

The tyrosine phosphorylation sites in *Drosophila* Ena are not conserved in the mammalian Ena/VASP proteins (Krause et al., 2003). Among all three mammalian Ena/VASP isoforms, Mena is the only one that has been found to be a substrate of Abl (Krause et al., 2003). Initially, only a specific neuronal isoform of Mena was shown to be phosphorylated by Abl (Gertler et al., 1996). Subsequently, it was found that Tyr296 of two more ubiquitously expressed isoforms of Mena could also be phosphorylated by Abl (Tani et al., 2003). Tyr296 of Mena is not conserved in VASP

and Evl, suggesting that at least in mammalian cells, only Mena is a specific substrate of Abl.

Our molecular understanding of the definitely regulation of Ena/VASP family proteins by phosphorylation is still relatively poor. Future work is required to address how the functions of Ena/VASP proteins in regulating the actin cytoskeleton are regulated by this important posttranslational modification.

1.7.6 The non-classical EVH1 interactors

It was believed that the EVH1 domain of Ena/VASP proteins could only interact with FPPPP-containing proteins until the identification of the non-classical EVH1 binding partner, Tes (Boeda et al., 2007). Tes, which is ubiquitously expressed, consists of an N-terminal PET domain of unknown function and three tandemly arranged LIM domains in its C-terminal half (Garvalov et al., 2003, Coutts et al., 2003) (Figure 1.15A). LIM domain is a protein-protein interaction domain. It consists of two contiguous zinc finger domains, which are separated by a hydrophobic linker in the middle (Kadrmas and Beckerle, 2004). The C-terminal half of Tes can interact with a variety of cytoskeletal proteins such as Zyxin and Arp7A (Coutts et al., 2003, Boeda et al., 2011). The interaction between the LIM1 domain of Tes and Zyxin is required for recruiting Tes to focal adhesions (Garvalov et al., 2003). Tes is found to be down regulated in cancer cell lines and primary tumours (Tatarelli et al., 2000, Tobias et al., 2001, Drusco et al., 2005, Mueller et al., 2007, Sarti et al., 2005). Moreover, overexpression of Tes inhibits cancer cell growth in nude mice (Sarti et al., 2005). Based on these studies, it is proposed that Tes is a tumour suppressor.

Tes was shown to specifically bind the EVH1 domain of Mena but not VASP and Evl (Boeda et al., 2007). In contrast to previous EVH1 binding partners, the interaction between Tes and Mena is not mediated by an FPPPP motif. Instead, the LIM3 domain of Tes is responsible for the direct interaction with the EVH1 domain of Mena (Figure 1.15B). Tes thus represents the first non-FPPPP containing protein, which can specifically interact with a single Ena/VASP family member. The same study also demonstrated that the LIM3 domain of Tes regulates the ability of the EVH1 domain of Mena to bind to FPPPP containing ligands such as Zyxin. Moreover, this study showed that Tes negatively regulates cell migration in a Mena dependent manner.

Based on these observations, it suggests previously unidentified non-FPPPP containing EVH1 binding proteins can potentially regulate Ena/VASP proteins.

In addition, a subsequent study demonstrated that nuclear factor of activated T-cells, cytoplasmic, calcineurin-dependent 2 (NFATc2), which lacks a polyproline region, is also capable of interacting directly with the EVH1 domain of homeopathic Ena/VASP homologue (Homer), although the structure showed that NFATc2 binds to a site that is located opposite the FPPPP binding pocket on the EVH1 domain (Huang et al., 2008).

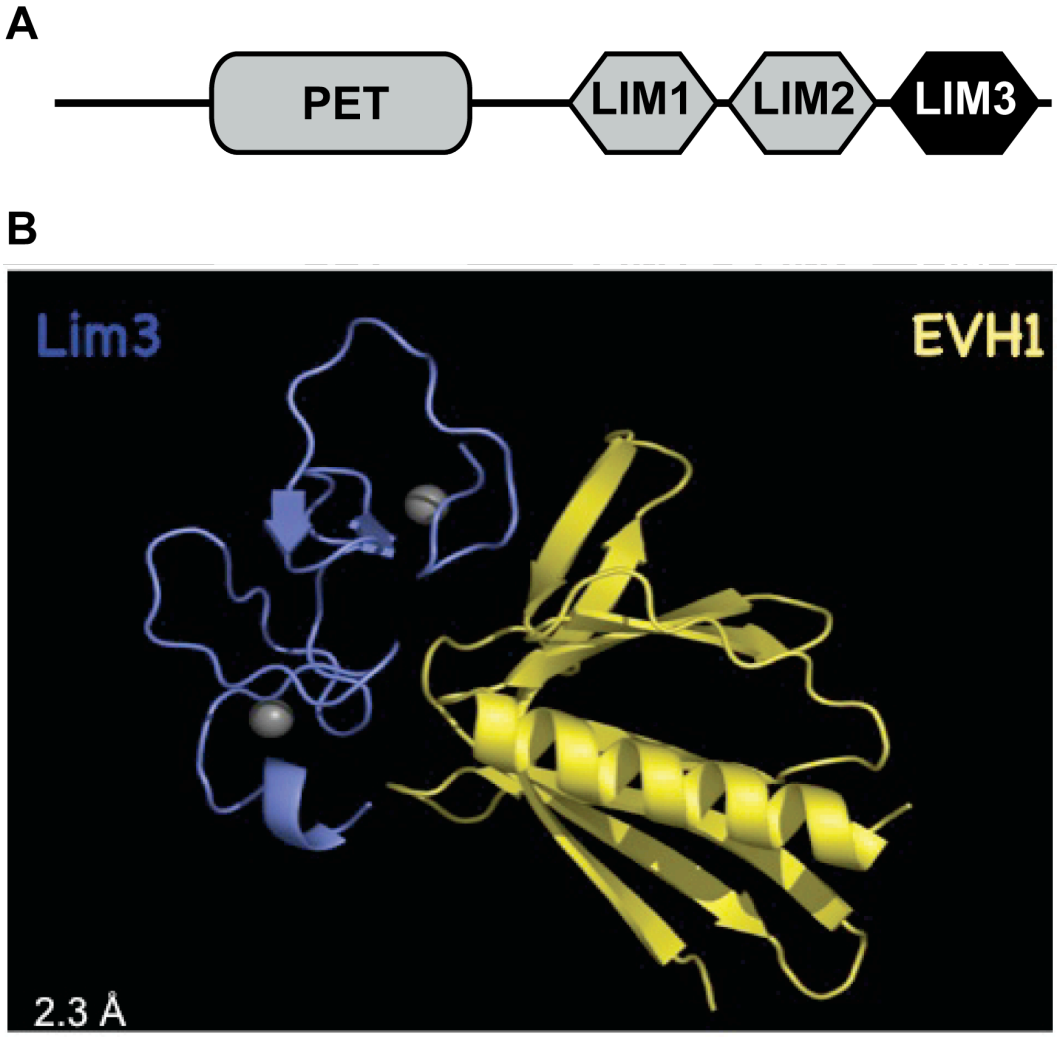

Figure 1.15 The non-classical EVH1 binding partner:Tes.
A. A cartoon of the domain organisation of Tes. Tes consists of a N-terminal PET domain and 3 C-terminal LIM domains. The LIM3 domain of Tes (black) is responsible for interacting with the EVH1 domain of Mena. **B**. The structure of the LIM3:EVH1 complex. The LIM3 domain is shown in blue and the EVH1 domain of Mena is shown in yellow. The grey spheres indicate the coordinated zinc atoms.

1.8 Aim of my thesis

Given that Tes, which lacks a FPPPP motif, can interact directly with the EVH1 domain of Mena, it is highly likely that other unique non-FPPPP containing binding partners and potential regulators of Ena/VASP proteins will exist. My thesis project was to identify new EVH1 binding partners that lack FPPPP motifs and elucidate their possible roles during cell migration. Using biochemical approaches, I found that Ena/VASP proteins are capable of interacting with the WAVE complex via their EVH1 domain. My subsequent studies verified the direct interaction between Ena/VASP proteins and the WAVE complex and examined the physiological importance of this interaction in actin-mediated cell motility.

Chapter 2. Materials and Methods

2.1 General buffers and culture media

General buffers and culture media were provided by the in-house central service at Cancer Research UK and their recipes are listed below. Buffers and solutions for specific applications are described at the end of the relevant sections.

2.1.1 General Buffers

Phosphate Buffered Saline A (PBSA)

8.00 g NaCl
0.25 g KCl
1.43 g Na_2HPO_4
0.25 g KH_2PO_4,

The reagents were dissolved in distilled water; the pH was adjusted to 7.2 before the solution was adjusted to a total volume of 1 L. The solution was autoclaved.

Tris/EDTA (TE) Buffer, pH 8.0

1.21 g Trizma Base
0.37 g Ethyldiaminotetraacetic acid disodium salt (EDTA),

The reagents were dissolved in distilled water; the pH was adjusted to 8.0 with hydrochloric acid (HCl) before the solution was adjusted to a total volume of 1 L.

2.1.2 Cell Culture Media

Trypsin Solution: 0.25% in Tris Saline

Tris Saline (TS)

8.00 g NaCl
2.00 ml 19% (w/v) KCl solution
0.10 g $Na_2H_2PO_4$
1.00 g D-Glucose
3.00 g Trizma Base
1.50 ml 1% (w/v) Phenol red solution
0.06 g Penicillin
0.10 g Streptomycin

The Tris Saline reagents were dissolved in distilled water, the pH was adjusted to 7.7 with HCl and the solution was made to a final volume of 200 ml. Penicillin (0.06 g) and

0.1 g streptomycin were then added to the Tris Saline solution. The trypsin solution was prepared by dissolving 2.5 g trypsin (Difco 1:250) in 200 ml of distilled water (pH 7.7). The Tris Saline and the trypsin solution were mixed and made up to a final volume of 1 L with distilled water. The pH was adjusted to 7.7. The solution was then sterilised by filtration through a 0.22 µm filters and stored at -20 ºC until needed.

Versene Solution

8.00 g	NaCl
0.20 g	KCl
1.15 g	Na_2HPO_4
0.20 g	KH_2PO_4, pH 7.2
0.20 g	EDTA
1.50 ml	1% (w/v) Phenol red solution

The reagents were dissolved in distilled water, the pH was adjusted to 7.2 with HCl and the solution was made up to 1 L. The solution was autoclaved and stored at room temperature until use.

Glutamine Solution

A 10x stock solution (0.24 M) was prepared by dissolving 35.05 g of L-Glutamine in 1 L of distilled water. The solution was sterilised by filtration through a 0.22 µm filter and stored at -20 ºC until required.

Minimal Essential Medium (MEM)

9.68 g	MEM powder
3.70 g	$NaHCO_3$,

The reagents were dissolved in 10 litres of distilled water and the pH was adjusted to 7.0 with CO_2. The solution was sterilised by filtration through a 0.22 µm filter and stored at room temperature until use.

2.1.3 Bacteriological Media

Luria-Bertani (LB) Medium

10 g	Bacto-tryptone
5 g	Bacto-yeast extract
10 g	NaCl

The reagents were dissolved in distilled water, the pH was adjusted to 7.2 with NaOH (1 M) and the solution was made up to a total volume of 1 L with water. The resulting solution was autoclaved and stored at room temperature.

LB Agar

15 g of Bacto-agar were dissolved in 1 L of LB medium and the resulting solution was autoclaved.

2.2 Tissue culture

2.2.1 Culture and Freezing stocks

All cell lines used in this thesis and their respective culture media are listed in Table 2.1.

Table 2.1 Cell lines and media

Cell lines	Species	Medium	Glutamine	Serum	Antibiotics	Source
HeLa	Human	MEM	2mM	10% FCS[5]	Pen/Strep[7]	Way lab stock
HEK 293T	Human	DMEM high glucose[1]	2mM	10% FCS[5]	Pen/Strep[7]	Way lab stock
MVD7	Mouse	DMEM high glucose[1]	2mM	10% FCS[5]	Pen/Strep[7]	Frank Gertler MIT
B16-F1	Mouse	DMEM high glucose[1]	2mM	10% FCS[5]	Pen/Strep[7]	Vic Small IMBA
Rat-2	Rat	DMEM high glucose[1]	2mM	5% FCS[5]	Pen/Strep[7]	Matthias Krause KCL
$S2R^+$	Fly	M3[3]	2mM +2mM[4]	10% FCS[6]	Pen/Strep[7]	Nic Tapon LRI
S2	Fly	Sch[2]	2mM +2mM[4]	10% FCS[6]	Pen/Strep[7]	Nic Tapon LRI

Notes

[1]Dulbecco's modified eagle medium 4500 mg/dm^3 glucose from Sigma (D-6546)

[2]Schneider's *Drosophila* Medium from Invitrogen (21720-024)

[3]Shields and Sang M3 Insect Medium from Sigma (S3652)

[4]GlutaMAX™-1 from Sigma (35050-079)

[5]Fetal calf serum, from PAA Laboratories (A15-041)

[6]Fetal calf serum, from Sigma (F9665)

[7]100 units/ml penicillin G sodium, 100 µg/ml streptomycin sulphate, from 100x stock, Invitrogen (15140-122)

2.2.1.1 Mammalian cell culture

Cells were grown in 10 cm plastic tissue culture dishes at 37 ºC in 5% CO_2 and depending on cell type passaged every 2-3 days when they reached a confluence of around 70%. Cells to be passaged were washed once with PBSA and 0.5 ml 0.05% trypsine/versene solution was subsequently added. The plate was kept at 37 ºC until all the cells had detached. Then 10 ml complete medium was added and the cells were plated in a new dish at the required confluence. Cells were then cultured in the appropriate complete medium.

To generate frozen stocks, cells from one 10 cm tissue culture dish were trypsinised at a confluence of 70%, re-suspended in complete medium and collected by centrifugation at 1000 rpm for 5 min at room temperature. Cells were then re-suspended in 0.5 ml FCS containing 10% DMSO, aliquoted into cryo-vials and transferred to -80 ºC freezer. The cryo-vials containing cells were transferred into liquid nitrogen 7 days later.

To recover cells, a cryo-vial of cells stored in liquid nitrogen was resuspended in 10 ml complete medium and plated on to a 10 cm dish. After cells had settled down and spread on the bottom of the dish, the DMSO containing medium was substituted with 10 ml fresh complete medium.

2.2.1.2 Drosophila haemocyte culture

S2 and $S2R^+$ cells were grown in 160 ml tissue culture flasks at 25 ºC and passaged every 7 days at a confluence of 100%. For passaging $S2R^+$ cells, they were washed twice with PBSA and 1 ml of 0.05% trypsine/versene solution was subsequently added. The flask was put at 37 ºC for 1 min before being moved to room temperature until all the cells detached. The detached cells were washed once with 10 ml complete medium and collected by centrifugation at 1000 rpm for 5 min at room temperature. Cells were then resuspended in 10 ml complete medium and plated in to a new flask at the required confluence. S2 cells were passaged by centrifugation at 1000 rpm for 5 min at room temperature, washed once with PBSA before they were resuspended in 10 ml complete medium and subsequently transferred to a new flask at the required confluence.

To generate frozen stocks, $S2R^+$ cells and S2 cells were collected from their flasks by trypsinising and resuspending respectively. Following centrifugation, cells were resuspended in 0.5 ml complete medium containing 10% FCS and 10% DMSO, aliquoted into cryo-vials and transferred to the -80 ºC freezer. The vials were transferred into liquid nitrogen 7 days later.

To recover cells, a cryo-vial containing either $S2R^+$ or S2 cells stored in liquid nitrogen was resuspended in 10 ml complete medium and transferred into a 160 ml flask. After cells settled down and spread on the bottom of the flask, the DMSO containing medium was substituted with 10 ml fresh complete medium.

2.2.2 Transfection

In this thesis, two different transfection protocols were used for overexpressing proteins in mammalian or insect cells depending on the assay, the cell type used and the transfection efficiency required.

2.2.2.1 Calcium Phosphate

Tissue culture cells were transfected with a CMV-based (CB6) or an actin promoter based (pAC) vector using a calcium phosphate method (De Rivoyre et al., 2006, Rietdorf et al., 2001). This method was used when large-scale transfections were required with a relatively low cost compared to lipid based transfection methods. Before transfection, cells were seeded and allowed to adhere for 3 hours. To transfect a 10 cm dish, 5 µg DNA was incubated in 0.5 ml $CaCl_2$ solution (0.25 M) for 20 min at room temperature. Following drop-wise addition of 0.5 ml HBS (280 mM NaCl, 10 mM KCl, 1.5 mM Na_2HPO_4, 12 mM glucose, 50 mM HEPES (Gibco), pH 7.05), the mix was incubated for another 20 min at room temperature and added to the prepared cells. After incubating the cells for 20 hr at 37 ºC with the transfection mix, the medium was replaced with fresh complete medium. Cells were analysed immediately or incubated for another 24 h depending on the experiment.

2.2.2.2 Effectene

Effectene-based transfection (Qiagen) was used to transfect cells when calcium phosphate transfection could not be used for certain cell types or when a higher transfection efficiency was required. Cells were plated at 70% confluence in complete medium one day before transfection. To transfect a 10 cm dish, 2 µg of DNA was

diluted in EC buffer to a final volume of 300 µl. Enhancer (16 µl) was added and the solution was incubated for 5 min at room temperature. Afterwards, 50 µl of Effectene was added and the mix was incubated for another 15 min at room temperature. The resulting transfection solution was mixed with 3 ml complete medium and added to the cells, which were analysed after 24-48 hr depending on the cell type used and the experiment.

2.2.3 RNA interference

2.2.3.1 Abi siRNA

siRNAs that specifically target the three different rat Abi isoforms were purchased from Dharmacon and Invitrogen (Table 2.2). The non-targeting oligos containing random DNA sequences (Invitrogen) were used as control. The siRNAs were resuspended in siRNA buffer (Dharmacon) at a concentration of 20 µM and were stored in aliquots at -20 ºC. For siRNA transfection, $2x10^5$ Rat-2 cells were seeded in 12 well plates in antibiotic-free complete medium one day before the transfection. On the day of transfection, 5 µM siRNA solution in RNAase free buffer was prepared. 5 µl of the 5 µM siRNA solution was added to 95 µl serum free medium. In parallel, 100 µl transfection reagent was prepared by diluting 0.5 µl DharmaFECT 1 transfection reagent in 99.5 µl serum free medium. The siRNAs were added to the transfection reagent and incubated for 20 min at room temperature. Antibiotic-free complete medium (0.8 ml) was added to the mixture to obtain a final volume of 1 ml of transfection medium. Culture medium in each well was replaced by the prepared transfection medium. Cells were incubated with the transfection medium at their normal growing condition for 24-48 hr before qRT-PCR analysis.

Table 2.2 siRNA oligonucleotides duplexes used to knockdown rat Abi isoforms.

Rat Abi isoform	Target Sequence	Size (bp)	Source
Abi1	5'-GCUGUAAGGACGCGCUAAU-3' 3'-CGACAUUCCUGCGCGAUUA-5'	19	Dharmacon
Abi1	5'-GUGAAAUGUGGUAGGUACU-3' 3'-CACUUUACACCAUCCAUGA-5'	19	Dharmacon
Abi1	5'-UGACAUUGGACAUGGCGUA-3' 3'-ACUGUAACCTGUACCGCAU-5'	19	Dharmacon
Abi1	5'-GCACAUCUGUCUAGCGAGU-3' 3'-CGUGUAGACAGAUCGCUCA-5'	19	Dharmacon
Abi2	5'-GAACAAAUCCUCCCACGCA-3' 3'-CUUGUUUAGGAGGGTGCGU-5'	19	Dharmacon
Abi2	5'-AUGGAGUUAAGCACGGAAA-3' 3'-UACCUCAAUUCGUGCCUUU-5'	19	Dharmacon
Abi2	5'-UCUGGUGGAUAUAGACGAA-3' 3'-AGACCACCUAUAUCTGCUU-5'	19	Dharmacon
Abi2	5'-CCUCUGUGACUGCGCAAUU-3' 3'-GGAGACACUGACGCGUUAA-5'	19	Dharmacon
Abi3	5'-ACACGCUUCGAAUGCUGGAUCUACA-3' 3'-UGUGCGAAGCUUACGACCUAGAUGU-5'	25	Invitrogen
Abi3	5'-GCCAGAUGGUGAACAUGCACCUGGA-3' 3'-CGGUCUACCACUUGUACGTGGACCU-5'	25	Invitrogen
Abi3	5'-CAAGAGCAUAAAGGCGCCCGCUACA-3' 3'-GUUCUCGTAUUUCCGCGGGCGAUGU-5'	25	Invitrogen

2.2.3.2 Drosophila Abi (dAbi) dsRNA

2.2.3.2.1 Generation of dsRNA

Individual DNA fragments for the 3' untranslated region (3'UTR) of dAbi, the open reading frame (ORF) of dAbi were amplified from a *Drosophila* cDNA library using PCR (Chapter 2.3). The DNA fragment of LacZ (control) was amplified using PCR from a LacZ clone that was kindly provided by the Tapon lab at Cancer Research UK. The PCR primers also contain a 5' T7 RNA polymerase binding site (TAATACGACTCACTATAGGG) in front of the gene specific sequence that were

designed using E-RNAi (http://www.dkfz.de/signaling/e-rnai3/) (Table 2.3). The purified PCR products were used as templates for single stranded RNA (ssRNA) synthesis as described in the manufacturers instructions for the Ambion MEGAscript High yield Transcription T7 kit. The synthesised ssRNAs were incubated with TURBO DNase for 15 min at 37 °C and their complementary strands were annealed by heating to 70º C for 10 min followed by cooling down to 25 ºC at 0.1 ºC per second. Double stranded RNA (dsRNA) products were purified as described in the manufacturers instruction for the Ambion MEGAclear™ kit. Annealing was performed once more after purification. The purity of the obtained dsRNA was confirmed using gel electrophoresis. All purified dsRNA products were stored in aliquots at -80 ºC until required.

Table 2.3 Primers designed to generate dsRNA.

Targeted Gene	**Oligonucleotide Sequence (T7 RNA polymerase binding site sequence is indicated in red)**	**Size of PCR Amplicon (bp)**
dAbi ORF	For TAATACGACTCACTATAGGGCGCAAGCCCATCGACTACTC	230
	Rev TAATACGACTCACTATAGGGAGTGTCCCGGTATTGCTGAC	
dAbi 3'UTR	For TAATACGACTCACTATAGGGGGTCTGTTCCAGTCCTCTGC	216
	Rev TAATACGACTCACTATAGGGTTAGACTAAATGCGGTTGG	
LacZ	For TAATACGACTCACTATAGGGGCCTTCCTGTTTTTGCTCAC	520
	Rev TAATACGACTCACTATAGGGTTGCCGGAAGCTAGAGTAA	

2.2.3.2.2 Knockdown of dAbi

$S2R^+$ and S2 cells were seeded in 24 well plates at a density of $1x10^5$ cells per well in 0.5 ml complete medium at least 3 hr before performing RNAi knockdown. After cells adhered to the bottom of the dish, 4 µg dsRNA was added into each well. The plate was swirled gently and the cells were allowed to grow at 25 ºC for 3 days. dAbi expression in the cells was assayed by qRT-PCR as well as western blot analysis.

For parallel knockdown of endogenous dAbi and overexpression of dAbi, $S2R^+$ and S2 cells were treated with dsRNA one day before transfection with effectene based approaches. Cells were incubated 25 ºC in complete medium containing dsRNA and the transfection mix for another two days before being analysed by western blot, immunofluorescence and live cell imaging.

2.2.3.3 qRT-PCR

Knockdown efficiencies of purchased siRNAs and self-made dsRNA were determined by qRT-PCR. mRNAs from siRNA treated Rat-2 or dsRNA treated insect cells were extracted and purified using the Qiagen RNeasy Mini kit. The mRNA concentration in each sample was adjusted to 50 ng/µl using RNase-free water as required. For first strand cDNA synthesis, 500 ng mRNA, 200 ng random primers (Invitrogen) and 10 mM dNTP were mixed and incubated at 70 ºC for 10 min. Subsequently, First-Strand Buffer, 0.1 M DTT and 200 units SuperScipt II Reverse Transcriptase (Invitrogen) were added to the reaction mix, which was then incubated at 42 ºC for 45 min. The reaction was terminated by heating to 70 ºC for 15 min. The qRT-PCR primers as listed in Table 2.4 were designed using the Roche Universal ProbeLibrary Assay Design Center (https://www.roche-applied-science.com/sis/rtpcr/upl/index.jsp?id=uplct_030000). All qRT-PCR primers that can only amplify a single target gene were verified and confirmed using melting curve analysis following qRT-PCR. For each qRT-PCR reaction, 2 µl cDNA (approximately 100-500 ng), 200 ng primer mix and 5 µl EXPRESS SYBR Green ER™ qRT-PCR SuperMix Universal (Invitrogen) were mixed and adjusted to 10 µl with distilled water. qRT-PCR reactions were set up in MicroAmp Fast Optical 96-Well Reaction Plates (Applied Biosystems) and performed/analyzed using the 7500 Fast Real-Time PCR System (Applied Biosystems). The standard cycling program was set up as follows.

Holding stage:	50 °C	2 min	
	95 °C	10 min	
	---	---	
Cycling stage:	96 °C	15 sec ⎫	
	60 °C	1 min ⎭	40 cycles
	---	---	
Melting curve stage:	95 °C	15 sec	
	60 °C	1 min *	
	95 °C	30 sec *	
	60 °C	15 sec	

* Running speed was slowed down between the steps.

For statistical analysis, all data generated from qRT-PCR experiments was normalised to an endogenous β-Actin control. The relative standard curve method was used to

quantify mRNA expression of each Abi isoform in Rat-2 cells. The comparative C_T method was used to quantify mRNA expression of the RNAi targeted proteins in siRNA treated Rat-2 and dsRNA treated S2 and $S2R^+$ cells.

Table 2.4 Primers designed to perform qRT-PCR.

Targeted Gene	Oligonucleotide Sequence	Size (bp)
Rat Abi1	For AATTTCTATTGCCCCCCCTC	20
	Rev GTGGAGTTGGGCTATCAGCA	20
Rat Abi2	For CACCATGGGCACCAAGGTCT	20
	Rev AGCCCAGTCACTCCATTCAT	20
Rat Abi3	For CGCCCTGCTACGGGTGGCCA	20
	Rev GGCTTCCACCTGCCGCAGGG	20
Rat β-Actin	For GACATCCGTAAAGACCTCTATGCC	24
	Rev ATAGAGCCACCAATCCACACAGAG	24
dAbi	For GGGACGCAATATCAACAGGA	20
	Rev TGGTCGTCCGAAGTCTTGAT	20
Drosophila β-Actin	For TGCCTCATCGCCGACATAA	19
	Rev CACGTCACCAGGGCGTAAT	19

2.2.4 Stable Rat-2 cell lines

2.2.4.1 Lentivirus system

Stable Rat-2 cell lines were generated using the lentiviral expression vectors, a modified pL/L3.7 (Robinson et al., 2001), the HIV-1 based pLVX-Puro and pLVX-IRES-Hyg from Clontech. All lentiviral expression vectors containing the gene of interest that were used in this thesis are listed in Table 2.5. For generating lentiviruses encoding the protein of interest, $2x10^6$ HEK 293T cells were seeded into each of the 6 cm dishes. On the following day, the medium in each dish was replaced with fresh medium 3 hr before transfection. Using the calcium phosphate method, cells were transfected with pL/L3.7 vectors containing the gene of interest together with 5 µg of the viral packaging vector, RRE (gag-pol plasmid), RER (RNA export protein) and VSVG (Virus envelope). Transfected cells were incubated overnight at their normal growing condition. On the third day, the transfection media were replaced with fresh media containing 10 mM sodium butyrate (Sigma). After 8 hr, the media containing sodium butyrate was

replaced with 3 ml fresh medium. On the fourth day, the medium containing the packaged lentivirus was passed through a 0.45 μm filter.

For lentivirus infection, Rat-2 cells were seeded into 6 well plates at least 12 hr before infection at 50% confluence. The filtered, 3ml of virus-containing medium from each the of the 6 cm dishes was added to each well. Rat-2 cells were incubated with virus-containing media for 2 days at their normal growing condition. On day 6, Rat-2 cells were washed with PBSA and fresh medium was added. Cells were then either expanded for FACS sorting or treated with drugs for antibiotic selection.

Table 2.5 Lentiviral expression vectors used to generate stable Rat-2 cell lines.

Vector	Used 1st in figure	Created by
pL/L3.7 RFP-APPPP-mito	5.3	X. Chen
pL/L3.7 RFP-FPPPP-mito	5.3	X. Chen
pL/L3.7 GFP	5.5	B. Boëda
pL/L3.7 GFP-Abi	5.5	X. Chen
pL/L3.7 GFP-Abi mut	5.5	X. Chen
pLVX-Puro GFP-VASP	5.12	X. Chen
pLVX-IRES-Hyg Abi-RFP	5.12	X. Chen
pLVX-IRES-Hyg Abi mut-RFP	5.12	X. Chen

2.2.4.2 Fluorescence activated cell sorting (FACS)

GFP, RFP or both GFP and RFP-positive Rat-2 cell lines that were generated using the lentiviral approaches, were obtained by performing flow cytometry in the FACS facility at Cancer Research UK. The lentivirus-infected cells were trypsinised and harvested by centrifugation at 1000 rpm for 5 min at 4 °C. The cell pellet was resuspended in the PBSA containing 1% FCS and passed through a cell strainer to remove cell aggregates and debris. For each cell line created, non-lentivirus-infected Rat-2 cells were used as negative controls to set up the gating on the FACS machine. For each cell line, cells at 90% confluence from a 15 cm dish were sorted. Due to the problems of over-expressing Abi in cells, FACS sorting of GFP/RFP-tagged Abi expressing cells was repeated twice. Cells were expanded between each sorting. The sorted fluorescence positive cells were expanded and stored in aliquots at -80 °C before they were transferred to liquid nitrogen for future use.

2.2.4.3 Antibiotic selection

GFP- and RFP-positive Rat-2 cells, which were generated using the lentiviral expression vectors pLVX-Puro and pLVX-IRES-Hygro were selected and expanded under antibiotic selection. A minimum amount of each drug was used in order to keep infected cells growing healthy when growing under constant selection pressure. This was determined by performing a drug kill curve by examining the level of Rat-2 survival in different concentrations of Puromycin (Sigma), Hygromycin B (Sigma) or both drugs. After infection, Rat-2 cells were incubated with the complete medium containing 5 µg/ml Puromycin and 400 µg/ml Hygromycin B for 1-2 weeks in their normal growing condition. The antibiotic containing medium was changed every 3 days. Cells were not split during the drug selection. Hygromycin B and Puromycin double resistant cells were then expanded. GFP and RFP-positive antibiotic resistant cells were FACS sorted once and expanded again before they were used immediately in the FRAP analyses.

2.3 Molecular biology

2.3.1 General buffers and solutions for molecular biology

TBE

89 mM Tris-HCL pH 7.5
89 mM Borate
2 mM EDTA

Ethidium Bromide

The stock solution was made to 10 mg/ml and was used at 0.5 µg/ml.

10x DNA Loading Buffer

0.25% (w/v) Bromophenol Blue
30% (v/v) Glycerol

10x dNTPs (Amersham Pharmacia Biotech)

2 mM dATP
2 mM dCTP
2 mM dGTP
2 mM dTTP

2.3.2 Expression vectors

In addition to the lentiviral expression vectors that were used to generate Rat-2 stable cell lines, six different vectors were used for protein expression. For expression in mammalian cells, the CB6 vector (CMV promoter) (Reckmann et al., 1997) was used, for bacteria expression, the pMW172 vector (T7 promoter) (Way et al., 1990) was used, for expression in *Drosophila* haemocytes, the pAC vector (Ac5 promoter) (modified pAc5.1/V5-His (Invitrogen) from Tapon lab at Cancer Research UK, unpublished), the pAW vector (Ac5 promoter) (modified pAW from Tapon lab at Cancer Research UK, unpublished) and the pUAST vector (GAL4-inducible UAS promoter) (Brand and Perrimon, 1994) were used and for expression in baculoviruses, the pBacPAK vector (Clonetech) from protein expression facility at Cancer Research UK, unpublished) were used. All six vectors contained a tag at the N- or C-termini of the proteins of interest. The tags that were used were green fluorescent protein (GFP) (Chalfie et al., 1994), red fluorescent protein (RFP/mCherry) (Campbell et al., 2002, Shaner et al., 2004), 6-Histidine (HIS) or glutathione-S-transferase (GST) (Smith and Johnson, 1988). All DNA constructs used to express proteins are listed in Table 2.6.

Table 2.6 Expression vectors used in this thesis.

Vector	**Used first in figure**	**Created by**
pMW GST-EVH1-VASP	3.1	B. Boëda
pMW GST-EVH1-Evl	3.1	B. Boëda
pMW GST-EVH1-Mena	3.1	B. Boëda
pMW GST	3.2	Way Laboratory
CB6 GFP	3.3	Way Laboratory
CB6 GFP-Nap1	3.3	X. Chen
CB6 GFP-PIR121	3.3	X. Chen
CB6 GFP-LIM3 Tes	3.3	B. Boëda
pMW GST-Nap1	3.4	X. Chen
pMW GST-PIR121	3.4	X. Chen
pMW HIS-EVH1-Mena	3.4	B. Boëda
pMW HIS-Grb2	3.4	I. Weisswange

pMW HIS-LIM3 Tes	3.4	B. Boëda
pBacPAK HIS-PIR121	3.4	X. Chen
pBacPAK GST-Nap1	3.4	X. Chen
pMW GST-FPPPP-Zyxin	3.5	B. Boëda
pMW GST-LIM3-Tes	3.5	B. Boëda
pMW HIS-Nap1	3.5	X. Chen
pMW HIS-Abi	3.5	X. Chen
pMW GST-Abi	4.1	X. Chen
pMW GST-Abi N-term-PR1	4.1	X. Chen
pMW GST-Abi PR2-SH3	4.1	X. Chen
pMW GST-Abi ΔSH3	4.1	X. Chen
pMW GST-Abi PR2	4.1	X. Chen
pMW GST-Abi PR1-PR2-SH3	4.1	X. Chen
pMW GST-Abi PR1-PR2	4.1	X. Chen
pMW GST-Abi P366G/P367G/P368G (mutant 1)	4.8	X. Chen
pMW GST-Abi F375A (mutant 2)	4.8	X. Chen
pMW GST-Abi P383G/P384G/P385G (mutant 3)	4.8	X. Chen
pMW GST-Abi P366G/P367G/P368G/F375A (mutant 1+2)	4.8	X. Chen
pMW GST-Abi P366G/P367G/P368G/P383G/P384G/P385G (mutant 1+3)	4.8	X. Chen
pMW GST-Abi F375A/P383G/P384G/P385G (mutant 2+3)	4.8	X. Chen
pMW GST-Abi P366G/P367G/P368G/F375A/P383G/P384G/P385G (mutant 1+2+3, mut)	4.8	X. Chen
CB6 GFP-Abi	4.9	X. Chen
CB6 GFP-Abi P366G/P367G/P368G/F375A/P383G/P384G/P385G (mut)	4.9	X. Chen
pMW GST-EVH1 Ena	6.2	X. Chen
CB6 GFP-dAbi	6.4	X. Chen

CB6 GFP-dAbi L311A/P312G/P313G/P314G/P315G (mutant 1)	6.4	X. Chen
CB6 GFP-dAbi L374A/P375G/P376G/P377G/P378G (mutant 2)	6.4	X. Chen
CB6 GFP-dAbi L311A/P312G/P313G/P314G/P315G/ L374A/P375G/P376G/P377G/P378G (mutant 1+2, mut)	6.4	X. Chen
pAC GFP	6.5	Tapon Lab
pAC dAbi-GFP	6.5	X. Chen
pAC dAbi-GFP L311A/P312G/P313G/P314G/P315G/ L374A/P375G/P376G/P377G/P378G (mut)	6.5	X. Chen
pAW Ena-mCherry	6.14	X. Chen
pMW HIS-VASP	7.3	X. Chen

2.3.3 Amplification of DNA using PCR

Polymerase chain reactions (PCR) were performed to amplify or modify genes from pre-existing DNA constructs or cDNA libraries. For each PCR reaction, a forward (for) and a reverse (rev) primer were designed to amplify the DNA sequence of interest together with a suitable restriction site for sub-cloning. A stop codon was included in each rev primer for sub-cloning if required. A 100 µl PCR reaction contained 100 ng of DNA template, 10 pmol of each primer, 1x Taqplus Precision DNA polymerase buffer, 5 units Taqplus Precision DNA polymerase (Stratagene) and 25 nmol dNTP mix (Invitrogen). The reactions were performed on an Applied Biosystems GeneAmp PCR machine using the conditions described below.

96°C 4 min

Denaturation : 96 °C 30 sec ⎫

Annealing : 55 °C 30 sec ⎬ 25 cycles

Extension : 72 °C 1 min * ⎭

---

72 °C 7 min

---

4 °C ∞

- *Extension time: 1 min/kb of amplified product length.

2.3.4 Sub-cloning

All restriction enzymes that were used in this thesis were purchased from New England Biolabs (United Kingdom). Insert and vector were digested in a total volume of 25 µl containing 5000 units of each of the two enzymes, the adequate buffer for the enzymes, the DNA and BSA. The reaction was incubated for at least 1 hr at 37 ºC. The reaction was then loaded on a 1% agarose gel in TBE with 0.5 µg/ml ethidium bromide. The DNA was visualised using a UV lamp, bands corresponding to the correct size were cut out from the gel, purified with the Qiagen QIAquick gel extraction kit and eluted from the column in 30 µl distilled water. A 10 µl ligation reaction was set up containing 100-500 ng of the digested vector DNA, an excess of purified insert DNA, 200 units T4 DNA ligase and 1x ligase buffer (New England Biolabs). The reaction was incubated for at least 1 hr at room temperature or incubated overnight at 16 ºC before 5 µl of the ligation were transformed into 50 µl chemical competent *E. coli* (Chapter 2.3.5). Digestions of purified DNA were performed to check for correct insertion.

2.3.5 Preparing chemical competent bacteria (Calcium chloride method)

Chemical competent *E. coli* XL-10 or BL21 (DE3) Rosetta strain were prepared by incubating 2 ml of an overnight culture in 500 ml of LB medium. To ensure the bacteria where in an exponential growth phase, the culture was grown with constant shaking at 37 ºC until an OD_{600} of 0.5 was reached. Subsequently, the bacterial culture was incubated for 30 min on ice before it was centrifuged for 12 min at 2500 rpm. The pellet was resuspended in 20 ml of cold RF1 buffer, incubated on ice for 15 min and centrifuged for 9 min at 2500 rpm. The pellet was resuspended in 7 ml cold RF2 buffer and the suspension was stored in 100 µl aliquots at -80ºC.

RF1 Buffer

12.00 g	Rubidium chloride, RbCl
9.00 g	Manganese chloride, $MnCl_2$
2.94 g	Potassium acetate
150.00 g	Glycerol

The reagents were dissolved in 900 ml of distilled water and the pH was adjusted to pH 5.8 with acetic acid, before the volume was made up to 1 L. The buffer was subsequently sterile filtered through a 0.22 μm filter and stored at 4 °C.

RF2 Buffer

2.09 g	3-(N-morpholino)propanesulfonic acid, MOPS
1.20 g	Rubidium chloride, RbCl
11.00 g	Calcium chloride, $CaCl_2$
150.00 g	Glycerol

The reagents were dissolved in 900 ml of distilled water and the pH was adjusted to 6.8 with sodium hydroxide, before the volume was made up to 1 L. The buffer was subsequently sterile filtered through a 0.22 μm filter and stored at 4 °C.

2.3.6 Plasmid DNA transformation of bacteria

To transform bacteria, 5 μl of ligation reaction or 50 ng of plasmid DNA was incubated with 50 μl chemical competent *E. coli* on ice. After 20 min, the bacteria were heat shocked for 30 sec at 42 ºC, before the addition of 500 μl LB medium and incubation at 37 ºC with constant shaking for 30 min. The bacteria culture (50 μl to 500 μl) was plated on LB-agar plates containing the appropriate antibiotics for the vector.

2.3.7 Plasmid DNA preparation

For plasmid DNA preparation, 5 ml and 100 ml overnight cultures from single colonies for mini and midi preparations were set up respectively. The bacteria cultures were spun down at 3000 rpm and the pellets were processed as described in the Qiagen Plasmid Miniprep and Midiprep Kit instructions.

2.3.8 DNA sequencing

For sequencing reactions, oligonucleotide primers matching to sequences in the insert-flanking regions of the vector and every 500 bp inside the insert were used. For each sequencing reaction, 200 ng plasmid DNA, 3.2 pmol oligonucleotide primer and 8 μl BDT reaction mix (Big Dye Terminator Cycle sequencing kit) were mixed and adjusted to the total volume of 20 μl using distilled water. The sequencing reactions were performed on an Applied Biosystems GeneAmp PCR machine. Following amplification, the reaction was cleaned using the Qiagen Dye-Ex 2.0 Spin kit, and vacuum dried. The samples were sequenced using an Applied Biosystems DNA

sequencer in the sequencing facility at Cancer Research UK. The resulting sequences were analysed using the DNAstar software package (Madison, USA).

2.3.9 Site-Directed Mutagenesis

Mutations in genes of interest were introduced by site-directed mutagenesis using two complementary synthetic primers containing the desired bases. All primers used to introduce mutations in the EVH1 binding site of both human and *Drosophila* Abi are listed in Table 2.7. For each mutagenesis, 100 ng plasmid DNA template, 125 ng of each oligonucleotide primer, 10 mM dNTP mix, 1x Cloned Pfu DNA polymerase reaction buffer and 2.5 units PfuTurbo DNA polymerase (Stratagene) were mixed and adjusted to the total volume of 50 µl using distilled water. The mutated plasmids containing staggered nicks were generated during temperature cycling as shown below.

95°C	30 sec	

Denaturation :	95 °C 30 sec ⎫	
Annealing :	55 °C 30 sec ⎬	18 cycles
Extension :	68 °C 1 min * ⎭	
	---	
	4 °C ∞	

- *Extension time: 2 min/kb of plasmid length.

The amplification reaction was subsequently incubated with 20 units DpnI (New England Biolabs) at 37 ºC for 1 hr to digest the methylated, non-mutated parental DNA templates. The nicked plasmid DNA incorporating the desired mutations was then transformed into XL-10 *E. coli* (Chapter 2.3.6). Mutations of the gene of interest were confirmed by sequencing DNA mini-preps of individual clones.

Table 2.7 Primers used to modify Abi sequence

Mutated amino acids	Oligonucleotide Sequence	Size (bp)
Abi P366G/P367G/P368G (Mutant 1)	For CCAACTCCACCGCCAGGCGGCGGCCCAGATGACATTCCC	39
	Rev GGGAATGTCATCTGGGCCGCCGCCTGGCGGTGGAGTTGG	39
Abi F375A (Mutant 2)	For GCCCAGATGACATTCCCATGGCGGATGACTCTCCACCTCCCCC	43
	Rev GGGGGAGGTGGAGAGTCATCCGCCATGGGAATGTCATCTGGGC	43
Abi P383G/P384G/P385G (Mutant 3)	For CCTCTCCACCTCCCCCAGGCGGCGGCCCAGTGGATTATGAAG	41
	Rev CTTCATAATCCACTGGGCCGCCGCCTGGGGGAGGTGGAGAG	41
dAbi L311A/P312G/P313G/ P314G/P315G (Mutant 1)	For GCGGGCATGATGCAATCGGCGGGCGGCGGCGGCCCCACTACGTACGACGAT	51
	Rev ATCGTCGTACGTAGTGGGGCCGCCGCCGCCCGCCGATTGCATCATGCCCGC	51
dAbi L374A/P375G/P376G/ P377G/P378G (Mutant 2)	For GGCTCACAGTCGCCTCCCGCGGGCGGCGGCGGCCCGCCGGAGGATGAGCAT	51
	Rev ATGCTCATCCTCCGGCGGGCCGCCGCCGCCCGCGGGAGGCGACTGTGAGCC	51

2.4 Immunofluorescence

2.4.1 General buffers and solutions for Immunofluorescence

1x Cytoskeletal Buffer (CB)

10 mM	MES pH 6.1
150 mM	NaCl
5 mM	EGTA
5 mM	$MgCl_2$
5 mM	Glucose

The reagents were dissolved in distilled water.

Immunofluorescence (IF) Blocking Buffer

1%	BSA
2%	FCS

The reagents were dissolved in 1x Cytoskeletal Buffer.

Mowiol

Mowiol (2.4 g) and glycerol (6 g) were dissolved in 6 ml distilled water. The mix was incubated for 2 hr at room temperature before 12 ml of 200 mM Tris-HCL (pH8.5) was added. The resulting solution was stirred for 10 min at 60 ºC, spun down for 5 min at 5000 rpm and was stored in 500 µl aliquots at -20 ºC.

3% Paraformaldehyde in 1x CB

Paraformaldehyde (15 g) was added to 500 ml of pre-heated 1xCB. The solution was stirred under heating and 1 M NaOH tablets were added until the solution became clear. The solution was left to cool down to room temperature and the pH was adjusted to 8.8. The mix was passed through a 0.45 µm filter (Millipore) and aliquots were stored at -20 ºC.

2.4.2 Fixation methods

Paraformaldehyde (PFA) fixation methods were generally used to fix cells for immunofluorescence staining. Cells were fixed in 3% PFA/CB for 10 min at room temperature and washed 3 times with PBSA and stored at 4 ºC until processed for immunofluorescence.

2.4.3 Staining and mounting

To permeabilise cells before labelling with primary antibodies, the cover slips containing PFA fixed cells were incubated with a 0.1% Triton X-100/ PBSA solution for 45 sec and washed 2 times with PBSA. Following permeabilisation, cover slips were incubated for 15-30 min in IF-blocking buffer at room temperature. Cells were incubated with the primary antibody (diluted in IF blocking buffer) for at least 1 hr at room temperature (Table 2.8). After incubation with the primary antibody, the cover slips were washed 3 times with IF-blocking buffer and incubated for at least 30 min with the secondary antibody (diluted in IF-blocking buffer) at room temperature (Table 2.9). Phalloidin that binds to F-actin was added to the secondary antibody solution in a 1:500 dilution where required. During incubation, cover slips were protected from light. After incubation with the secondary antibody the cover slips were washed 3 times with IF-blocking buffer. DNA was visualized by incubating the cover slips for at least 10 sec in distilled water containing 1 mg/ml 4',6-diamidine-2-phenylidole dihydrochloride (DAPI) (Roche Diagnositcs, Mannheim, Germany) where required. The cover slips were then washed once with distilled water and mounted on microscopy slides using Molviol (Calbiochem, Bad Soden, Germany) with 1 mg/ml p-phenylendiamine (Sigma). The prepared microscopy slides were dried at RT for at least 30 min before use.

Table 2.8 Primary Antibodies

Antibody	Specificity	Species	Dilution	Origin
α-Abi1	Abi1 and 2	Rabbit	1:1000	Dr Theresia Stradal
α-Abi1	Abi1	Mouse	1:1000	Abcam
α-Mena	Mena	Mouse	1:75	BD Transduction Laboratories
α-VASP	VASP	Rabbit	1:1000	Dr Frank Gertler
α-Paxillin	Paxillin	Mouse	1:1000	BD Transduction Laboratories
α-WAVE2 (1735)	WAVE2	Rabbit	1:1000	Dr Theresia Stradal
α-Nap1 (4952)	Nap1	Rabbit	1:1000	Dr Theresia Stradal
α-SCAR	SCAR	Guinea pig	1:1000	Dr Sven Bogdan
α-Ena	Ena	Mouse	1:10	Dr Sven Bogdan
Alexa 568-phallodin	Actin		1:500	Molecular Probes

Table 2.9 Secondary antibodies

Antigen	Species raised in:	Label	Dilution	Origin
Mouse	Rabbit	FITC	1:500	Jackson ImmunoResearch
Mouse	Rabbit	Texas Red	1:500	Jackson ImmunoResearch
Rabbit	Donkey	FITC	1:500	Jackson ImmunoResearch
Rabbit	Donkey	Texas Red	1:500	Jackson ImmunoResearch
Guinea pig	Goat	Texas Red	1:500	Santa Cruz

2.5 Microscopy

2.5.1 Microscopes

2.5.1.1 Zeiss Axioplan 2 Upright

To image fixed samples, a Zeiss Axioplan2 equipped with a Photometrics Cool Snap HQ cooled CCD camera, external Prior Scientific filter wheels (DAPI; FITC; Texas Red; Cy5) and a 63x/1.4NA Plan Apochromat objective was used. The system was controlled by MetaMorph software version 6.3r7 (Universal Imaging Corporation Ltd.). Images were analysed using MetaMorph and processed with the Adobe software package (Adobe Systems Incorporated, San Jose, CA, USA).

2.5.1.2 Zeiss Inverted

To image live cells, a Zeiss Axiovert 200 equipped with a Photometrics Cool Snap HQ cooled CCD camera, external Prior Scientific filter wheels (GFP, RFP) and a 63x/1.4NA Oil Plan Apochromate objective was used. The system was controlled by MetaMorph software version 6.3r7, Universal Imaging Corporation Ltd. Movies and images were analysed using the MetaMorph and processed with the Adobe software package and Quick Time Player (Apple Computer, Incorporated).

2.5.1.3 Nikon Inverted

To image live cells in the LRI imaging facility, a Nikon ECLIPSE TE2000-E equipped with a Andor iXon^{EM} + DU-888 back-illuminated EMCCD scientific camera, filter wheel (FITC) and a Dry 10x/0.3 Plan Fluor objective was used. The system was controlled by MetaMorph software version 7.7.3.0, Universal Imaging Corporation Ltd. Movies and images were analysed using the MetaMorph software and processed with the Adobe software package and Quick Time Player (Apple Computer, Incorporated).

2.5.1.4 Zeiss confocal LSM 710

To perform FRAP experiments, a Zeiss FObserver.Z1 confocal microscope equipped with photomultiplier spectral detector, dichroic mirrors and beam splitter (MBS 488, MBS 488/561), Argon laser (458nm, 488nm, 514nm), a DPSS laser (561nm), filter for FITC and TRITC and a 63x/1.4NA Oil DIC Plan Apochromate objective was used. The system was controlled by the ZEN software version 2009 (Carl Zeiss MicroImaging GmbH). Movies and images were analysed using the ZEN 2009 software.

2.5.2 Live-cell imaging of cell migration

Rat-2 cells stably expressing either GFP, GFP-tagged Abi or Abi mut were seeded into the 6 well MatTek dishes pre-coated with 10 µg/ml fibronectin (Invitrogen) at a density of $1x10^4$ cells per well in complete medium lacking phenol red and grown over night. On the following day, the 6 well MatTek dish was transferred to the Nikon Inverted microscope and after 30 min, images were collected every 10 min for 20 hr in multiple stage positions at 37 ºC in a 5% CO_2 atmosphere.

2.5.3 Fluorescence Recovery After Photo-Bleaching (FRAP)

Rat-2 cells were seeded onto fibronectin coated 3.5 cm MaTek dishes one day before performing FRAP analysis. *Drosophila* S2 and $S2R^+$ cells were seeded on to Concanavalin A (conA) (Sigma) coated 3.5 cm MaTek dishes 30 min before performing FRAP analysis. To analyse the turnover rate of GFP-tagged Abi/dAbi, VASP and mCherry-tagged Ena at the cell plasma membrane in Rat-2 cells, S2 or $S2R^+$ cells, the conditions for each FRAP assay were optimised by testing several imaging parameters, laser power and iteration times. All FRAP assays were performed using a Zeiss LSM 710 confocal. After the pre-seeded cells were transferred to the confocal microscope, cells to be imaged were first identified under low light fluorescence using the eyepiece. In all cases, a region of 300x100 pixels for each cell at a higher magnification (digital zoom 2.0x) was recorded using a fast scan speed of 1.27 µs per pixel with either laser power setting of 1% for 488 nm and pinhole adjustment of 90 µm (GFP) or laser power setting of 2% for 561 nm and pinhole adjustment of 68 µm (mCherry). A selected region within the imaging area of 90x25 pixels covering parts of protruding lamellipodia was bleached using either 30 iterations of the 488 nm laser at 100% power (GFP) or 10 iterations of the 516 nm laser at 100 % (mCherry). Five images in all cases were recorded before the GFP or mCherry signal was bleached. In all cases, 500 images were acquired without time delay for each FRAP experiment.

2.6 Analysis of microscopy data

2.6.1 Quantification of the fluorescence intensities at the tip of lamellipodia

Analysis was performed using a plug-in for ImageJ (version 1.44p) developed by Dr David Barry, a postdoctoral researcher in the lab. Only non-adjoining cells were considered. Cells were segmented from background by grey-level thresholding of the dAbi-GFP signal (channel 1). Unwanted artefacts were removed using morphological

thresholds (minimum area and circularity). The resulting binary image was used to construct a Eucidean Distance Map (EDM), in which each pixel within an object was assigned a grey level proportional to its distance from the nearest background pixel. Dividing the original channel 1 image by the EDM resulted in the suppression of pixels distant from the cell boundary (plasma membrane), providing an estimate of dAbi signal strength at the cell periphery. Dividing the signal of the immunolabeled endogenous Ena (Ena antibody) by the same EDM provided an estimate of Ena signal strength at the plasma membrane and the mean Ena:dAbi ratio was estimated. Ten cells were quantified per population per timepoint. The results of three independent experiments were presented.

2.6.2 Single-cell tracking assay

Cells were tracked manually using the single cell track feature of MetaMorph. In all cases, the cell nucleus was tracked for 120 time points over a period of 15 hr. No dividing or attaching cells were tracked. Each day 13 cells from each cell line were tracked and the experiment was repeated on 3 separate days. Data that was generated using MetaMorph was subsequently imported into Excel (Microsoft Office 2007). Using Excel, the directionality, velocity and persistence of each cell over the tracking period was calculated.

2.6.3 FRAP analysis

The fluorescence intensity of FRAP movies was analysed using the FRAP analysis feature in the ZEN 2009. A region of 88x23 pixels, which was created inside the bleaching area (90x25 pixels), was used to measure the recovery of the fluorescence intensity after photobleaching. To subtract the background, the fluorescence intensity in a region of 20x20 pixels outside the cell boundary was measured. The FRAP data was normalised to the first pre-bleached image and subsequently normalised to the background fluorescence intensity. Kinetic modelling of normalised data was performed using the equation $Y_{(T)} = (Y_{max} – Y_{min}) (1\text{-}e^{-kt}) + Y_{min}$ in the Prim 5.0 software. The rate of recovery k and the half time ($t_{1/2} = -\ln k$) was obtained from a fitted curve. The maximum recovery after photobleaching (% recovery) was calculated. Each curve corresponds to an average of at least 20 cells, which were acquired on 3 different days.

2.6.4 Quantification of lamellipodia formation in *Drosophila* haemocytes.

GFP or GFP-tagged dAbi rescued dsRNA treated cells were seeded on ConA coated cover slips to allow cells to spread. Afterwards, cells were fixed, permeabilised and stained with phalloidin to label F-actin as described in (Section 2.4). Only GFP positive cells, were counted. Each day 200 cells were counted and the experiment was repeated on 3 different days. The cells were scored for the morphology of their lamellipodial structures.

2.6.5 Statistical analysis of microscopy data

Data in all graphs are presented as mean and standard error of the mean. Prism 5.0 (GraphPad Software, CA) was used to perform standard statistical analysis of measured data sets. When two data sets were compared, a student's t-test was performed. If more than two data sets were compared with each other, a One Way ANOVA test followed by a Newman-Keuls multiple comparison test was performed. Statistical analysis of fitted FRAP data was performed using the extra sum-of-squares F test in Prism 5.0 to test whether the rate constants k differ significantly from each other. All experiments were repeated at least three times on three different days. The P value represents the probability of obtaining the observed values, under the assumption that the null hypothesis (means or k are equal) is true: the lower the P value, the lower the probability that the difference of the observed means or k was obtained by chance. A P value of <0.05 was considered statistically significant. *indicates $P<0.05$, ** indicates $P<0.01$ and *** indicates $P<0.001$.

2.7 Biochemistry

2.7.1 Total cell lysate

Bacteria or tissue culture cells were washed once in PBSA before preparing total cell lysates. After PBSA aspiration, the appropriate amount of protein sample buffer (PSB) to cover the entire dish was added and cells were scraped. The lysate was then transferred to an microcentrifuge tube, mixed by vortexing and boiled for 10 min at 95 ºC. The samples were stored at -20 ºC before being used in SDS-PAGE prior to immuno-blot analysis (Section 2.7.2). To digest DNA in the sample before immuno-blot analysis, 0.5 µl of 10 mg/ml Sigma D4527 deoxyribonuclease I (DNase I) was added where required.

Protein Sample Buffer (PSB)

50%	Glycerol
3%	SDS
50 mM	Tris.HCl pH 6.8
2%	β-Mercaptoethanol
+	Solid Bromophenol Blue

2.7.2 SDS-PAGE and Western blotting

2.7.2.1 SDS-PAGE

Pre-cast NuPAGE 4-12% Bis-Tris 1.0 mm gels (Invitrogen) were used throughout my studies. Gels were loaded with at least one lane containing the SeeBluePlus2 Prestained standard protein marker (Invitrogen) and were run using MES Running buffer (Invitrogen). Gels were run at 200 V for at least 35 min using Invitrogen mini gel tanks. Gels were run for 2-4 hr if proteins of similar size needed to be separated. After the proteins were separated, gels were either transferred for immuno-blot analysis or stained with Coomassie solution (0.5% Coomassie Brilliant Blue, 50% methanol, 10% acetic acid) for 30 min, followed by destaining in high destain (50% methanol, 10% acetic acid) for 5 min, and then low destain (5% methanol, 10% acetic acid) for as long as necessary to visualise the protein bands.

20x MES Running Buffer (Invitrogen)

MES	97.6 g (1 M)
Tris Base	60.6 g (1 M)
SDS	10.0 g (69.3 mM)
EDTA	3.0 g (20.5 mM)

2.7.2.2 Immuno blot analysis

After proteins were separated by size using SDS-PAGE, they were transferred onto a nitrocellulose membrane for immuno-blot analysis. Gels were transferred using the iBlotter and the iBlot gel Transfer kit from Invitrogen. After the transfer, the membrane was stained with Ponceau S solution to control for equal loading and successful transfer. Afterwards, the membrane was blocked for 30 min in blocking buffer (5% milk in PBSA, 0.1% Tween20 (Sigma)) and incubated with the primary antibody (in blocking buffer) for a period of 1 hr at room temperature to over night at 4 °C depending on the antibody used (Table 2.10). The membrane was then washed 3 times in PBT (PBSA,

0.1% Tween20) before it was incubated in blocking buffer containing the secondary antibody conjugated to HRP for 30 min (Table 2.11). The membrane was then washed 5 times in PBT before developing using ECL reagent according to manufacturer's instructions (Amersham Bioscences), before being exposed on Hyperfilm-ECL (Amersham Biosciences) and developed using an IGP Compact automated developer (IPG limited).

Table 2.10 Primary antibodies used for Western blot analysis

Antibody	Specificity	Species	Dilution	Time	Origin
α-GFP (3E12)	GFP	monoclonal mouse	1:1000	1 h	Way lab
α-GST (G-7781)	GST	polyclonal rabbit	1:2000	1 h	Sigma
α-HIS	HIS	monoclonal mouse	1:2000	1 h	Sigma
α-Nap1 (4952)	Nap1	polyclonal rabbit	1:2000	1 h	Dr Theresia Stradal
α-PIR121 (4955-B)	PIR121	polyclonal rabbit	1:1000	O/N	Dr Theresia Stradal
α-Abi1 (4996)	Abi1 and Abi2	polyclonal rabbit	1:1000	1 h	Dr Theresia Stradal
α-Zyxin (164D4)	Zyxin	monoclonal mouse	1:1000	1 h	Dr Matthias Krause
α-dAbi	dAbi	polyclonal rabbit	1:1000	O/N	Dr Sven Bogdan
α-SCAR	SCAR	Polyclonal guinea pig	1:1000	O/N	Dr Sven Bogdan
α-α Tubulin	α Tubulin	monoclonal mouse	1:5000	1 h	Sigma

Table 2.11 Secondary antibodies used for Western blot analysis

Antigen	Species	Label	Dilution	Origin
Rabbit	Goat	HRP	1:2000	Jackson ImmunoResearch
Mouse	Goat	HRP	1:5000	Jackson ImmunoResearch
Guinea Pig	Donkey	HRP	1:10000	Jackson ImmunoResearch

2.7.3 Expression and purification of proteins in *E. coli*

In thesis, the conditions of each protein produced in bacteria are listed in Table 2.12.

2.7.3.1 Leaky Protein expression

Chemically competent BL21 (DE3) Rosetta *E. coli* were transformed with the pMW172 DNA vector carrying the gene of interest. Bacteria from single colonies were used to inoculate 5 ml LB-ampicillin starter cultures, which were grown during the day under vigorous shaking at 37 °C. Starter culture (1 ml) was then used to inoculate 1 L of LB-ampicillin overnight cultures, which were then incubated either overnight with vigorous shaking at 30/37 °C or over 20 hr at 20/25 °C depending on the protein (Table 2.12). Bacteria were then harvested by centrifugation at 3500 rpm for 20 min at 4 °C. The resulting bacterial cell pellet was snap frozen in liquid nitrogen and thawed at room temperature. Afterwards, the cell pellet was resuspended in 25 ml bacterial lysis buffer (50 mM Tris HCl pH 8.0, 1 mM EDTA, 25% sucrose, 1x protease inhibitors (Complete EDTA-free protease inhibitor tablets (Roche)) at room temperature, and 3 mg lysozyme was added. After 30 min incubation at room temperature, 240 µl of 1 M $MgCl_2$, 24 µl $MnCl_2$ and 10 µl of 10 mg/ml DNase I were added to the lysate and incubated at room temperature for another 30 min. Subsequently, the lysate was centrifuged at 12,000 rpm for 15 min at 4 °C. The supernatant was retained as the bacterial soluble fraction, which was then either snap frozen in liquid nitrogen and stored in aliquots at -20 °C or stored on ice at 4 °C with 1% sodium azide until they were used.

2.7.3.2 Isopropyl β-D-1-thiogalactopyranoside (IPTG) induced Protein expression

Chemically competent BL21 (DE3) Rosetta *E. coli* were transformed with the pMW172 DNA vector carrying the gene of interest. Fresh single colonies were used to inoculate a 10 ml LB-ampicillin starter culture, which was grown over night with vigorous shaking at 37 °C. On the following day, the starter culture was used to inoculate 1 L of LB-ampicillin media, which was then grown under vigorous shaking at 37 °C until the culture reached an OD_{600} of 0.6-0.7. Cultures were incubated at 30 °C for 30 min before 1 mM IPTG (Sigma) was added. After adding IPTG, cultures were grown for 2 hr under vigorous shaking at 30 °C. Afterwards, cells were harvested by centrifugation and the bacterial soluble fraction was obtained as described in Chapter 2.7.3.1.

Table 2.12 Expression conditions used to produce recombinant proteins in bacteria

Recombinant proteins	Condition of expression
GST-EVH1 VASP	37 °C O/N
GST-EVH1 Evl	37 °C O/N
GST-EVH1 Mena	37 °C O/N
GST	37 °C O/N
GST-Nap1	IPTG induced
GST-PIR121	IPTG induced
HIS-Grb2	30 °C O/N
HIS-EVH1 Mena	37 °C O/N
HIS-Nap1	IPTG induced
HIS-PIR121	IPTG induced
HIS-Abi	IPTG induced
GST-Abi	20 °C O/N
GST-Abi N-term-PR1	30 °C O/N
GST-Abi PR2-SH3	25 °C O/N
GST-Abi ΔSH3	20 °C O/N
GST-Abi PR2	20 °C O/N
GST-Abi PR1-PR2-SH3	20 °C O/N
GST-Abi PR1-PR2	20 °C O/N
GST-Abi Mutant 1	20 °C O/N
GST-Abi Mutant 2	20 °C O/N
GST-Abi Mutant 3	20 °C O/N
GST-Abi Mutant 1+2	20 °C O/N
GST-Abi Mutant 1+3	20 °C O/N
GST-Abi Mutant 2+3	20 °C O/N
GST-Abi Mutant 1+2+3 (mut)	20 °C O/N
pMW GST-EVH1 Ena	IPTG induced
HIS-VASP	IPTG induced

2.7.3.3 Purification of HIS-tagged proteins on Ni-resin

Imidazole (1 M, pH 7.8) was added to soluble fractions to a final concentration of 50 mM. Ni-NTA resin (Qiagen), prewashed in bacterial lysis buffer, was added to the soluble fraction, and incubated under constant rotation at 4 °C for at least 60 min. The

resin was pelleted by centrifugation at 2000 rpm, and washed 3 times in bacterial Ni wash buffer (50 mM Tris HCl pH 8.0, 250 mM NaCl, 0.1% Triton X-100, 50 mM imidazole pH 7.8).

2.7.3.4 Purification of GST-tagged proteins on glutathione resin

Glutathione sepharose resin (Amersham Biosciences), prewashed in bacterial lysis buffer, was added to soluble fractions, and incubated under rotation at 4 ºC for at least 1 hr. The resin was pelleted by centrifugation at 2000 rpm, and washed 3 times in bacterial GST-wash buffer (150 mM NaCl, 0.1% Triton X-100, 5% glycerol in PBSA).

2.7.4 Expression and purification of HIS-tagged PIR121:Nap1 protein complex using the Baculovirus system

Full-length Nap1 and PIR121 were cloned into the baculovirus transfer vector pBacPAK-His3 (Clontech) or pBacPAK-GST (modified pBacPAK-GST (Clontech) from the protein expression facility at Cancer Research UK). Expression and purification of HIS-tagged PIR121:Nap1 protein complex from Sf9 cells were performed by the in-house facility at Cancer Research UK.

2.7.5 *In vitro* EVH1 pull-downs

The amounts of proteins in all soluble fractions used in each *in vitro* pull down assay were estimated using SDS-PAGE following by coomassie staining. In each assay, all samples were adjusted to contain a similar amount of GST- and HIS-tagged protein or protein complex, which were mixed in approximately a 1:1 ratio. About 10% of the soluble fraction used in each pull-down was purified by glutathione sepharose resin or Ni-NTA resin and used as the input.

2.7.5.1 HIS-EVH1 and bacterially produced GST-Nap1/PIR121 pull-down assay

Soluble bacterial fractions containing HIS-EVH1/Grb2 and GST, GST-tagged Nap1 or PIR121 were mixed and incubated at 4 °C for 60 min. Subsequently, pre-washed Ni-NTA resin was added to the mixed soluble fractions, and incubated at 4 °C for 1 hr with rotation. The resin was pelleted by centrifugation at 2000 rpm, washed 3 times in bacterial Ni wash buffer. Samples were then boiled with PSB and subjected to SDS-PAGE. Afterwards, proteins were visualized by coomassie staining or immuno analysis.

2.7.5.2 GST-EVH1 and Sf9 cells produced HIS-PIR121:Nap1 pull-down assay

Soluble bacterial fractions containing GST/GST-EVH1 and pre-washed glutathione sepharose resin were incubated with rotation at 4 °C for 1 hr. Afterwards, the resin was pelleted by centrifugation at 2000 rpm, and washed 3 times in bacterial GST wash buffer. The resin was then incubated with the Sf9 cells produced HIS-PIR121:Nap1 protein complex or the soluble bacterial fraction of HIS-LIM3 with rotation at 4 °C for 1 hr. These resins were pelleted by centrifugation at 2000 rpm, and washed 3 times in bacterial GST wash buffer. Samples were then boiled with PSB and subjected to SDS-PAGE. Proteins were subsequently visualized by immuno-blot analysis with antibodies.

2.7.5.3 GST-EVH1, HIS-Abi and HIS-Nap1 pull down-assays

For GST/GST-EVH1 resin preparation, soluble bacterial fractions containing GST/GST-EVH1 were incubated with pre-washed glutathione sepharose resin with rotation at 4 °C for 1 hr. For GST/GST-EVH1:HIS-Abi resin preparation, soluble bacterial fractions containing GST/GST-EVH1 and HIS-Abi were mixed and allowed to incubated with rotation at 4 °C for 1 hr. Subsequently, pre-washed glutathione sepharose resin was added to the mixed soluble fractions and incubated with rotation at 4 °C for 1 hr. All resins were pelleted by centrifugation at 2000 rpm, washed 3 times in bacterial GST wash buffer, mixed with the soluble bacterial fraction containing HIS-Nap1 and incubated under rotation at 4 °C for 1 hr. Following incubation, resins were pelleted by centrifugation at 2000 rpm and washed 3 times in bacterial GST wash buffer. Samples were boiled with PSB and then subjected to SDS-PAGE prior to be stained with coomassie solution.

2.7.5.4 GST-EVH1 and HIS-Abi pull-down assays

Soluble bacterial fractions containing GST/GST-EVH1 and HIS-Abi were incubated with rotation at 4 °C for 1 hr. Subsequently, pre-washed glutathione sepharose resin was added to the mixed soluble fractions, and incubated with rotation at 4 °C for 1 hr. Resins were pelleted by centrifugation at 2000 rpm, and washed 3 times in bacterial GST wash buffer. Samples were boiled with PSB and then subjected to SDS-PAGE prior to be stained with coomassie solution.

2.7.5.5 HIS-EVH1, GST-Abi full length and deletion mutant pull-down assays

Soluble bacterial fractions containing either HIS-EVH1 or GST/GST-tagged Abi full length and Abi deletion mutants were mixed and incubated with rotation at 4 °C for 1 hr. Subsequently, pre-washed Ni-NTA resin was added to soluble fractions, and incubated with rotation at 4 °C for 1 hr. Resin was pelleted by centrifugation at 2000 rpm, and washed 3 times in bacterial Ni wash buffer. Samples were boiled with PSB and then subjected to SDS-PAGE prior to be stained with coomassie solution.

2.7.6 Pull-downs from cell lysates and protein identification by mass spectrometry

Cells on a 10 or 15 cm dish were washed 2 times with PBSA at 4 °C and resuspended in 0.7 ml culture cell lysis buffer (50 mM Tris HCl pH 8.0, 150 mM NaCl, 20 mM Na_3VO_4, 10 mM NaF, 5% glycerol, 1% Triton X-100, 1x protease inhibitors). Cells were disrupted by vigorous pipetting and resulting cell lysate was cleared of nuclei and membranes by centrifugation at 13000 rpm for 10 min at 4 °C. Clarified cell lysates were the incubated with GST/GST-EVH1 resin previously washed in culture cell lysis buffer for 1 hr at 4 °C with rotation. The resin was then pelleted by centrifugation at 2000 rpm, and washed 3 times in culture cell lysis buffer. Samples were then subjected to SDS-PAGE and followed by coomassie staining or immuno blot analysis. For protein identification, the coomassie stained gels were given to the Mass Spectrometry facility at Cancer Research UK. The bands corresponding to the proteins of interest were then cut out and analysed using mass spectrometry.

2.7.7 EVH1 binding competition assay

For generating HIS-EVH1 affinity resin, soluble bacterial fractions containing HIS-EVH1 domain of Mena were incubated with pre-washed Ni-NTA resin with rotation at 4 °C for 1 hr. For generating HIS-EVH1:GST-FPPPP and HIS-EVH1:GST-LIM3 affinity resins, soluble bacterial fractions containing HIS-EVH1 were mixed with the soluble fractions containing GST-FPPPP or GST-LIM3 and incubated with rotation at 4 °C for 1 hr. Subsequently, pre-washed Ni-NTA resin was added to soluble fractions, and incubated with rotation at 4 °C for another 1 hr. Following incubation, all resins were pelleted by centrifugation at 2000 rpm, and washed 3 times in bacterial Ni wash buffer. The resulting resins were then incubated with pre-prepared MVD7 cell lysates (Chapter

2.7.6). Subsequently, the standard protocol for pull-downs from cell lysates was followed.

2.7.8 Immunoprecipitation

All immunoprecipitations were performed using the purified mouse monoclonal anti-GFP antibody except one immunoprecipitation that was performed using the ChromoTek GFP-Trap_A, as described in the manufacture's instructions. Cell lysates that contain over-expressed GFP or GFP-tagged protein were prepared (Chapter 2.7.6) and incubated with pre-washed Protein G resin (Pierce) with rotation at 4 °C for 1 hr. The resin was pelleted by centrifugation at 2000 rpm, and the cell lysates were subsequently transferred into a fresh tube, in which 2 µg of purified rabbit anti-GFP antibody was added to each pre-clarified cell lysate. The samples were incubated with rotation at 4 °C for 2 hr. Then pre-washed Protein G resin was added to the cell lysate/antibody mix and incubated with rotation at 4 °C for 1 hr. The resin was pelleted by centrifugation at 2000 rpm, and washed 3 times in culture cell lysis buffer. Samples were boiled with PSB and then subjected to SDS-PAGE. The precipitated proteins were analysed by immuno blot analysis.

2.7.9 Far western analysis of peptide arrays

2.7.9.1 Purification of GST-tagged EVH1 for far western analysis

To purify GST-tagged EVH1 domains of Mena, VASP, Evl and Ena under a more stringent salt and glycerol condition, NaCl and glycerol was added to soluble bacterial fractions to a final concentration of 500 mM NaCl and 10% glycerol. Glutathione sepharose resin was prewashed in bacterial lysis buffer, was added to soluble fractions, and incubated under rotation at 4 °C for at least 1 hr. Resin was pelleted and washed 4 times in bacterial GST wash buffer (150 mM NaCl, 0.1% Triton X-100, 5% glycerol in PBSA). Bound GST-tagged EVH1 domains were eluted from beads using 4 washes of 800 µl elution buffer (10 mM glutathione in 50 mM Tris HCl pH 8.0). The elution buffer containing the purified GST-tagged EVH1 was subsequently passed through PD-10 desalting columns according to the manufacturer's instruction (GE Healthcare). Protein concentrations were measured by spectrophotometry methods (Absorbance at 280 nm) using a NanoDrop spectrophotometer (Thermo Scientific).

2.7.9.2 Probing peptide arrays

The peptide arrays containing overlapping peptides covering full length Abi or the proline rich C-terminus of Abi were generated by the peptide service at Cancer Research UK. For all arrays, peptides of 20 amino acids that overlap with each other by 1 amino acid residue were synthesised and spotted onto a cellulose membrane. To perform far western analysis, the dried peptide arrays were first moistened with 100% Ethanol, followed by 3 washes with PBT for 5 min each. Subsequently, non-specific binding sites on the array were blocked by 1 hr or overnight incubation in blocking buffer (5% milk in PBSA, 0.1% Tween20). Purified GST or GST-EVH1 was diluted to a concentration of 2 µg/µl in blocking buffer. The peptide array was incubated upside down a parafilm in plastic box using 2-3 ml of diluted purified protein at room temperature for 1 hr. The array was then washed 3 times for 10 min with blocking buffer followed by incubation with rabbit anti-GST primary antibody (diluted 1/10000 in blocking buffer) at room temperature for 1 hr. After these 10 min washes with blocking buffer, the peptide array was incubated with goat anti-rabbit HRP secondary antibody (diluted 1/6000 in blocking buffer) at room temperature for 45 min. After 3 washes for 5 min with PBT, the peptide arrays were washed once with PBT containing 0.5 M NaCl to reduce non-specific binding. The peptide arrays containing the mutated peptides of Abi were probed in a similar fashion. Peptide arrays were subsequently developed using the ECL reagent as described before Chapter 2.7.2.2.

Chapter 3. Abi mediates the interaction between Ena/VASP proteins and the WAVE complex

3.1 Introduction

Ena/VASP proteins have been found to play important roles in regulating actin dynamics during filopodia and lamellipodia formation. It was previously thought that the EVH1 domain of Ena/VASP proteins could only interact with proteins containing FPPPP motifs. However, it has been demonstrated that Tes, which lacks a FPPPP motif, binds to the EVH1 domain of Mena via its LIM3 domain, but does not bind VASP and Evl (Boeda et al., 2007). Tes is therefore the first example of an EVH1 binding protein lacking a FPPPP motif that specifically regulates only one Ena/VASP family member. Given these results, we speculated that other non-FPPPP containing binding partners and potential regulators of Ena/VASP proteins could exist. I therefore set out to identify new EVH1 binding partners of Ena/VASP proteins using a combination of biochemical approaches and mass spectrometry.

3.2 Results

3.2.1 The EVH1 domain of Ena/VASP proteins interacts with the WAVE complex.

To identify new binding partners of the EVH1 domain and potential regulators of Ena/VASP proteins, I made recombinant EVH1 domains of Mena, VASP and Evl with a GST-tag at their N-terminus. All the GST-tagged EVH1 domains could be expressed in bacteria and were readily purified from the soluble fraction in high yield (Figure 3.1).

I used the bacterially expressed GST-EVH1 domains of Mena, VASP and Evl as well as GST (control) to perform pull-down assays on HEK 293T cell lysates. Several proteins were specifically retained by the GST-EVH1 domains, but not by the GST negative control (Figure 3.2A). These proteins were identified by mass spectrometric analysis. A number of known FPPPP containing binding partners of EVH1 domains were found, including zyxin (Reinhard et al., 1995, Drees et al., 2000) and palladin (Boukhelifa et al., 2004). We also indentified a number of novel potential EVH1 binding proteins, including Zap3 (240 kDa), WAVE2 (68 kDa), Nap1 (125 kDa) and PIR121 (140 kDa) (Figure 3.2B).

For Zap3, a nuclear protein, no link to the actin cytoskeleton has been described. However, all other three potential EVH1 binding partners (WAVE2, Nap1 and PIR121) are part of the WAVE complex (Gautreau et al., 2004, Echarri et al., 2004, Innocenti et al., 2004, Leng et al., 2005). This indicates that Ena/VASP proteins may cooperate with the WAVE complex to regulate actin dynamics at the leading edge.

To verify the interaction between the EVH1 domain and components of the WAVE complex, I repeated my pull down assays using MVD7 cells, which are mouse embryonic fibroblasts that lack endogenous Mena/VASP and only express low levels of Evl (Bear et al., 2000). By using this cell line, the competition for binding between bacterially produced GST-EVH1 and the EVH1 domains of endogenous Ena/VASP proteins is reduced. Mass spectrometric analysis found that the GST-tagged EVH1 domain also retained Nap1 and PIR121 from MVD7 cells (Figure 3.2C). This assay did not, however, indentify any bands corresponding to WAVE2. The EVH1 pull-down assay using MVD7 cells was repeated one more time under more stringent conditions. Nap1 and PIR121 were also found to bind the GST-EVH1 in a phosphate-based buffer containing 300mM NaCl and 10% glycerol (Figure 3.2D). WAVE2 was also present albeit weakening in this more stringent condition. In contrast, Zyxin was always detected in my pull down assays (Figure 3.2).

It should be noted that Zap3 and WAVE2 were not readily detected in the pull-downs from MVD7 cells using a phosphate-based buffer containing 150 mM NaCl and 5% glycerol (Figure 3.2C). It is possible that due to the lower band intensity of Zap3 and WAVE2 (Figure 3.2A), only Zyxin, Nap1 and PIR121, were found as distinct bands in the EVH1 pull-down compared to the control pull-downs. The apparent difference in the intensity of the bands may either be due to the fact that more Nap1 and PIR121 compared to Zap3 and WAVE2 were pulled-down by EVH1 or that Nap1 and PIR121 have a higher affinity for the coomassie dye than Zap3 and WAVE2.

However, coomassie detectable levels of WAVE2 were pulled-down by GST-EVH1 from MVD7 cell lysates under more stringent conditions (Figure 3.2D). Additionally, C77080, a FPPPP motif-containing protein, was pulled down by GST-EVH1 that was not found in the other conditions (Figure 3.2D). These two findings can be explained by the reduced unspecific binding to GST and GST-EVH1 (compare Figure 3.2D to 3.2C) under the more stringent conditions. When comparing GST-EVH1 to GST alone,

bands corresponding to WAVE2 and C77080 may have been masked by other unspecific bands in the less stringent conditions. Given Nap1, PIR121 and WAVE2 are binding to GST-EVH1 under the more stringent conditions strengthens the idea that the WAVE complex is a *bona fide* interaction partner of the EVH1 domain of Ena/VASP proteins.

In my pull-down assays, five novel potential binding partners of the EVH1 domain were identified: Zap3 (240 kDa), WAVE2 (68 kDa), Nap1 (125 kDa), PIR121 (140 kDa) and C77080 (120 kDa). Zap3 contains multiple FPPPP motifs and is thought to serve as a scaffold protein for type 1 serine/threonine protein phosphatases (PP1s) and several RNA binding proteins within the nucleolus (Armstrong et al., 2004). C77080 also contains FPPPP motifs. Neither the cellular localisation nor its functions are known. The other three proteins belong to the WAVE complex, and Nap1 and PIR121 have been always detected in my pull down assays. Given the function of Ena/VASP proteins and the WAVE complex in regulating the actin cytoskeleton at the leading edge, I therefore decided to verify if the non-FPPPP containing proteins Nap1/PIR121 and the EVH1 domains of Ena/VASP proteins interact.

In order to confirm the mass spectrometric results for Nap1 and PIR121, I performed pull-down assays using HEK 293T cells overexpressing N-terminally GFP-tagged Nap1 or PIR121, and the bacterially produced GST-EVH1 domain of Mena. HEK 293T cells overexpressing GFP alone or the GFP-LIM3 domain of Tes (Boeda et al., 2007) were used as negative and positive controls respectively. Western blot analysis with a GFP antibody revealed that the GST-EVH1 domain of Mena but not GST alone retained GFP-tagged Nap1 and PIR121 from cell lysates that were overexpressed separately or co-overexpressed (Figure 3.3). Together, these results suggest that Nap1 and PIR121, which both lack a classical FPPPP motif, may provide a link between Ena/VASP proteins and the WAVE complex.

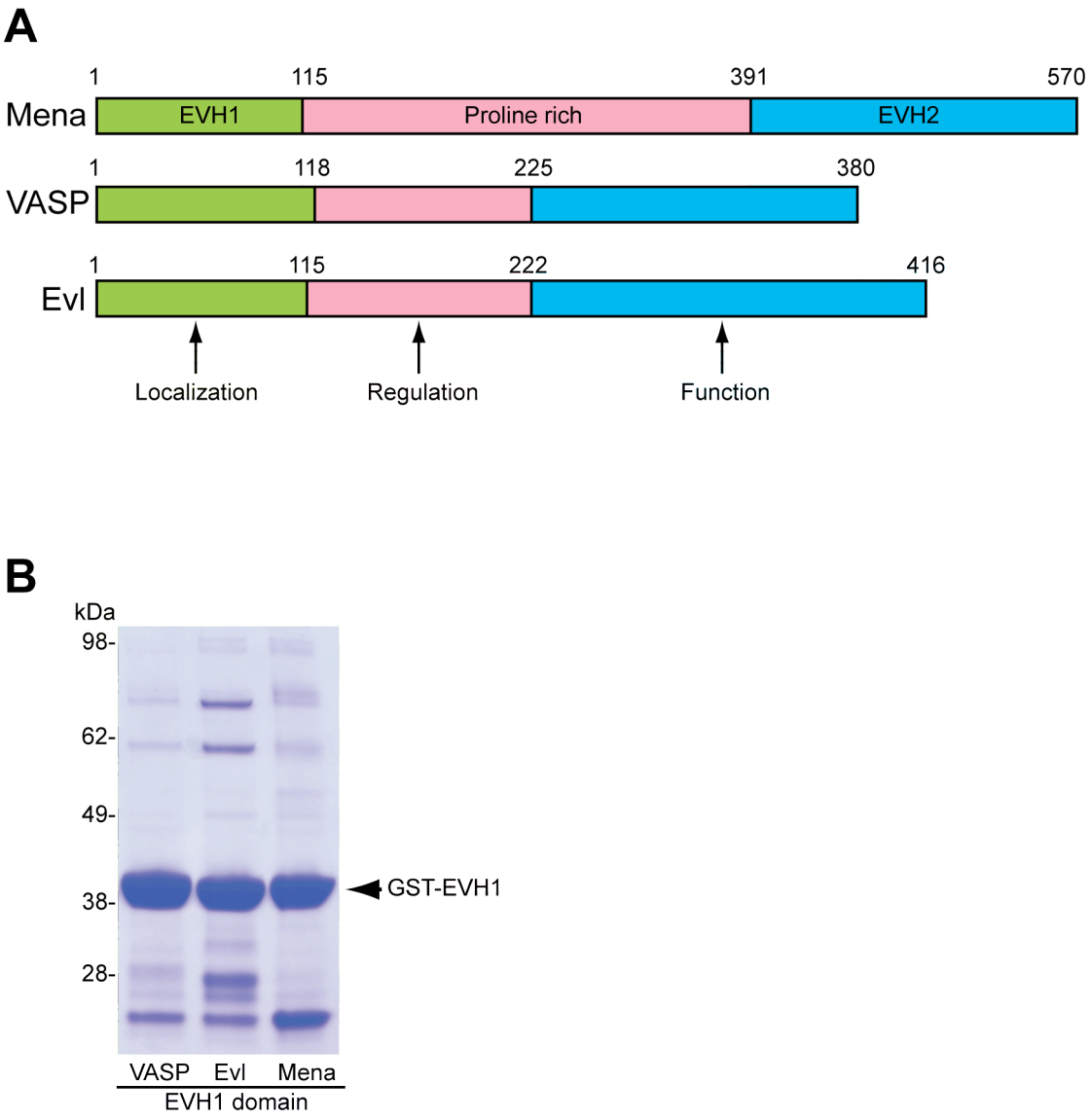

Figure 3.1 Purification of recombinant GST- EVH1 domains of Ena/VASP proteins.
A. Schematic representation of Ena/VASP proteins. The N-terminal EVH1 domain (green) and the C-terminal EVH2 domain (blue) are separated by the middle proline rich region (pink). Numbers indicate the first and last residue of each domain. **B.** Coomassie stained gel illustrating the successful production and purification of soluble GST-EVH1 domains of Mena, VASP and Evl in bacteria.

A

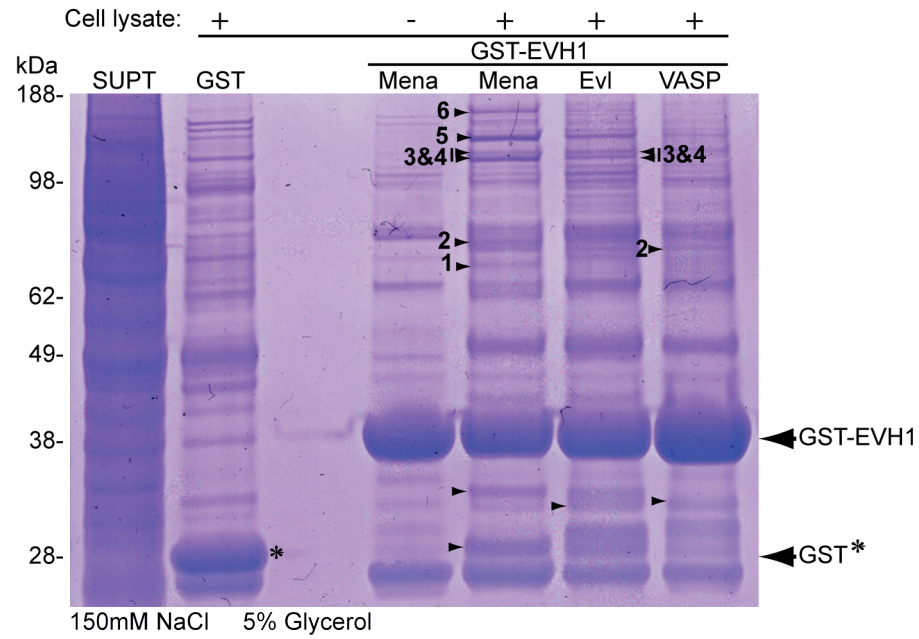

B Results from Mass spectrometric analysis:

No.	Protein	Size (kDa)	Proline Rich	Retained by	EVH1 Interaction
1	WAVE2	68	Yes	Mena	unknown
2	Zyxin	83	Yes	Mena and VASP	known
3	Palladin	90	Yes	Mena and Evl	known
4	Nap1	125	No	Mena and Evl	unknown
5	PIR121	140	No	Mena	unknown
6	Zap3	240	Yes	Mena	unknown

Figure 3.2 The non-FPPPP containing proteins Nap1 and PIR121 are potential binding partners of Ena/VASP proteins.
A. Coomassie stained gel showing pull-downs from HEK 293T cell lysates using GST-EVH1 domains. The protein bands that are indicated by small black arrowheads were sent for mass spectrometric analysis. Identified proteins are indicated with numbers. Pull-downs were performed in a PBS buffer containing 150 mM NaCl and 5% glycerol. **B.** Table of proteins from **A** that were identified by mass spectrometric analysis.

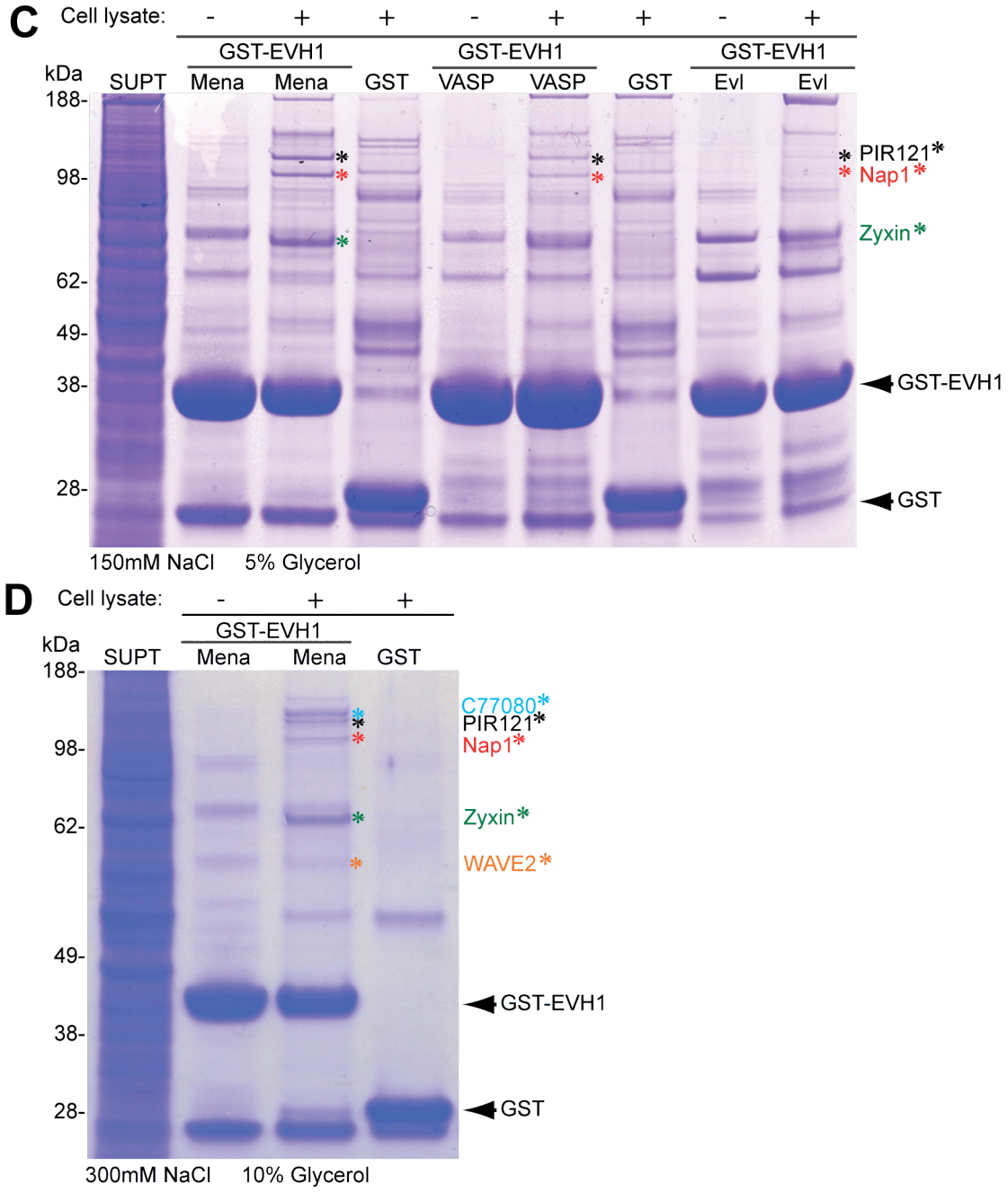

C. Coomassie stained gel showing pull-downs from MVD7 cell lysates using the GST-EVH1 domain of Ena/VASP proteins. Pull downs were performed in a PBS buffer containing 150 mM NaCl and 5% glycerol. Coloured asterisks indicate protein bands that were identified by mass spectrometric analysis.
D. Coomassie stained gel of GST-EVH1 pull-down from MVD7 cell lysates using more stringent conditions (PBS buffer containing 300 mM NaCl and 10% glycerol). Nap1 (red asterisk), PIR121 (black asterisk), WAVE2 (yellow asterisk), Zyxin (green asterisk) and C77080 (blue asterisk) were identified by mass spectrometric analysis. In all panels, the large black arrowheads indicate GST or the GST-EVH1 domain of Ena/VASP proteins. 4% of the cell lysate used in each pull down was used as the input.

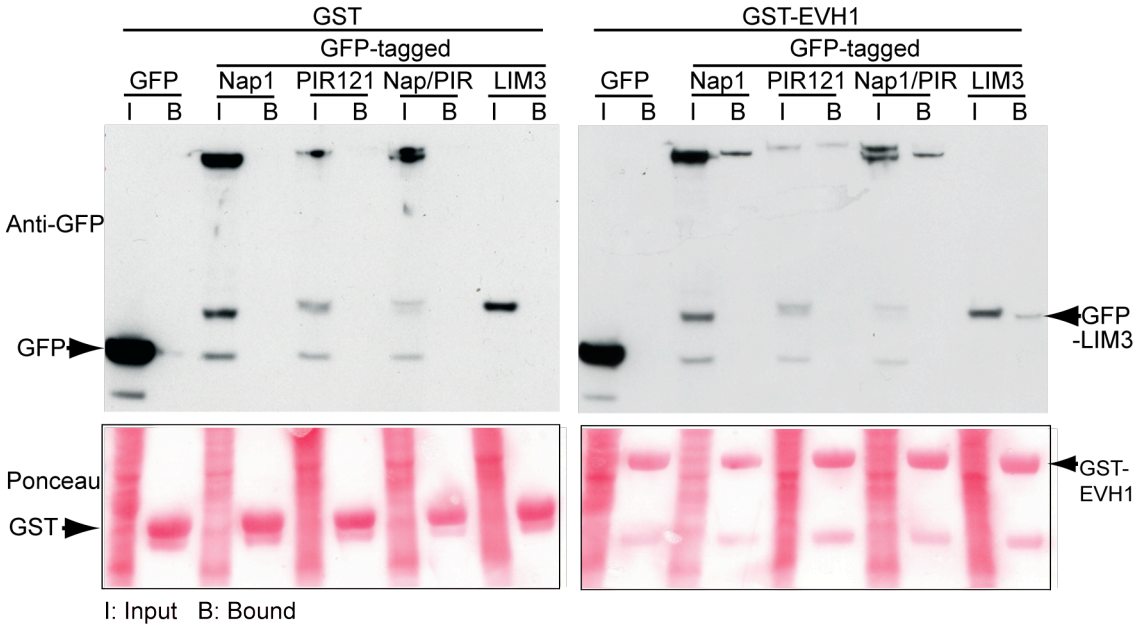

Figure 3.3 The EVH1 domain of Mena retains GFP-Nap1 and GFP-PIR121 from HEK 293T cell lysates.
Immunoblot analysis of pull-downs using GST-EVH1 domain of Mena (right panel) or GST alone (left panel) incubated with HEK 293T cell lysates containing overexpressed GFP-Nap1 and GFP-PIR121. GFP alone and GFP-LIM3 domain of Tes were used as controls. The input (I) and bound (B) samples with the respective GFP-tagged proteins are indicated. The Ponceau S staining shows equivalent amounts of GST and GST-EVH1 domain of Mena were present on the resin.

3.2.2 Nap1/PIR121 do not interact directly with the EVH1 domain of Mena

To test if the interactions between the EVH1 domain and Nap1/PIR121 are direct, I carried out an *in vitro* pull-down assay using recombinant proteins. I expressed and purified full-length Nap1 and PIR121 with either a GST- or HIS-tag at their N-terminus from *E. coli*. The expression of these proteins in bacteria was problematic, presumably at least in part due to the size of the proteins. However, after testing different *E. coli* strains and expressing under different conditions, I did obtain small amounts of soluble full length Nap1 and PIR121 by performing IPTG induced protein expression in *E. coli* BL21 (DE3) Rosetta strain. Although full length Nap1 and PIR121 with either a GST- or HIS-tag were soluble, a lot of breakdown products of the full-length proteins were observed (data only shows the GST-tagged Nap1 and PIR121 in figure 3.4 A). In the end, I decided to use N-terminally GST-tagged Nap1 and PIR121 instead of the HIS-tagged versions for the following experiments as they had better expression.

In the *in vitro* pull-down assays, HIS-EVH1 domain of Mena or HIS-Grb2 (as negative control) was bound to the resin and GST-Nap1/PIR121, GST (as negative control) or GST-LIM3 domain of Tes (as positive control) was added. The coomassie stained gel revealed that GST-LIM3, but not GST binds directly to HIS-EVH1 as expected. However, no convincing binding of HIS-EVH1 to GST-Nap1 or GST-PIR121 was detected (Figure 3.4A). This suggests that the interaction between Nap1/PIR121 and the EVH1 domain of Mena is indirect. In order to confirm this result, I performed western blot analysis on the same samples. Also using specific antibodies no interaction between GST-Nap1 or GST-PIR121 and the HIS-EVH1 domain of Mena was detected (Figure 3.4B). However, I detected binding of a fragment of PIR121 to the EVH1 domain (Figure 3.4B). The nature of this fragment, which may be an artefact, is unknown. However, EVH1 pull-down assays on HEK 293T cell lysates overexpressing GFP-PIR121 deletion mutant (residue 1-536) showed that GST-EVH1 was able to retain this GFP-PIR121 deletion mutant from cell lysates (data not shown). Based on these observations, it suggests that PIR121 may actually contain an atypical EVH1 binding site in its N-terminus, which is hidden in the full-length protein. However, subsequent *in vitro* binding assays with the N-terminal mutant of PIR121 (residue 1-536) produced in bacteria confirmed that this was not the case, as no binding to the EVH1 domain of Mena was detected using western blot analysis with GST antibody (data not shown).

Given the fact that obtaining soluble recombinant HIS or GST-tagged Nap1 and PIR121 from bacteria was problematic, I repeated the *in vitro* pull-down assays using a Nap1 and HIS-tagged PIR121 protein complex that was purified from insect cells by the protein expression facility at Cancer Research UK (Figure 3.4C). Although no breakdown products were observed, the purified protein complex was unstable as it rapidly precipitated after purification (data not shown). Consequently, the complex had to be used in the *in vitro* EVH1 pull-down assays on the same day when it was purified. In this pull-down assay, GST alone and HIS-LIM3 domain of Tes were used as controls. Western blot analysis with a HIS-tag antibody showed no binding of the HIS-tagged Nap1/PIR121 complex to the GST-EVH1 domain of Mena (Figure 3.4D). This data is in line with the results from the *in vitro* pull-down assays using bacterially produced Nap1 and PIR121. Although the quality of recombinant Nap1 and PIR121 used in the *in vitro* pull-down assays were not great, overall, the results suggest that both, Nap1 and PIR121 do not bind directly to the EVH1 domain of Ena/VASP proteins.

Figure 3.4

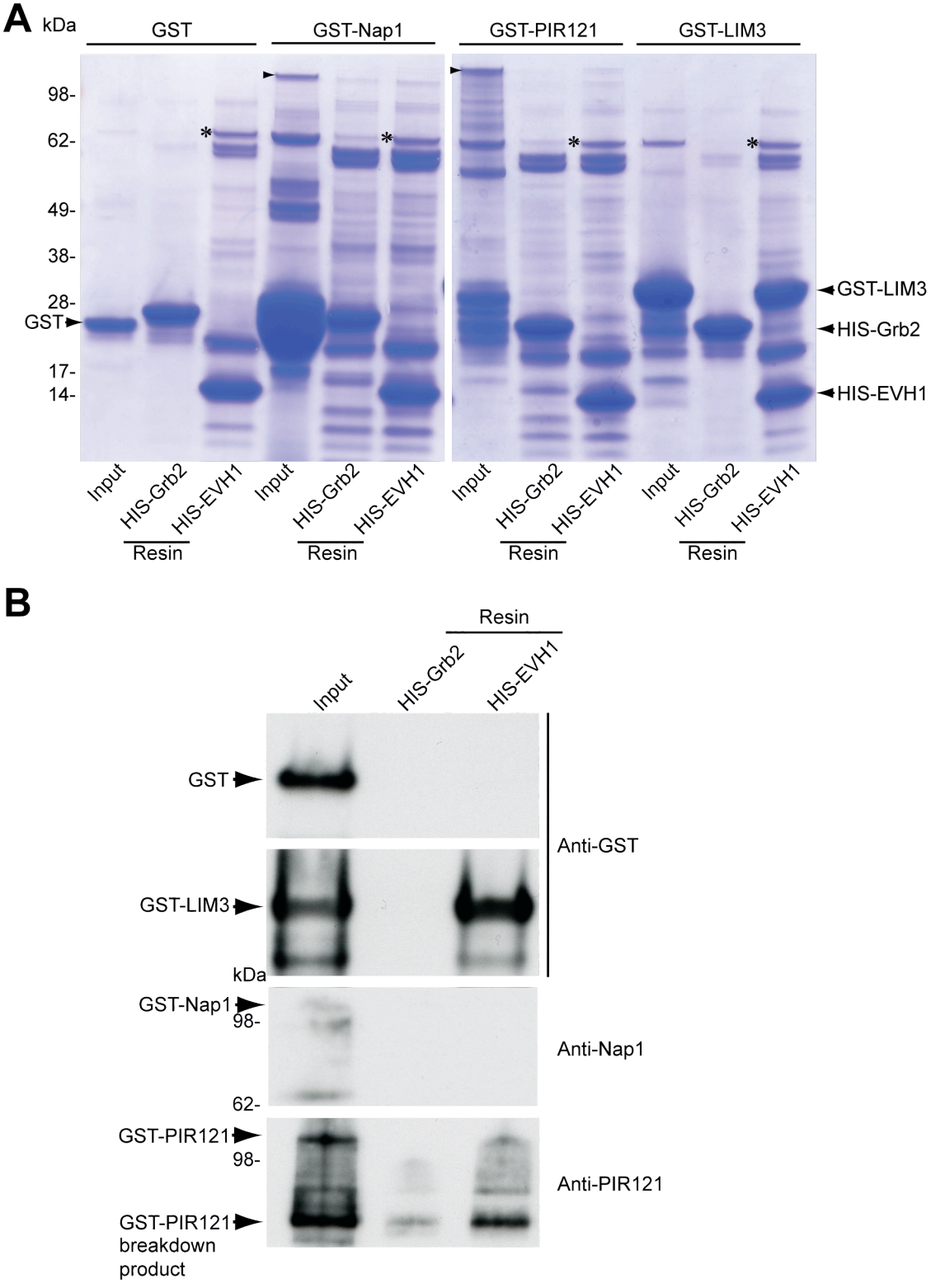
A
kDa
GST
GST-Nap1
GST-PIR121
GST-LIM3
98-
62-
49-
38-
28-
GST
17-
14-
GST-LIM3
HIS-Grb2
HIS-EVH1
Input
HIS-Grb2
HIS-EVH1
Resin
B
Resin
Input
HIS-Grb2
HIS-EVH1
GST
GST-LIM3
Anti-GST
kDa
GST-Nap1
98-
62-
Anti-Nap1
GST-PIR121
98-
GST-PIR121
breakdown
product
Anti-PIR121

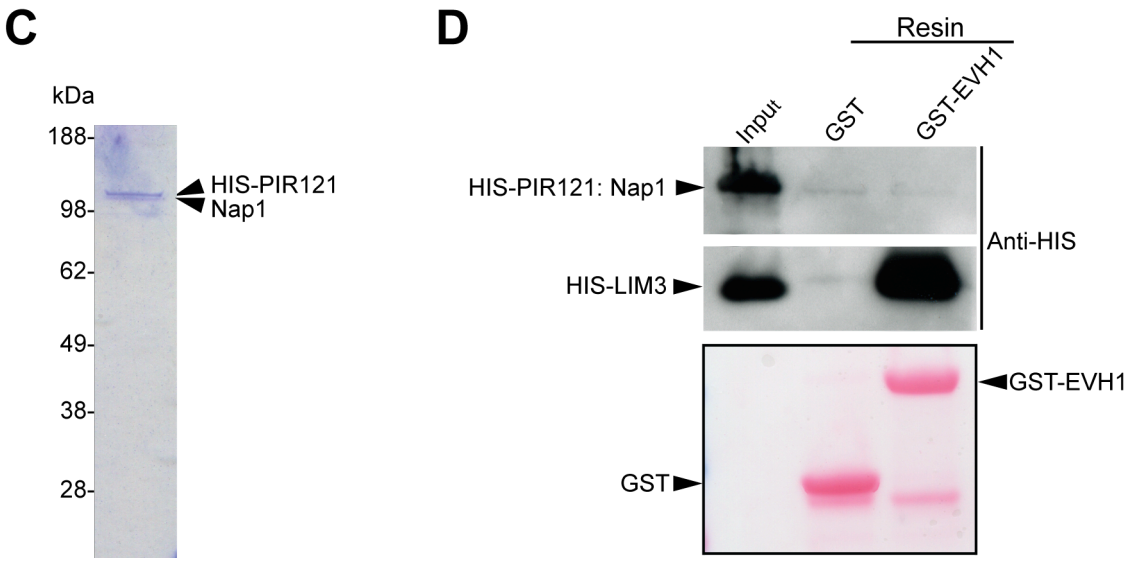

Figure 3.4 Nap1 and PIR121 do not bind directly to the EVH1 domain of Mena. **A.** Coomassie-stained gel of *in vitro* pull-downs using HIS-EVH1 domain of Mena and GST-Nap1/GST-PIR121. HIS-EVH1 domain of Mena and HIS-Grb2 (control) were pre-incubated with resin. GST-Nap1, GST-PIR121, GST alone or GST-LIM3 was added to the resin. GST-Nap1 and GST-PIR121 (indicated by small arrowheads) do not interact with the HIS-EVH1 domain of Mena or HIS-Grb2. Asterisks indicate bands corresponding to bacterial proteins that are present in all HIS-EVH1 fractions. Note that this band is not specific for GST-Nap1 or GST-PIR121, since it can also be observed in the GST and GST-LIM3 lanes. **B.** The results shown in **A** were confirmed by western blot analysis. The input and HIS-tagged proteins, which were pre-incubated with resin, are indicated at the top of the panels. GST and GST-tagged proteins are indicated on the left of the panels. Antibodies are indicated on the right of the panels. PIR121 breakdown product that can bind the EVH1 domain of Mena is indicated. **C.** Coomassie stained gel of purified recombinant HIS-tagged Nap1/PIR121 protein complex produced in insect cells. **D.** Western blot analysis of *in vitro* pull-downs using HIS-tagged Nap1/PIR121 protein complex produced in insect cells. As bacterially produced Nap1 and PIR121, the insect cell produced proteins do not bind the EVH1 domain of Mena. The input and GST-tagged proteins, which were pre-incubated with resin, are indicated at the top of the panels. HIS-tagged Nap1/PIR121 and HIS-tagged LIM3 domain of Tes (control) are indicated on the left of the panels. Anti-HIS antibody is indicated on the right of the panels. The Ponceau S stain shows equivalent amounts of GST and the GST-EVH1 domain of Mena was present on the resin.

3.2.3 Abi mediates the interaction between the EVH1 domain and the WAVE complex

My analysis reveals that Nap1 and PIR121 do not directly interact with the EVH1 domain of Mena. However, the pull-down of three subunits of the WAVE complex (Nap1, PIR121 and WAVE2) by the EVH1 domain suggests that the interaction may be mediated by another component of the WAVE complex. A potential candidate is Abi. Previous biochemical studies have demonstrated that Abi binds directly to the EVH1 domains of Mena and VASP through its C-terminal proline rich region (Tani et al., 2003, Dittrich et al., 2010). However, none of these studies have mapped the EVH1 binding site in Abi, as Abi does not contain classical FPPPP motifs.

Curiously, Abi was not detected by coomassie staining in GST-EVH1 pull-down assays (Figure 3.2). However, the stability of the WAVE complex and the 1:1:1:1:1 stoichiometry of its components suggested that Abi should have been retained if Ena/VASP proteins bind to the WAVE complex (Eden et al., 2002). To test if Abi was present in my previous pull downs assays, I performed western blot analysis using antibodies that recognise individual WAVE complex components. Using these antibodies, additional to Nap1 and PIR121 that were detected by mass spectrometry, I also found that Abi was associated with the EVH1 domain of Mena (Figure 3.5B). Since the interaction between coomassie dyes and proteins are dependent on a variety of factors such as the overall composition of a protein and it is known that the coomassie staining of Abi is less efficient than other components of the WAVE complex (personal communication with Dr Michael Rosen), it is likely that the amount of Abi that was pulled down could only be detected by western blot analysis, but not by coomassie staining.

To test if the WAVE components bind to the same site on EVH1 as the FPPPP-containing proteins and Tes, I pre-incubated the EVH1 domain with the FPPPP region of zyxin (human zyxin polyproline region, residues 61-141) or the LIM3 domain of Tes (Boeda et al., 2007). The results showed that the interaction between EVH1 and the components of the WAVE complex as well as Zyxin were inhibited by GST-FPPPP and GST-LIM3 (Figure 3.5A, B). This suggests that the components of the WAVE complex, Zyxin and Tes all compete for the same binding site on the EVH1 domain of Ena/VASP protein.

Since Nap1 and PIR121 do not directly bind to the EVH1 domain, I set up an *in vitro* pull-down assay to examine if Abi acts as a bridging protein to mediate the interaction between the WAVE complex and Ena/VASP proteins. There are three mammalian Abi isoforms Abi1, Abi2 and Abi3 (Hirao et al., 2006). As all three isoforms share similar domain organisation and associate with the WAVE complex. I only used the human Abi1 isoform, which I designated as Abi. Full-length soluble recombinant Abi was produced in bacteria with an N-terminal HIS-tag (Figure 3.5C). Pull-down assays using bacterially produced proteins revealed that the GST-EVH1 domain of Mena but not GST alone interacts directly with HIS-Abi. Moreover, Nap1, which does not interact directly with EVH1, but is known to interact directly with Abi (Yamamoto et al., 2001), can bind the Abi-EVH1 complex (Figure 3.5D). Together, my data indicate that Abi acts as the link between Mena and the rest of the WAVE complex.

The sequences of the EVH1 domains of Ena/VASP proteins are very similar, although not totally identical (Figure 3.6A). Given Tes only binds Mena and not VASP and Evl (Boeda et al., 2007), I wanted to investigate if Abi, is a specific binding partner of Mena or if it also binds to VASP or Evl. To address this question, I performed an *in vitro* pull-down assay using bacterially produced GST-EVH1 domains of Mena, VASP and Evl together with HIS-Abi. GST was used as a negative control. The coomassie stained gel revealed direct interactions between Abi and the GST-tagged EVH1 domains of all three mammalian Ena/VASP isoforms but not GST (Figure 3.6B). These results indicate that Abi is not a specific Mena interactor. This is consistent with the previous pull-down assays demonstrating that Nap1 and PIR121 were retained from cell lysates by the EVH1 domains of all three mammalian Ena/VASP proteins (Figure 3.2).

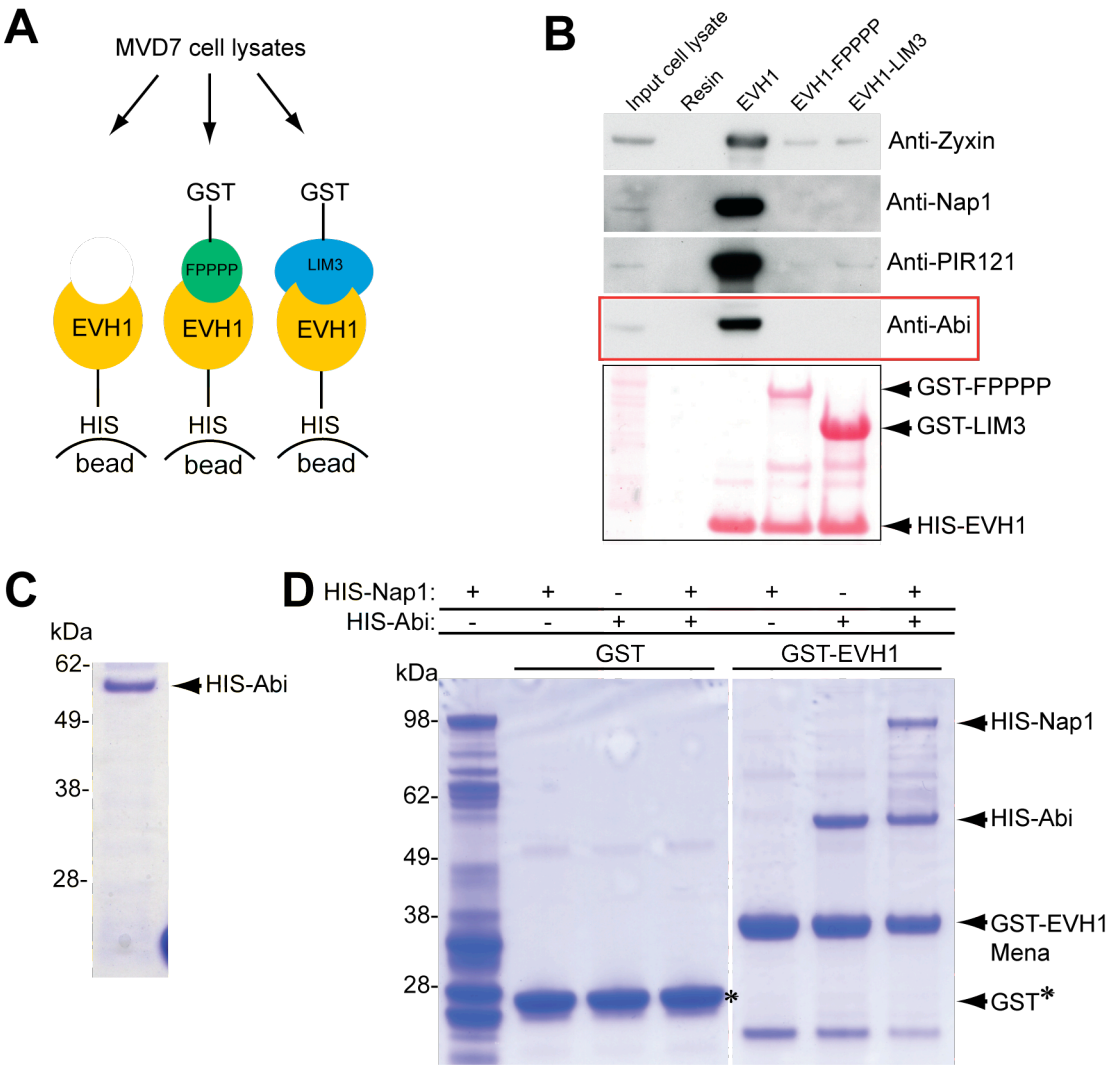

Figure 3.5 Abi binds directly to the EVH1 domain.
A. Schematic representation of the competitive binding assay that is shown in **B**. **B.** Western blot analysis of GST-EVH1 pull-downs shows that endogenous Abi is only retained from MVD7 cell lysates together with Nap1, PIR121 and Zyxin (control) by the EVH1 resin not by the resins that were pre-incubated with the EVH1:FPPPP or EVH1:LIM3 complexes. The input and pull-downs are indicated at the top of the panels. The Ponceau S panel shows proteins that are on the resins. **C.** Coomassie stained gel shows the bacterially produced HIS-Abi. **D.** Coomassie stained gel of *in vitro* pull-down assays demonstrating that Nap1 can only interact with the EVH1 domain of Mena in the presence of Abi. Resins were pre-incubated with either GST (control) or GST-EVH1. The pre-bound resins were then incubated with either HIS-Abi or HIS-Nap1. The GST-EVH1:HIS-Abi bound resins were incubated with HIS-Nap1. The presences of HIS-tagged proteins are indicated at the top of the gel. The large arrowheads indicate the bands representing HIS-Nap1, HIS-Abi as well as the GST-EVH1 domain of Mena and GST respectively.

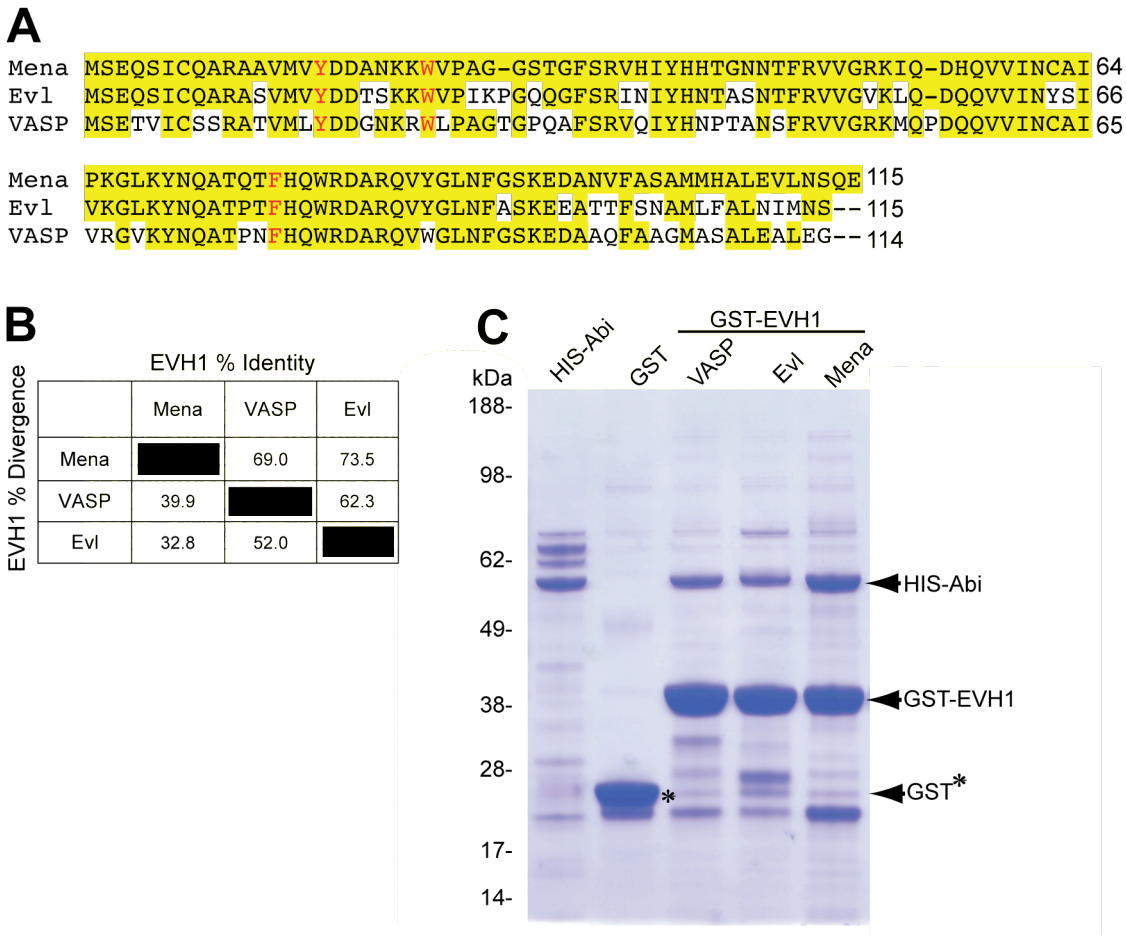

Figure 3.6 Abi does not bind specifically to Mena.
A. Sequence alignment of the EVH1 domains of human Mena, VASP and Evl. Conserved residues are highlighted in yellow. Gaps are indicated by -. The three conserved aromatic residues that are essential for FPPPP binding are indicated in red. **B.** The table lists the sequence identity and divergence between the EVH1 sequences of human Mena, VASP and Evl. ClustalW2-Multiple Sequence Alignment (EMBL-EBL) was used to generated both **A** and **B.** **C.** A coomassie stained gel of an *in vitro* pull-down assay demonstrating that Abi interacts directly with the EVH1 domains of Mena, VASP and Evl. HIS-Abi, GST, and GST-tagged proteins are indicated at the top of the gel. Large black arrowheads indicate the protein bands corresponding to HIS-Abi, GST and the different GST-EVH1 domains.

3.3 Summary

Using EVH1 pull-down assays combined with mass spectrometry, I identified the WAVE complex components Nap1 and PIR121 as potential binding partners for the EVH1 domain of Ena/VASP proteins. However, data from *in vitro* pull-down assays showed that this interaction is indirect and actually dependent on Abi, another component of the WAVE complex, which also lacks a classical FPPPP motif. My data is consistent with published data, which demonstrated a direct interaction between Abi and Ena/VASP proteins (Dittrich et al., 2010, Tani et al., 2003). Moreover, in contrast to Tes, which only binds Mena, Abi can interact with all three mammalian Ena/VASP proteins *in vitro*. These results suggest that Abi may act as a linker to mediate an interaction between Ena/VASP proteins and the rest of the WAVE complex.

Chapter 4. Identification of the EVH1 binding site in Abi

4.1 Introduction

My data suggests Abi, which is an integral component of the WAVE complex interacts directly with the EVH1 domain of Ena/VASP proteins *in vitro.* Both, the WAVE complex and Ena/VASP proteins are key regulators of actin dynamics at the leading edge during cell migration. I wondered if uncoupling the interaction of Ena/VASP proteins from the WAVE complex would therefore affect the actin-based motility of the cell. In order to study the physiological significance of the Abi-EVH1 interaction *in vivo,* I aimed to make a mutant Abi that could not bind the EVH1 domain of Ena/VASP proteins but could still incorporate into the WAVE complex. The first stage of this goal required the identification of the EVH1 binding site in Abi.

4.2 Results

4.2.1 The C-terminal proline rich region of Abi binds the EVH1 domain of Ena/VASP proteins

To identify the EVH1 binding site in Abi, I generated a series of deletion mutants. The same boundaries for the deletion mutants were selected as in previous work that partially mapped the EVH1 binding region in Abi (Tani et al., 2003) (Figure 4.1A). N-terminal GST-tagged Abi deletion mutants were expressed and purified from bacteria (Figure 4.1B, C, D). In contrast to the expression of GST-Abi-N-term-PR1, which was not detected by western blot analysis with GST antibody, other GST-tagged Abi deletion mutants were expressed and soluble, although their expression levels were somewhat variable (Figure 4.1B, C, D). Most of the recombinant GST-tagged Abi deletion mutants, however, were generally less stable than full length Abi as precipitation of Abi deletion mutants was often observed (data not shown). These recombinant Abi deletion mutants, together with full length Abi were used in EVH1 in vitro pull-down assays with GST alone as a control. The results demonstrated that the HIS-EVH1 domain of Mena bound full length Abi and only the GST-tagged Abi deletion mutants containing the proline rich region (PR1+PR2 or PR2) (Figure 4.2). These results suggest the EVH1 binding region of Abi may also involve a proline rich motif.

The problem of producing stable recombinant Abi deletion mutants in significant qualities in bacteria led to difficulties in narrowing down the essential region for EVH1

binding within the proline rich regions of Abi. Interestingly, far western approaches using the EVH1 domain on peptide arrays were successful used to initially identify the FPPPP motif in ActA from *Listeria* as the binding site for the EVH1 domain of Ena/VASP proteins (Niebuhr et al., 1997). Given this I decided to use this approach to try to identify the EVH1 binding site in Abi. A peptide array containing a series of overlapping peptides of 20 amino acids in length that covered the full length of Abi was generated by the peptide service facility at Cancer Research UK (Figure 4.3A). The overlapping peptides were spaced one amino acid residue apart. The peptide array was probed with bacterially produced GST-EVH1 domain of Mena. The interaction between the GST-EVH1 domain of Mena and binding peptides was subsequently detected by GST antibodies, followed by secondary antibodies and ECL detection (Figure 4.3B). As shown in Figure 4.4A, the black spots represent peptides that bound to the GST-EVH1 domain of Mena. These peptides covered only the PR2 region, but not the PR1 region of Abi. To confirm this data, I repeated the far western analysis using the GST-EVH1 domain of Mena and GST alone (control) on a peptide array consisting of a series of overlapping 20 residue peptides corresponding to the residues 320-415 of Abi, which contains both PR1 and PR2 regions. Again, the overlapping peptides in this peptide array were spaced one amino acid apart. The same peptides, which were shown to bind EVH1 in the previous experiment, were detected by probing with the GST-EVH1 domain of Mena but not GST (Figure 4.4B). Discontinuous detections within the overlapping peptides in the potential EVH1 binding site of Abi were observed in both experiments (Figure 4.4C). These gaps in signal could be due to errors or defects that occurred during peptide synthesis. Taken together, the far western analyses of both peptide arrays indicate that Abi interacts with the EVH1 domain of Ena/VASP proteins through residues 352-394 in its PR2 region. The results obtained from these far western experiments are consistent with my data from the *in vitro* pull-down assays as well as the previously published data from yeast two-hybrid screening (Tani et al., 2003).

Curiously, it has been shown that an extended WIP sequence (residue 454-459 and 475-478) and a central polyproline rich motif are essential for binding to the WH1 domain of WASP family proteins (Peterson et al., 2007, Zettl and Way, 2002, Volkman et al., 2002). Given the binding site in Abi I identified appears to cover 43 amino acid residues, it may be that Abi binds the EVH1 domain of Ena/VASP proteins in a similar fashion to the WIP and WASP family interaction

The EVH1 domains of all three mammalian Ena/VASP proteins are highly conserved (Figure 3.6A, B). In order to test if Abi binds to the EVH1 domains of VASP and Evl in a similar fashion to that of the EVH1 domain of Mena, I performed far western analysis using the GST-EVH1 domains of Mena, VASP, and Evl on individual peptide arrays consisting of overlapping 20 residue peptides covering the residues 320-415 of Abi. Although similar peptide binding patterns were observed for the three different GST-EVH1 domains, these peptide-binding patterns were not identical (Figure 4.5). The difference in peptide binding patterns for different GST-EVH1 domains may reflect variation in peptide binding affinities. My results suggest that the EVH1 domains of all three mammalian Ena/VASP proteins interact with Abi in a similar fashion.

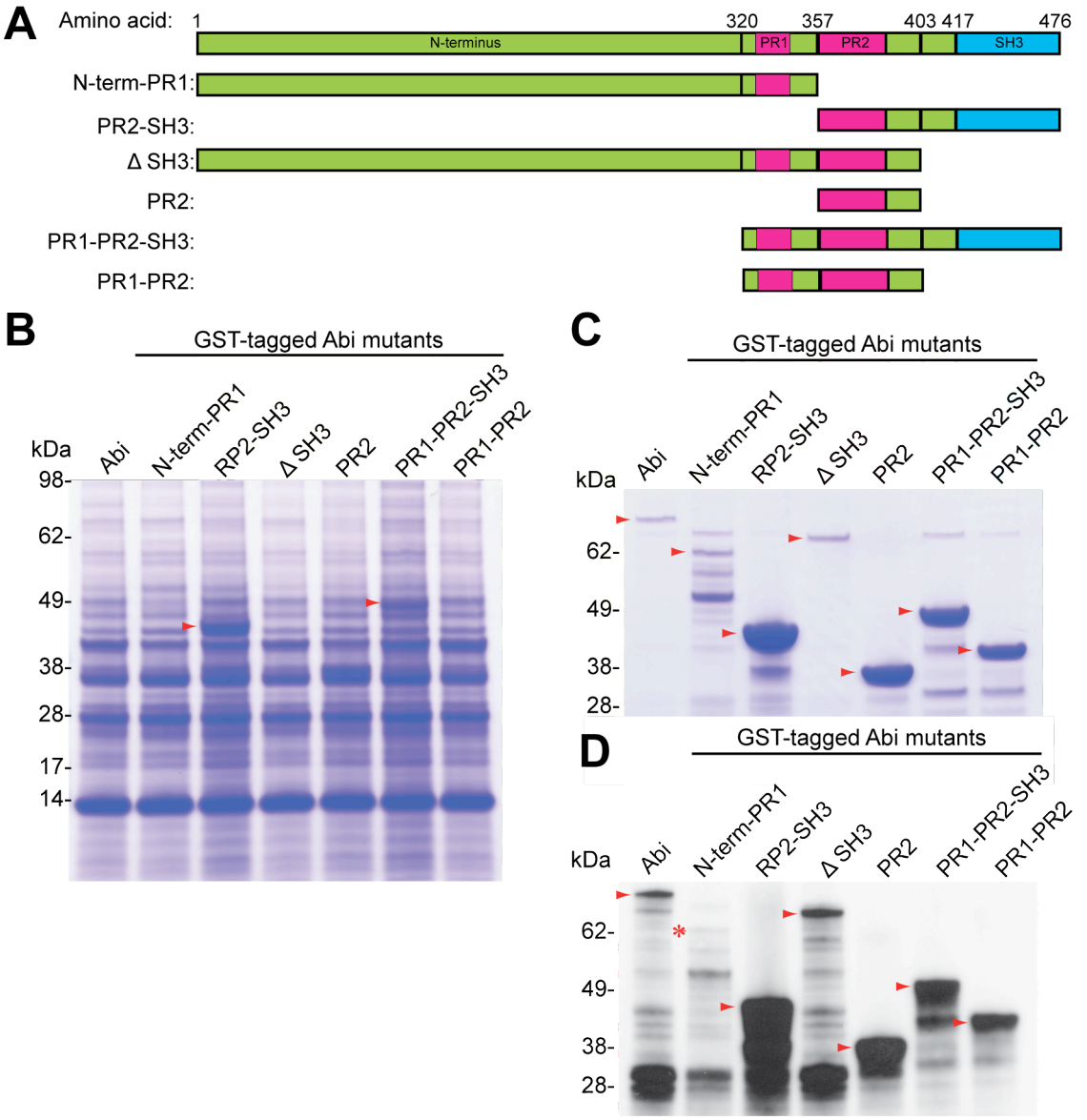

Figure 4.1 Generation deletion mutants of Abi.
A. Schematic representation of Abi and the deletion mutants that were used to map the EVH1 binding site. The PR1 and PR2 regions (pink) and SH3 domain (blue) are indicated. The corresponding name of each deletion mutant is shown on the left. **B.** Coomassie-stained gel of soluble fractions of GST-tagged Abi and Abi deletion mutants produced in bacteria indicates that except for GST-tagged PR2-SH3 and PR1-PR2-SH3 (red arrows) no other recombinant proteins could be clearly detected. **C.** Coomassie-stained gel of GST-tagged Abi and Abi deletion mutants purified from the soluble fraction on glutathione beads (red arrows). **D.** Western blot analysis confirms the bands indicated by red arrows in **C** (except GST-Abi-N-term-PR1) are GST-tagged Abi and its deletion mutants (red arrows). GST-Abi-N-term-PR1, which was not detected by GST antibody, is indicated by red asterisk.

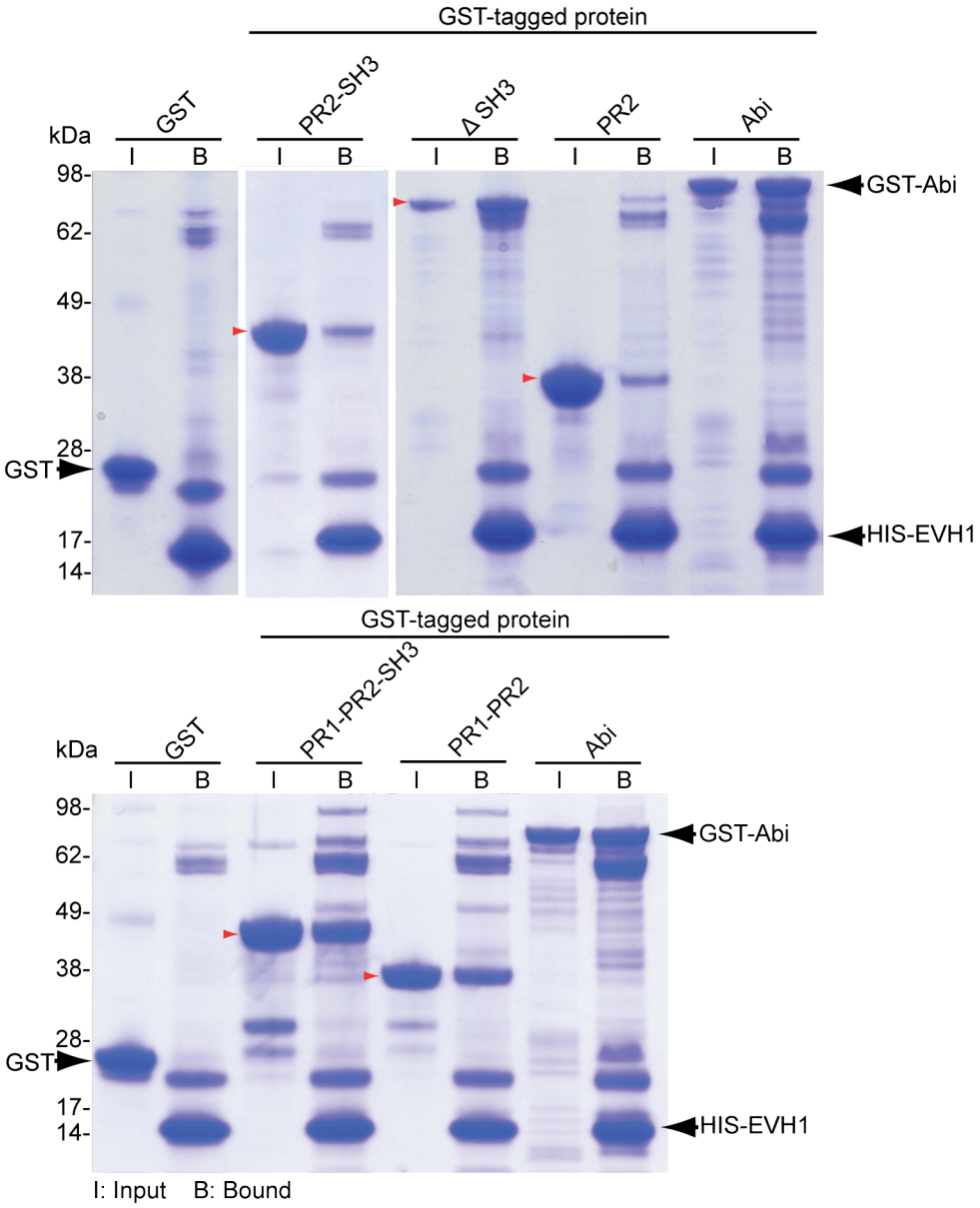

Figure 4.2 The proline rich region of Abi is essential for EVH1 binding.
Coomassie stained gels of pull-down assays using the indicated GST-tagged Abi deletion mutants and GST with HIS-EVH1 domain of Mena as a resin. Only the GST-tagged Abi mutants containing both PR1 and PR2 regions bound strongly to the EVH1 domain of Mena. The input (I) and bound (B) samples of the respective GST-tagged inputs are indicated at the top of the gel. Red small arrowheads indicate the bands representing GST-tagged Abi mutants. Black arrowheads at the side of the gels indicate the bands representing GST, GST-Abi and HIS-EVH1 domain of Mena (resin).

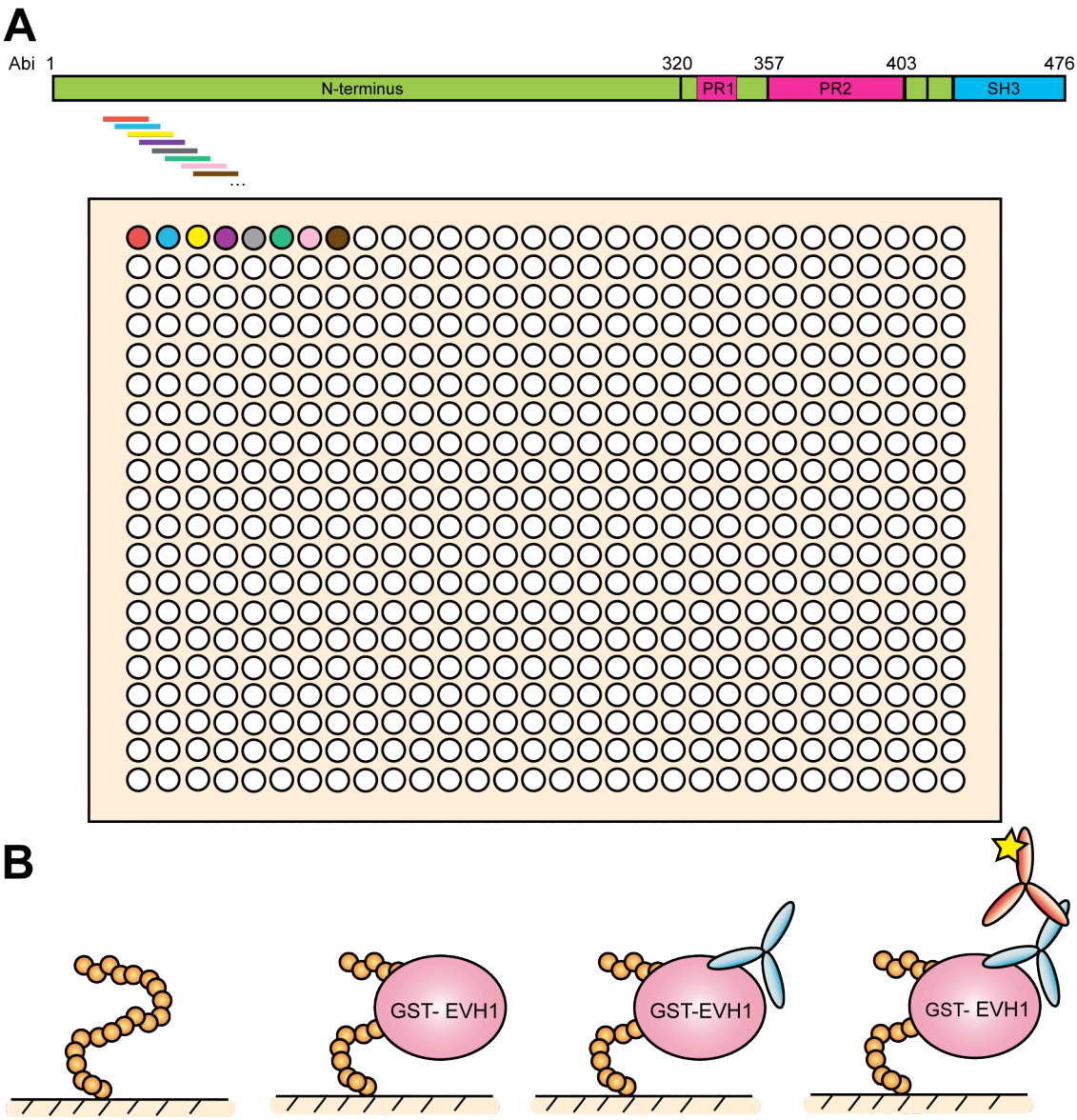

Figure 4.3 Schematic representation of the far western approach used to map the EVH1 binding site in Abi.
A. Overlapping peptides corresponding to the amino acid sequence of Abi were synthesised on a cellulose membrane. Each peptide consists of 20 residues displaced by one residue starting with amino acids 1-20 of Abi at position 1 on the array and ending with amino acids 457-476 at position 457. **B.** The peptide array was probed with GST-EVH1 domain of Mena. The potential interactions between the peptides and the EVH1 domain were subsequently detected by immunoblot using anti-GST (blue), followed by antibody conjugated to HRP (orange).

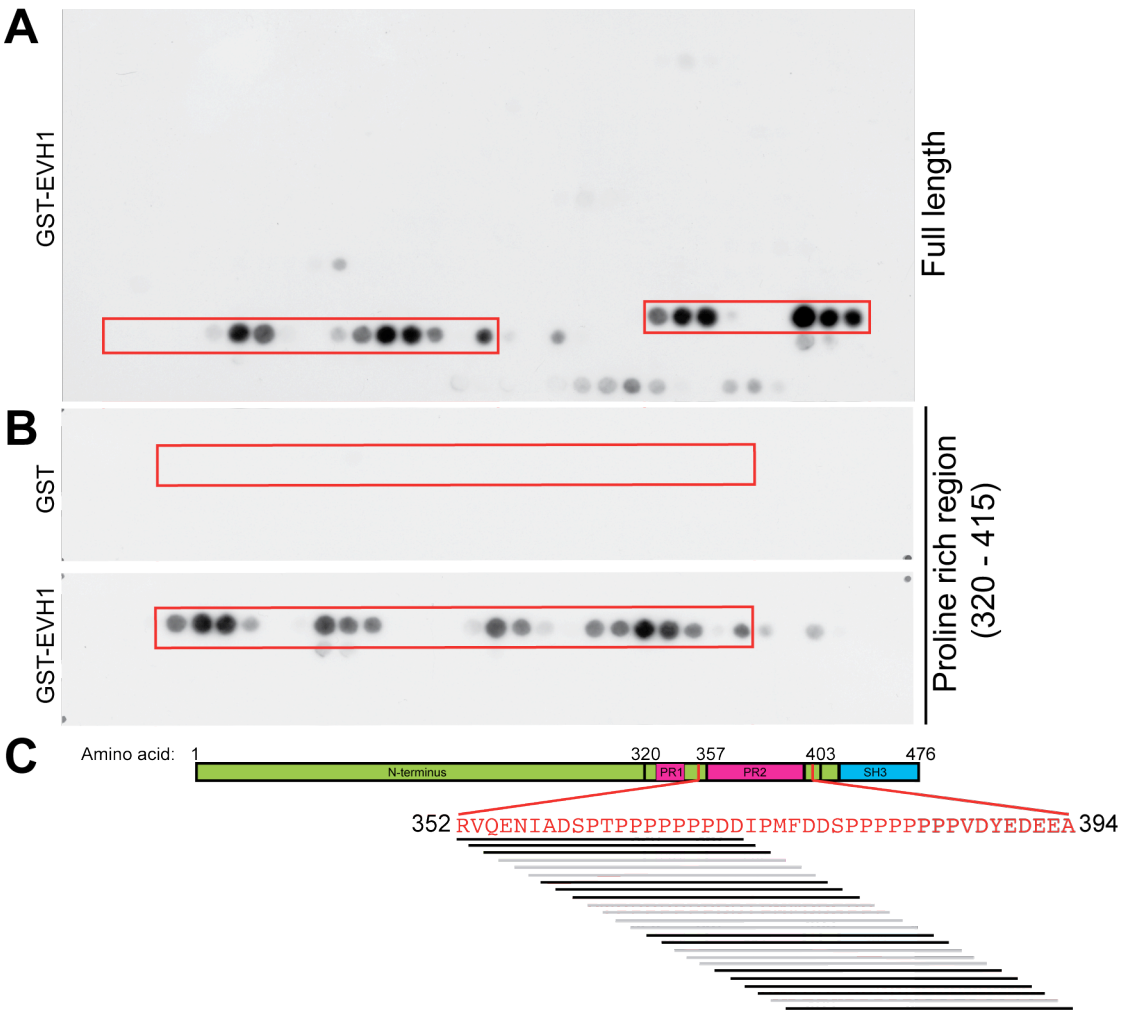

Figure 4.4 Residues 352-394 of Abi bind the EVH1 domain of Mena.
A. Far western analysis on a peptide array of the overlapping peptides that cover the full length of Abi. The black spots identify the peptides that interact with the GST-EVH1 domain of Mena. The spots that cover the proline rich region (residues 352-394) of Abi are highlighted in the red box **B.** Far western analyses of peptide arrays consisting of overlapping peptides covering residues 320-415 of Abi. The black spots represent the peptides that bound the GST-EVH1 domain of Mena. No black spots were observed on the peptide array that had been probed with GST. Red boxes in both arrays indicate the positions of the peptides that cover the proline rich region of Abi (residues 352-394). **C.** Schematic representation of the peptides of Abi that bind the EVH1 domain of Mena. The sequence of the EVH1 binding site in Abi is indicated in red. Each line represents a peptide of 20 amino acids, which partially covers the EVH1 binding site in Abi. The intensities of the lines from darkest (black) to lightest (light grey) reflect the binding efficiencies of the EVH1 domain to the different peptides from strongest to weakest.

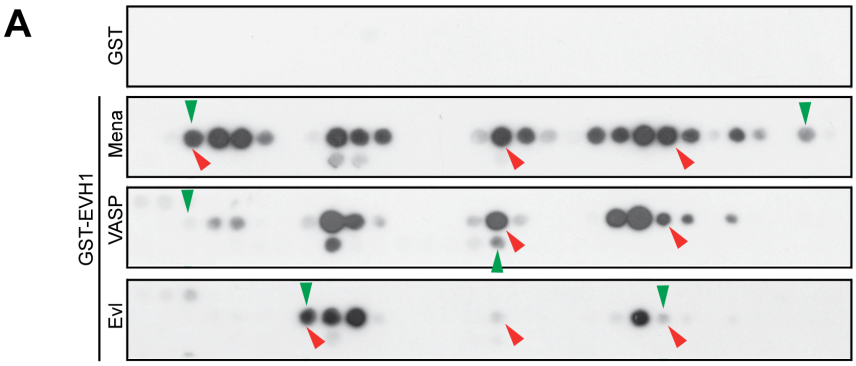

B

Mena		VASP		Evl	
RVQENIADSPTPPPPPPPDD	**++**	RVQENIADSPTPPPPPPPDD	-/+		
VQENIADSPTPPPPPPPDDI	**+++**	VQENIADSPTPPPPPPPDDI	+		
QENIADSPTPPPPPPPDDIP	**+++**	QENIADSPTPPPPPPPDDIP	+		
ENIADSPTPPPPPPPDDIPM	+	ENIADSPTPPPPPPPDDIPM	-		
NIADSPTPPPPPPPDDIPMF	-	NIADSPTPPPPPPPDDIPMF	-		
IADSPTPPPPPPPDDIPMFD	-/+	IADSPTPPPPPPPDDIPMFD	-/+	**IADSPTPPPPPPPDDIPMFD**	**++**
ADSPTPPPPPPPDDIPMFDD	**+++**	**ADSPTPPPPPPPDDIPMFDD**	**++++**	**ADSPTPPPPPPPDDIPMFDD**	**++**
DSPTPPPPPPPDDIPMFDDS	**++**	**DSPTPPPPPPPDDIPMFDDS**	**+++**	**DSPTPPPPPPPDDIPMFDDS**	**+++**
SPTPPPPPPPDDIPMFDDSP	**++**	SPTPPPPPPPDDIPMFDDSP	-/+	SPTPPPPPPPDDIPMFDDSP	-/+
PTPPPPPPPDDIPMFDDSPP	-	PTPPPPPPPDDIPMFDDSPP	-	PTPPPPPPPDDIPMFDDSPP	-
TPPPPPPPDDIPMFDDSPPP	-	TPPPPPPPDDIPMFDDSPPP	-	TPPPPPPPDDIPMFDDSPPP	-
PPPPPPPDDIPMFDDSPPPP	-	PPPPPPPDDIPMFDDSPPPP	-	PPPPPPPDDIPMFDDSPPPP	-
PPPPPPDDIPMFDDSPPPPP	-/+	PPPPPPDDIPMFDDSPPPPP	-/+	PPPPPPDDIPMFDDSPPPPP	-
PPPPPDDIPMFDDSPPPPPP	**+++**	**PPPPPDDIPMFDDSPPPPPP**	**+++**	PPPPPDDIPMFDDSPPPPPP	-/+
PPPPDDIPMFDDSPPPPPPP	**++**	PPPPDDIPMFDDSPPPPPPP	-/+	PPPPDDIPMFDDSPPPPPPP	-
PPPDDIPMFDDSPPPPPPPP	-/+	PPPDDIPMFDDSPPPPPPPP	-	PPPDDIPMFDDSPPPPPPPP	-
PPDDIPMFDDSPPPPPPPPV	-	PPDDIPMFDDSPPPPPPPPV	-	PPDDIPMFDDSPPPPPPPPV	-
PDDIPMFDDSPPPPPPPPVD	**++**	PDDIPMFDDSPPPPPPPPVD	-	PDDIPMFDDSPPPPPPPPVD	-
DDIPMFDDSPPPPPPPPVDY	**++**	**DDIPMFDDSPPPPPPPPVDY**	**+++**	DDIPMFDDSPPPPPPPPVDY	-/+
DIPMFDDSPPPPPPPPVDYE	**+++**	**DIPMFDDSPPPPPPPPVDYE**	**++++**	**DIPMFDDSPPPPPPPPVDYE**	**+++**
IPMFDDSPPPPPPPPVDYED	**+++**	**IPMFDDSPPPPPPPPVDYED**	**++**	IPMFDDSPPPPPPPPVDYED	-/+
PMFDDSPPPPPPPPVDYEDE	**++**	**PMFDDSPPPPPPPPVDYEDE**	**++**		
MFDDSPPPPPPPPVDYEDEE	-/+	MFDDSPPPPPPPPVDYEDEE	-		
FDDSPPPPPPPPVDYEDEEA	**++**	FDDSPPPPPPPPVDYEDEEA	+		
DDSPPPPPPPPVDYEDEEAA	+	DDSPPPPPPPPVDYEDEEAA	-		
DSPPPPPPPPVDYEDEEAAV	-	DSPPPPPPPPVDYEDEEAAV	-		
SPPPPPPPPVDYEDEEAAVV	+	SPPPPPPPPVDYEDEEAAVV	-		
		PPPPPPPPVDYEDEEAAVVQ	-		
		PPPPPPPVDYEDEEAAVVQY	-		
		PPPPPPVDYEDEEAAVVQYN	-		
		PPPPPVDYEDEEAAVVQYND	-		
		PPPPVDYEDEEAAVVQYNDP	-		
		PPPVDYEDEEAAVVQYNDPY	-		
		PPVDYEDEEAAVVQYNDPYA	-		
		PVDYEDEEAAVVQYNDPYAD	-		
		VDYEDEEAAVVQYNDPYADG	-		
		DYEDEEAAVVQYNDPYADGD	**++**		
		YEDEEAAVVQYNDPYADGDP	-		
		EDEEAAVVQYNDPYADGDPA	-		
		DEEAAVVQYNDPYADGDPAW	-		
		EEAAVVQYNDPYADGDPAWA	-		
		EAAVVQYNDPYADGDPAWAP	-		
		AAVVQYNDPYADGDPAWAPK	-/+		
		AVVQYNDPYADGDPAWAPKN	+		

Figure 4.5 The EVH1 domains of Mena, VASP and Evl bind the same region of Abi.

A. Far western analysis with GST-EVH1 domains of Mena, VASP and Evl on peptide arrays consisting of overlapping peptides covering residues 320-415 of Abi. The peptide arrays were probed with either GST or the purified GST-tagged EVH1 domain of different Ena/VASP proteins. Similar peptides were found to interact with all three EVH1 domains, but not GST alone. Red arrowheads indicate the examples of non-identical peptide binding patterns. Green arrowheads indicate the first and the last peptide in each array that are listed in **B.** **B.** A List of peptides that interact with the EVH1 domain of Mena, VASP or Evl. The intensity of the spots were scored with "- " and/or "+". The peptides with the strongest intensities are highlighted in black.

4.2.2 Identification of key residues in Abi required for EVH1 binding

My data has shown that the PR2 region of Abi (residues 352-394) contains the EVH1 binding site of Ena/VASP proteins. To make an Abi mutant that cannot bind EVH1 with minimal disruption, I needed to identify key residues that are required for mediating this interaction within this region of Abi.

Given that the length of peptide that can be synthesised on peptide array is limiting, generation of a peptide that spans residues 352-394 of Abi is problematic. Therefore, based on my far western results, I picked three peptides, which bound strongly to the GST-EVH1 domain of Mena and covered residues 352-394 of Abi, and used them for mutational analysis (Figure 4.6A). Each residue of the three peptides was mutated into the 20 different possible amino acids combinations and spotted onto a peptide array. Far western analysis was performed using the GST-EVH1 domain of Mena and the binding subsequently detected by anti-GST as described previously (Figure 4.3). The results revealed that the interactions between the peptides and the GST-EVH1 domain of Mena was significantly reduced when the proline residues 366-368 and 383-385 as well as phenylalanine 375 of Abi were substituted to the majority of other amino acids (Figure 4.6B). These results suggest that the two sets of proline residues as well as the single phenylalanine residue within the EVH1 binding site of Abi are important for the Abi-EVH1 interaction.

However, it is noticeable that mutating the proline residues 366-368 of Abi in the first peptide dramatically reduced binding, whereas mutating the same proline residues in the second peptide had no effect on EVH1 binding (Figure 4.6B). Similarly, in contrast to the effects of mutating the phenylalanine 375 of Abi in the second peptide on EVH1 binding, no effect on EVH1 binding was observed when this phenylalanine residue of Abi in the third peptide was mutated (Figure 4.6B). It is possible that these residues become less essential for the entire peptide to interact with the EVH1 domain when they are placed at the end of the peptide.

Additional effects of mutating proline 369 and the following two aspartic acids of Abi in the first peptide but not the second peptide were observed (Figure 4.6B). This could be explained by the fact that errors or defects may occur during peptide synthesis, as potential errors in peptide synthesis were observed in previous experiments (Figure 4.4).

To confirm that the proline and phenylalanine residues in Abi identified by mutational analysis are important for EVH1 binding, I substituted proline 366, 367, 368, 383, 384 and 385 with glycine residues and phenylalanine 375 with alanine (Figure 4.7A). I then examined whether these substitutions disrupted the interaction between Abi peptides and the EVH1 domain of Ena/VASP proteins using the far western approach. The data demonstrated that, in contrast to the wild type peptides, the mutated peptides were no longer able to bind to the EVH1 domain of any of the three Ena/VASP proteins (Figure 4.7B). The amino acid substitutions I designed are clearly sufficient to disrupt the interaction between the EVH1 domain of Ena/VASP proteins and linear peptides. However, these substitutions may not be sufficient to disrupt the interaction between the EVH1 domain and full length Abi. Therefore, it is essential to examine the effects of changing these residues in Abi on EVH1 binding in the context of the full length protein. To address this question, I expressed and purified full length Abi containing P366G, P367G and P368G substitutions (mutant 1), F375A substitution (mutant 2), P383G, P384G and P385G substitutions (mutant 3), mutant 1+2, mutant 1+3, mutant 2+3 or mutant 1+2+3 with a GST tag at their N terminus (Figure 4.8A). These bacterially produced mutant Abi proteins, together with the wild type Abi, were used in *in vitro* pull-down assays. The coomassie stained gel revealed that each mutant in isolation was not sufficient to block the binding between Abi and EVH1 (Figure 4.8B). However, when any two mutants were combined, the binding of Abi to the EVH1 domain was reduced. The combinations of mutant 2 with either mutant 1 or mutant 3 partially affected the interaction between Abi and EVH1 to a similar level. In contrast, the interaction between Abi and EVH1 domain was significantly disrupted when mutant 1 and 3 were combined. The effects of mutant 1+3 on EVH1 binding are almost the same as the effects of combining all three mutants on EVH1 binding. Based on these observations, it suggests that all three mutants are required to block the binding of Abi to the EVH1 domain of Mena, although mutant 1 and 3 appear to play major role in disrupting this interaction. To ensure the maximum disruption of the binding between Abi and EVH1 for future experiments, the mutant Abi carrying all three mutants (P366/367/368G, F375A and P383/384/385G) (Abi mut) was used in future experiments.

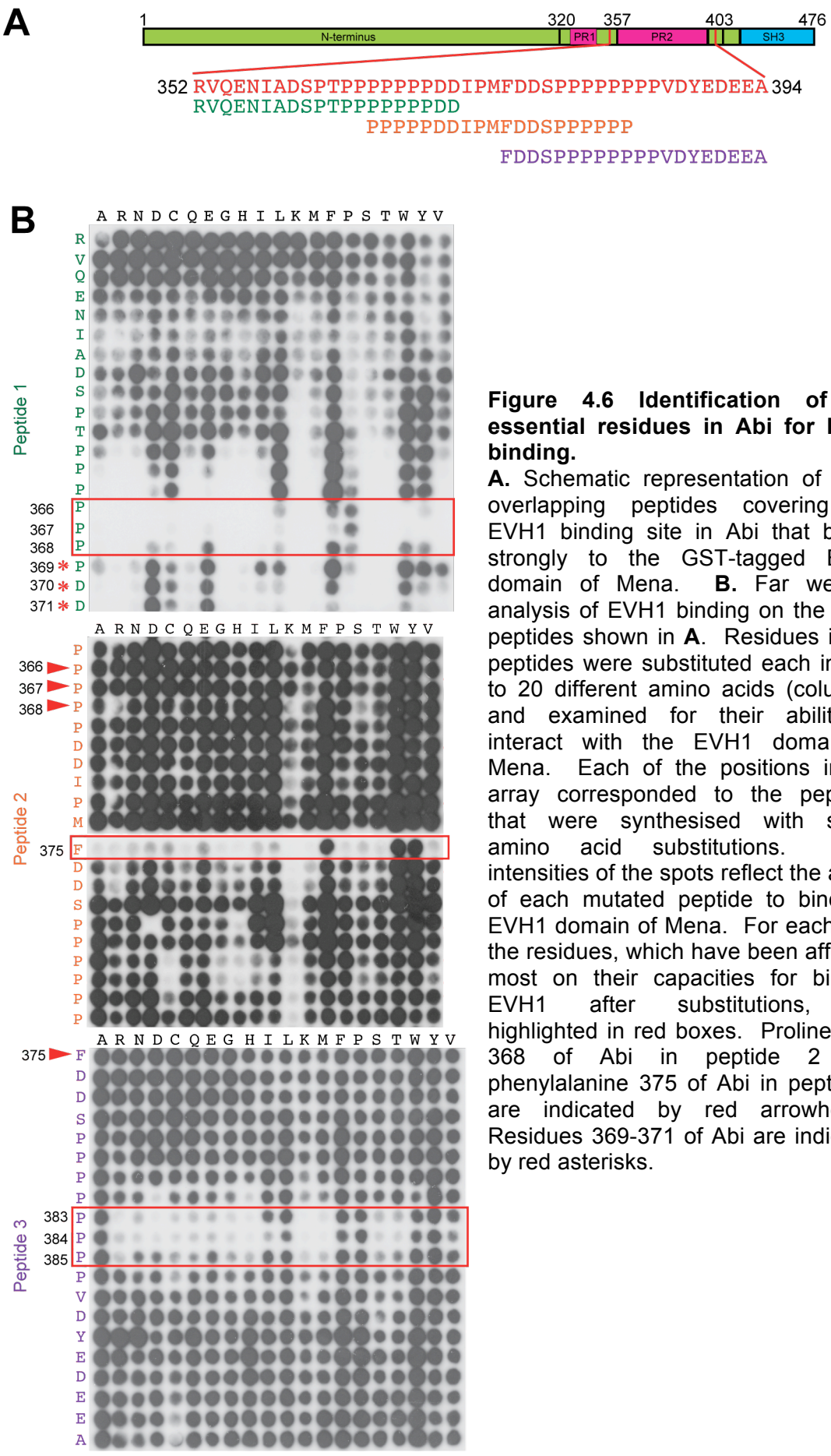

Figure 4.6 Identification of the essential residues in Abi for EVH1 binding.

A. Schematic representation of three overlapping peptides covering the EVH1 binding site in Abi that bound strongly to the GST-tagged EVH1 domain of Mena. **B.** Far western analysis of EVH1 binding on the three peptides shown in **A**. Residues in the peptides were substituted each in turn to 20 different amino acids (columns) and examined for their ability to interact with the EVH1 domain of Mena. Each of the positions in the array corresponded to the peptides that were synthesised with single amino acid substitutions. The intensities of the spots reflect the ability of each mutated peptide to bind the EVH1 domain of Mena. For each blot, the residues, which have been affected most on their capacities for binding EVH1 after substitutions, are highlighted in red boxes. Proline 366-368 of Abi in peptide 2 and phenylalanine 375 of Abi in peptide 3 are indicated by red arrowheads. Residues 369-371 of Abi are indicated by red asterisks.

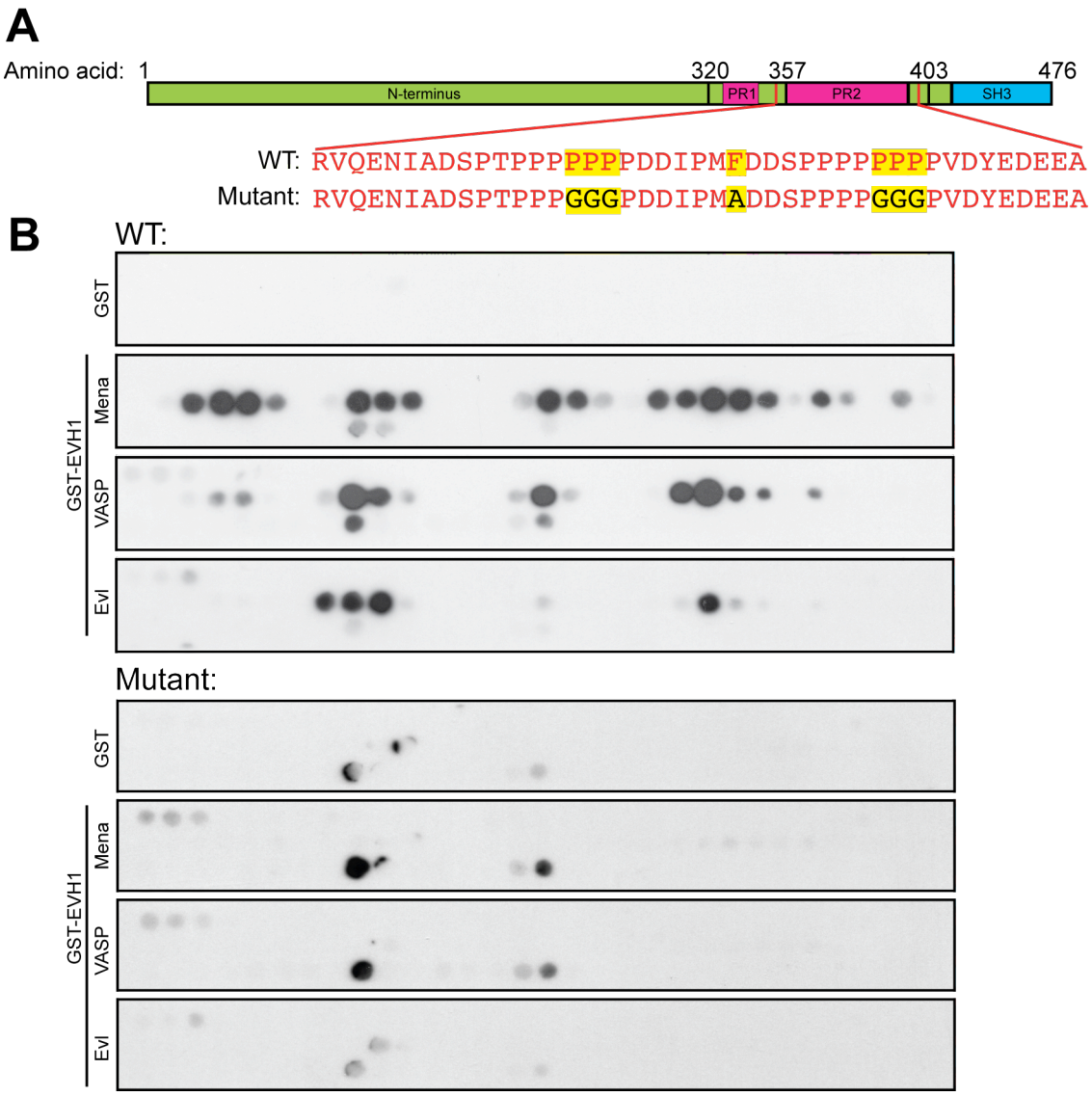

Figure 4.7 The amino acids substitutions in Abi peptides disrupt their interaction with the EVH1 domain of Mena.
A. Schematic representation of the strategy for blocking the interaction between Abi and EVH1. The key residues that are important to mediate the Abi-EVH1 interactions are highlighted in yellow. These residues were replaced with either glycine or alanine (black) to generate a mutant Abi that is deficient in EVH1 binding. **B.** Far western analyses on the peptide arrays that contain either the wild type (top panel) or the mutated overlapping peptides (bottom panel) covering residues 320-415 of Abi. Each set of peptide arrays was probed with either GST or GST-EVH1 domain of the different Ena/VASP proteins. In contrast to the wild type peptides, the mutated peptides lost their ability to interact with EVH1 domains. GST and the GST-tagged recombinant proteins that were used as probes are indicated on the left of the arrays.

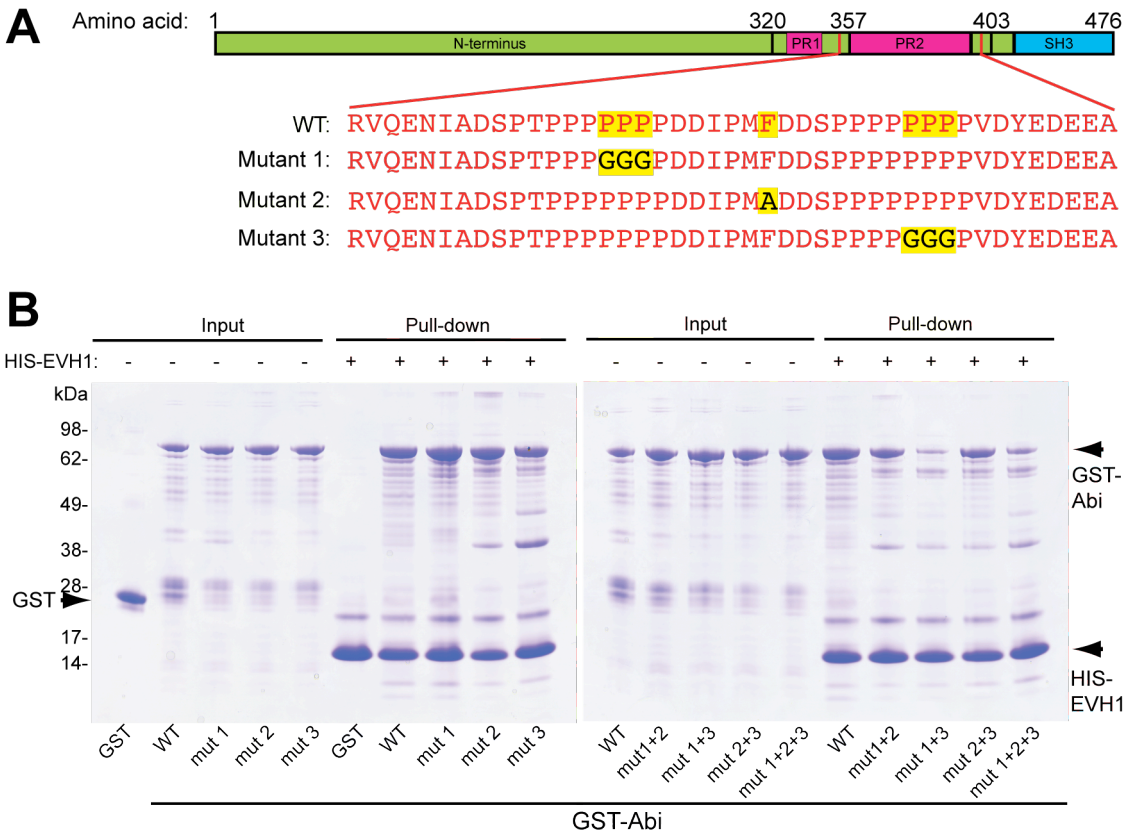

Figure 4.8 Abi mutant 1+2+3 is deficient in EVH1 binding.
A. Schematic representation of 3 different sets of amino acid substitutions that were introduced into the bacterially produced GST-full length Abi. The three sets of amino acid substitutions are referred to mutant 1, 2 and 3. **B.** Coomassie stained gel of HIS-EVH1 pull-downs reveals that the combinations of double or triple mutants had a larger impact on EVH1 binding than the single substitution mutants. Input and HIS-tagged EVH1 pull-down are indicated at the top of the gels. GST and GST-tagged Abi and Abi mutants are indicated at the bottom of the gels. The bands corresponding to GST, GST-tagged Abi or its mutants, and the HIS-EVH1 domain of Mena are indicated by arrowheads on each side of the gels.

4.2.3 Abi mut is incorporated into the WAVE complex but cannot bind Mena

To ensure the amino acids substitutions I created in Abi mut do not affect the ability of the protein to incorporate with the WAVE complex, I performed immunoprecipitation experiments using anti-GFP on HEK 293T cells over-expressing GFP-Abi or GFP-Abi mut. As shown in Figure 4.9, GFP-Abi but not GFP-Abi mut or GFP interacted with Mena. Both, GFP-Abi and GFP-Abi mut, however, pulled-down the endogenous PIR121 from cell lysates. This suggests the amino acids substitutions I created in Abi mut only disrupt its interaction with EVH1 domains and not its capacity to associate with the rest of the WAVE complex.

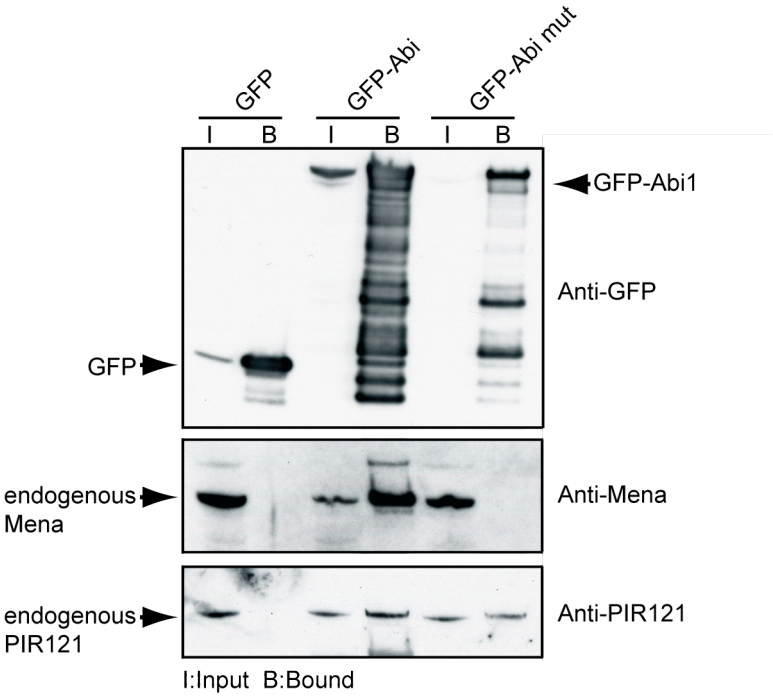

Figure 4.9 Abi mut incorporates into the WAVE complex but cannot associate with Mena.
Abi and Abi mut with an N-terminal GFP tag were over-expressed in HEK 293T cells. The GFP-tagged proteins were immunoprecipitated from cell lysates using a mouse monoclonal antibody against GFP. The precipitated proteins were analysed by western blotting with antibodies against Mena and PIR121. To estimate the amounts of over-expressed proteins, 4% of each lysate was used as the input (I).

4.3 Summary

Work presented in this chapter was aimed at generating a mutant Abi that cannot bind Ena/VASP proteins but can still associate with the other components of the WAVE complex. A far western approach was used to identify key residues, which when mutated, are sufficient to disrupt the interaction of Abi with EVH1. I found that the EVH1 binding site is in the PR2 region of Abi by performing *in vitro* pull-down assays using recombinant proteins as well as the far western analysis on peptide arrays. Moreover, the amino acid substitutions that disrupt the EVH1 interaction do not affect the interaction between Abi and PIR121. This mutant Abi can therefore be used in cell based assays to study the physiological importance of the interaction between Ena/VASP proteins and the WAVE complex.

Chapter 5. Is the interaction between Ena/VASP proteins and the WAVE complex important for cell migration?

5.1 Introduction

To study the physiological role of the interaction between Ena/VASP proteins and the WAVE complex in lamellipodia formation during cell migration, I used Rat-2 cells as the model system, as they have been extensively used to study the role of Ena/VASP proteins in lamellipodia formation and cell migration (Bear et al., 2000, Bear et al., 2002, Krause et al., 2004, Cai et al., 2007, Cai et al., 2008). Since Rat-2 cells are very difficult to transfect transiently, I generated a series of stable Rat-2 cell lines expressing GFP/RFP-tagged proteins using a Lentivirus system (Figure 5.1). Using these stable Rat-2 cell lines, I tested if the cellular localisation of the WAVE complex is dependent on Ena/VASP proteins. I also examined the effect of uncoupling Ena/VASP from the WAVE complex on the rate of cell migration and the turnover of each protein at the leading edge.

5.2 Results

5.2.1 The localisation of the WAVE complex is independent of Ena/VASP proteins

I wondered whether Ena/VASP proteins play a role in recruiting the WAVE complex to the leading edge, as they co-localise at the plasma membrane of migrating cells (Boeda et al., 2007, Nozumi et al., 2003). In order to address this question, I performed immunofluorescence analysis of stable Rat-2 cell lines that express either RFP-APPPP-mito or RFP-FPPPP-mito. FPPPP-mito, which is derived from the ActA protein of *Listeria*, contains four FPPPP EVH1 interaction motifs and a mitochondria-targeting domain at its C-terminus (Bear et al., 2000). FPPPP-mito, when overexpressed in cells, depletes Ena/VASP proteins from the leading edge and focal adhesions (Disanza et al., 2006, Bear et al., 2000, Bear et al., 2002, Gates et al., 2009, Tucker et al., 2011, Evans et al., 2007). APPPP-mito, which has phenylalanine to alanine substitution in each of the four FPPPP can no longer interact with EVH1 and provides a negative control (Figure 5.2). These two constructs have been widely used

to sequester Ena/VASP proteins form their normal cellular locations to mitochondria (Bear et al., 2000, Bear et al., 2002, Gates et al., 2009, Tucker et al., 2011).

Stable Rat-2 cells that express either RFP-tagged APPPP-mito or FPPPP-mito were established using a Lentivirus system (Figure 5.1) (Chapter 2). The RFP-positive cells were sorted using fluorescence based activated cell sorting (FACS) (Figure 5.3). Uninfected Rat-2 cells were used as the RFP-negative control to set the gating parameters to ensure only RFP positive cells are collected (Figure 5.3A). Expression of RFP-FPPPP-mito and RFP-APPPP-mito in the FACS sorted Rat-2 cells, (from here called Rat-2-RFP-FP and Rat-2-RFP-AP cells respectively), was confirmed by western blot analysis with an antibody against RFP (Figure 5.3B).

Using Rat-2-RFP-FP and Rat-2-RFP-AP cells, I examined the role of the EVH1 domain in recruiting the WAVE complex to the plasma membrane by immunofluorescence analysis using antibodies against endogenous VASP and Abi. An antibody that recognises endogenous Paxillin, a focal adhesion protein, was used as a control. As shown in Figure 5.4, Paxillin and Abi were present at their normal cellular localisations of focal adhesions and the plasma membrane respectively, in both Rat-2-RFP-AP and Rat-2-RFP-FP cells. In contrast, VASP was dramatically re-localised to mitochondria in Rat-2-RFP-FP cells. This result indicates that the FPPPP-mito construct effectively recruits VASP and presumably Mena and Evl from focal adhesions and the plasma membrane to the surface of mitochondria. However, the sequestration of VASP to mitochondria did not affect the cellular localisation of Abi, suggesting that the localisation of the WAVE complex at the plasma membrane is not dependent on Ena/VASP proteins.

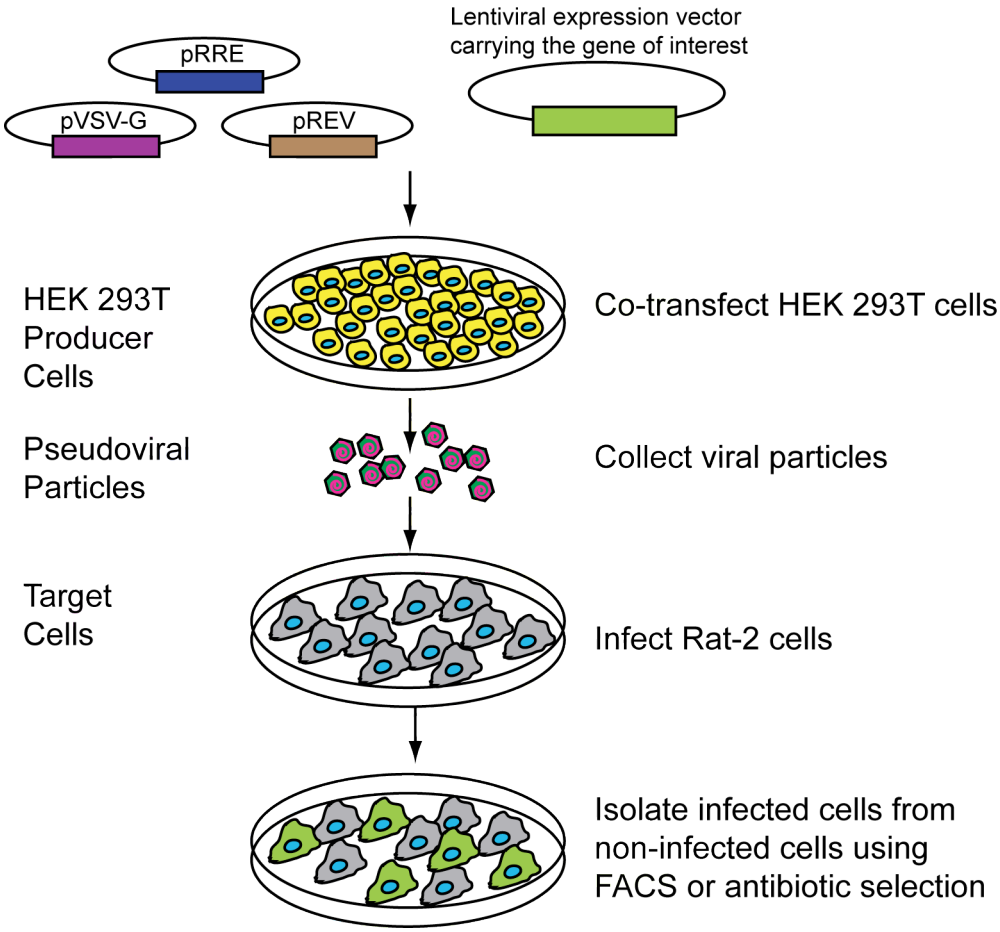

Figure 5.1 Schematic representation of Lentivirus–mediated generation of stable Rat-2 cell lines.
Lentivirus expression vectors pL.L 3.7 or pLVX-Puro/Hygro that contain a GFP/RFP-tagged protein of interest (green) and the three packaging vectors: pRRE (gag-pol plasmid) (blue), pREV (RNA export protein) (brown), pVSV-G (virus envelope) (purple) were co-transfected into HEK 293T cells using a calcium phosphate method. Lentivirus particles encoding the GFP/RFP-tagged protein of interest are released into the supernatant media. This viral-supernatant is then collected after two days, filtered and can then be used to infect Rat-2 cells. The lentivirus-infected cells that express GFP/RFP-tagged proteins were selected by FACS (Chapter 2.2.4.2) or by antibiotic selection (Chapter 2.2.4.3).

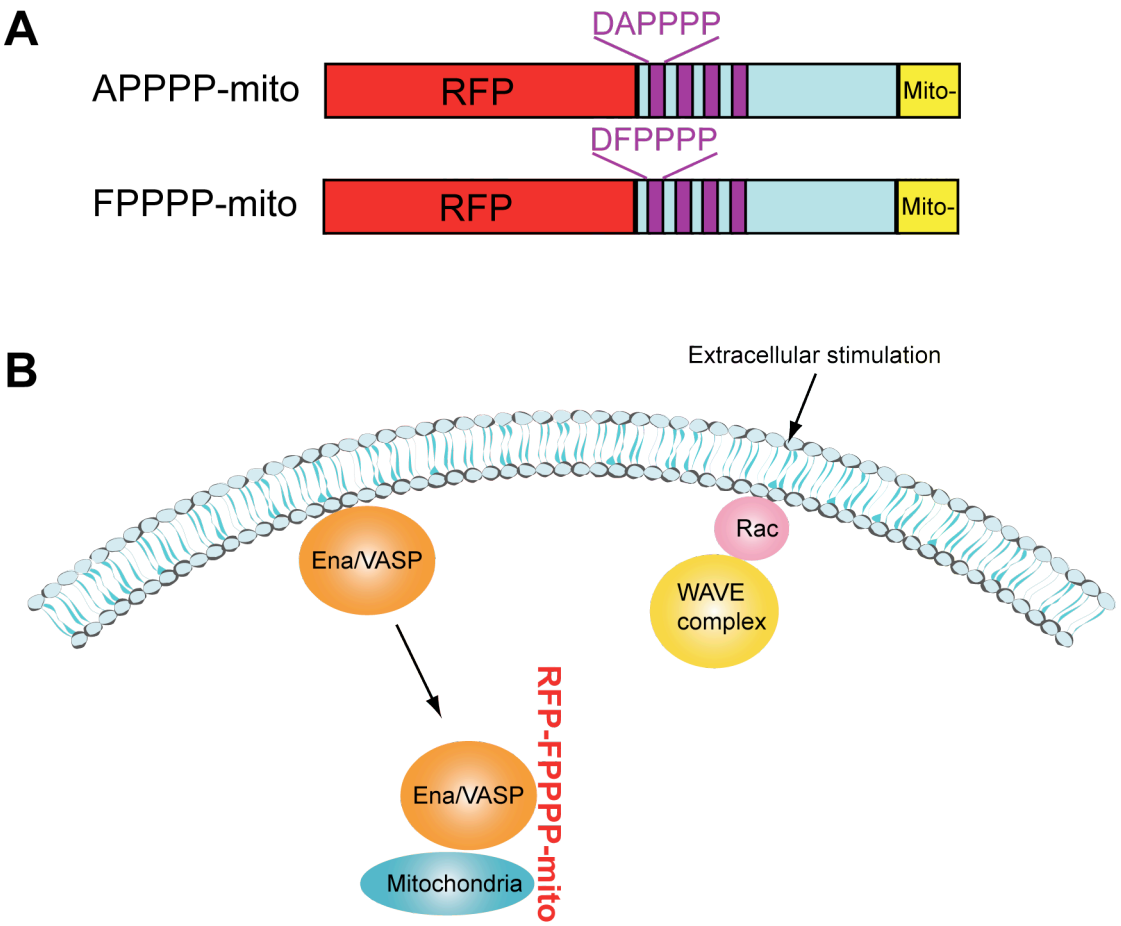

Figure 5.2 Schematic representation of sequestration of Ena/VASP proteins to mitochondria.
A. Schematic illustration of FPPPP-mito and APPPP-mito (control) constructs. FPPPP-mito, which is derived from the ActA protein of *Listeria*, contains four FPPPP EVH1 interaction motifs (purple) and a mitochondria-targeting domain (yellow) at its C-terminus. Adapted from (Bear et al., 2000) with the permission of Elsevier. **B.** Schematic representation of depleting Ena/VASP proteins from the plasma membrane where the WAVE complex is localised by targeting them to mitochondria using RFP-FPPPP-mito.

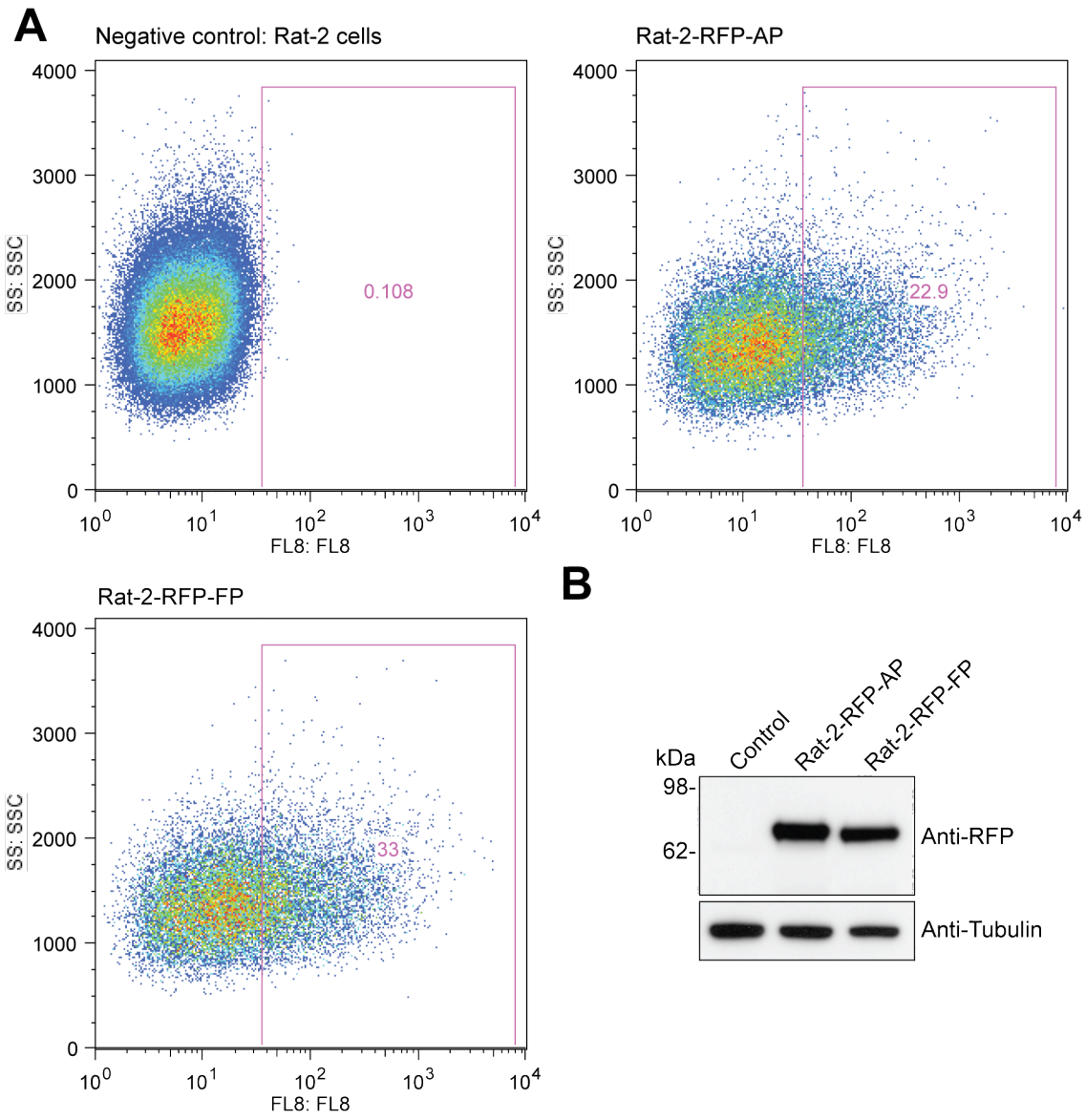

Figure 5.3 FACS sort to establish Rat-2-RFP-FP and Rat-2-RFP-AP cell lines. **A.** Bivariate dot plot of control Rat-2 cells were used to set up the gating parameters to select RFP-positive cells. The cells in the pink boxes correspond to the cells that showed a strong RFP fluorescence signal. For Rat-2-RFP-AP 22.9% and for Rat-2-RFP-FP 33% of the cells were sorted as RFP-positive. **B.** Immunoblot analysis showing that RFP-tagged proteins were expressed at the predicted size in each cell line. The control and RFP-positive cell lines are indicated at the top and antibodies are indicated on the right of the panels. Tubulin levels were used as loading control.

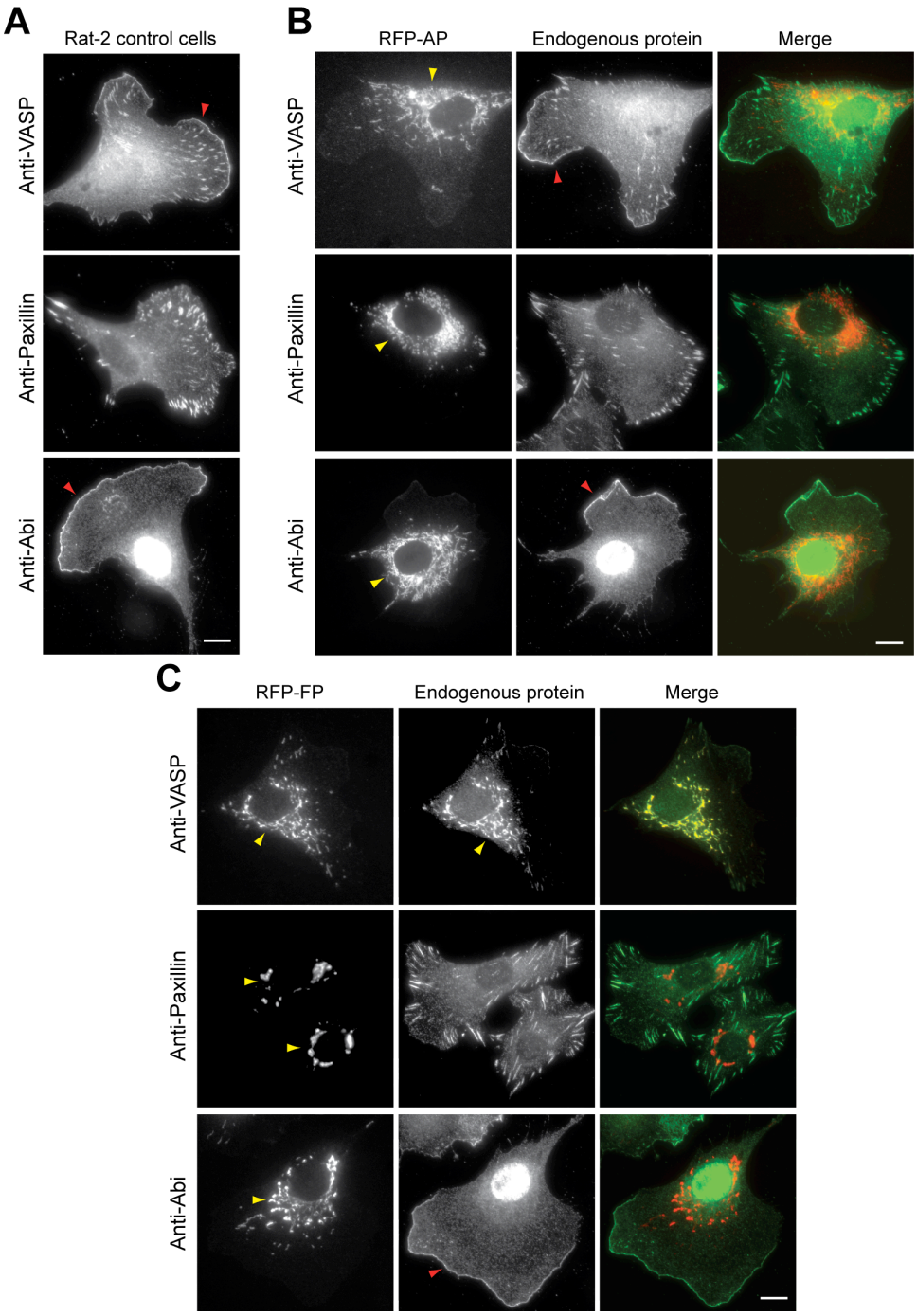

Figure 5.4 Sequestration of Ena/VASP proteins to mitochondria does not deplete Abi from the plasma membrane.
A. Immunofluorescence images showing the localisations of VASP, Paxillin and Abi in Rat-2 control cells. **B**. Overexpression of RFP-AP does not affect the normal cellular localisation of VASP, Paxillin and Abi in Rat-2 cells. **C**.VASP, but not Paxillin or Abi is depleted from its normal cellular localisation by overexpressing RFP-FP in Rat-2 cells. Red arrowheads indicate the leading edge of cells. Yellow arrowheads indicate mitochondria of cells. The primary antibodies are indicated on the left of the panels. Scale bar represents 10μm.

5.2.2 The physiological significance of Abi-EVH1 interaction during cell migration

Ena/VASP proteins and the WAVE complex are key players in the regulation of the actin cytoskeleton during cell migration (Chapter 1). I therefore examined the effect of disrupting the binding of Abi to EVH1 on cell migration using the Abi mutant deficient in EVH1 binding.

I generated Rat-2 cells stably expressing GFP, GFP-Abi or GFP-Abi mut using the lentivirus system. GFP-positive cells were subsequently sorted using FACS (Figure 5.5A). Western blot analysis demonstrated that the expression of GFP-Abi and GFP-Abi mut was much lower than GFP alone (Figure 5.5B). Moreover, the expression level of GFP-Abi or GFP-Abi mut decreased rapidly at early cell passages compared with GFP alone, which remained stable (data not shown). These observations suggest that over-expression of GFP-Abi is poorly tolerated in Rat-2 cells. *Dictyostelium* cells lacking Abi exhibited a serious defect in cytokinesis (Pollitt and Insall, 2008). This suggests that in addition to the role of the WAVE complex in regulating actin cytoskeleton during cell migration, the activity of the WAVE complex is required for cytokinesis. Thus, alterations in the expression level of Abi may cause cell stress or inhibit cell division and survival. If GFP-Abi expressing Rat-2 cells are unable to properly undergo cytokinesis, then cells expressing higher levels of GFP-Abi may either undergo apoptosis or attempt to survive by down regulating the expression of GFP-Abi. All these possibilities could contribute to the poor expression of GFP-Abi constructs in Rat-2 cells as well as the rapid loss of signal in the stable Rat-2 cells lines. To over come the problem of losing GFP/RFP-tagged Abi expression at early cell passages, all the GFP/RFP-positive cells were amplified and further sorted at least two more rounds by FACS. Only the data from the last FACS sort for each of the Rat-2 stable cell lines expressing GFP/RFP-tagged Abi is shown.

To ensure the over-expressed GFP-Abi and Abi mut can still co-localise with other components of the WAVE complex at the plasma membrane in Rat-2 cells, I performed immunofluorescence analysis using antibodies against endogenous Abi, Nap1 and WAVE. This immunofluorescence analysis demonstrated that GFP-Abi and GFP-Abi mut but not GFP alone, co-localise with endogenous Nap1 and WAVE, suggesting that the overexpressed GFP-tagged proteins retain their capacity to interact with the rest of the WAVE complex (Figure 5.6A). This suggestion was confirmed by performing

immunoprecipitation using anti-GFP and antibodies against endogenous PIR121 (Figure 5.6B). My data demonstrate that exogenously expressed GFP-Abi and its mutant is incorporated into the WAVE complex and localises to the plasma membrane in my stable Rat-2 cell lines.

Using these stable Rat-2 cell lines, I performed single cell-tracking assays using time-lapse imaging to examine whether there are any differences in the migration of cells that expressing GFP-Abi or GFP-Abi mut. The parental Rat-2 cells and GFP-expressing cells were used as controls in these experiments. The data from the single cell-tracking assays, in which 30 cells were tracked, demonstrate that the GFP-Abi mut expressing cells migrate at a slightly higher velocity than the GFP-Abi expressing cells (Figure 5.7B). However, the difference between the two cell populations was not statistically significant (Figure 5.7B). Additionally, no differences in directionality or persistency during migration were observed (Figure 5.7A,C). My analysis reveals that there is no obvious alteration in migration of Rat-2 cells when GFP-Abi mut is overexpressed as compared to wild type Abi.

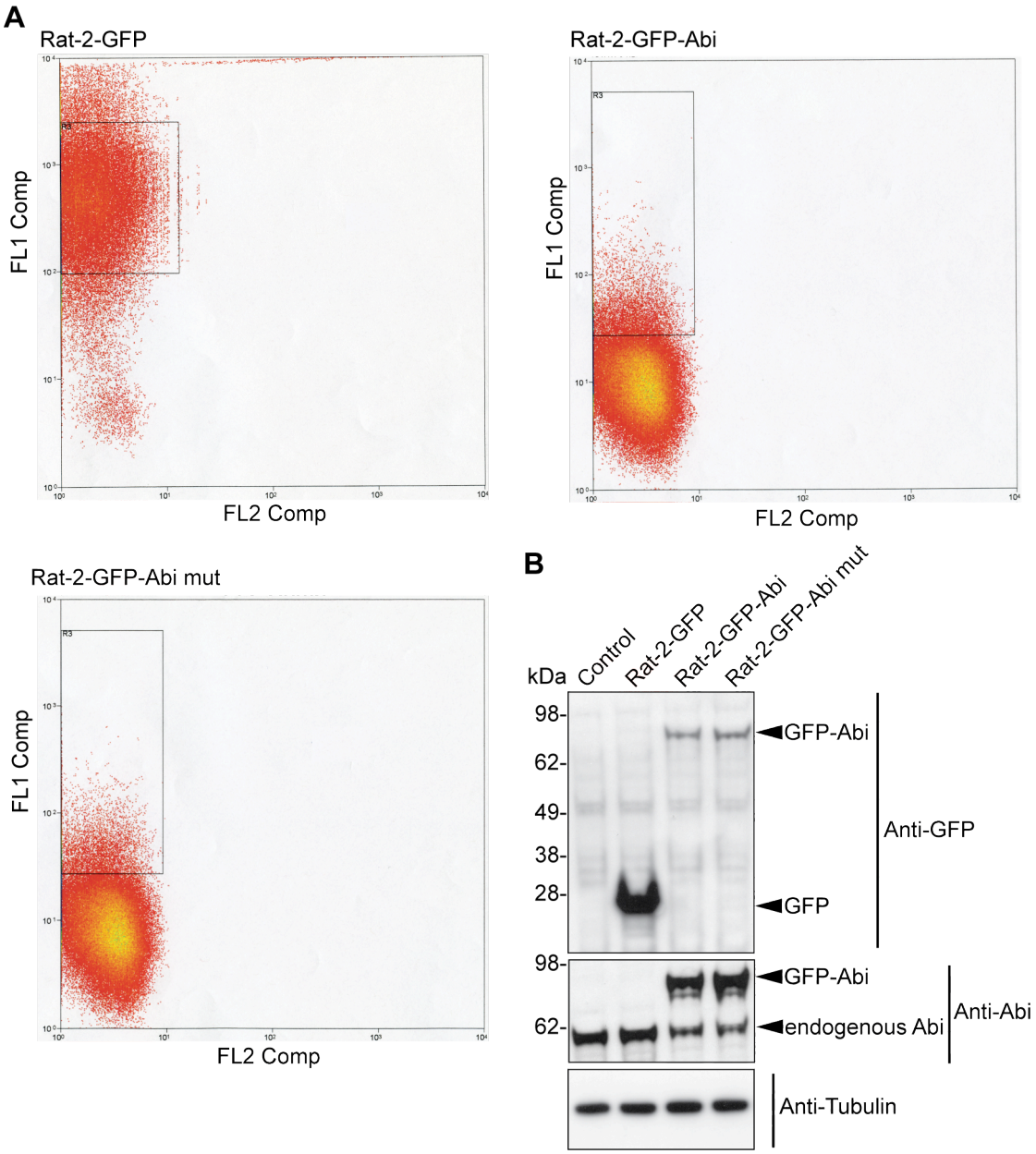

Figure 5.5 FACS sort to establish GFP, GFP-Abi and GFP-Abi mut Rat-2 cell lines. **A.** Bivariate dot plot showing GFP-positive cells (inside the red box) in each cell population that were collected. More cells expressing GFP alone were collected than cells expressing either GFP-Abi or GFP-Abi mut. Control Rat-2 cells were used to set up the gating parameters to select GFP-positive cells only (data not shown). **B.** Immunoblot analysis showing that GFP-tagged and endogenous Abi were expressed at the predicted size in each cell line. The control and GFP-positive cell lines are indicated at the top of the panels and the antibodies are indicated on the right of the panels. Tubulin levels were used as loading control.

Figure 5.6

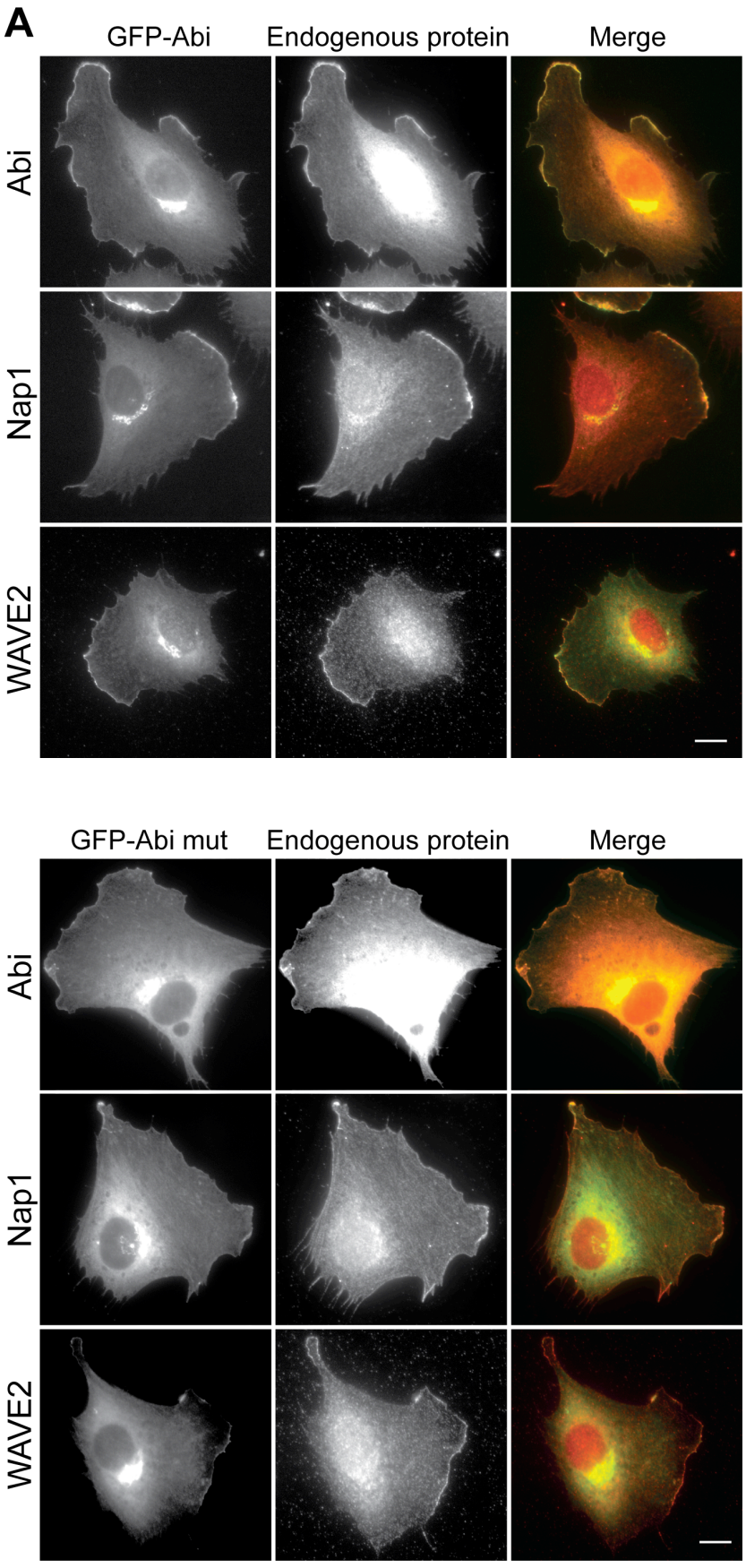
A
GFP-Abi
Endogenous protein
Merge
Abi
Nap1
WAVE2
GFP-Abi mut
Endogenous protein
Merge
Abi
Nap1
WAVE2

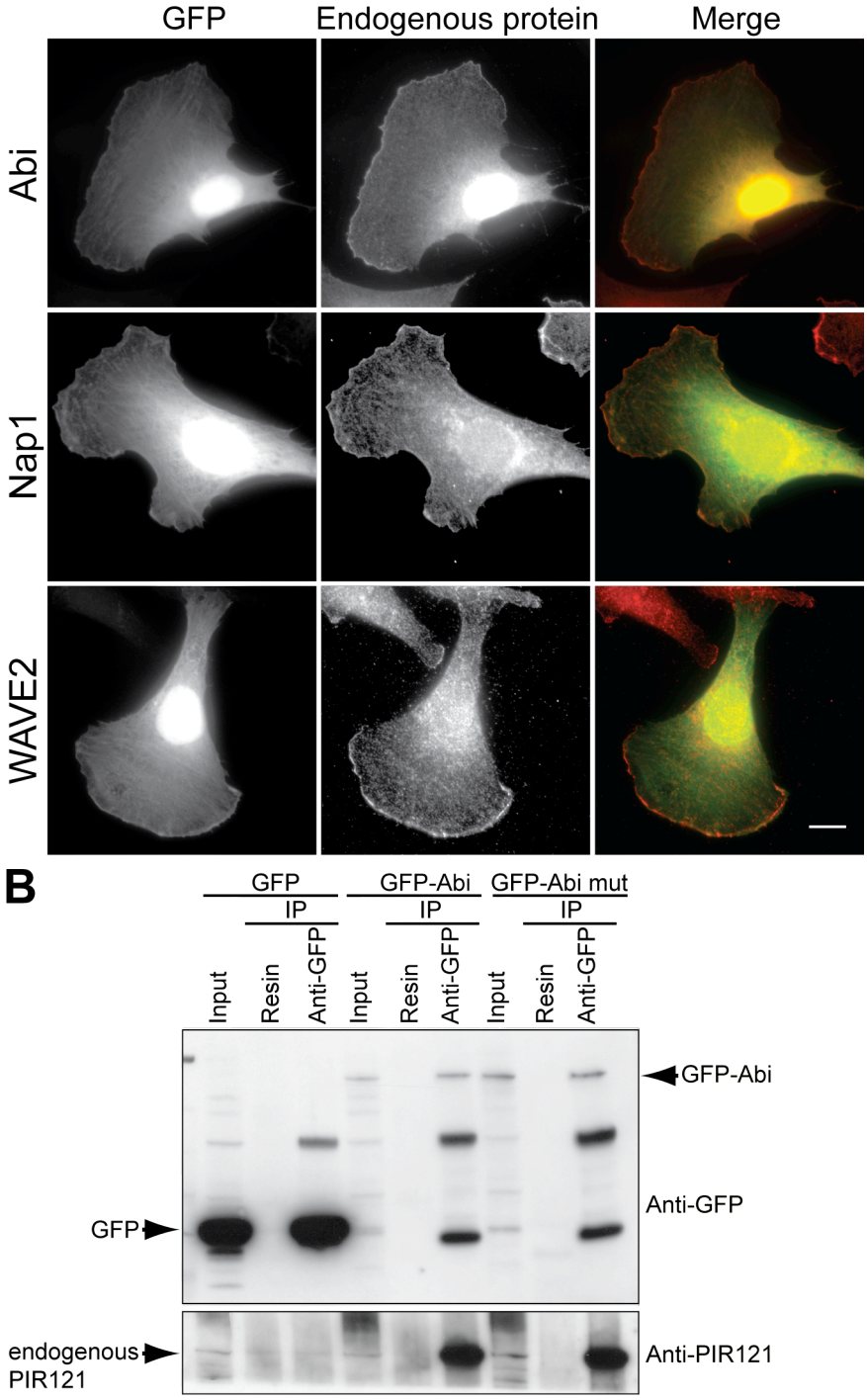

Figure 5.6 GFP-Abi is incorporated into the WAVE complex in Rat-2 cells.
A. Immunofluorescence analysis demonstrating that GFP-Abi and GFP-Abi mut, but not GFP, are recruited to the leading edge of Rat-2 cells, where they co-localise with endogenous Nap1 and WAVE. Scale bar represents 10 μm. **B**. Immunoprecipitation analysis reveals that endogenous PIR121 can be retained by GFP-Abi and GFP-Abi mut, but not GFP from Rat-2 cell lysates. 4% of each lysate was used as input.

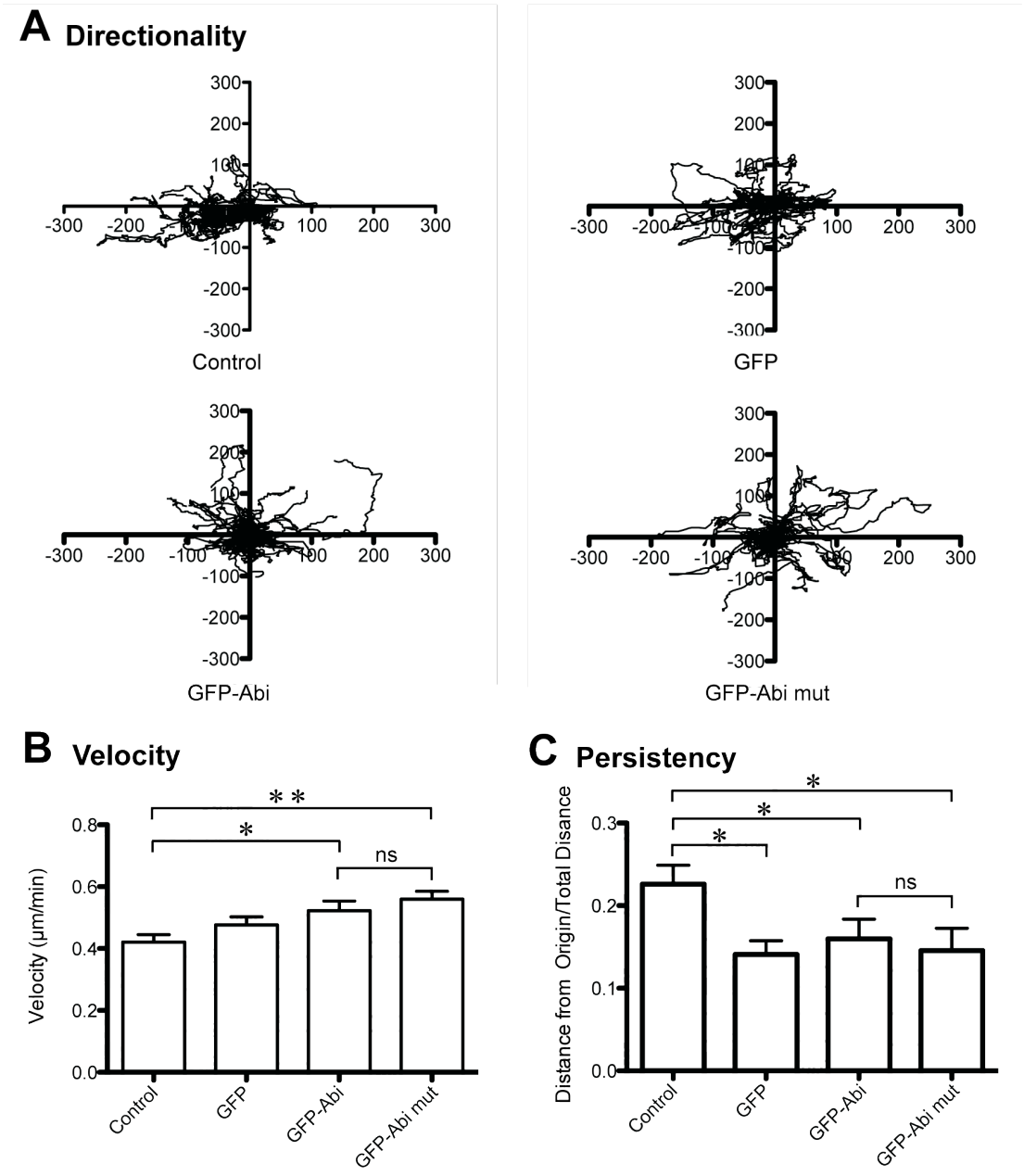

Figure 5.7 Uncoupling Ena/VASP proteins from the WAVE complex does not effect cell migration.

A. Representative centroid plots showing the trajectory of Rat-2 cells with and without expression of GFP, GFP-Abi and GFP-Abi mut over 15 hr. Scale unit is µm. **B.** Analysis of migration speeds of the four cell lines from **A**. A One Way ANOVA test was performed and the P value was found to be <0.01. **C.** Quantitative analysis of the migration persistence of the four cell lines. A One Way ANOVA test was performed and the P value was found to be <0.05. In **B** and **C, a** Newman-Keuls multiple comparison test was performed for paired comparisons after the One Way ANOVA test found means to be significantly different. *indicates P<0.05; **indicates P<0.01; ns indicates no significance. The data presented in this figure was collected from 3 independent experiments, in which 30 cells from each group were tracked. Bars represent the mean +/- SEM. n = 30.

5.2.3 Ena/VASP proteins stabilise the WAVE complex at the plasma membrane

My data suggest that Abi-EVH1 interactions neither affect the cellular localisation of the WAVE complex nor play a role in regulating the rate of cell migration. To test if Ena/VASP proteins affect the dynamics of the WAVE complex at the leading edge, I performed fluorescence recovery after photobleaching (FRAP) analysis using my stable Rat-2 cells lines (Figure 5.5).

FRAP is an optical technique that was first established in 1985 and has been used successfully to study the turnover of proteins in the leading edge of migrating cells (Lai et al., 2008, Wang, 1985). FRAP is based on selectively photobleaching fluorescently tagged-proteins within a selected region in a live cell and then measuring the reappearance of fluorescently tagged-proteins into the selected region. The rate, at which non-photobleached fluorescently tagged-proteins reappear within the photobleached region, reflects the turnover or exchange rate of the protein in this region of the cell (Figure 5.8). FRAP is therefore a powerful tool to study the dynamics of proteins in living cells. The key for performing a successful FRAP assay is to acquire as many time points as possible after rapid photobleaching while avoiding photobleaching damage that affects the cell. To achieve optimal conditions to analyse the turnover rate of GFP-Abi at the leading edge of Rat-2 cells, several imaging parameters and photobleaching parameters (laser power and times of iteration) were tested with the assistance from the light microscopy facility at Cancer Research UK (Chapter 2.5.4).

As shown in Figure 5.9, both, GFP-Abi and GFP-Abi mut fully recovered to ~100% after photobleaching within 20 seconds, suggesting these proteins are highly dynamic and turnover in a time scale of seconds. Interestingly, the red curve that represents the turnover rate of GFP-Abi mut is shifted slightly to the left compared to the curve corresponding to GFP-Abi. This suggests the Abi mut turns over faster than Abi. Importantly, the difference in the turnover rates between GFP-Abi and GFP-Abi mut is statistically significant (Figure 5.9B). My FRAP results suggest that the WAVE complex becomes more dynamic after being uncoupled from Ena/VASP proteins at the plasma membrane.

To further study the effects of uncoupling Ena/VASP proteins on the dynamics of the WAVE complex at the cell plasma membrane, I also performed FRAP analysis using Rat-2 cell lines that express GFP-Abi with either RFP-AP or RFP-FP. My aim was to determine the turnover rates of GFP-Abi at the plasma membrane using FRAP in the presence or absence of Ena/VASP. To generate these new cell lines, I expressed GFP-Abi in the Rat-2-RFP-FP and Rat-2-RFP-AP cell lines that I established earlier (Figure 5.3). The GFP-positive Rat-2 cells stably expressing RFP-tagged proteins were subsequently sorted using FACS (Figure 5.10A). Moreover, the expression of the GFP and RFP-tagged proteins in these new Rat-2 cell lines was confirmed by western blot analysis using antibodies against GFP and RFP (Figure 5.10B).

FRAP analysis using my Rat-2 cell lines stably expressing GFP-Abi with either RFP-FP or RFP-AP revealed that the turnover rate of GFP-Abi at the plasma membrane was not affected by the presence of Ena/VASP proteins at the plasma membrane (the black and red curves overlap; Figure 5.11). This result was unexpected, as I found that uncoupling Ena/VASP proteins from Abi reduced the turnover rate of Abi at the plasma membrane. Depletion of Ena/VASP proteins from the plasma membrane is therefore expected to have a similar or greater effect on the turnover rate of Abi. However, sequestration of Ena/VASP proteins from their normal cellular localisations to the surface of mitochondria will not only disrupt their interaction with Abi, but will also disrupt interactions with other proteins at both focal adhesion and the plasma membrane. Loss of Ena/VASP proteins will also affect actin dynamics at the leading edge (Bear et al., 2000, Bear et al., 2002, Tucker et al., 2011). I can only assume that the global effects of depleting Ena/VASP proteins from their normal cellular localisations may mask or cancel out the effect of disrupting the interaction between Ena/VASP proteins and Abi on the dynamics of the WAVE complex at the plasma membrane.

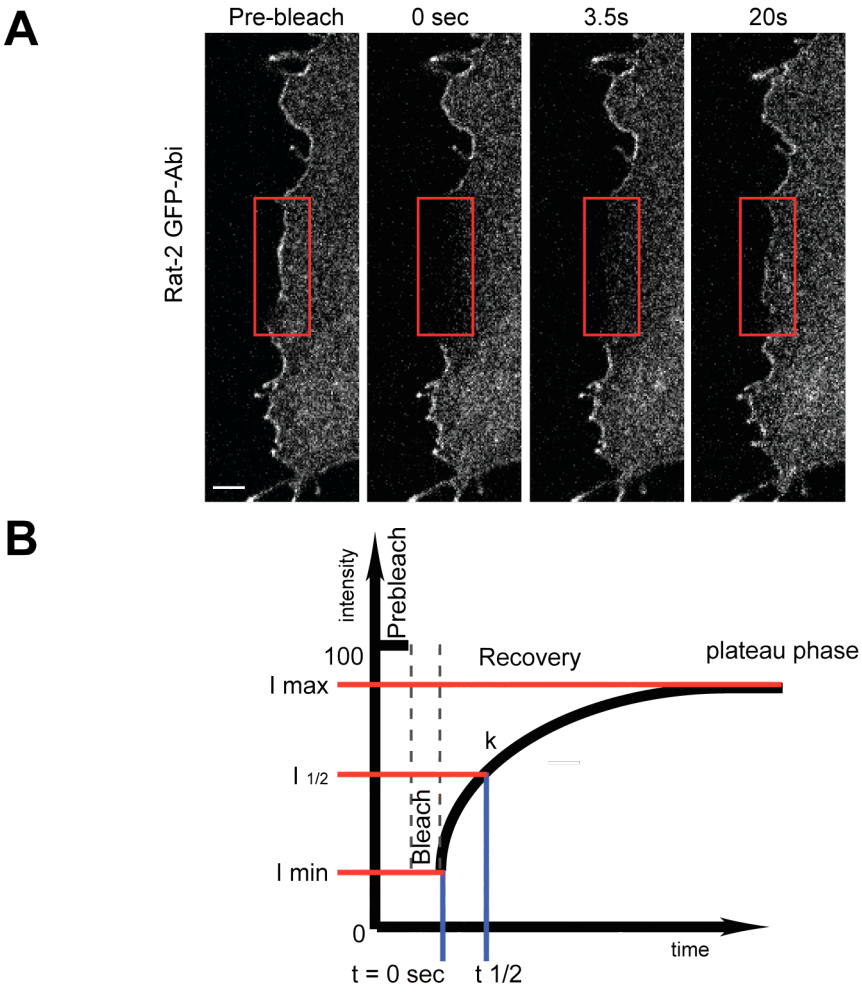

Figure 5.8 Analysis of GFP-Abi dynamics at the plasma membrane using FRAP. **A.** Movie stills showing the recovery over time of GFP-Abi after photobleaching in the selected area (red box). Time points after photobleaching are indicated at the top of the panels. Scale bar represents 2µm. **B.** Schematic of normalised data collected during an idealised FRAP experiment. The fluorescence intensity in the photobleached area (Y-axis) is plotted over time (X-axis). The steeper the curve, the faster the recovery, which means the protein is more dynamic. I_{max} represents the fluorescence intensity when the signal reaches a plateau phase after recovery. $I_{1/2}$ represents the fluorescence intensity reaches half of the final recovered intensity. I_{min} represents the remaining fluorescence intensity after photobleaching. t_0 represents the first time point after photobleaching. $t_{1/2}$ represents the time point when the fluorescence intensity reaches half of the final recovered intensity. **C.** The rate constant of recovery (k) was calculated using the non-linear regression curve-fitting formula in the Prism software. $t_{1/2}$ was calculated from the value of k.

A

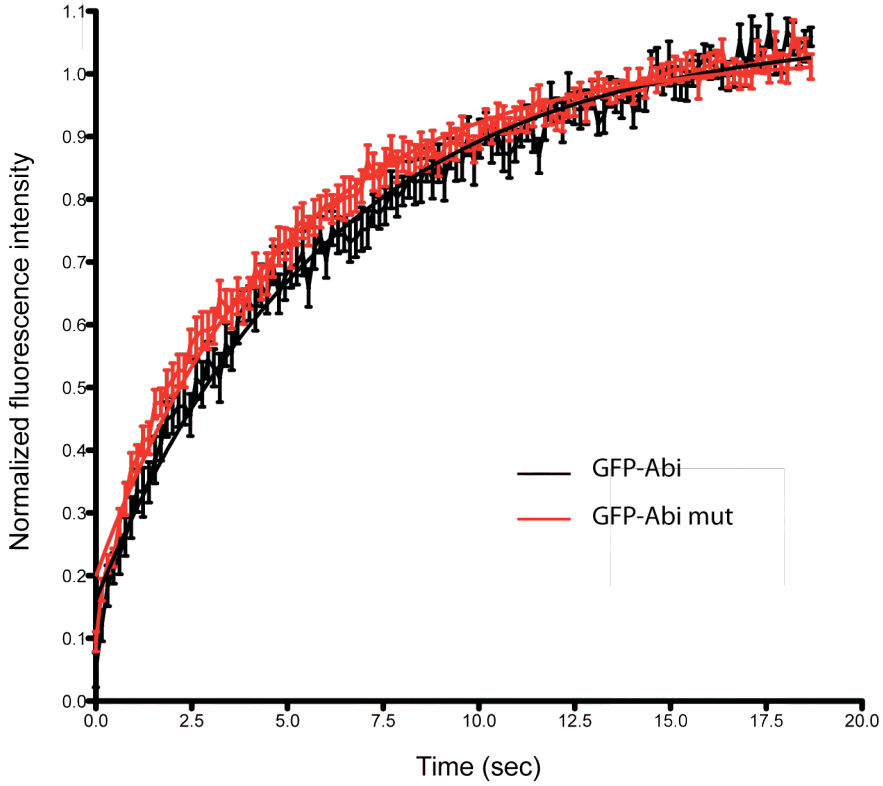

B

Protein	% Recovery	Rate constant of recovery (sec^{-1})	$t_{1/2}$ (sec)
GFP-Abi	100.0 ± 0.9	0.16 ± 0.01	4.22 ± 0.14
GFP-Abi mut	100.0 ± 0.5	0.21 ± 0.01***	3.37 ± 0.09***

Figure 5.9 Ena/VASP proteins stabilise the WAVE complex at the plasma membrane.
A. The graph illustrates the recovery rates of GFP-Abi (black) and GFP-Abi mut (red) at the plasma membrane after photobleaching. Intensity values of the GFP-tagged proteins were normalised to the pre-bleached intensity values. Linear curves correspond to best fits of averaged data obtained from 30 data sets. Bars represent the SEM. n = 30. **B.** The table lists the values derived from 30 fitted recovery curves together with the SEM for the percentage, rate constant and half-time of recovery of GFP-tagged Abi as well as Abi mut in Rat-2 cells. *** indicates P<0.001.

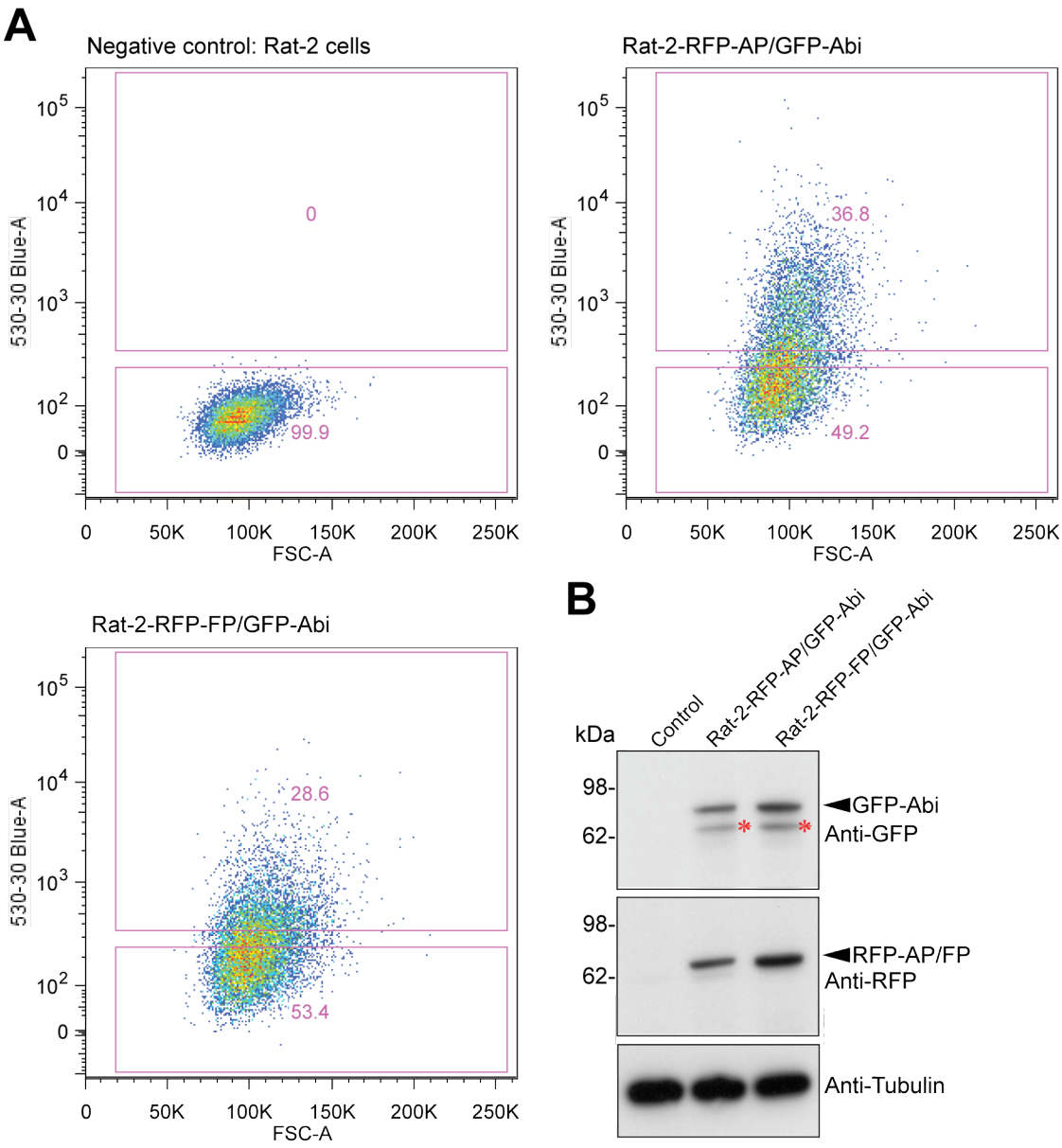

Figure 5.10 FACS sort to establish RFP-AP/GFP-Abi and RFP-FP/GFP-Abi Rat-2 cell lines.
A. Bivariate dot plot showing control Rat-2 cells that were used to set up the gating parameters to select GFP-positive cells. The cells in the bottom pink box represent the background fluorescence of GFP negative cells and 99.9% of cells are in this range. Only cells which showed a strong fluorescence signal (top pink box) were sorted. For RFP-AP/GFP-Abi 36.8% and for RFP-FP/GFP-Abi 28.6% of the cells were sorted as GFP-positive. **B.** Immunoblot analysis revealing that the GFP and RFP-tagged proteins were expressed at the predicted size in each cell line. The bands that are indicated by red asterisks are likely to be RFP-tagged proteins, as the GFP antibody may also weakly recognise RFP. The different cell lines are indicated at the top of the panels. GFP/RFP-tagged proteins and antibodies are indicated on the right of the panels. Tubulin levels were used as loading control.

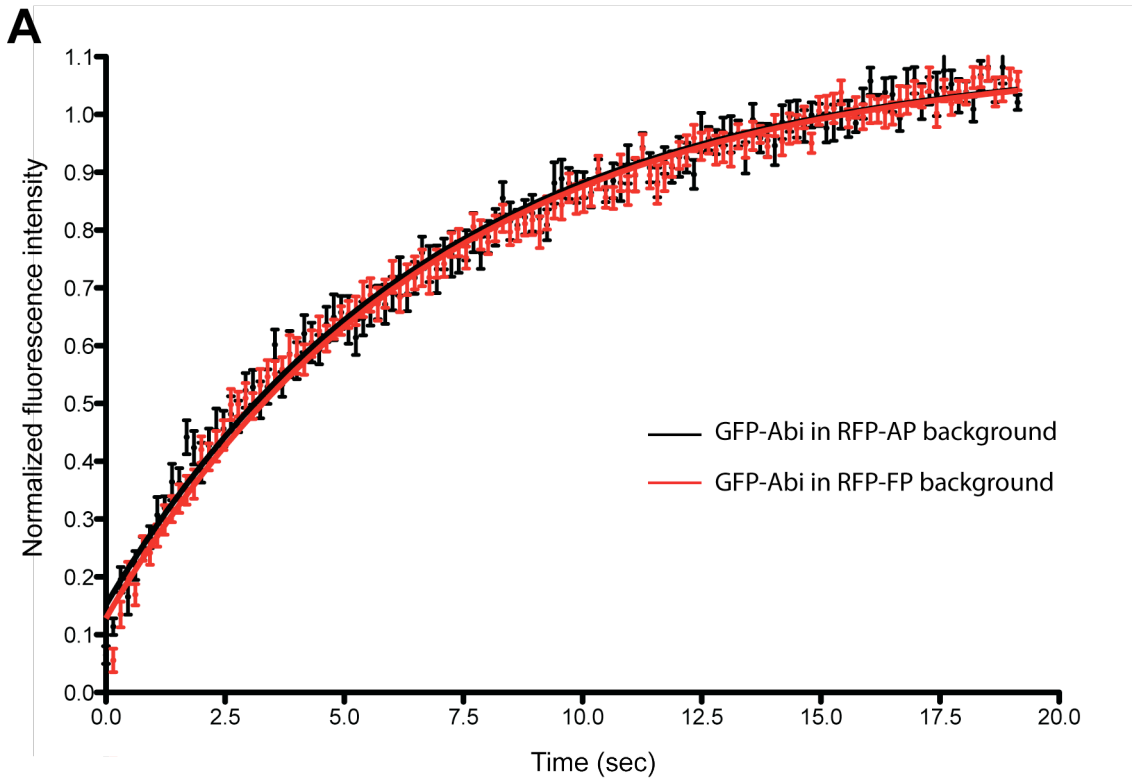

B

GFP-Abi	% Recovery	Rate constant of recovery (sec $^{-1}$)	$t_{1/2}$ (sec)
GFP-Abi/RFP-AP	100 ± 1.1	0.140 ± 0.005	4.95 ± 0.17
GFP-Abi/RFP-FP	100 ± 0.8	0.153 ± 0.004	4.54 ± 0.12

Figure 5.11 Loss of Ena/VASP proteins from the leading edge does not affect the dynamics of Abi.
A. The graph illustrating the recovery rate of GFP-Abi at the plasma membrane after photobleaching in cells expressing either RFP-AP (black) or RFP-FP (red). Intensity values of the GFP-Abi were normalised to the pre-bleached intensity value. Linear curves corresponded to best fits of averaged data. Bars represent the SEM and n = 20. **B.** The table lists the values derived from 20 fitted recovery curves together with the SEM, for the percentage, rate constant and half time of recovery of GFP-Abi in the presence of the indicated RFP-tagged protein.

5.2.4 The WAVE complex may help stabilise Ena/VASP proteins at the plasma membrane

I next wanted to ask if the WAVE complex plays a role in regulating the dynamics of Ena/VASP proteins at the plasma membrane. In order to address this question, I generated stable Rat-2 cell lines that co-express GFP-VASP with either Abi-RFP or Abi mut-RFP. For these lines I used lentivirus system, in which the expression vectors (pLVX-Puromycin and pLVX-IRES-Hygromycin) also contain an antibiotic resistant cassette to allow for antibiotic selection of cells expressing my protein of interest (Chapter 2.2.4.3). In contrast to the stable expression of GFP-VASP, I found that expression of Abi-RFP and Abi mut-RFP in Rat-2 cells rapidly decreased with three days despite continuous selection with antibiotics (data not shown). This observation is consistent with my previous observations on the stability of GFP-Abi expression in Rat-2 cells and again suggest that overexpression of Abi is poorly tolerated. To overcome this problem, GFP and RFP-positive cells were again re-selected using FACS after antibiotic selection and cell amplification (Figure 5.12A). Due to the limited numbers of cells, co-expression of GFP-VASP and Abi-RFP in Rat-2 cells is illustrated by fluorescence microscopy rather than western blot analysis (Figure 5.12B).

FRAP analysis using these stable cell lines demonstrated that there was a small but significant reduction in the turnover rate of the GFP-VASP in the presence of Abi mut-RFP compared to Abi-RFP (Figure 5.13). My FRAP data suggests that an interaction with the WAVE complex increases the dynamics of GFP-VASP at the plasma membrane. By contrast, my previous FRAP data indicates Ena/VASP proteins stabilise the WAVE complex at the plasma membrane (Figure 5.9). Taken together, my data suggests that Ena/VASP proteins and the WAVE complex might regulate the dynamics of each other at the plasma membrane.

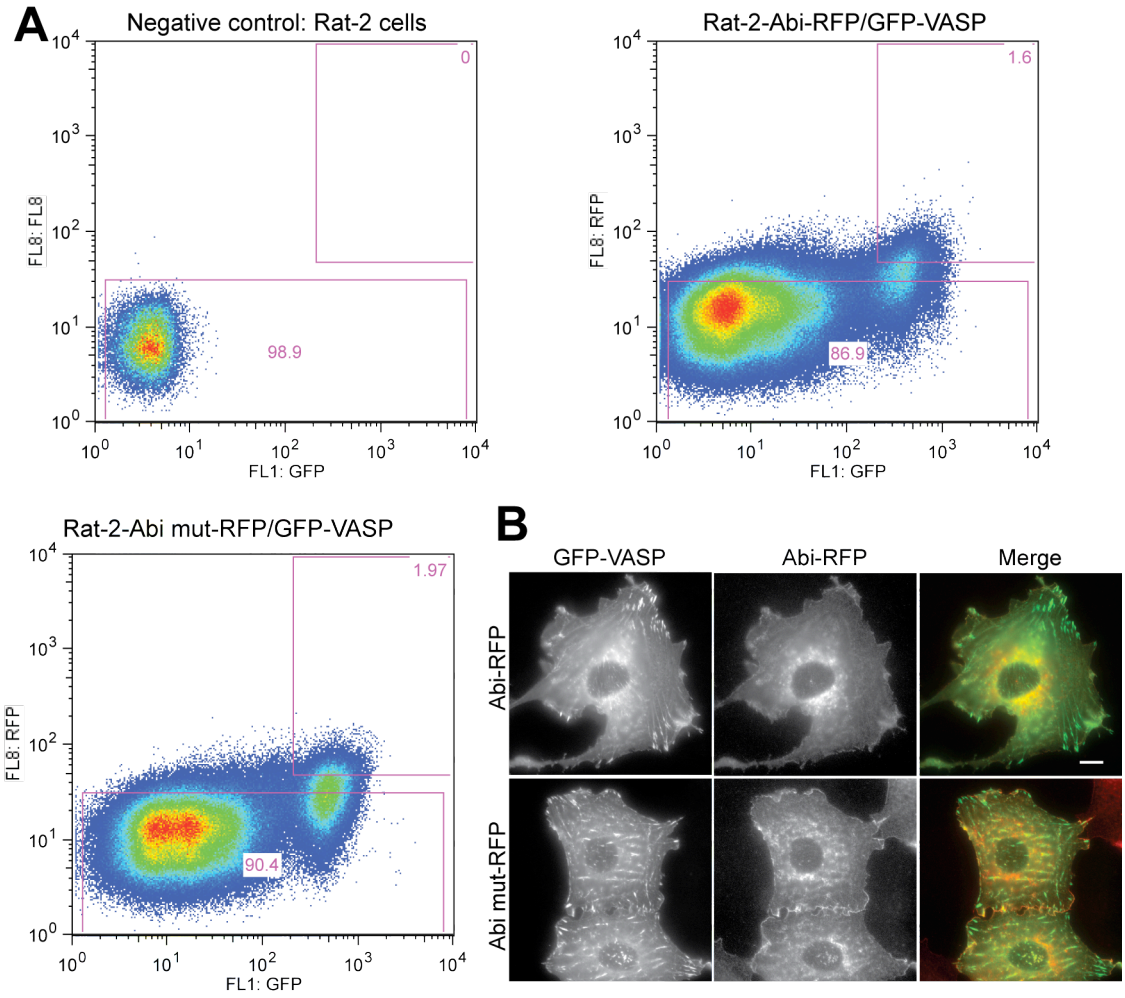

Figure 5.12 FACS sort to establish Abi-RFP/GFP-VASP and Abi mut-RFP/GFP-VASP Rat-2 cell lines.
A. Bivariate dot plot showing control Rat-2 cells that were used to set up the gating parameters to select RFP and GFP-positive cells. The cells in the bottom pink box represent the background fluorescence of RFP negative cells and 98.9% of cells are in this range. Only cells which showed a strong signal for both RFP and GFP (top pink box) were sorted. For Abi-RFP/GFP-VASP 1.6% and for Abi mut-RFP/GFP-VASP 1.97% of the cells were sorted as RFP and GFP-positive. **B.** The GFP and RFP-positive cells were fixed and analysed by fluorescence microscopy. GFP-VASP and Abi-RFP localised at their predicated cellular localisations. Cell lines are indicated on the side of the panels. The fluorescence channels that were used are indicated on the top of the panels. Scale bar represents 10 µm.

A

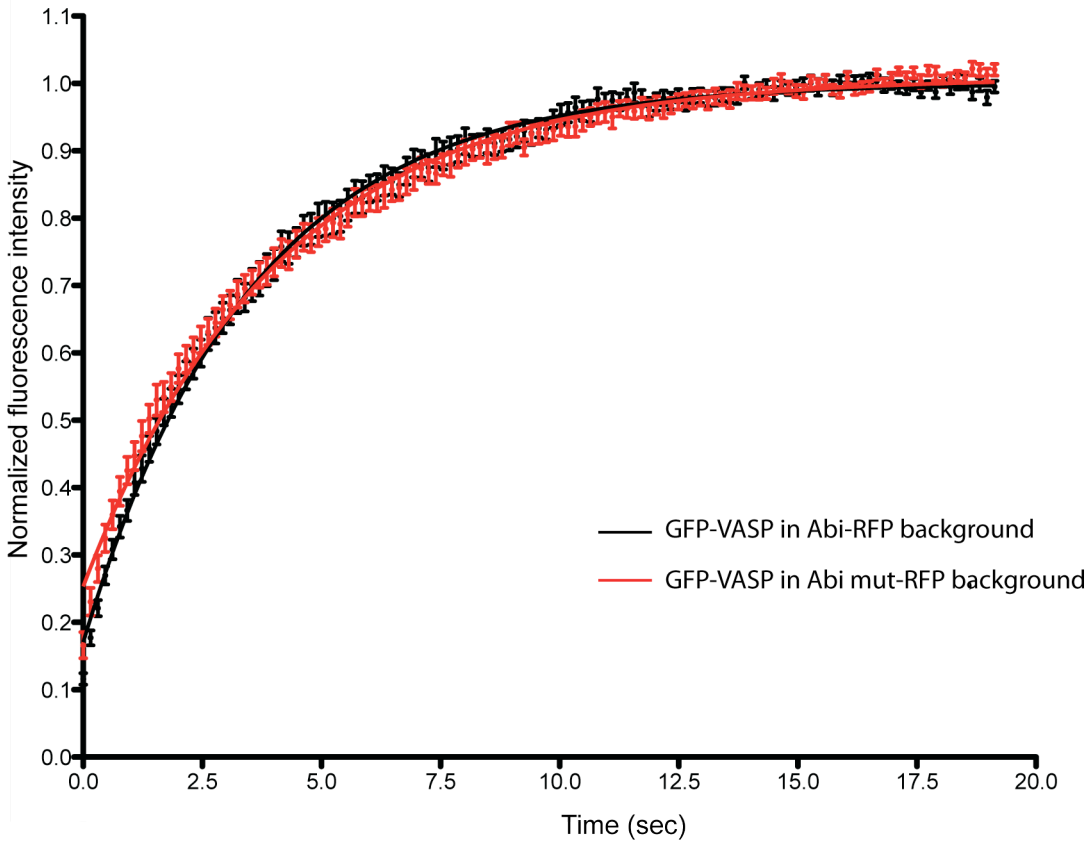

B

GFP-VASP	% Recovery	Rate constant of recovery (sec $^{-1}$)	$t_{1/2}$ (sec)
GFP-VASP/Abi-RFP	100 ± 0.003	0.284 ± 0.005	2.44 ± 0.04
GFP-VASP/Abi mut-RFP	100 ± 0.003	0.247 ± 0.004***	2.80 ± 0.05***

Figure 5.13 The WAVE complex regulates the turnover of Ena/VASP proteins at the plasma membrane.
A. The graph illustrating the recovery rate of GFP-VASP at the plasma membrane after photobleaching in cells expressing either Abi-RFP (black) or Abi mut-RFP (red). Intensity values of the GFP-VASP were normalised to the pre-bleached intensity value. Linear curves corresponded to best fits of averaged data. Bars represent the SEM and n = 20. **B.** The table lists the values derived from 20 fitted recovery curves together with the SEM, for the percentage, rate constant and half time of recovery of GFP-VASP in the presence of the indicated RFP-tagged protein. *** indicates P<0.001

5.2.5 Knockdown of endogenous Abi proteins in Rat-2 cells is problematic

My FRAP analysis established that the GFP-Abi mut is more dynamic at the leading edge compared with GFP-Abi (Figure 5.9). In contrast, GFP-VASP is less dynamic when it was co-expressed with the Abi mut-RFP. However, single cell tracking assays showed that the overexpression of the GFP-Abi mut did not lead to a major difference in the rate of cell migration. It may be that the absence of a migration phenotype for the GFP or RFP-tagged Abi mut is masked by the presence of endogenous Abi. I therefore aimed to repeat all my previous experiments using my Rat-2 cell lines that lack endogenous Abi.

To deplete endogenous Abi in Rat-2 cells, I needed to know how many Abi isoforms are present in this cell line, as mammals express three Abi isoforms (Hirao et al., 2006). To address this question, I performed quantitative real-time polymerase chain reaction (qRT-PCR). The results revealed that Rat-2 cells expressed all three Abi isoforms (Figure 5.14A). The amount of Abi1 mRNA was almost 3.5 times more than that of Abi3. The Abi 2 mRNA was more than double that of Abi3. While mRNA levels do not immediately predict protein levels, it is likely that Abi1 represents the most abundant isoform in Rat-2 cells. Importantly, all three Abi isoforms are known to interact with Mena and WAVE (Hirao et al., 2006). Therefore, in order to obtain a clearer phenotype of overexpressed GFP or RFP-tagged Abi mut, RNAi knockdown of all three endogenous Abi isoforms in Rat-2 cells was required.

Small interfering RNA (siRNA) oligonucleotides, which do not target GFP or RFP tagged human Abi and Abi mut, were used to knockdown each Abi isoform in Rat-2 cells. The efficiency of each siRNA oligonucleotide to deplete the different Abi isoforms was examined in Rat-2 cells. The best siRNA oligonucleotide for each Abi isoform would then be combined to generate a siRNA pool, which could be used to simultaneously knockdown all three Abi isoforms in the GFP or RFP-tagged Abi expressing Rat-2 cells. Due to a lack of antibodies that recognise the three different Abi isoforms, qRT-PCR was performed to determine the changes in mRNA level of each of isoform in Rat-2 cells. The mRNA level of β-actin was used as the internal control. Even after many attempts, I found no statistically significant decrease in the mRNA level of any Abi isoform when cells were treated with the appropriate siRNA (Figure 5.14). Given this and the lack of suitable antibodies to detect all three Abi

isoforms, I abandoned the knockdown of endogenous Abi isoforms in Rat-2 cells using RNAi approaches.

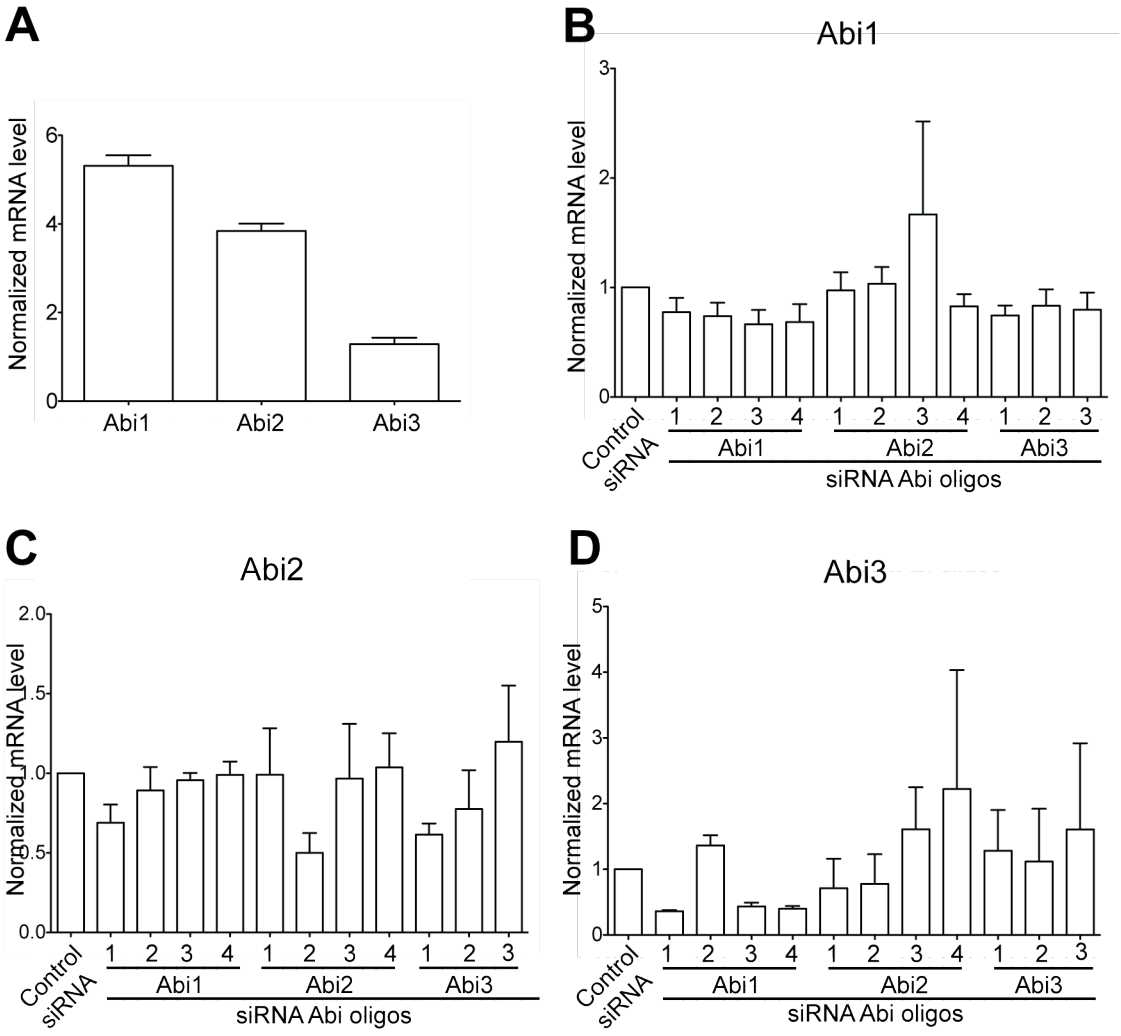

Figure 5.14 siRNA depletion of 3 Abi isoforms in Rat-2 cells.
A. The qRT-PCR reveals the mRNA levels of three Abi isoforms in Rat-2 cells, which were normalised to the mRNA level of β-actin. **B-D.** The qRT-PCR analyses show that the normalised mRNA expressions of three Abi isoforms in Rat-2 cells when the cells were treated with different siRNA oligonucleotides that target specific Abi isoforms. The mRNA levels of Abi isoforms in cells that were treated with non-targeting siRNA oligonucleotides were used as control. Rat-2 Abi isoforms are indicated in each bar chart. siRNA oligonucleotides used are indicated at the bottom of each bar chart.
Bars represent the SEM. n = 3.

5.3 Summary

In order to study the physiological importance of the interaction between Ena/VASP proteins and the WAVE complex in regulating the actin cytoskeleton during cell migration, I generated a series of stable Rat-2 cell lines expressing GFP or RFP-tagged proteins using a lentivirus system. Immunofluorescence analysis revealed that Ena/VASP proteins did not drive plasma membrane targeting of the WAVE complex. Moreover, time-lapse live cell imaging did not show any significant effects of over-expressing GFP-Abi mut on the migration of Rat-2 cells. FRAP analysis, however, demonstrated that uncoupling Abi from EVH1 increased the dynamics of the WAVE complex but decreased the dynamics of Ena/VASP proteins at the plasma membrane. This suggests a negative feedback loop might be involved in regulating the dynamics of the two groups of proteins at the plasma memberane. To try and obtain a clearer phenotype from overexpressing Abi mut in Rat-2 cell, it is likely that depletion of the endogenous Abi isoforms will be required. However, RNAi knockdown of the all three endogenous Abi isoforms in Rat-2 cells proved unsuccessful. I therefore decided to investigate the physiological significance of Abi-EVH1 interaction in regulation of actin cytoskeleton using a different model system, which is more amenable to RNAi techniques and only expresses one Abi isoform.

Chapter 6. Characterisation of the interaction between Ena and the WAVE complex in *Drosophila* haemocytes

6.1 Introduction

Given that depletion of the three Abi isoforms in Rat-2 cells is problematic (Figure 5.14) and antibodies that recognise specific Abi isoforms are currently unavailable, I decided to investigate the interplay between Ena/VASP proteins and the WAVE complex using *Drosophila* S2 and S2R$^+$ cells. S2 cell lines were originally derived from an embryonic macrophage-like lineage in *Drosophila* (Schneider, 1972). The S2R$^+$ cell line, which is positive for the Wingless (Wg) receptor, was subsequently identified and characterised (Yanagawa et al., 1998). This is an easier cellular system to study the potential role of this interaction as *Drosophila* only express one Abi isoform (dAbi) and one Ena (*Drosophila* homologue of Mena). Moreover, both, *Drosophila* S2 and S2R$^+$ cells have been widely used to study lamellipodial dynamics (LeClaire et al., 2008, Biyasheva et al., 2004, Jovceva et al., 2007, Iwasa and Mullins, 2007, Kim et al., 2011). Although the EVH1 domain of Ena/VASP proteins is highly conserved from fly to human, *Drosophila* Abi and human Abi (hAbi) have significantly less sequence similarity (Figure 6.1). Given the differences between the proline rich regions in human and *Drosophila* Abi, it is difficult to predict the location of the EVH1 binding site in dAbi based on the location of the EVH1 binding site in hAbi. Therefore, to generate a mutant dAbi that is deficient in EVH1 binding, I used similar biochemical approaches to those used to generate the hAbi mutant (Chapter 4). This dAbi mutant was then used to study the physiological importance of the dAbi-EVH1 interaction in *Drosophila* S2 and S2R$^+$ cells that had been depleted of endogenous dAbi using dsRNA.

6.2 Results

6.2.1 Generation of a mutant dAbi that is deficient in EVH1 binding

Given that the far western analysis of peptide arrays was successfully used to identify the EVH1 binding site in hAbi, the same approach was used to map the EVH1 binding site in dAbi. A peptide array was generated by the peptide service facility at Cancer Research UK, which contained a series of overlapping peptides 20 amino acid residues in length, and covering the full length of dAbi. The GST-EVH1 domain of Ena from *Drosophila* was expressed and purified in bacteria and used as a probe. Potential

interactions between peptides and the EVH1 domain were subsequently detected by GST antibodies as previously described (Figure 4.3B). As shown in Figure 6.2A, two regions in the C-terminal half of dAbi which both contain a single LPPPP motif were detected by GST antibodies. This suggests that these two LPPPP-containing regions of dAbi may be responsible for EVH1 binding. This data was confirmed by repeating the far western analysis on peptide arrays covering only the C-terminus of dAbi (residues 291-429), which includes the two potential EVH1 binding sites. In addition to using GST-EVH1 of Ena as a probe, purified GST alone was used as a negative control probe in this second assay. The results from this second experiment highlighted the same peptides that were detected in the previous array (Figure 6.2A). These peptides were detected only by GST-EVH1 and not GST (Figure 6.2B). Similar to my results from previous far western analyses (Figure 4.4), discontinuous detections of overlapping peptides was also observed with dAbi (Figure 6.2A, B). This may be due to errors or the efficiency of peptide synthesis. Taken together, my results suggest that residues 301-322 and 362-387 of dAbi are potential sites for EVH1 binding (Figure 6.2 C).

Given that the length of peptide that can be synthesised on a peptide array is limiting, generation of a peptide that covers the entire EVH1 binding site of dAbi is problematic. Therefore, to identify residues within the EVH1 binding sites of dAbi that are essential for EVH1 binding, I selected two dAbi peptides that bound strongly to the EVH1 domain of Ena (Figure 6.3A). Each amino acid position in the two peptides was sequentially mutated into the possible 20 different amino acids and spotted on to a peptide array. The peptide arrays with the mutated peptides were probed with GST-EVH1 of Ena and binding subsequently detected using GST antibodies. As shown in Figure 6.3B, substituting any of the residues in the LPPPP motifs for alternative amino acids significantly disrupted binding between the peptides and the EVH1 domain. These results suggest that these two LPPPP motifs are key residues for mediating the interaction between dAbi and EVH1.

Additionally, mutating the proline immediately after the LPPPP motif or mutating any of the last three amino acids in peptide 1 dramatically reduced binding (Figure 6.3B). In contrast, mutating the proline at the position after the LPPPP motif in peptide 2 had minimal effects on EVH1 binding. The different effects of mutating the proline immediately after the LPPPP motif on EVH1 binding between peptide 1 and 2 may be

due to the different sequences that are present downstream of this proline residue in these two peptides. For peptide 1, it should be noted that all the spots for the last two aspartic acids (last two rows) appear to be weaker (Figure 6.3B). This can be seen in the intensity of the spots where the aspartic acids remain unchanged, when compared to other spots representing unchanged residues. Therefore, it is likely that the decrease in binding seen when mutating any of these residues may be due to errors during peptide synthesis. However, it is curious that changing downstream acidic residues in both human and *Drosophila* Abi does seem to have an effect on EVH1 binding.

Identification of the two LPPPP motifs as being involved in EVH1 binding is consistent with previous studies that demonstrate FPPPP motifs as the classical binding motif for the EVH1 domain of Ena/VASP proteins (Niebuhr et al., 1997, Ball et al., 2000, Carl et al., 1999). Therefore, I hypothesised that the interaction between dAbi and the EVH1 domain of Ena is mediated by the two LPPPP motifs in dAbi. To test my hypothesis, I generated mutant dAbi, in which the first, second or both LPPPP motifs were substituted with "AGGGG" (Figure 6.4A). I then used these mutants to examine their effects on the dAbi-EVH1 interaction. Initially, I tried to perform *in vitro* pull-down assays with bacterially produced proteins. However, production of recombinant dAbi in bacteria proved unsuccessful, as no expression of dAbi with either GST or HIS tag in *E. coli* was observed (data not shown). I therefore performed pull-down assays on lysates from HEK 293T cells overexpressing dAbi containing the different mutations tagged at their N-terminus with GFP using the bacterially produced GST-EVH1 domain of Ena. Cell lysates with expressed GFP and GFP-dAbi were used as negative and positive controls respectively. Western blot analysis with a GFP antibody revealed that the GST-EVH1 domain of Ena but not GST alone retained GFP-dAbi but not GFP from cell lysates. In contrast, the GST-EVH1 domain of Ena only partially retained GFP-dAbi containing mutant 1 and was unable to retain dAbi containing either mutant 2 or both mutants (Figure 6.4B). These results suggest that both of the mutants affect binding of dAbi to the EVH1 domain of Ena, although mutating the second LPPPP motif at position 374-378 gives the greatest effect. To ensure a complete absence of interaction between dAbi and EVH1, a mutant dAbi that carries both sets of amino acids substitutions (L311A/P312G/P313G/P314G/P315G/ and L374A/P375G/P376G/P377G/P378G) is referred to as dAbi mut and used in future experiments.

To ensure overexpressed GFP-tagged dAbi and dAbi mut could still co-localise with other components of the WAVE complex at the plasma membrane, I performed immunofluorescence analysis using antibodies against endogenous SCAR (*Drosophila* homologue of WAVE) on S2 cells expressing GFP, dAbi-GFP or dAbi mut-GFP. DAbi-GFP and dAbi mut-GFP but not GFP alone co-localised with endogenous SCAR (Figure 6.5A). This suggests that overexpressed dAbi-GFP and dAbi mut-GFP retain their capacity to interact with rest of the WAVE complex. This suggestion was confirmed through immunoprecipitation using anti-GFP and antibodies against endogenous SCAR (Figure 6.5B). The same experiments were repeated using $S2R^+$ cells. Results from experiments using $S2R^+$ cells are consistent with those from S2 cells (Figure 6.6). Taken together, my data indicate that exogenously expressed dAbi-GFP and dAbi mut-GFP are properly incorporated into the WAVE complex in S2 cells and $S2R^+$ cells.

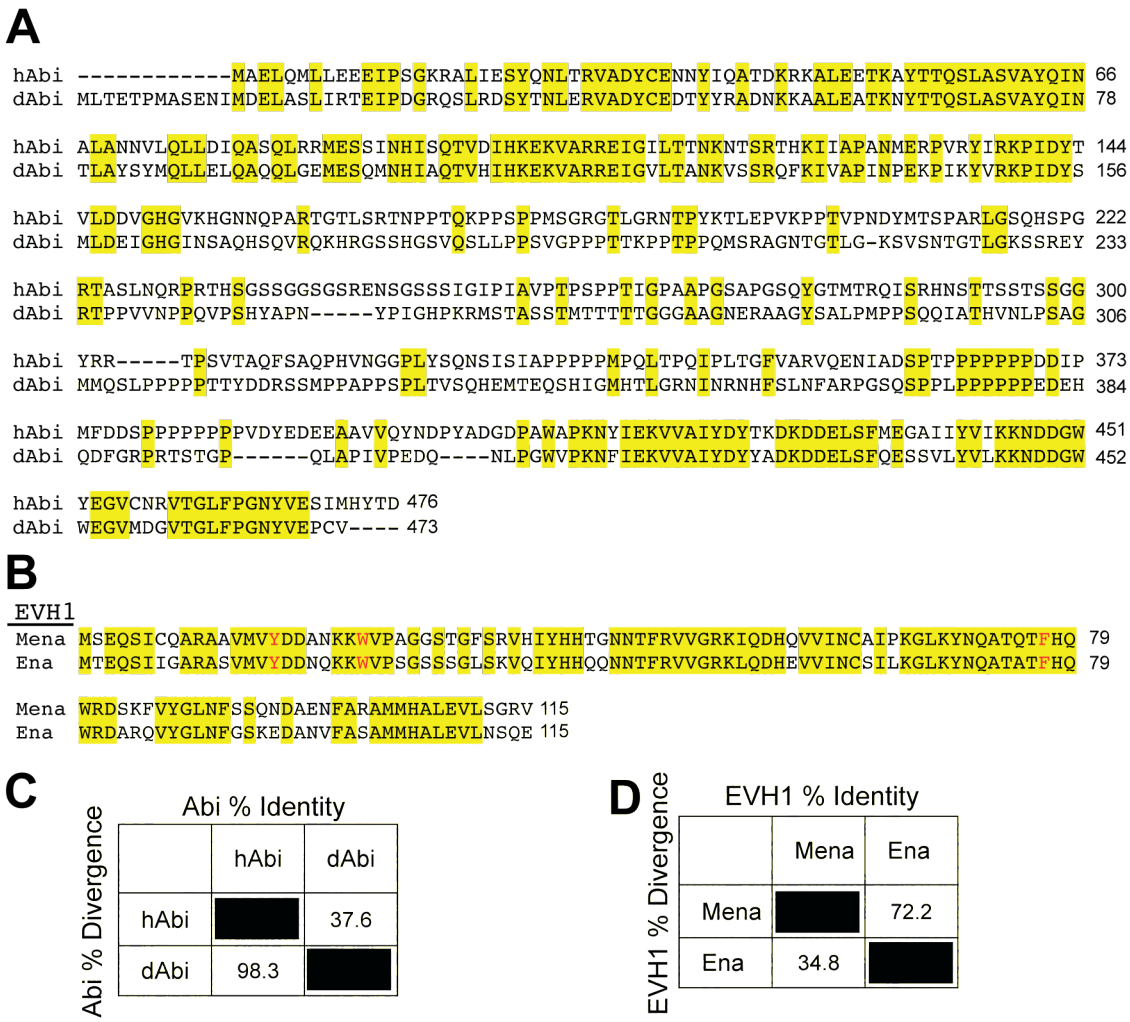

Figure 6.1 Sequence conservation of *Drosophila* and human Abi and the EVH1 domain of Mena/Ena.

A. Alignment of the sequence of human Abi (hAbi) and *Drosophila* (dAbi). Conserved amino acids are highlighted in yellow. **B**. Alignment of the EVH1 sequences of human Mena and *Drosophila* Ena. Conserved amino acids are highlighted in yellow. The conserved aromatic residues binding FPPPP ligands are indicated in red. **C**. The divergence and identity between the sequences of human Abi and *Drosophila* Abi. **D**. The divergence and identity between the EVH1 sequences of human Mena and *Drosophila* Ena. Figure was generated using ClustalW2-Multiple Sequence Alignment (EMBL-EBL).

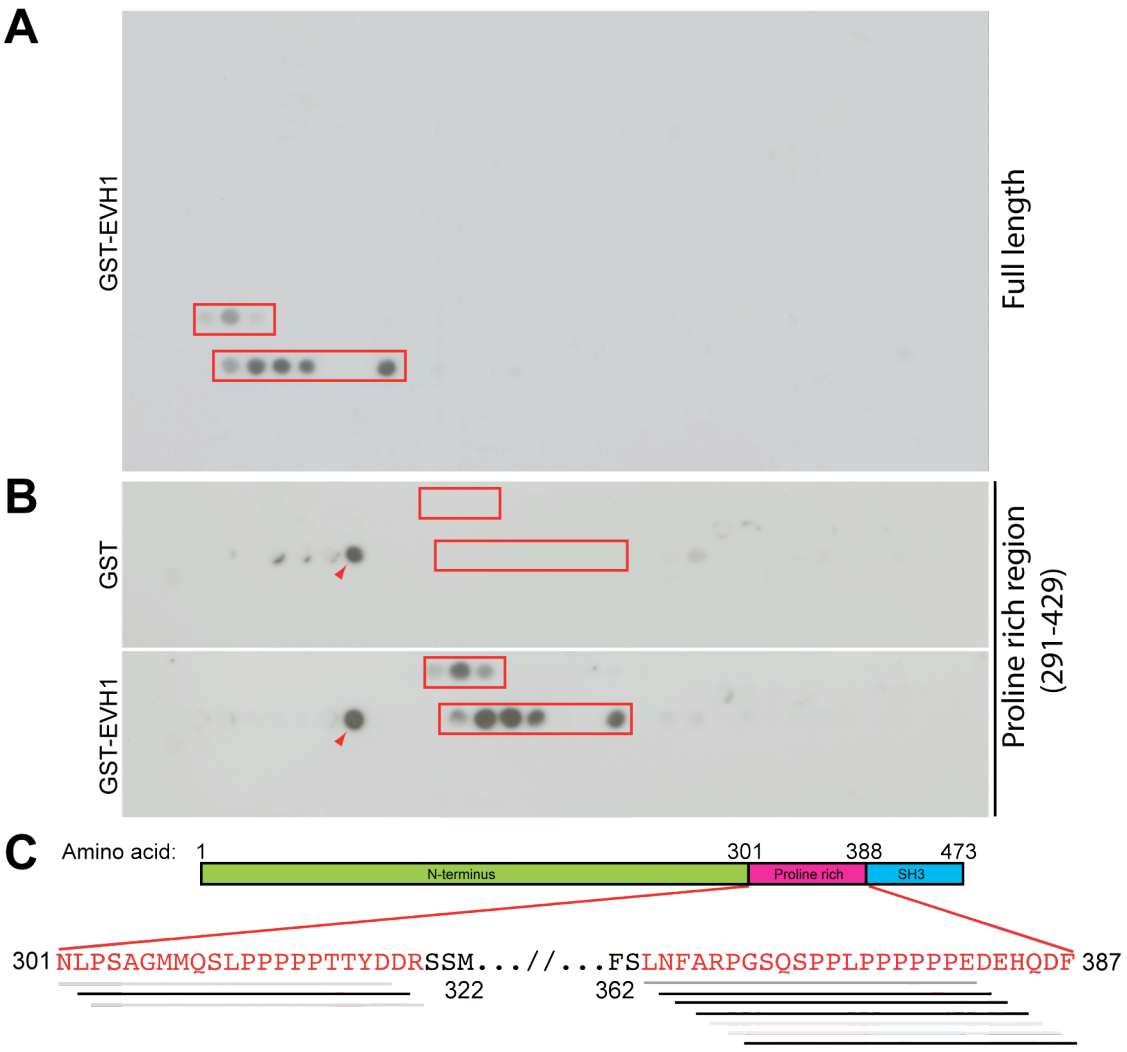

Figure 6.2 Residues 301-322 and 362-387 of dAbi can bind the EVH1 domain of Ena.

A. Far western analysis of a peptide array that contains overlapping peptides covering full length dAbi. Black spots highlight an interaction between a peptide and the GST-EVH1 domain of Ena. The spots that cover residues 301-322 and 362-387 in the proline rich region of dAbi are highlighted by red boxes. **B**. Far western analyses of peptide arrays that contain overlapping peptides covering residues 291-429 of dAbi. Black sports represent peptides that bound the GST-EVH1 domain of Ena. No black spots were observed in the peptide array that was probed with GST. Red boxes in both arrays indicate the positions of the peptides that cover residues 301-322 and 362-387 of dAbi. Red arrowheads indicate non-specific binding peptides. **C**. Schematic representation of the peptides of dAbi that bind the EVH1 domain of Ena. The sequence of the EVH1 binding sites in dAbi is indicated in red. Each line represents a peptide of 20 amino acids, which partially covers the EVH1 binding site in dAbi. The colours of the lines from darkest (black) to lightest (light grey) reflect the binding intensities observed in the peptide arrays.

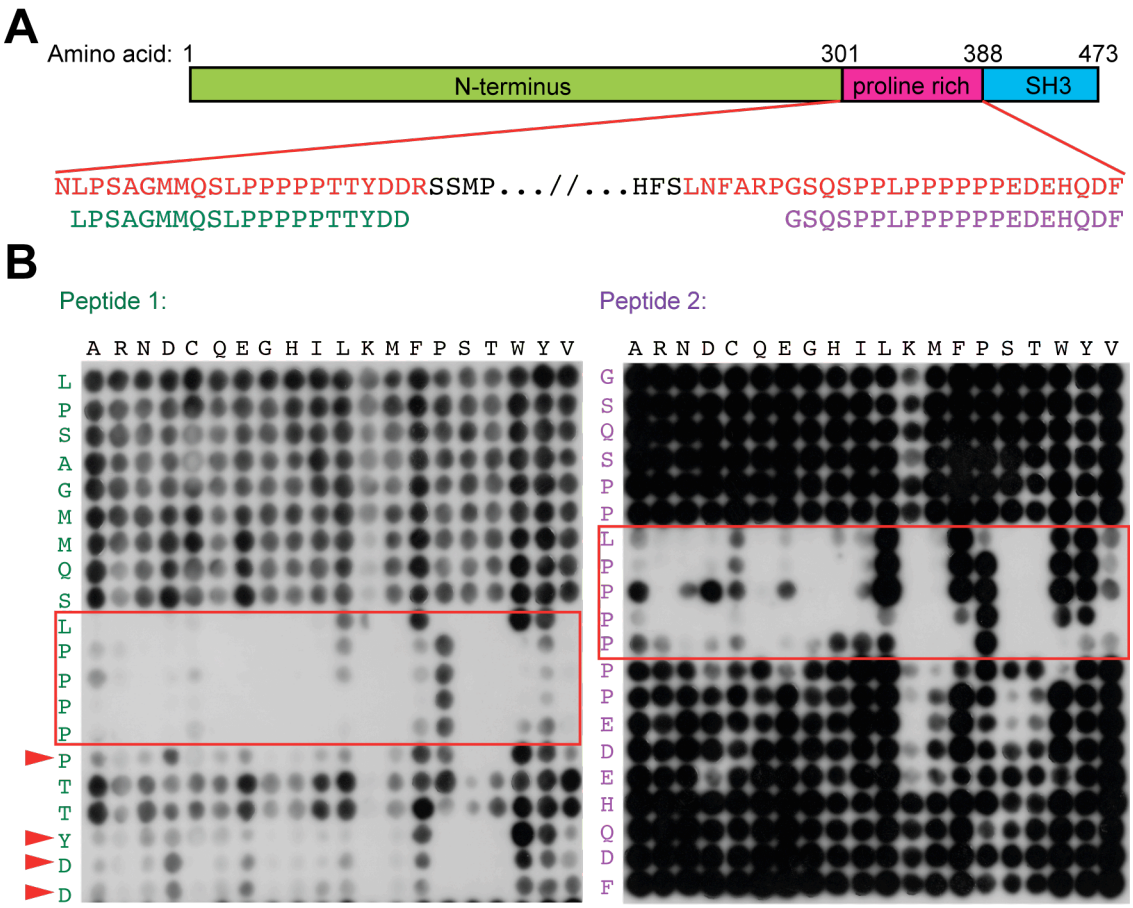

Figure 6.3 Identification of the residues in dAbi required for EVH1 binding.
A. Schematic representation of two peptides from dAbi that bound strongly to the GST-EVH1 domain of Ena. **B**. Residues in the two selected peptides were substituted in turn to the 20 different amino acids and examined for their interaction with the EVH1 domain of Ena. The intensities of the spots represent the comparative binding affinities of each mutated peptide to the EVH1 domain of Ena. The residues, which have largely lost the capacity to bind EVH1, are highlighted in red boxes. Red arrowheads indicate other residues that have also been also affected after substitution, although this may be due to problems in peptide synthesis.

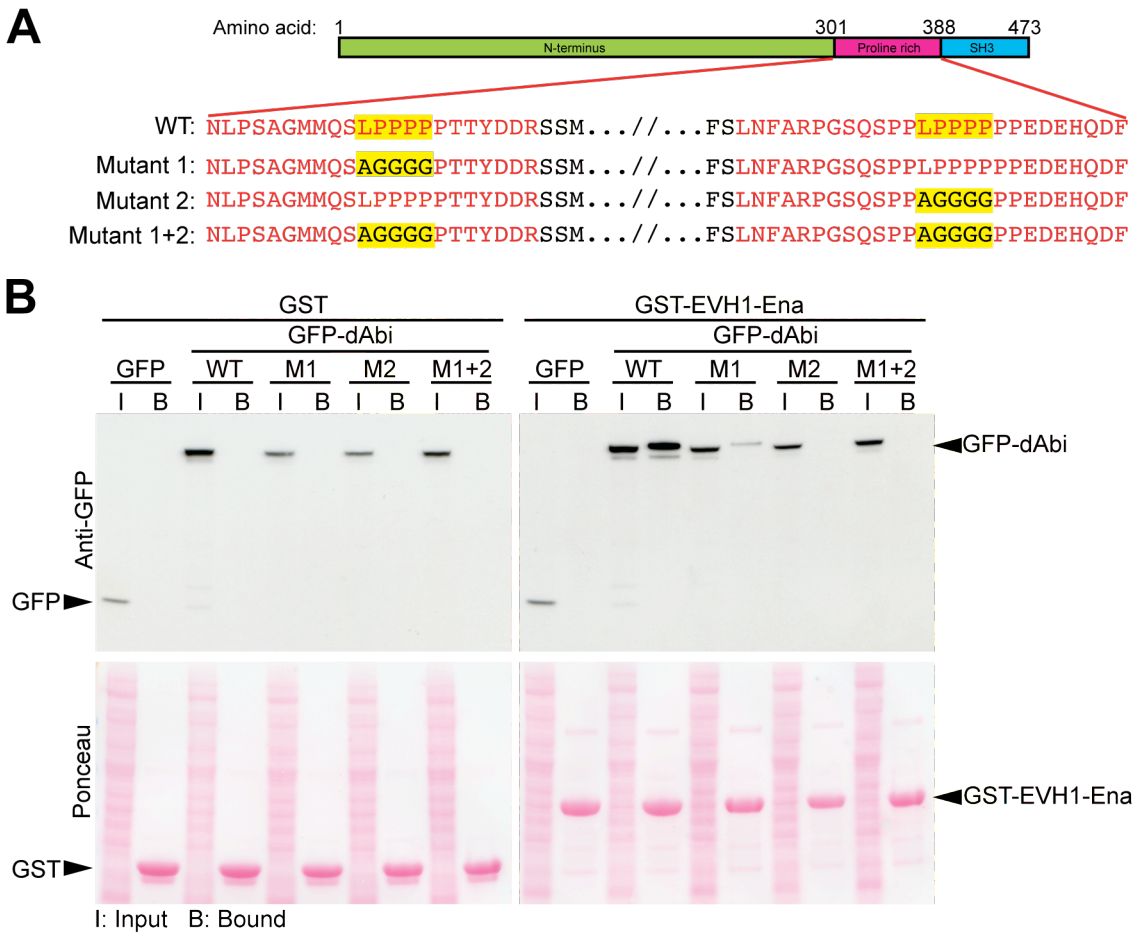

Figure 6.4 Mutation of LPPPP motifs in dAbi disrupts EVH1 binding.
A. Schematic representation of dAbi and LPPPP motif substitutions. The LPPPP motifs that mediate EVH1 interactions are highlighted in yellow. These residues were substituted to either glycine or alanine (black) to generate the indicated dAbi mutants. **B**. Immunoblot analysis of pull-downs using the GST-EVH1 domain of Ena (right panel) or GST alone (left panel) incubated with cell lysates containing GFP, GFP-tagged dAbi or dAbi mutants 1, 2 or 1+2. The input (I) and bound (B) samples with their respective GFP-tagged proteins are indicated. The Ponceau S stain shows equivalent amounts of GST and GST-EVH1 domain of Ena were present on the resin.

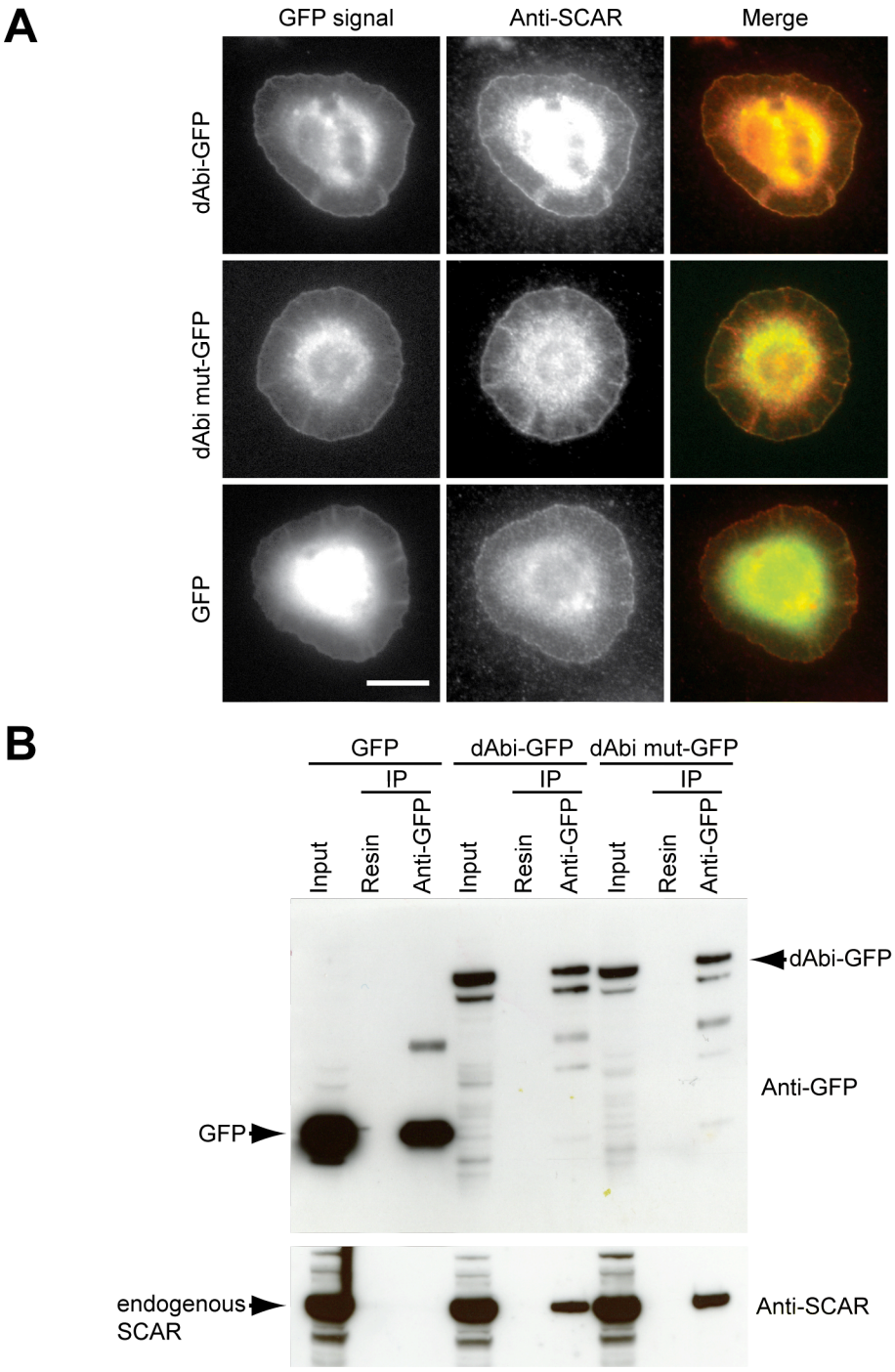

Figure 6.5 dAbi-GFP is incorporated into the WAVE complex in S2 cells.
A. Immunofluorescence analysis demonstrating that dAbi-GFP, dAbi mut-GFP but not GFP, are recruited to the plasma membrane of S2 cells, where they co-localise with endogenous SCAR. Scale bar represents 10µm. **B**. Immunoprecipitation analysis revealing that endogenous SCAR associates with dAbi-GFP, dAbi mut-GFP but not GFP in S2 cell lysates. 4% of each lysate was used as input.

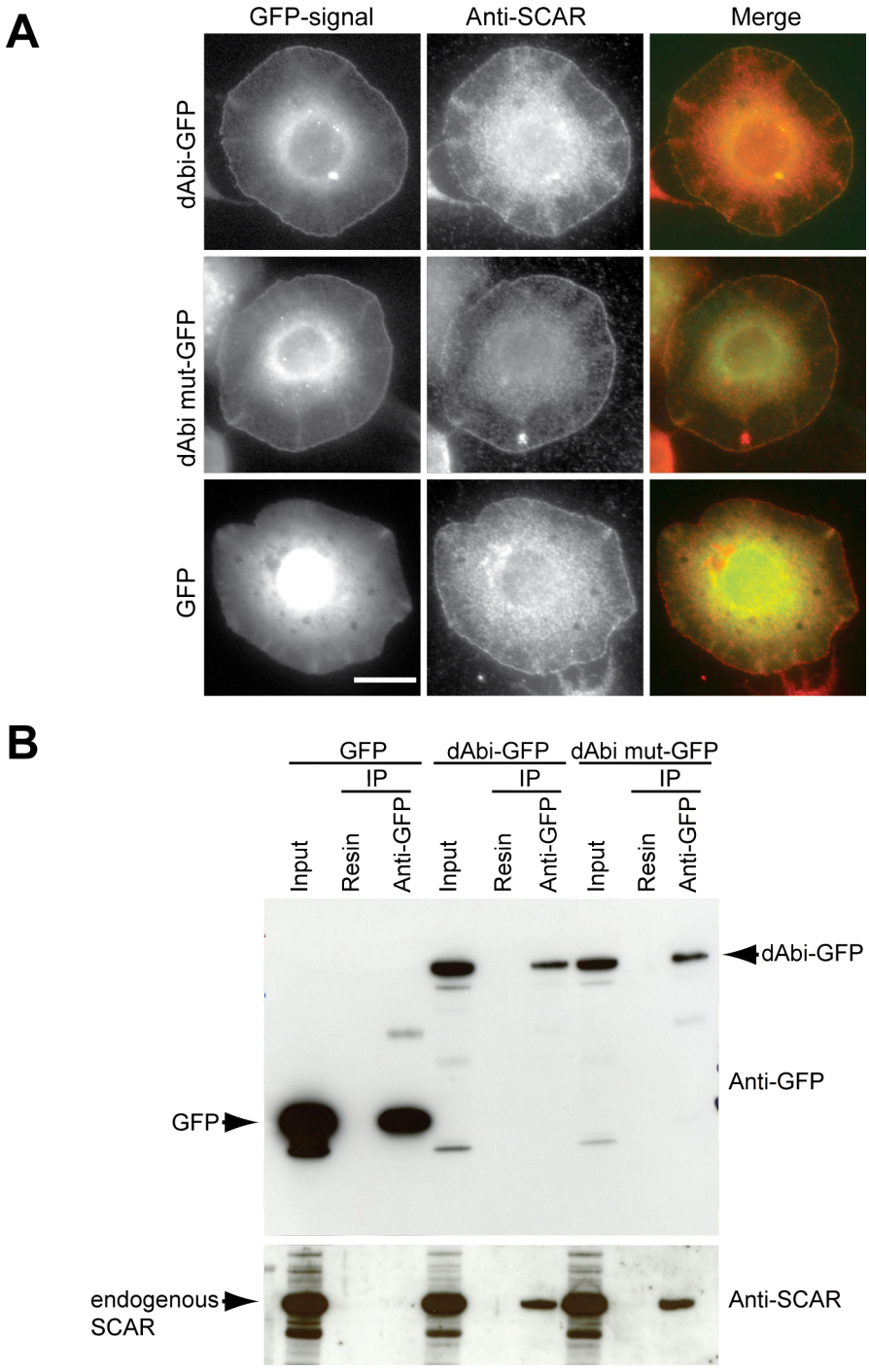

Figure 6.6 dAbi-GFP is incorporated into the WAVE complex in S2R$^+$cells.
A. Immunofluorescence analysis demonstrating that dAbi-GFP, dAbi mut-GFP but not GFP, are recruited to the plasma membrane of S2R$^+$ cells, where they co-localise with endogenous SCAR. Scale bar represents 10µm. **B**. immunoprecipitation analysis revealing that endogenous SCAR associates with dAbi-GFP, dAbi mut-GFP but not GFP in S2R$^+$cell lysates. 4% of each lysate was used as input.

6.2.2 S2 and S2R$^+$ cells lacking dAbi have defects in lamellipodia formation

Large double stranded RNA (dsRNA) has been successfully used to suppress gene expression in *Drosophila* haemocytes (Clemens et al., 2000, Kiger et al., 2003, Liu et al., 2009b). To inhibit the expression of endogenous dAbi in S2 and S2R$^+$ cells, I generated dsRNAs that targeted either the opening reading frame of dAbi (ORF) or the 3 prime untranslated region of dAbi (3'UTR) (Chapter 2.2.3.2). The ORF dsRNA, which is able to target both exogenous dAbi-GFP and endogenous dAbi, was used as a control to avoid unexpected off-target effects. In contrast, the 3'UTR dsRNA, which can only target dAbi and not dAbi-GFP, was used to reduce expression of endogenous dAbi in S2 and S2R$^+$ cells (Figure 6.7). In addition, dsRNA that suppresses *Drosophila* β-galactosidase (LacZ) expression was also generated and used as negative control (Chapter 2.2.3.2).

To verify the knockdown efficiency in S2 cells, I performed western blot analysis using an antibody that recognises endogenous dAbi on cell lysates derived from either non-transfected S2 cells or S2 cells expressing dAbi-GFP. LacZ dsRNA treated cells and non-dsRNA treated cells (mock) were used as controls. Western blot analysis revealed that the ORF dsRNA knocked down both the expression of endogenous dAbi and dAbi-GFP effectively. In contrast, the 3'UTR dsRNA only reduced expression of the endogenous dAbi (Figure 6.8A). Furthermore, qRT-PCR analysis also confirmed that both, ORF and 3'UTR dsRNA but not LacZ dsRNA are able to reduce the mRNA levels of the endogenous dAbi (Figure 6.8B). My results show that the 3'UTR dsRNA I generated can suppress the expression of endogenous dAbi but not that of dAbi-GFP in S2 cells.

To examine the phenotype of S2 cells lacking endogenous dAbi, I stained cells with phalloidin, which labels actin filaments. In contrast to LacZ dsRNA treated cells, which exhibited normal lamellipodia, both, the ORF and 3'UTR dsRNA transfected cells showed severe defects in lamellipodia formation and had spikey morphologies (Figure 6.8C). This appearance is consistent with previous results (Huang et al., 2007) and confirms that dAbi plays a central role in lamellipodia formation in S2 cells.

Using similar approaches, the knockdown efficiency of dAbi in S2R$^+$ cells and the resulting phenotype were examined. As observed in S2 cells, the expression levels of

endogenous dAbi and exogenously expressed dAbi-GFP were both reduced significantly by treating the $S2R^+$ cells with the ORF dsRNA (Figure 6.9A, B). In addition, the 3'UTR dsRNA was only able to knock down endogenous dAbi (Figure 6.9A, B). Moreover, $S2R^+$ cells lacking endogenous dAbi exhibited similar defects in lamellipodia formation as observed in ORF/3'UTR treated S2 cells (Figure 6.9C).

Given my results, I was now ready to study the significance of the interaction between Ena and the WAVE complex in S2 and $S2R^+$ cells lacking endogenous dAbi using my dAbi mutant that is deficient in EVH1 binding.

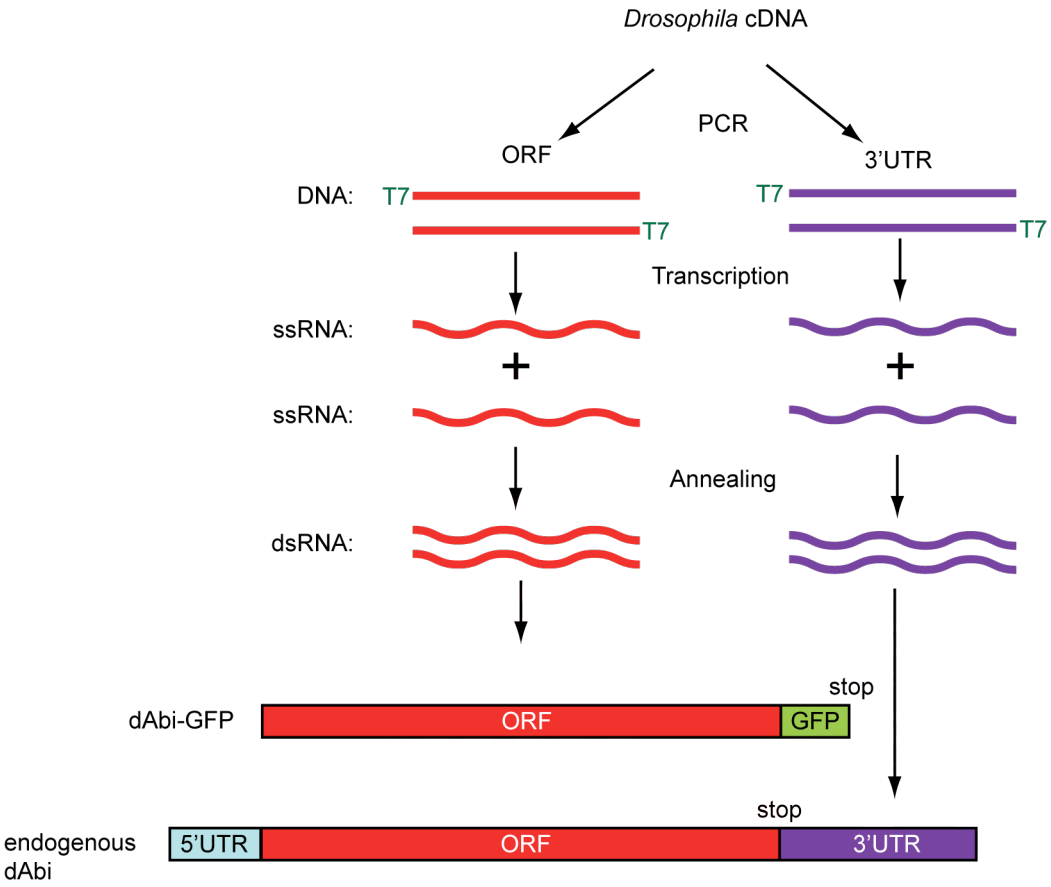

Figure 6.7 Schematic representation of dsRNA targeting the ORF or 3'UTR of dAbi.
Individual DNA fragments corresponding to the ORF or the 3'UTR of dAbi were amplified from a *Drosophila* cDNA library by using PCR. Each primer used in the PCR contains a 5 prime T7 RNA polymerase-binding site followed by sequences for the targeted gene (not shown). The resulting DNA fragments were used as templates for ssRNA synthesis using a transcription T7 kit. The ssRNAs were annealed to generate the dsRNA (Chapter 2.2.3.2). The dsRNA, which recognises the ORF of dAbi (red), targets both dAbi-GFP and endogenous dAbi. The dsRNA, which recognises the 3'UTR of dAbi (purple), only targets endogenous dAbi.

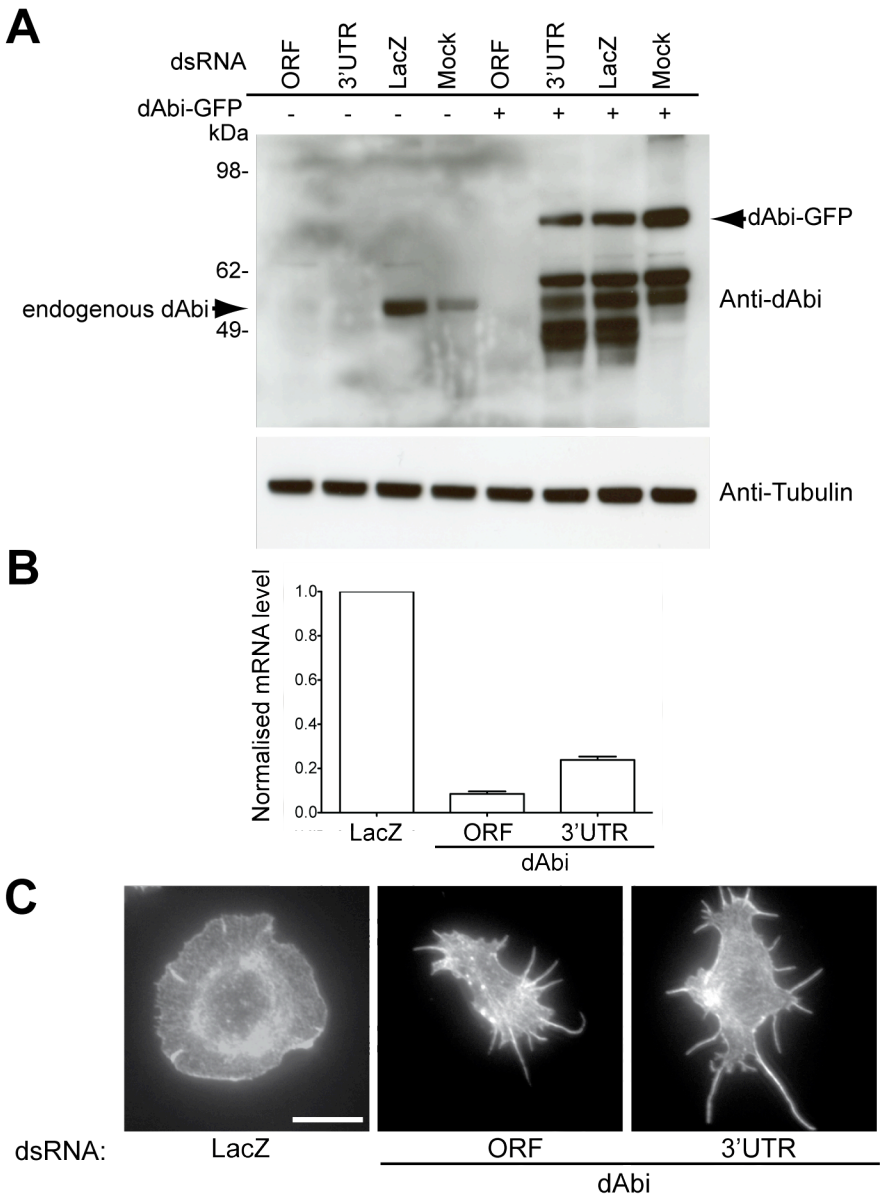

Figure 6.8 Knockdown of endogenous dAbi in S2 cells using dsRNA.
A. Immunoblot analysis of dAbi and dAbi-GFP expression in S2 cells treated with the indicated dsRNA (top of blot). DsRNA and cell lysates derived from untransfected cells or cells expressing dAbi-GFP are indicated. **B**. qRT-PCR analysis showing the normalised mRNA levels of dAbi in S2 cells when they are treated with dsRNA that targets either the ORF or the 3'UTR of dAbi. The mRNA level of dAbi in LacZ dsRNA treated S2 cells was used as control. dsRNA are indicated at the bottom of the bar chart. Error bars represent the SEM and n = 3. **C**. Immunofluorescent images of S2 cells that were treated with dsRNA targeting LacZ, the ORF or the 3'UTR of dAbi plated on con-A and stained with phalloidin. Loss of endogenous dAbi leads to a loss of lamellipodia and a spikey appearance. dsRNA are indicated below the panels. Scale bar represents 10 μm.

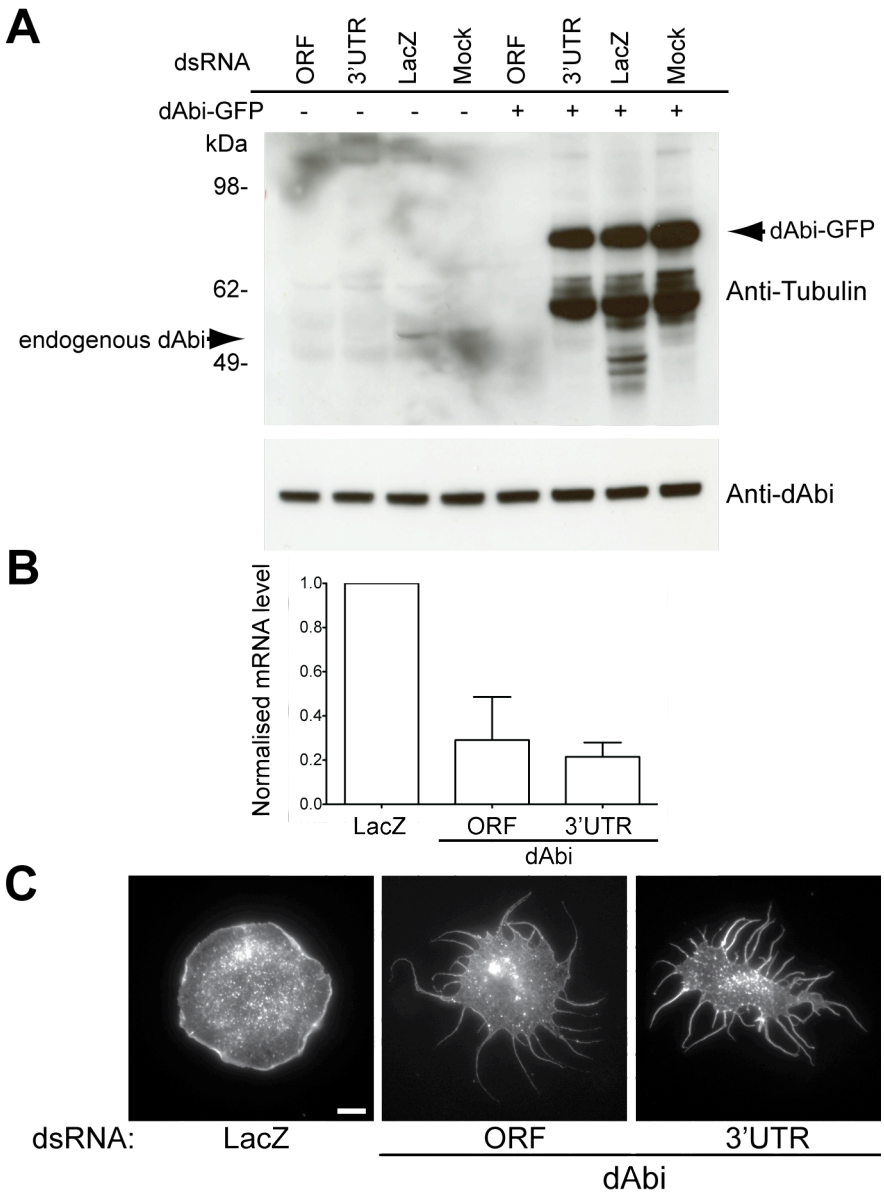

Figure 6.9 Knockdown of endogenous dAbi in S2R$^+$ cells using dsRNA.
A. Immunoblot analysis of dAbi and dAbi-GFP expression in S2R$^+$ cells treated with the indicated dsRNA (top of blot). DsRNA and cell lysates derived from untransfected cells or cells expressing dAbi-GFP are indicated on the top of the panels. **B**. qRT-PCR analysis showing the normalised mRNA levels of dAbi in S2R$^+$ cells when they are treated with dsRNA that targets either the ORF or the 3'UTR of dAbi. The mRNA level of dAbi in LacZ dsRNA treated S2R$^+$ cells was used as control. dsRNA are indicated at the bottom of the bar chart. Error bars represent the SEM and n =3. **C**. Immunofluorescent images of S2R$^+$ cells that were treated with dsRNA targeting LacZ, the ORF or the 3'UTR of dAbi plated on con-A and stained with phalloidin. Loss of endogenous dAbi leads to a loss of lamellipodia and spikey appearance. dsRNA are indicated below the panels. Scale bar represents10µm.

6.2.3 Uncoupling Ena from the WAVE complex does not affect lamellipodia formation

My previous results show that dAbi (WAVE complex) is essential for lamellipodia formation. I now wondered whether the interaction of dAbi with Ena plays a role in regulating lamellipodia formation. To address this question, I treated S2 cells with four different knockdown/re-expression strategies. I overexpressed GFP in S2 cells that had been pre-treated with either LacZ or 3'UTR dsRNA. Alternatively I overexpressed GFP-tagged dAbi or dAbi mut in S2 cells that had been pre-treated with 3'UTR dsRNA. After two days, I then performed immunofluorescence analysis and GFP-positive cells in each group were scored based on their morphology. As shown in Figure 6.10A, approximately 80% of the LacZ dsRNA-treated cells that express GFP exhibited normal lamellipodia, whereas only 25% of the 3'UTR dsRNA treated cells that express GFP had lamellipodia. Lamellipodia formation is rescued by expression of dAbi-GFP in 3'UTR dsRNA treated cells. Expression of dAbi mut-GFP also rescues lamellipodia formation to almost the same extent as the wild type protein. Similar results were obtained in the experiments using $S2R^+$ cells (Figure 6.10B). These experiments demonstrate that the dAbi mut-GFP is as efficient as the wild type in rescuing the defect in lamellipodia formation in both, S2 and $S2R^+$ cells that lack endogenous dAbi. Taken together the results suggest that the interaction between Ena and dAbi is not required for lamellipodia formation.

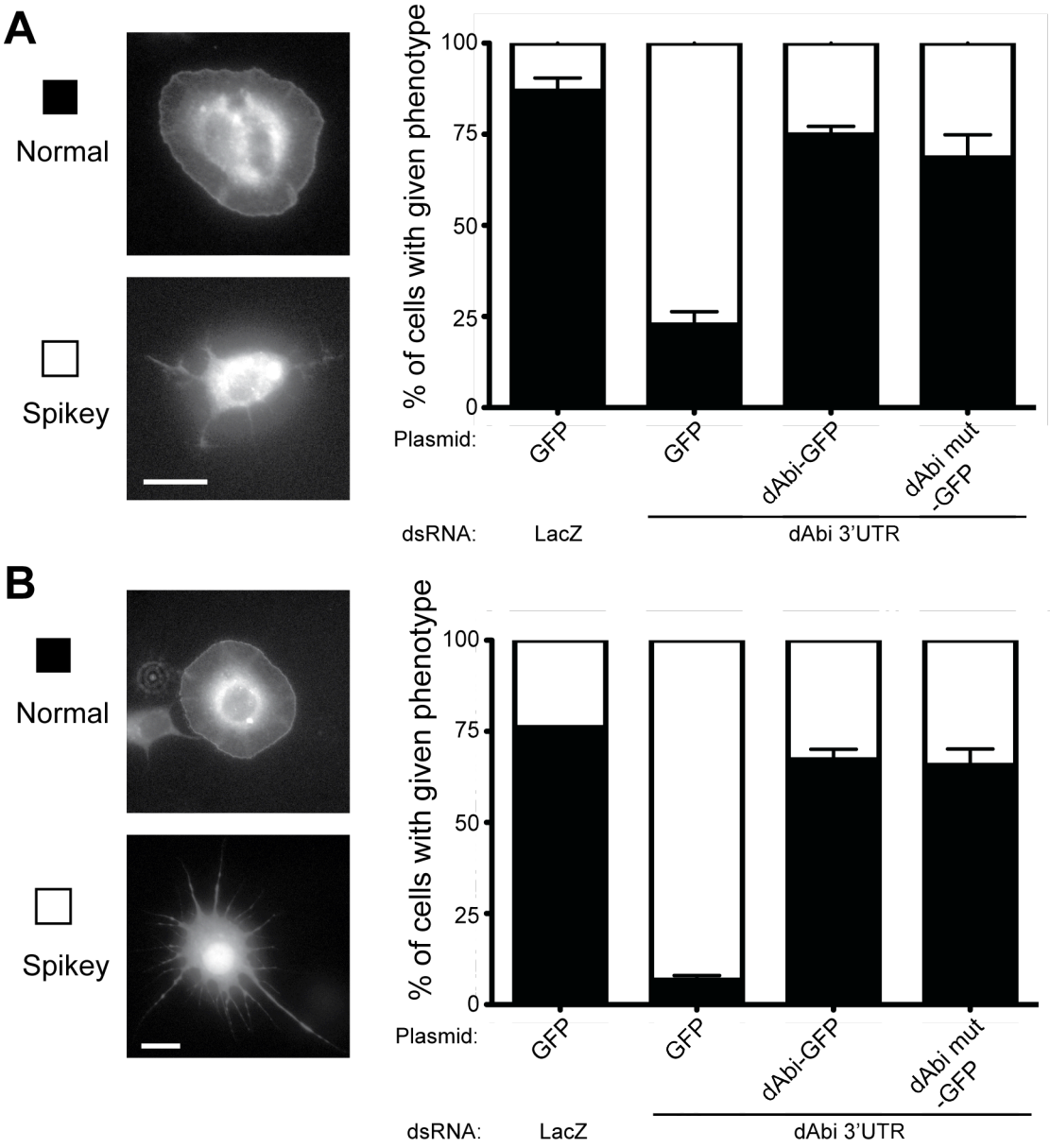

Figure 6.10 dAbi-GFP and dAbi mut-GFP can rescue lamellipodia formation in S2 and S2R$^+$ cells lacking endogenous dAbi.
A. Quantification of the ability of GFP-tagged dAbi or dAbi mut to rescue lamellipodia formation in S2 cells lacking endogenous dAbi. The phenotypes of lamellipodial structures were quantified based on the image standards shown in the left panel. Treatments used are indicated at the bottom of the graphs. **B**. The experiment described in **A** was repeated using S2R$^+$ cells. In both cases, error bars represent the SEM and n = 600. Scale bar represents 10μm.

6.2.4 The localisation of Ena at the plasma membrane is independent of dAbi

It is known that the localisation of Ena/VASP proteins at the plasma membrane is mediated by the direct interactions between their EVH1 domains and the FPPPP-containing MRL family proteins such as lamellipodin (Krause et al., 2004, Michael et al., 2010). I wanted to ask if the WAVE complex cooperates with MRL proteins to drive the cellular localisation of Ena/VASP proteins to the plasma membrane. To address this question, I perfomed rescue experiments in which 3'UTR-treated S2 cells were transfected with either dAbi-GFP or dAbi mut-GFP. Using these cells, I performed immunofluorescence analysis with an antibody that recognises endogenous Ena. Both overexpressed dAbi-GFP and dAbi mut-GFP were found to co-localise with endogenous Ena at the plasma membrane in S2 cells (Figure 6.11A). Quantification of the fluorescence intensity of Ena in cells that either express dAbi-GFP or dAbi mut-GFP revealed that there was no significant difference in the amount of Ena at the plasma membrane (Figure 6.11B) (Chapter 2.6.1). This result suggests that localisation of Ena at the plasma membrane is not dependent on the WAVE complex. Unfortunately, I was unable to repeat this experiment in $S2R^{+}$ cells, as the Ena antibody does not detect endogenous Ena in these cells (data not shown). Together with my previous results in migrating Rat-2 cells (Figure 5.4), this suggests that recruitment of Ena/VASP proteins and the WAVE complex at the plasma membrane is not mediated by an Abi-EVH1 interaction.

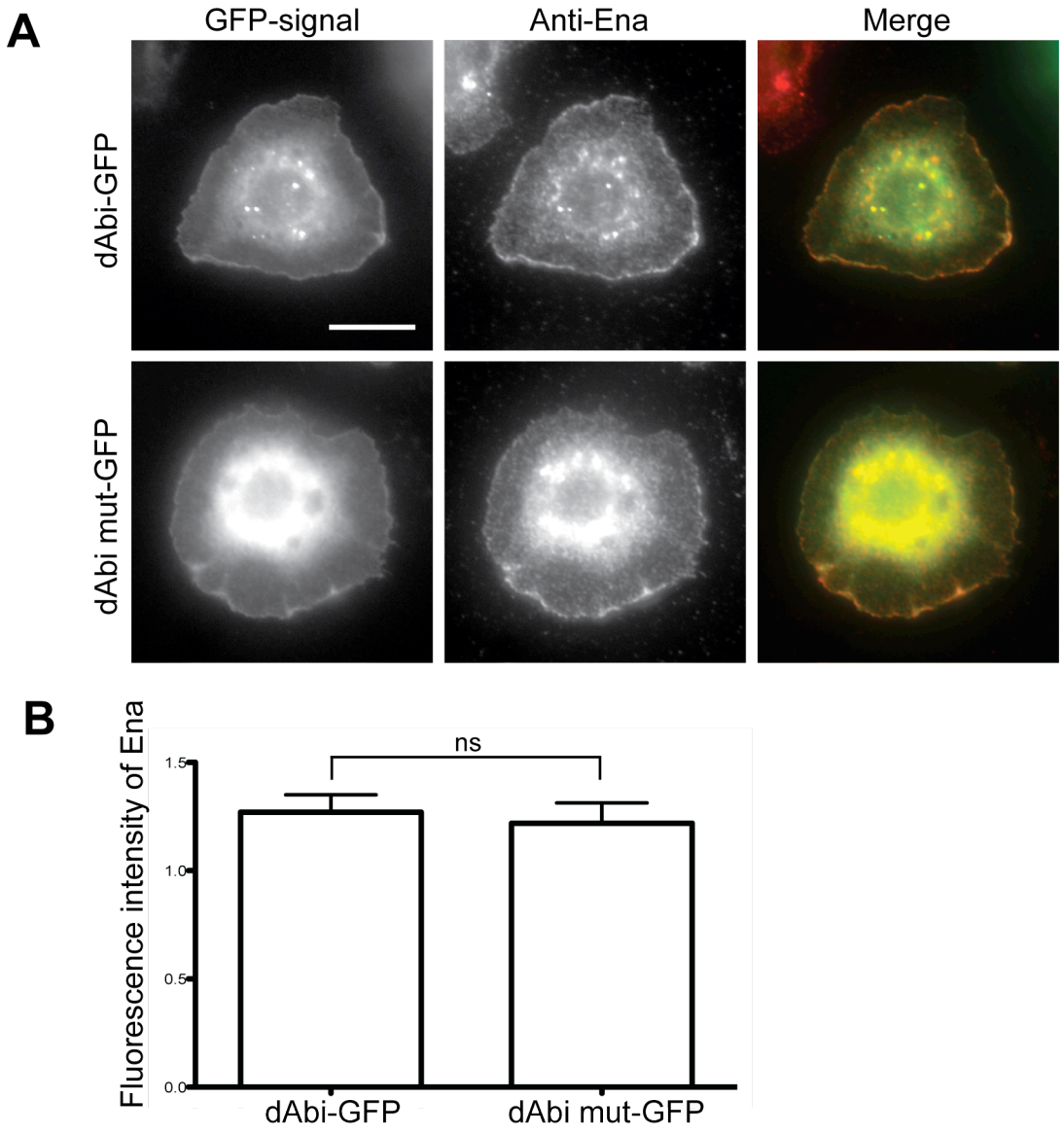

Figure 6.11 Uncoupling of Ena from dAbi does not affect the localisation of Ena at the plasma membrane.
A. Immunofluorescence images showing the localisation of endogenous Ena together with GFP-tagged dAbi or dAbi mut in S2 cells. Ena antibody is indicated on the top of the panels and GFP-tagged proteins are indicated on the left of the panels. Scale bar represents 10μm. **B**. Quantification of the fluorescence intensity of Ena at the plasma membrane in S2 cells expressing either GFP-tagged dAbi or dAbi mut. A student's t-test was performed. ns indicates no significance. Error bars represent the SEM. n = 30.

6.2.5 dAbi-EVH1 interaction regulates the dynamics of the WAVE complex at the plamsma membrane

The results from previous FRAP analyses using the stable Rat-2 cell lines suggest that uncoupling Ena/VASP proteins from the WAVE complex increases the dynamics of the WAVE complex but not the former at the leading edge of migrating cells (Figure 5.9 and 5.13). However, the stable Rat-2 cell lines that were used in these FRAP experiments had endogenous Abi, which could partially mask any phenotype of the overexpressed GFP-Abi mut. Therefore I wanted to examine the effects of the dAbi-EVH1 interaction on the dynamics of both Ena and the WAVE complex at the plasma membrane in S2 and S2R$^+$ cells lacking endogenous dAbi.

To test the effects of abrogating the interaction between dAbi and Ena on the dynamics of the WAVE complex at the plasma membrane, I performed FRAP analysis on 3'UTR dsRNA-treated S2 and S2R$^+$ cells that express either dAbi-GFP or dAbi mut-GFP. After photobleaching, the dAbi mut-GFP recovered faster than the dAbi-GFP at the plasma membrane in both S2 and S2R$^+$ cells lacking endogenous dAbi (Figure 6.12A and 6.13A). Furthermore, statistical analysis revealed that the difference in the turnover rates of dAbi-GFP and dAbi mut-GFP is significant (Figure 6.12B and 6.13B). These results are consistent with my previous FRAP results in Rat-2 cells (Figure 5.9). Together, this suggests that the WAVE complex is more dynamic if it does not interact with Ena/VASP proteins. Notably, the turnover rate of dAbi mut-GFP is almost 30% higher than that of dAbi-GFP in S2 cells lacking endogenous dAbi (Figure 6.12B). In contrast, there was only approximately 20% difference in the turnover rates between GFP-Abi and GFP-Abi mut in Rat-2 cells containing the endogenous Abi (Figure 5.9B). These differences may be due to the presence or absence of endogenous dAbi. My observations from the FRAP analyses using both, mammalian and insect cells suggest that Ena/VASP proteins play a role in helping to stabilise the WAVE complex at the plasma membrane.

To test if uncoupling Ena from the WAVE complex also affects the dynamnics of Ena at the plasma membrane, I performed FRAP analysis using S2 cells co-overexpressing Ena-mCherry with either GFP-tagged dAbi or dAbi mut in the absence of the endogenous dAbi. As shown in Figure 6.14A, the black curve that represents the recovery rate of Ena in the dAbi-GFP background overlapped with the red curve that

corresponds to the recovery rate in the dAbi mut-GFP expressing cells. The statistical analysis showed that there was no difference in the turnover rate of Ena-mCherry when co-overexpressed with dAbi or its mutant (Figure 6.14B). The results suggest that the dynamics of Ena at the plasma membrane is not dependent on the WAVE complex. The overexpression of Ena-mCherry in $S2R^+$ cells was problematic (data not shown). The low expression level of Ena-mCherry led to difficulties in performing FRAP analysis. Therefore, the interplay between Ena and the WAVE complex in regulating the dynamics of Ena at the plasma membrane could not be studied in $S2R^+$ cells.

The results from the FRAP analysis using stable Rat-2 cell lines suggest that the WAVE complex regulates the dynamics of VASP at the plasma membrane (Figure 5.13), whereas the results from the FRAP analysis using S2 cells suggest that the dynamics of Ena at the plasma membrane is not affected by the WAVE complex (Figure 6.14). It is not clear why different results were obtained from the two experiments. I am sure that this is at least in part due to the problems of overexpressing Abi-RFP in Rat-2 cells. The difficulties in overexpressing Abi-RFP in Rat-2 cells led to limited numbers of RFP positive cells that could be analysed using FRAP (n=20). The results from the FRAP analysis using Rat-2 stable are therefore likely to be less reliable due to the limited sample size as well as the inconsistent expression and aggregation problem of Abi-RFP and Abi mut-RFP. In contrast, the expression level of dAbi-GFP in transiently transfected S2 cells was always relatively high (data not shown). More cells were also measured in the FRAP analysis of S2 cells (n=45). Furthermore, the phenotype of the overexpressed dAbi mut-GFP in S2 cells was fully uncovered through knocking down endogenous dAbi. Thus, I feel a firm conclusion can be better drawn from the FRAP analysis of S2 cells.

Taken together, my data from FRAP analyses using different model systems suggests that the interaction between Ena/VASP proteins and the WAVE complex is essential for stabilising the WAVE complex at the plasma membrane, although the dynamics of Ena at the plasma membrane does not appear to be affected by the WAVE complex.

A

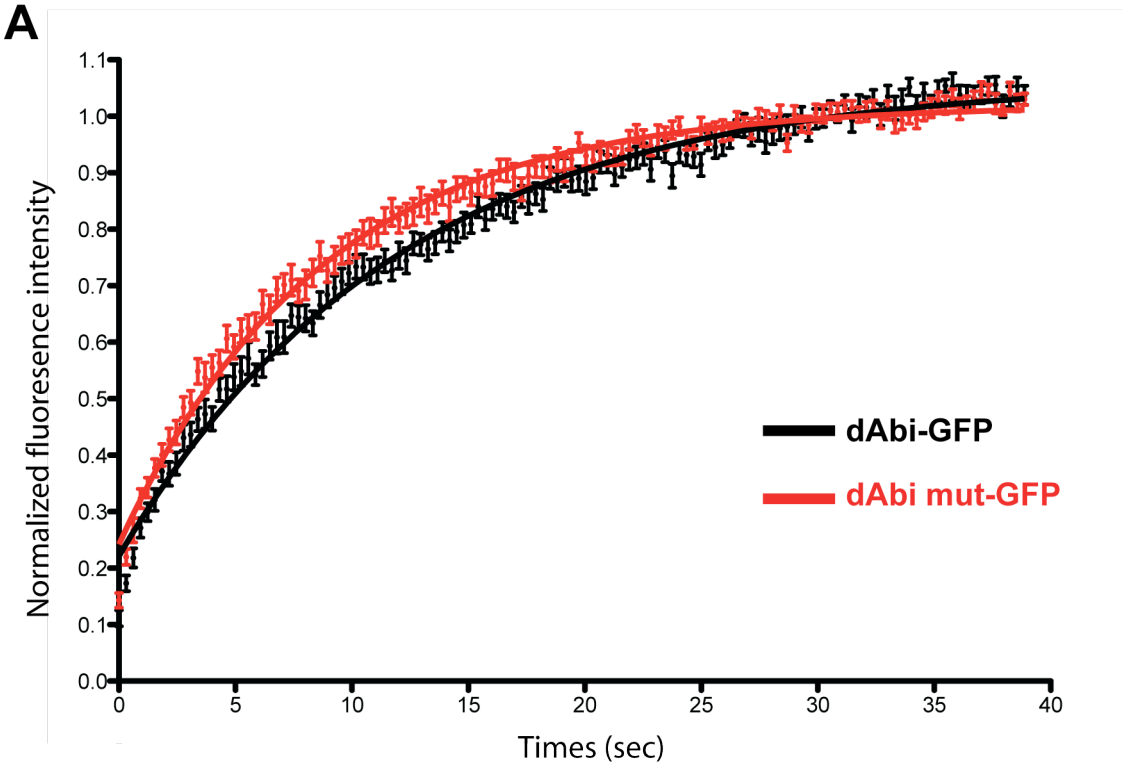

B

Protein	% Recovery	Rate constant of recovery (sec $^{-1}$)	$t_{1/2}$ (sec)
dAbi-GFP	100 ± 0.006	0.084 ± 0.002	8.282 ± 0.196
dAbi mut-GFP	100 ± 0.004	0.116 ± 0.002	6.002 ± 0.127***

Figure 6.12 Ena stabilises the WAVE complex at the plasma membrane in S2 cells.

A. The graph illustrates the recovery rates of dAbi-GFP (black) and dAbi mut-GFP (red) at the plasma membrane in the absence of endogenous dAbi after photobleaching. Intensity values of the GFP-tagged proteins were normalised to a pre-bleach image. Linear curves correspond to best fits of averaged data. Error bars represent the SEM and n = 30. **B**. The table lists values derived from the 30 fitted recovery curves together with the SEM for the percentage, rate constant and half time of recovery of dAbi-GFP and dAbi mut-GFP in S2 cells. *** indicates P<0.001.

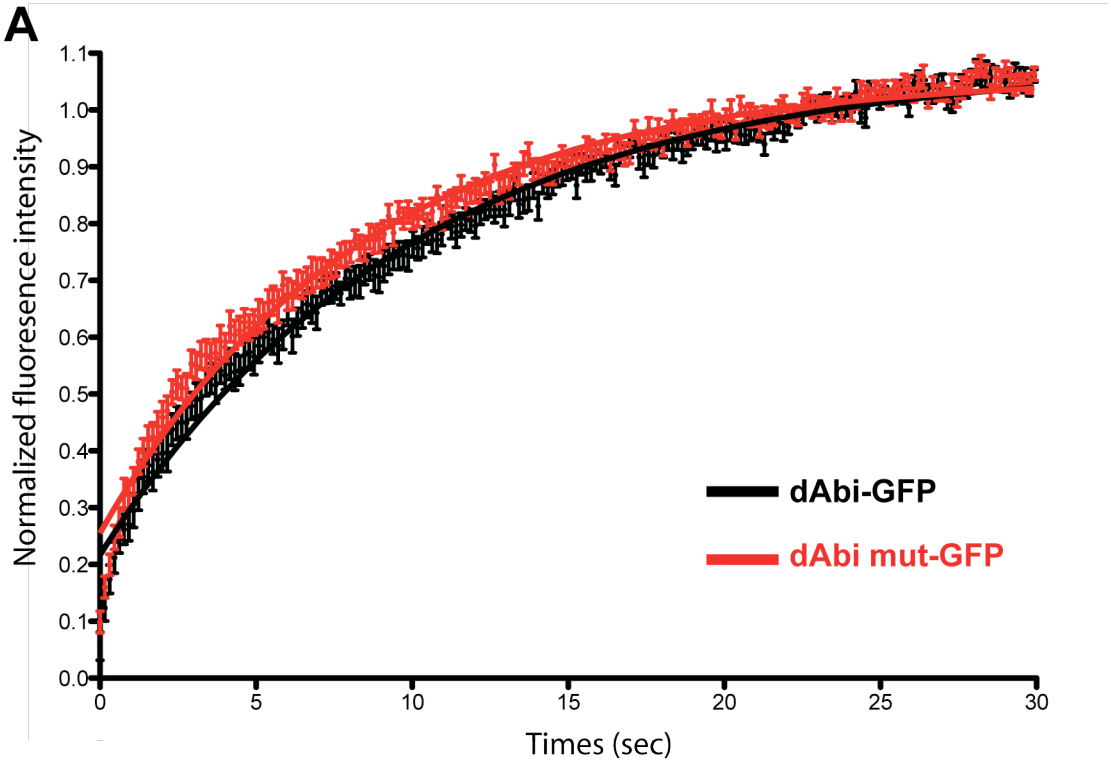

B

Protein	% Recovery	Rate constant of recovery (sec $^{-1}$)	$t_{1/2}$ (sec)
dAbi-GFP	100 ± 0.006	0.101 ± 0.002	6.884 ± 0.148
dAbi mut-GFP	100 ± 0.004	0.120 ± 0.002	5.760 ± 0.109***

Figure 6.13 Ena stabilises the WAVE complex at the plasma membrane in S2R$^+$ cells.
A. The graph illustrates the recovery rates of dAbi-GFP (black) and dAbi mut-GFP (red) at the plasma membrane in the absence of endogenous dAbi after photobleaching. Intensity values of the GFP-tagged proteins were normalised to a pre-bleach image. Linear curves correspond to best fits of averaged data. Error bars represent the SEM and n = 30. **B**. The table lists values derived from the 30 fitted recovery curves together with the SEM for the percentage, rate constant and half time of recovery of dAbi-GFP and dAbi mut-GFP in S2R$^+$ cells. *** indicates P<0.001.

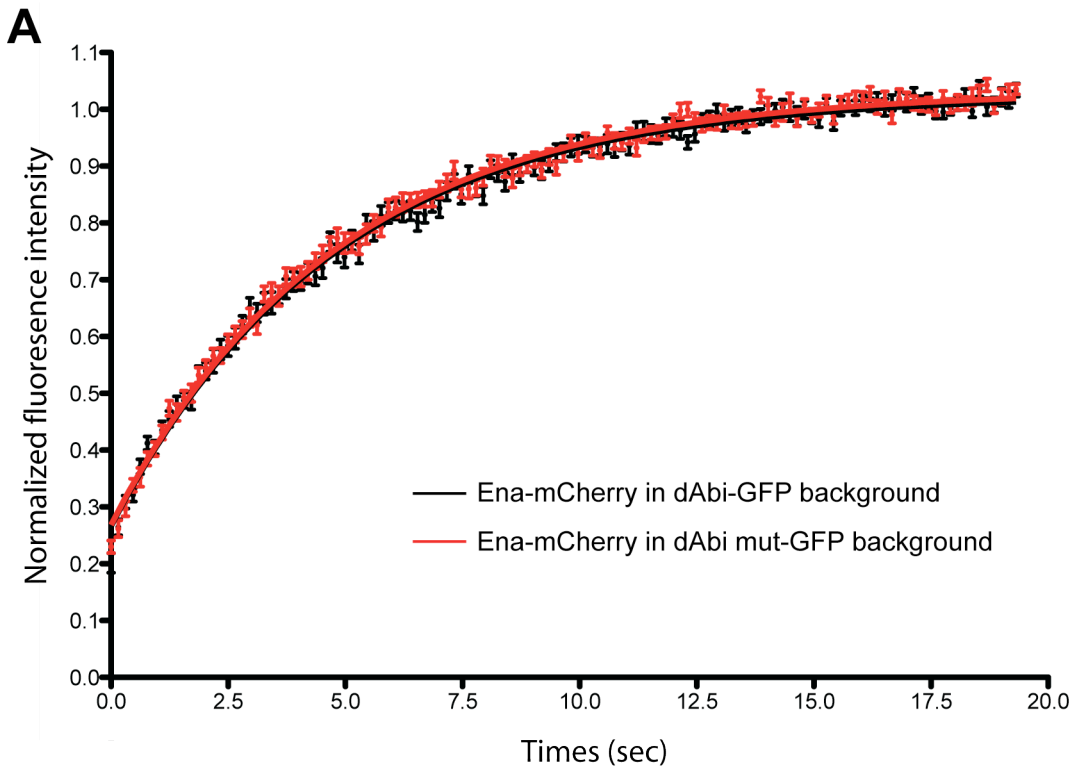

B

Ena-mCherry	% Recovery	Rate constant of recovery (sec $^{-1}$)	$t_{1/2}$ (sec)
Ena-mCherry/dAbi-GFP	100 ± 0.004	0.207 ± 0.004	3.35 ± 0.06
Ena-mCherry/dAbi mut-GFP	100 ± 0.003	0.213 ± 0.003	3.25 ± 0.05

Figure 6.14 The WAVE complex does not help stabilise Ena at the plasma membrane in S2 cells.
A. The graph illustrates the fluorescence recovery rate after photobleaching of Ena-mCherry at the plasma membrane of S2 cells co-overexpressing either dAbi-GFP (black) or dAbi mut-GFP (red) but lacking endogenous dAbi. Intensity values of the mCherry-Ena were normalised to a pre-bleach image. Linear curves corresponded to best fits of averaged data. Error bars represent the SEM and n = 45. **B**. The table lists the values derived from the 45 fitted recovery curves together with the SEM for the percentage, rate constant and half time of recovery of Ena-mCherry when it was co-expressed with the different GFP-tagged dAbi constructs.

6.3 Summary

Drosophila S2 and S2R$^+$ cells, which have a single dAbi and Ena isoform, were used as model systems to further investigate the significance of the Abi-EVH1 interaction in regulating actin dynamics. As the proline rich regions of hAbi are not conserved with those in dAbi, I identified the Ena EVH1 binding site in dAbi and generated a dAbi mutant that is deficient in EVH1 binding using the biochemical approaches I established earlier. Moreover, western blot analysis together with qRT-PCR analysis revealed that the expression of endogenous dAbi but not dAbi-GFP in S2 and S2R$^+$ cells could be knocked down efficiently by dsRNA targeting the 3'UTR of dAbi. Cells lacking endogenous dAbi exhibited several defects in lamellipodia formation, although overexpressing either dAbi-GFP or dAbi mut-GFP could rescue this defective phenotype. Furthermore, immunofluorescence analysis revealed that the localisation of Ena at the plasma membrane was independent of the WAVE complex. Consistent with the results from the FRAP analysis using Rat-2 cells, FRAP experiments using both, S2 and S2R$^+$ cells demonstrated that Ena helps stabilise the WAVE complex at the plasma membrane. However, in contrast to previous results Rat-2 cells, I found that in S2 cells, the WAVE complex does not regulate the dynamics of Ena at the plasma membrane.

Chapter 7. Discussion

Work presented in my thesis was aimed at identifying new non-FPPPP containing binding partners of the EVH1 domain of Ena/VASP proteins. Using a combination of biochemical approaches together with mass spectrometry, I initially identified the WAVE complex subunits Nap1 and PIR121, which both lack FPPPP motifs, as potential binding partners of the EVH1 domain of Ena/VASP proteins. However, subsequent *in vitro* binding assays showed that neither Nap1, nor PIR121 could interact with the EVH1 domain. Instead I found Abi, another component of the WAVE complex binds directly to the EVH1 domain of Ena/VASP proteins. I was then able to identify the EVH1 binding site in both human and *Drosophila* Abi. By expressing an Abi mutant deficient in EVH1 binding I was able to demonstrate that Ena/VASP proteins help stabilise the WAVE complex at the tip of lamellipodia in mammalian and *Drosophila* cells. My work has shown that Ena/VASP proteins are directly coupled to the WAVE complex, suggesting that they may regulate actin dynamics at the plasma membrane in a more coordinated fashion than previously thought.

7.1 The biochemistry of the Abi-EVH1 interaction

7.1.1 Human Abi is a non-classical EVH1 binding partner

The FPPPP motif in ActA from *Listeria* was the first binding site for the EVH1 domain of Ena/VASP proteins to be identified (Niebuhr et al., 1997). Subsequent studies solved the structure of the EVH1 domains of Mena or Evl in complex with a short FPPPP-containing peptide derived from ActA (Prehoda et al., 1999, Fedorov et al., 1999). As shown in Figure 7.1 A and B, a triad of three highly conserved aromatic residues in the EVH1 domain provides a V-shaped binding surface for the poly-proline core of the FPPPP ligand. The essential left-handed poly-proline type II helix required for FPPPP peptide binding will be disrupted if any proline is exchanged for another amino acid. In addition to the poly-proline core, a hydrophobic residue (F/W/Y/L) flanking the proline core docks into a pocket outside of the aromatic triad of the EVH1 domain. Data from far western approaches on peptide arrays suggests that the phenylalanine in the FPPPP motif can be replaced by leucine, tryptophan or tyrosine (Ball et al., 2000). However, most of the EVH1 binding partners of Ena/VASP proteins actually contain phenylalanine in their FPPPP motif (Figure 7.1 C). Moreover, the binding capacity of the LPPPP motif in lamellipodin has not been tested in the context of the full length protein. It is thought that the interaction between this hydrophobic residue and the

EVH1 domain determines the directionality of FPPPP binding (Fedorov et al., 1999). Based on the structure of the EVH1:FPPPP complex, it is clear that all five residues in the FPPPP motif are required for EVH1 binding. However, human Abi, which lacks the classical FPPPP motif, is still able to interact directly with the EVH1 domain of Ena/VASP proteins (Figure 3.5). This immediately raises questions about the molecular details of the interaction between human Abi and the EVH1 domain.

The results from my pull-down and far western assays demonstrated that the EVH1 domain interacts with the second proline rich region (PR2) of Abi. PR2 can be further divided into two subregions consisting of prolines 366-368 and 383-385. Both these proline regions were found to be important for EVH1 binding (Figure 4.8). Although the EVH1 binding sites in Abi mostly consist of prolines, they lack a hydrophobic residue that is essential for the interaction of FPPPP ligands with the EVH1 domain (Figure 7.1D). Instead, another proline can be found. Given the importance of the hydrophobic residue within the FPPPP motif in EVH1 binding (Fedorov et al., 1999, Prehoda et al., 1999, Peterson and Volkman, 2009), it is not immediately clear how the interaction between Abi and EVH1 is achieved. However, examination of the structure of EVH1 domains bound to their FPPPP peptides reveals that the phenylalanine does not form any hydrophobic contacts with the EVH1 domain. The binding cleft of phenylalanine residue could also easily accommodate a proline residue. In the absence of additional structural information using longer FPPPP peptides, it is hard to tell exactly why the phenylalanine is essential. However, one possible reason could be that the phenylalanine satisfies constraints imposed on this position by the residues upstream of the FPPPP motif that are lacking in all solved structures (Peterson and Volkman, 2009). Presumably, these upstream residues can be wrapped around the EVH1 domain as observed for the WH1 binding motif in WIP (Volkman et al., 2002, Zettl and Way, 2002, Peterson et al., 2007). Consistent with this suggestion, the EVH1 binding motif in Abi involves three separate motifs (prolines 366-368, phenylalanine 357 and prolines 383-385) in residues 352-394 of Abi (Figure 4.6). It is possible that the Abi interaction also involves an extended surface that wraps around the EVH1 domain in a similar fashion as observed in the interaction between WIP and the WH1 domain of N-WASP.

The idea that a proline can replace the hydrophobic residue of FPPPP motifs is further substantiated by the observation that several acidic residues follow both proline rich

subregions (Figure 7.1D). It has been shown that a cluster of negatively charged residues immediately downstream of the poly-proline core increases the binding affinity of FPPPP containing peptides for the EVH1 domain (Prehoda et al., 1999, Ball et al., 2000, Peterson and Volkman, 2009). Moreover, in binding assays, Abi was shown to compete with FPPPP containing peptides for binding to the EVH1 domain (Figure 3.5A, B).

My data show that human Abi contains two separate EVH1 binding motifs that appear to be equal (Figure 4.8). However, the structure of EVH1:FPPPP complexes suggests that only one FPPPP-motif can be packed into the binding pocket of the EVH1 domain (Fedorov et al., 1999, Prehoda et al., 1999). At least two models of binding between human Abi and the EVH1 domain are plausible. It is possible that both proline rich subregions are equivalent to the FPPPP-motif and compete with each other to interact with the EVH1 domain in a "classical" fashion. However, it may be that only one proline rich subregion of Abi is equivalent to the classic FPPPP-motif and the other subregion binds to the EVH1 domain at a different site as observed for the WH1 binding protein WIP (Peterson and Volkman, 2009). Additionally, it cannot be excluded that Abi may associate with more than one EVH1 domain using both of its proline rich subregions to form an EVH1:Abi:EVH1 trimer.

To determine which binding model is correct and whether a proline residue can replace the phenylalanine residue in the FPPPP-motif, future work should focus on determining the structure of the EVH1 domain and the binding regions of human Abi. Since sufficient amounts of recombinant EVH1 domain and the binding regions of human Abi can be produced in bacteria or as peptides, it is hoped that crystallisation trials can be started in the near future. Moreover, future experiments using biochemical assays such as gel filtration chromatography will shed light on the stoichiometric ratio between Abi and EVH1 when they are in a complex.

In addition to Abi1, mammals contain two additional Abi isoforms: Abi2 and Abi3 (Chapter 1). Similar to the overall sequence identity between the three isoforms, the second proline rich region of Abi1 and 2 are more similar to each other, whereas the second proline rich region of Abi3 shares less similarity with the second proline rich regions of the other two Abi isoforms (Figure 7.1 E). The residues that are essential for EVH1 binding in Abi1 (proline 366-368, 383-385 and phenylalanine 357) can be found

in Abi2. Similar to Abi1, in Abi2, acidic residues that are also important for EVH1 binding follow both of the two proline rich subregions. In Abi3, the prolines that correspond to the prolines in Abi1 that are essential for EVH1 binding can be found, however the phenylalanine is missing. Also, in contrast to the second proline rich region of Abi1 and Abi2, Abi3 contains two LPPPP motifs. This suggests that Abi3 may bind to the EVH1 domain of Ena/VASP proteins in a classical way. Overall, although Abi2 and Abi3 differ from Abi1, it is possible that they both bind to the EVH1 domain of Ena/VASP proteins. From the sequence alignment alone, no obvious binding specificity can be deduced.

7.1.2 *Drosophila* Abi is a classical EVH1 binding partner

In contrast to human Abi, which lacks the classical FPPPP-motif, dAbi contains two distinct LPPPP-motifs in its C-terminal half (Figure 6.1). All published data on EVH1 binding has only identified a single functional LPPPP interaction motif in lamellipodin (Krause et al., 2004) (Figure 7.1C). The assumption that leucine replaces phenylalanine is largely based on far western analysis of peptide arrays, which may not fully reflect the native situation in the full length protein (Ball et al., 2000). Sequence alignments reveal that the second LPPPP motif of dAbi is highly conserved and equivalent to the first proline rich subregion of human Abi (Figure 7.1F). This conservation suggests that these residues in human and *Drosophila* are likely to be functionally equivalent. Indeed, my pull down assays revealed that the second LPPPP motif in dAbi appears to be more important in mediating EVH1 binding than the first LPPPP motif, which is not conserved in human (Figure 6.4).

As for the human Abi:EVH1 complex, the molecular basis for the interaction as well as the stoichiometric ratio between the two proteins needs to be resolved. The EVH1 domain of Ena can be produced in bacteria, however, the production of full-length recombinant dAbi proved to be unsuccessful (data not shown). Future work to address these outstanding questions could attempt to produce dAbi deletion mutants that contain the EVH1 binding site in bacteria or as peptides instead of producing full-length Abi.

7.1.3 The interaction of Abi-EVH1 *in vivo*

In immunoprecipitation assays using HEK 293T cells I showed that endogenous Mena could be retained by GFP-Abi but not by GFP-Abi mut from cell lysates (Figure 4.9).

These results suggest that the overexpressed GFP-Abi interacts with Mena *in vivo* and that the mutation disrupted the interaction between GFP-Abi and the EVH1 domain of Mena in HEK 293T cells. To confirm that GFP-Abi binds the EVH1 domain of Ena/VASP proteins in the model systems that I used to study the physiological importance of the interaction between Ena/VASP proteins and the WAVE complex, the same immunoprecipitation assay was repeated using Rat-2 and *Drosophila* S2/S2R$^+$ cells. However, the antibodies against Mena or Ena could not detect the respective endogenous protein in these two cell lines (data not shown). To overcome this problem, the immunoprecipitation assay could be carried out using over-expressed tagged Abi and Ena/VASP proteins in Rat-2 and *Drosophila* S2/S2R$^+$ cells. Moreover, the interaction between Abi and Ena/VASP proteins in Rat-2 and *Drosophila* S2/S2R$^+$ cells could be examined by fluorescence resonance energy transfer (FRET). CFP-Abi/dAbi and YFP-Mena/Ena could be co-overexpressed in Rat-2 and *Drosophila* S2/S2R$^+$ cells. If both proteins interacted *in vivo* at the leading edge, the excitation of the CFP fluorophore should lead to the emission of light from the YFP fluorophore.

In addition, to test if endogenous components of the WAVE complex interact with Ena/VASP proteins *in vivo,* co-immunoprecipitation assays could be performed in the future using antibodies that recognise endogenous Abi (or other components of the WAVE complex). The precipitated protein could be subsequently detected using western blot analysis with antibodies that recognise endogenous Ena/VASP proteins. Alternatively, the co-immunoprecipitation assays could be performed using antibodies that recognise endogenous Ena/VASP proteins to pull down endogenous components of the WAVE complex.

It has been shown that both, Abi and Mena are substrates of the tyrosine kinase Abl (Tani et al., 2003, Huang et al., 2007). Abl can phosphorylate Mena on Tyr296 (Tani et al., 2003). In contrast, multiple tyrosine residues in Abi can be phosphorylated by Abl (Huang et al., 2007). Although the tyrosine phosphorylation sites in Mena and Abi are not at the Abi-EVH1 binding surface, it is possible that the phosphorylation state of Abi and Mena is affecting their binding to each other. Therefore, phospho-deficient mutants of both, Abi and Mena could be generated, or Abl could be co-overexpressed. Under these conditions, biochemical assays could be performed to investigate whether Abl-mediated phosphorylation influences the interaction between Abi and Mena.

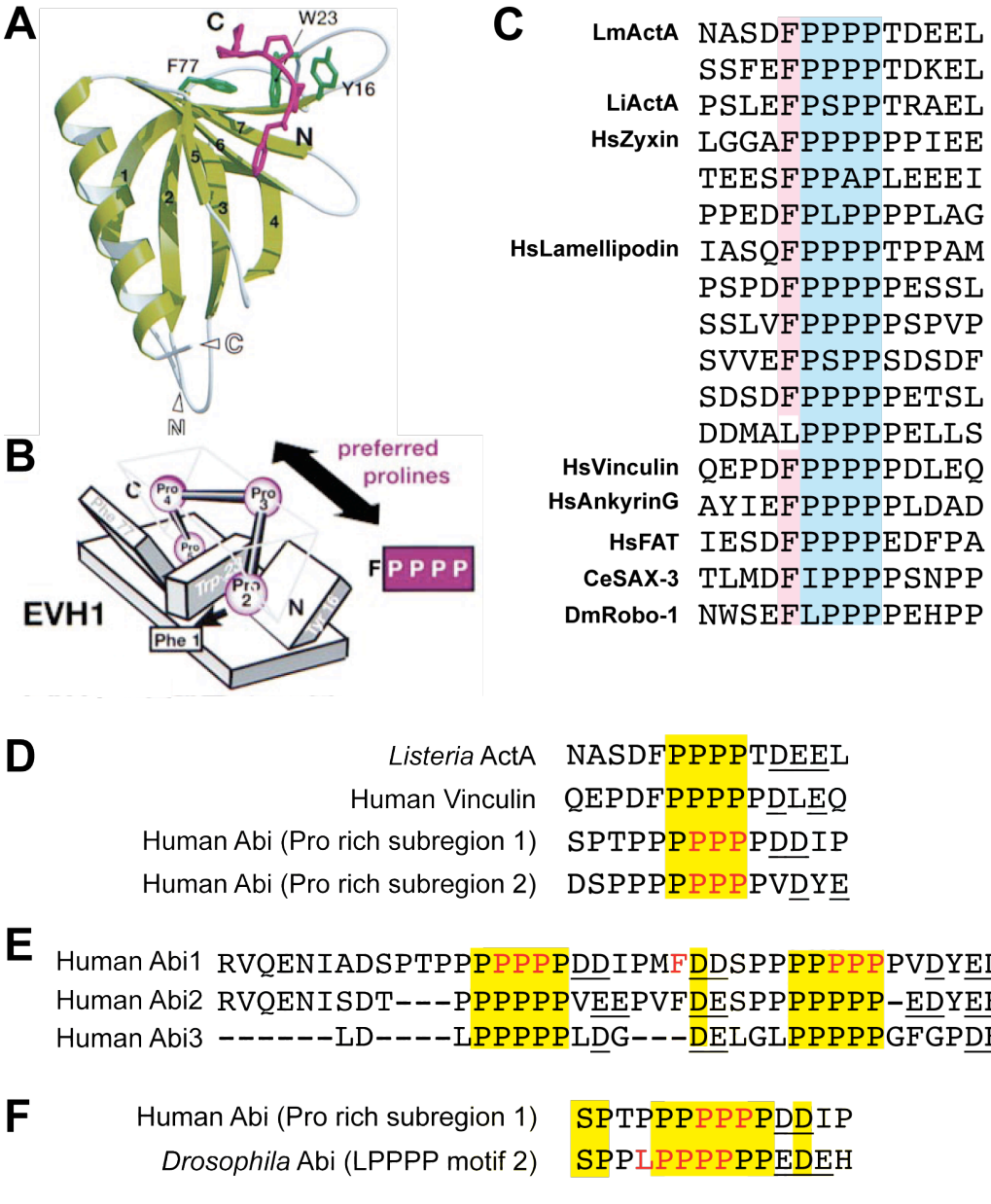

Figure 7.1 Human Abi may interact with the EVH1 domain of Ena/VASP proteins in a classical way.
A. Ribbon diagram illustrating the EVH1 domain of Mena (green) and the FPPPP peptide of *Listeria* ActA (purple). The triad of conserved aromatic residues in EVH1 that provide the pocket for binding the poly-proline core of the FPPPP-motif binding are shown in dark green. **B.** Schematic representation of the interaction that is shown in **A**. **C**. Alignment of FPPPP motifs of known EVH1 binding partners of Ena/VASP proteins. **D.** Alignment of two FPPPP containing motifs with the two proline rich subregions of human Abi. **E**. Alignment of the second proline rich region of all three human Abi isoforms. **F**. Alignment of the first proline rich subregion in human Abi with the second LPPPP motif in *Drosophila* Abi. In **D, E** and **F**, residues that were found to be key for EVH1 binding in human and *Drosophila* Abi are indicated in red. Acidic residues C-terminal to the polyproline core are underlined. **A** and **B** was taken from (Prehoda et al., 1999) with the permission of Elsevier.

7.2 Biology of the Abi-EVH1 interaction

7.2.1 Ena/VASP proteins stabilise the WAVE complex at the plasma membrane

Depletion of Ena/VASP proteins from the plasma membrane by overexpressing FPPPP-Mito in Rat-2 cells did not affect the localisation of Abi at the plasma membrane (Figure 5.4). Moreover, uncoupling of dAbi from Ena in S2 cells lacking endogenous dAbi had no effect on the localisation of Ena at the plasma membrane (Figure 6.11). Taken together, these results suggest that the localisation of Ena/VASP and the WAVE complex are independent of each other. Consistent with this, Ena/VASP proteins are recruited to the plasma membrane by binding to MRL family proteins (Lafuente et al., 2004, Krause et al., 2004, Michael et al., 2010, Quinn et al., 2006), whereas the WAVE complex is recruited to the plasma membrane through the action of Rac, membrane lipids and membrane-associated proteins such as IRSp53 (Takahashi and Suzuki, 2010, Suetsugu et al., 2006, Mattila et al., 2007, Oikawa et al., 2004, Miki et al., 1998, Steffen et al., 2004, Koronakis et al., 2011).

Although Ena/VASP proteins and Abi do not require each other for their localisation, my FRAP analysis in both Rat-2 and S2 cells, reveals that the Abi-EVH1 interaction appears to regulate the dynamics of Abi at the plasma membrane (Figures 5.9, 6.12 and 6.13). In contrast, my FRAP analysis in S2 cells showed no significant effects on the turnover of Ena at the plasma membrane when the interaction between dAbi and Ena was disrupted (Figure 6.14). These data suggest that the dynamics of Ena/VASP proteins at the plasma membrane is likely to be largely dependent on MRL family proteins.

Interestingly, the differences between the turnover rate of Abi and Abi mut in stable Rat-2 cell lines in the presence of endogenous Abi is smaller than the difference that was observed in S2 cells lacking endogenous dAbi (Figure 5.9 and 6.12). This may be explained by the ability of Abi to oligomerise (Fan et al., 2003, Echarri et al., 2004). I envisage that endogenous Abi that associates with Abi mut will effectively mask the binding deficiency in Abi mut. This idea also does not rule out that there is a direct competition between endogenous Abi and Abi mut to incorporate into the WAVE complex. In both cases, the difference between the turnover rate of Abi and Abi mut in Rat-2 cells would be expected to be reduced, which is what my data shows.

In addition, I also found that the turnover rate of Abi is slower than that of VASP at the plasma membrane in both stable Rat-2 cell lines and S2 cells (Figure 5.9, 5.13, 6.12 and 6.14). These differences suggest that in the cell lines I used, Abi and Ena/VASP are not turning over as one complex. However, a previous study suggested that Abi and VASP might form a complex at the plasma membrane as they had similar turnover rates (Lai et al., 2008). The discrepancies between my results and Lai et al. (2008) may be explained by the fact that in mouse melanoma (B16-F1) cells Abi and VASP are turned over as a complex, or that by chance they show a similar turnover rate in that cell line.

Using immunofluorescence analysis and immunoprecipitation, I have shown that the GFP-tagged human and *Drosophila* versions of Abi and Abi mut I generated are incorporated into the rest of the WAVE complex (Figure 5.6 and 6.5 and 6.6). Therefore, it is plausible that the dynamics of Abi could be coupled to the dynamics of the WAVE complex and that Ena/VASP proteins not only regulate the dynamics of Abi, but the whole WAVE complex. However, it has been shown that the turnover rate of Abi at the plasma membrane is different from the turnover rate of other components of the WAVE complex (Lai et al., 2008) and furthermore, Abi is found to interact with other proteins that localise at the plasma membrane, such as N-WASP (Liebau et al., 2011, Innocenti et al., 2005). Therefore, Abi may be turned over independent of the WAVE complex. The direct effects of overexpressing Abi mut in cells on the dynamics of other WAVE complex components at the plasma membrane has not yet been examined. Therefore, future analysis of the dynamics of other WAVE complex components in cells expressing either Abi or Abi mut will confirm the effect of Ena/VASP proteins on the dynamics of the WAVE complex at the plasma membrane.

It is unclear whether the increased dynamics of the WAVE complex will affect the rate of actin polymerisation at the plasma membrane. Ina Weisswange, a former PhD student in the laboratory showed that the stability of the N-WASP, another class I NPFs affects the length of actin tails and the speed of actin based motility of vaccina virus (Weisswange et al., 2009). Based on this, it is not unreasonable to think that the stability of the WAVE complex may also affect actin polymerisation at the plasma membrane. How the dynamics of the WAVE complex influences the rate and extent of Arp2/3 complex dependent actin polymerisation is an important area for future work,

since it clearly has a strong bearing on the fundamental mechanisms underlying the regulation of cell migration. The interaction between Abi and EVH1 that I have described could provide an important fine turning mechanism to control actin dependent motility.

7.2.2 Is the Abi-EVH1 interaction involved in actin-based protrusions?

Depletion of WAVE and other components of the WAVE complex leads to severe defects in lamellipodia formation (Suetsugu et al., 2003, Yamazaki et al., 2005, Yamazaki et al., 2003, D'Ambrosio and Vale, 2010). In contrast, the removal of Ena/VASP proteins from the plasma membrane only affects the rate of lamellipodial protrusion and not their formation (Bear et al., 2000, Bear et al., 2002, Tucker et al., 2011). Nevertheless, the regulation of lamellipodia formation by the WAVE complex may still involve the binding of Abi to Ena/VASP proteins. However, this interaction is not essential as the dAbi mut I generated can fully restore defects in lamellipodia formation in S2 cells lacking endogenous dAbi (Figure 6.10). My results indicate that the direct interaction between Ena/VASP proteins and the WAVE complex is not required for lamellipodia formation. Overexpression of WAVE, however, is known to negatively affect spontaneous lamellipodial protrusions (Hahne et al., 2001). Since Ena/VASP proteins regulate the rate of lamellipodial protrusions, it is possible that their direct interaction with the WAVE complex contributes to the regulation of lamellipodial protrusions. Future work will focus on determining if the rate of lamellipodial protrusion is dependent on the interaction between dAbi and EVH1 in *Drosophila* haemocytes, as these cells exhibit extensive membrane protrusions in tissue culture (Tucker et al., 2011) (Dr Sven Bogdan personal communication).

In addition to the role of Ena/VASP proteins in regulating lamellipodial protrusions, Ena/VASP proteins contribute to the formation of filopodia (Mattila and Lappalainen, 2008). It has been shown that filopodia can arise in existing lamellipodia at the leading edge of migrating cells (Svitkina et al., 2003). However, the molecular mechanism underlying the lamellipodia to filopodia transition is still not clear. Since Ena/VASP proteins and the WAVE complex primarily regulate filopodia and lamellipodia formation respectively, it is possible that the interaction between Ena/VASP proteins and the WAVE complex is also involved in the lamellipodia to filopodia transition. Unfortunately, S2 and S2R^{+} cells do not produce filopodia. Thus, a cell line needs to be identified that ideally contains a single Abi isoform, which is amenable for

knockdown using RNAi and has filopodial protrusions at the leading edge. A recent study using embryonic *Drosophila* primary neurons showed that the Arp2/3 complex cooperates with Ena to regulate filopodia formation (Goncalves-Pimentel et al., 2011). This co-operation may be via the WAVE complex. Future work could use embryonic *Drosophila* primary neurons as the model to study the dAbi-EVH1 interaction.

Ena/VASP proteins have emerged as important regulators of cancer cell metastasis and tumour invasion (Wang et al., 2004, Wang et al., 2007, Philippar et al., 2008, Han et al., 2008, Roussos et al., 2011, Gertler and Condeelis, 2011). Actin rich invadopodia are able to degrade ECM to promote cancer cell invasion (Buccione et al., 2009). Recent findings have suggested that Ena/VASP proteins and the WAVE complex are both required for invadopodia formation during tumour cell invasion (Philippar et al., 2008, Kikuchi and Takahashi, 2008). The direct interaction between Ena/VASP proteins and the WAVE complex may also be also involved in invadopodia stability during tumour cell invasion. Using the reagents I have developed, it would be possible to examine whether the Abi-EVH1 interaction promotes invadopodia formation and tumour cell invasion. Depending on the results from these experiments, further studies could be extended into mouse models of tumour invasion and metastasis.

7.2.3 Is the Abi-EVH1 interaction involved in actin-based cell motility?

Loss- and gain-of-function experiments have shown that Ena/VASP proteins regulate the speed of cell migration, although whether they enhance or decrease migration speed remains controversial (Chapter 1). Moreover, the WAVE complex provides the driving force for cell migration by activating Arp2/3 complex dependent actin polymerisation at the leading edge (Chapter 1). Considering that both Ena/VASP proteins and the WAVE complex are key regulators of actin-based cell motility, it is possible that their interaction will also regulate the speed of cell migration. This idea is based on the fact that Ena/VASP proteins stabilise Abi at the leading edge. However, single cell-tracking assays showed no difference in velocity, directionality and persistency during random cell migration between Rat-2 cells expressing Abi and Abi mut (Figure 5.7A). As discussed earlier, however, the endogenous Abi isoforms could not be knocked down by RNAi and thus may mask the phenotype of Abi mut in Rat-2 cells in these single cell-tracking assays (Figure 5.14). Changing to *Drosophila* haemocytes to study cell migration *in vitro* is also not possible, as they do not migrate in culture (Tucker et al., 2011).

To study the significance of the direct interaction between Ena/VASP proteins and the WAVE complex in regulating cell migration we therefore started a collaboration with Dr Sven Bogdan at the University of Münster, Germany. The group of Dr Sven Bogdan studies photoreceptor guidance in *Drosophila* larvae as a model system to examine the role WASP and WAVE family proteins in neuronal migration (Gohl et al., 2010) (Figure 7.2). They found that *abi* null mutants have over shooting axon projections in the photoreceptor (unpublished data). Currently they are examining the role of the Abi-EVH1 interaction in neuronal migration by performing rescue experiments in *abi* null mutants using my dAbi mutant that is deficient in EVH1 binding.

My dAbi binding mutant can also be used to test the significance of the Abi-EVH1 interaction in cell migration in other *Drosophila* models. For example cell migration can be studied in *Drosophila* embryos (Evans and Wood, 2011). Embryonic haemocytes that do not migrate *in vitro* are actually highly motile *in vivo* (Tucker et al., 2011). A recent study demonstrated that Ena increases the rate of haemocyte migration in *Drosophila* embryos (Tucker et al., 2011). In addition, Ena has also been found to promote border cell migration in *Drosophila* egg chambers during oogenesis (Gates et al., 2009). These systems can easily be used to test if the interaction between Ena and dAbi plays a role in regulating cell migration *in vivo*.

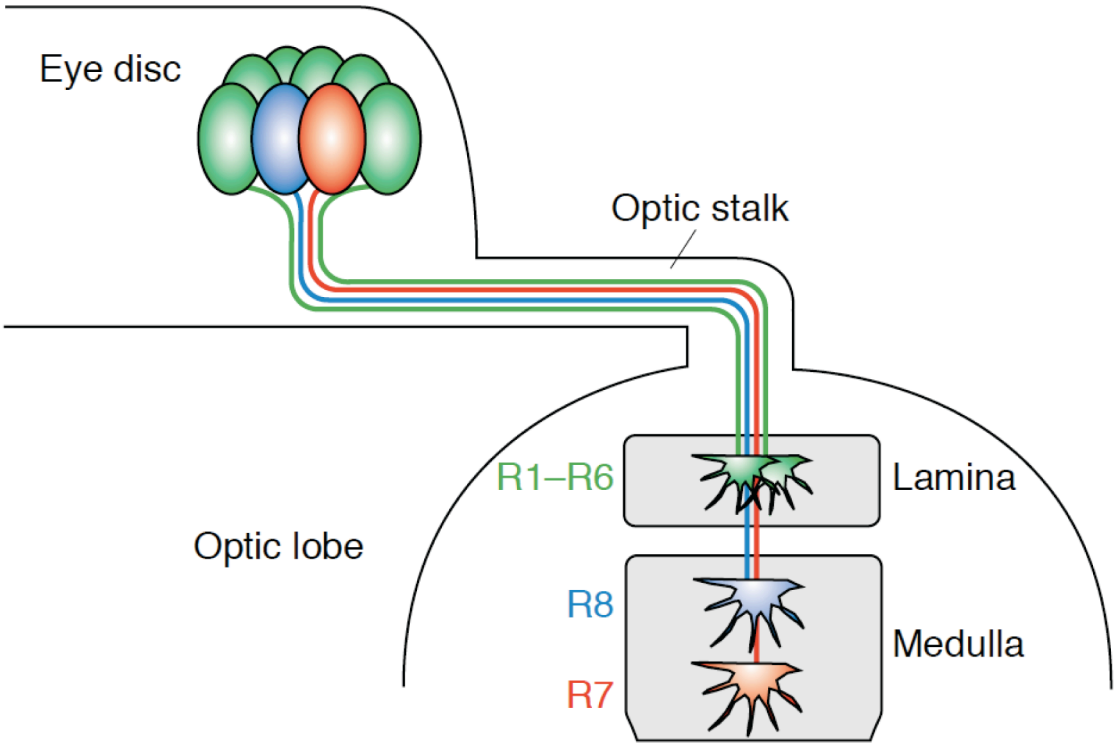

Figure 7.2 Schematic representation of photoreceptor connectivity in *Drosophila* larvae.
A compound eye of *Drosophila* consists of about 750 ommatidia, each of which possesses eight photoreceptor neurons (R-cells) that are uniquely identifiable. During development, these R-cells extend axons to target different areas of the fly brain. This neuronal targeting process provides a model system for studying cell migration as it occurs in very specific and organised fashion. Taken from (Tayler and Garrity, 2003) with the permission of Elsevier.

7.2.4 Can VASP activate the ability of the WAVE complex to stimulate Arp2/3 complex dependent actin nucleation?

FRAP analyses revealed that Ena/VASP proteins stabilise the WAVE complex at the plasma membrane. The next question was whether Ena/VASP proteins are able to directly activate the WAVE complex to induce Arp2/3 dependent actin polymerisation. To address this question, we have collaborated with the group of Dr Michael Rosen (University of Texas Southwestern Medical Center, Dallas, USA). Dr Baoyu Chen, a post-doctoral scientist in the Rosen laboratory performed WAVE complex dependent *in vitro* actin polymerisation assays in the presence or absence of VASP and/or its EVH1 domain that I produced and purified from bacteria.

These experiments are ongoing, although preliminary data reveal that in contrast to the EVH1 domain alone, full length VASP dramatically enhances the ability of the WAVE complex to stimulate the actin nucleating activity of the Arp2/3 complex (Figure 7.3A). This stimulation requires a direct interaction with the WAVE complex, as it does not occur in the absence of the proline rich region of Abi. Since Ena/VASP proteins can undergo tetramerisation via a coiled coil region at their C terminus (Bachmann et al., 1999, Zimmermann et al., 2002), it may be that clustering of four VASP proteins is required for the activation of the WAVE complex as the EVH1 domain has no effect (Figure 7.3A). Further mutational analysis using VASP that is unable to undergo tetramerisation will reveal whether tetramerisation is required for activating the WAVE complex. VASP on its own is also able to trigger actin polymerisation at a concentration of 50 nM. These observations agree with studies indicating that Ena/VASP proteins are capable of promoting the elongation of actin filaments (Breitsprecher et al., 2011, Breitsprecher et al., 2008).

The small GTPase Rac is the best-studied activator of the WAVE complex *in vitro* (Chen et al., 2010, Ismail et al., 2009, Lebensohn and Kirschner, 2009). *In vitro* actin polymerisation assays using Rac that is persistently bound to a non-hydrolysable GTP analogue revealed that Rac and VASP can activate the WAVE complex independently (Figure 7.3B). Moreover, VASP and Rac have an additive effect on actin polymerisation. These *in vitro* data strongly suggest that the Abi-EVH1 interaction I have described will have an impact on the rate of cell migration.

The fact that VASP activates the WAVE complex by a direct interaction raises important mechanistic questions about how this action occurs. Since the release of the C-terminal meander-VCA region of WAVE from PIR121 leads to the activation of the Arp2/3 complex (Chen et al., 2010, Ismail et al., 2009), it is possible that binding of Abi to EVH1 influences the binding interface between PIR121 and the C-terminus of WAVE. However, any conformational change induced in the WAVE complex must be different from the change that is induced by Rac, as the effects of VASP and Rac on activating the WAVE complex are additive. It has been shown that the dimerisation of VCA domains dramatically increases their affinity for Arp2/3 complex and the maximal Arp2/3 complex activation is thought to involve more than one VCA domain (Padrick et al., 2008, Padrick et al., 2011, Ti et al., 2011). It is therefore possible that the activation of WAVE complex is a consequence of clustering of WAVE complexes, as the VASP tetramer but not the monomeric EVH1 domain activates Arp2/3 dependent actin polymerisation. Unfortunately, the PR2 region of Abi is not present in the structure of the WAVE complex (Chen et al., 2010). Therefore, future experiments are required to uncover the underlying mechanism of the VASP mediated WAVE complex activation.

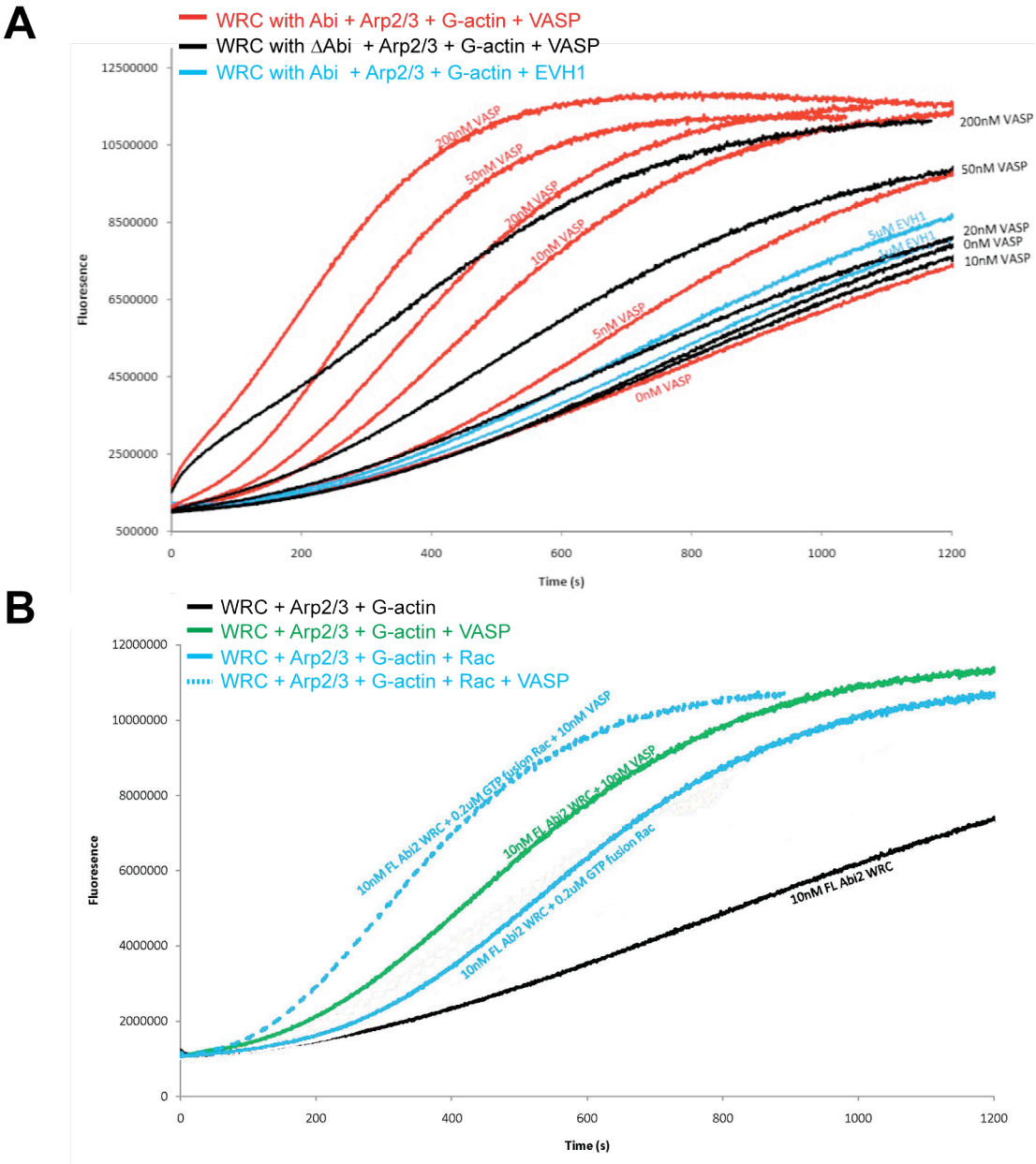

Figure 7.3 VASP activates the WAVE complex and enhances the effect of Rac on activating the WAVE complex *in vitro*.
A. *In vitro* pyrene actin polymerisation assay showing the affect of both, the EVH1 domain alone and full length VASP on activating the WAVE complex. **B.** *In vitro* pyrene actin polymerisation assays showing the effects of VASP and Rac on the ability of the WAVE complex to stimulate Arp2/3 dependent actin polymerisation. In all cases, the fluorescence indicates the amount of newly formed F-actin and was plotted against the time in seconds. A steeper curve represents a higher rate of actin polymerisation. Different combinations of proteins in each are indicated with different colours. Concentrations of proteins are indicated next to their respective curves. WRC represents the WAVE regulatory complex. ΔAbi represents a mutant Abi lacking the C-terminal region that contains the EVH1 binding site.

7.3 Working model for the role of the Abi-EVH1 interaction in cell migration

I have shown that Ena/VASP proteins can stabilise the WAVE complex at the plasma membrane *in vivo* and potentially activate the WAVE complex *in vitro*. Figure 7.4 shows a new model for the cooperation between Ena/VASP proteins and the WAVE complex in regulating actin-based membrane protrusions. The recruitment of Ena/VASP proteins and the WAVE complex are regulated by their respective signalling pathways. Once at the membrane, the EVH1 domain of Ena/VASP proteins binds directly to the WAVE complex via the PR2 region of Abi. This interaction helps stabilise the WAVE complex at the plasma membrane and enhances its ability to activate Arp2/3 dependent actin polymerisation. The interaction with Ena/VASP proteins also enhances the effect of Rac on activating the WAVE complex. Overall, this interaction helps regulate the coordination of actin polymerisation at the plasma membrane (Figure 7.4).

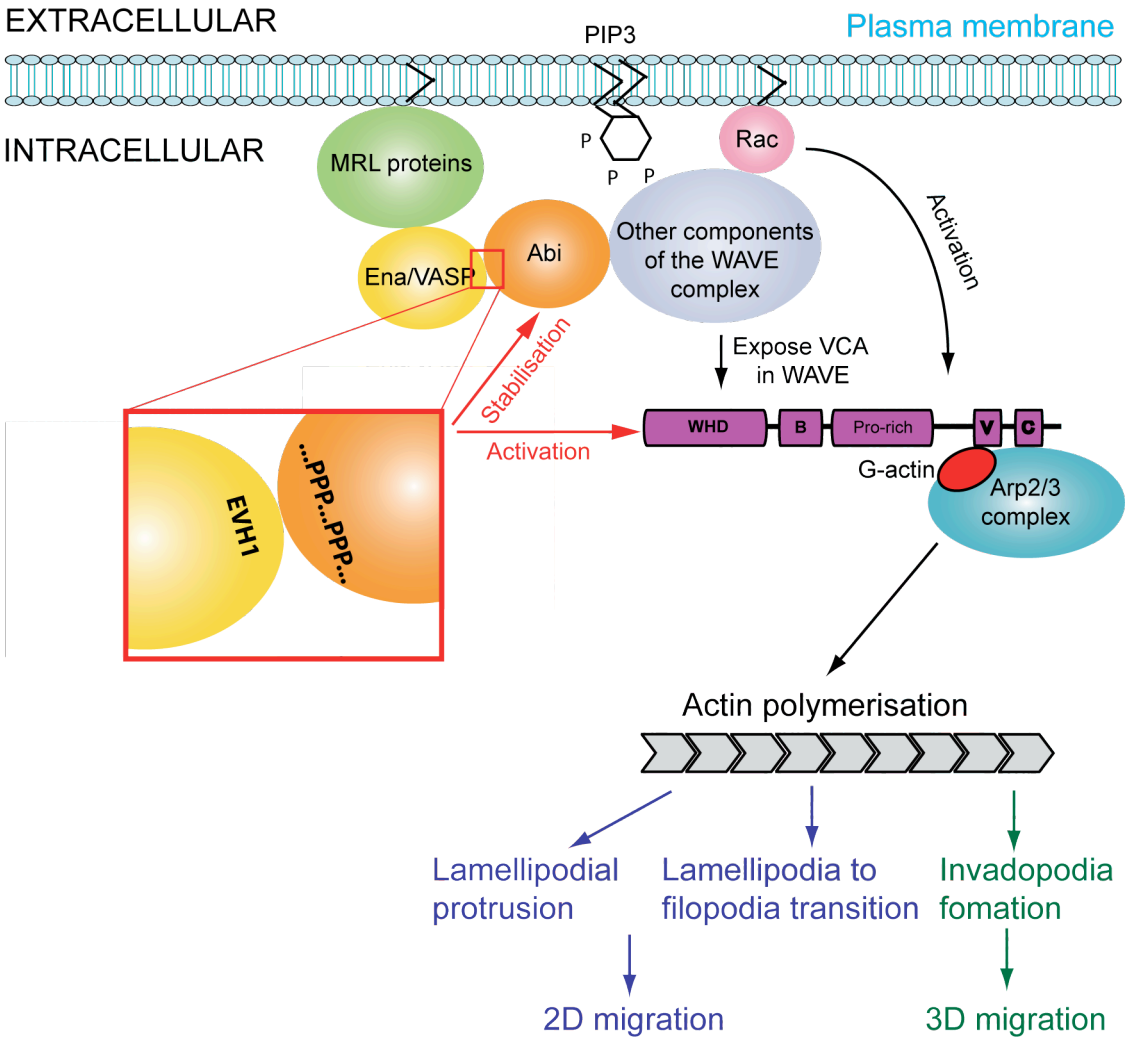

Figure 7.4 Hypothetical scheme of the consequences of the Abi-EVH1 interaction.

References

ABERCROMBIE, M. 1980. The Croonian Lecture, 1978: The Crawling Movement of Metazoan Cells. *Proceedings of the Royal Society of London. Series B. Biological Sciences,* 207**,** 129-147.

ABERCROMBIE, M., HEAYSMAN, J. E. & PEGRUM, S. M. 1970. The locomotion of fibroblasts in culture. II. "RRuffling". *Exp Cell Res,* 60**,** 437-44.

AHERN-DJAMALI, S. M., COMER, A. R., BACHMANN, C., KASTENMEIER, A. S., REDDY, S. K., BECKERLE, M. C., WALTER, U. & HOFFMANN, F. M. 1998. Mutations in Drosophila enabled and rescue by human vasodilator-stimulated phosphoprotein (VASP) indicate important functional roles for Ena/VASP homology domain 1 (EVH1) and EVH2 domains. *Mol Biol Cell,* 9**,** 2157-71.

AKIN, O. & MULLINS, R. D. 2008. Capping protein increases the rate of actin-based motility by promoting filament nucleation by the Arp2/3 complex. *Cell,* 133**,** 841-51.

ALBERTS, B., JOHNSON, A., LEWIS, J., RAFF, M., ROBERTS, K. & WALTER, P. 2007. *Molecular Biology of the Cell*, Garland Sience/Taylor & Francis Books, Inc.

AMAN, A. & PIOTROWSKI, T. 2010. Cell migration during morphogenesis. *Dev Biol,* 341**,** 20-33.

AMANN, K. J. & POLLARD, T. D. 2001a. The Arp2/3 complex nucleates actin filament branches from the sides of pre-existing filaments. *Nat Cell Biol,* 3**,** 306-10.

AMANN, K. J. & POLLARD, T. D. 2001b. Direct real-time observation of actin filament branching mediated by Arp2/3 complex using total internal reflection fluorescence microscopy. *Proc Natl Acad Sci U S A,* 98**,** 15009-13.

ANTON, I. M., JONES, G. E., WANDOSELL, F., GEHA, R. & RAMESH, N. 2007. WASP-interacting protein (WIP): working in polymerisation and much more. *Trends Cell Biol,* 17**,** 555-62.

ARDERN, H., SANDILANDS, E., MACHESKY, L. M., TIMPSON, P., FRAME, M. C. & BRUNTON, V. G. 2006. Src-dependent phosphorylation of Scar1 promotes its association with the Arp2/3 complex. *Cell Motil Cytoskeleton,* 63**,** 6-13.

ARMSTRONG, L., LAKO, M., VAN HERPE, I., EVANS, J., SARETZKI, G. & HOLE, N. 2004. A role for nucleoprotein Zap3 in the reduction of telomerase activity during embryonic stem cell differentiation. *Mech Dev,* 121**,** 1509-22.

AUERBUCH, V., LOUREIRO, J. J., GERTLER, F. B., THERIOT, J. A. & PORTNOY, D. A. 2003. Ena/VASP proteins contribute to Listeria monocytogenes pathogenesis by controlling temporal and spatial persistence of bacterial actin-based motility. *Mol Microbiol,* 49**,** 1361-75.

BACHMANN, C., FISCHER, L., WALTER, U. & REINHARD, M. 1999. The EVH2 domain of the vasodilator-stimulated phosphoprotein mediates tetramerization, F-actin binding, and actin bundle formation. *J Biol Chem,* 274**,** 23549-57.

BAILLY, M., ICHETOVKIN, I., GRANT, W., ZEBDA, N., MACHESKY, L. M., SEGALL, J. E. & CONDEELIS, J. 2001. The F-actin side binding activity of the Arp2/3 complex is essential for actin nucleation and lamellipod extension. *Curr Biol,* 11**,** 620-5.

BALL, L. J., KUHNE, R., HOFFMANN, B., HAFNER, A., SCHMIEDER, P., VOLKMER-ENGERT, R., HOF, M., WAHL, M., SCHNEIDER-MERGENER, J., WALTER, U., OSCHKINAT, H. & JARCHAU, T. 2000. Dual epitope recognition by the VASP EVH1 domain modulates polyproline ligand specificity and binding affinity. *EMBO J,* 19**,** 4903-14.

BARZIK, M., CARL, U. D., SCHUBERT, W. D., FRANK, R., WEHLAND, J. & HEINZ, D. W. 2001. The N-terminal domain of Homer/Vesl is a new class II EVH1 domain. *J Mol Biol,* 309**,** 155-69.

BARZIK, M., KOTOVA, T. I., HIGGS, H. N., HAZELWOOD, L., HANEIN, D., GERTLER, F. B. & SCHAFER, D. A. 2005. Ena/VASP proteins enhance actin polymerization in the presence of barbed end capping proteins. *J Biol Chem,* 280**,** 28653-62.

BASHAW, G. J., KIDD, T., MURRAY, D., PAWSON, T. & GOODMAN, C. S. 2000. Repulsive axon guidance: Abelson and Enabled play opposing roles downstream of the roundabout receptor. *Cell,* 101**,** 703-15.

BEAR, J. E. & GERTLER, F. B. 2009. Ena/VASP: towards resolving a pointed controversy at the barbed end. *Journal of cell science,* 122**,** 1947-53.

BEAR, J. E., LOUREIRO, J. J., LIBOVA, I., FASSLER, R., WEHLAND, J. & GERTLER, F. B. 2000. Negative regulation of fibroblast motility by Ena/VASP proteins. *Cell,* 101**,** 717-28.

BEAR, J. E., SVITKINA, T. M., KRAUSE, M., SCHAFER, D. A., LOUREIRO, J. J., STRASSER, G. A., MALY, I. V., CHAGA, O. Y., COOPER, J. A., BORISY, G. G. & GERTLER, F. B. 2002. Antagonism between Ena/VASP proteins and actin filament capping regulates fibroblast motility. *Cell,* 109**,** 509-21.

BELTZNER, C. C. & POLLARD, T. D. 2004. Identification of functionally important residues of Arp2/3 complex by analysis of homology models from diverse species. *J Mol Biol,* 336**,** 551-65.

BENEKEN, J., TU, J. C., XIAO, B., NURIYA, M., YUAN, J. P., WORLEY, P. F. & LEAHY, D. J. 2000. Structure of the Homer EVH1 domain-peptide complex reveals a new twist in polyproline recognition. *Neuron,* 26**,** 143-54.

BENESCH, S., POLO, S., LAI, F. P., ANDERSON, K. I., STRADAL, T. E., WEHLAND, J. & ROTTNER, K. 2005. N-WASP deficiency impairs EGF internalization and actin assembly at clathrin-coated pits. *J Cell Sci,* 118**,** 3103-15.

BENZ, P. M., BLUME, C., SEIFERT, S., WILHELM, S., WASCHKE, J., SCHUH, K., GERTLER, F., MUNZEL, T. & RENNE, T. 2009. Differential VASP phosphorylation controls remodeling of the actin cytoskeleton. *J Cell Sci,* 122**,** 3954-65.

BIYASHEVA, A., SVITKINA, T., KUNDA, P., BAUM, B. & BORISY, G. 2004. Cascade pathway of filopodia formation downstream of SCAR. *J Cell Sci,* 117**,** 837-48.

BLANCHOIN, L., AMANN, K. J., HIGGS, H. N., MARCHAND, J. B., KAISER, D. A. & POLLARD, T. D. 2000. Direct observation of dendritic actin filament networks nucleated by Arp2/3 complex and WASP/Scar proteins. *Nature,* 404**,** 1007-11.

BLASER, H., REICHMAN-FRIED, M., CASTANON, I., DUMSTREI, K., MARLOW, F. L., KAWAKAMI, K., SOLNICA-KREZEL, L., HEISENBERG,

C. P. & RAZ, E. 2006. Migration of zebrafish primordial germ cells: a role for myosin contraction and cytoplasmic flow. *Dev Cell,* 11**,** 613-27.

BLUME, C., BENZ, P. M., WALTER, U., HA, J., KEMP, B. E. & RENNE, T. 2007. AMP-activated protein kinase impairs endothelial actin cytoskeleton assembly by phosphorylating vasodilator-stimulated phosphoprotein. *J Biol Chem,* 282**,** 4601-12.

BLUNDELL, M. P., BOUMA, G., METELO, J., WORTH, A., CALLE, Y., COWELL, L. A., WESTERBERG, L. S., MOULDING, D. A., MIRANDO, S., KINNON, C., CORY, G. O., JONES, G. E., SNAPPER, S. B., BURNS, S. O. & THRASHER, A. J. 2009. Phosphorylation of WASp is a key regulator of activity and stability in vivo. *Proc Natl Acad Sci U S A,* 106**,** 15738-43.

BOCZKOWSKA, M., REBOWSKI, G., PETOUKHOV, M. V., HAYES, D. B., SVERGUN, D. I. & DOMINGUEZ, R. 2008. X-ray scattering study of activated Arp2/3 complex with bound actin-WCA. *Structure,* 16**,** 695-704.

BOEDA, B., BRIGGS, D. C., HIGGINS, T., GARVALOV, B. K., FADDEN, A. J., MCDONALD, N. Q. & WAY, M. 2007. Tes, a specific Mena interacting partner, breaks the rules for EVH1 binding. *Mol Cell,* 28**,** 1071-82.

BOEDA, B., KNOWLES, P. P., BRIGGS, D. C., MURRAY-RUST, J., SORIANO, E., GARVALOV, B. K., MCDONALD, N. Q. & WAY, M. 2011. Molecular recognition of the Tes LIM2-3 domains by the actin-related protein Arp7A. *J Biol Chem,* 286**,** 11543-54.

BOUKHELIFA, M., PARAST, M. M., BEAR, J. E., GERTLER, F. B. & OTEY, C. A. 2004. Palladin is a novel binding partner for Ena/VASP family members. *Cell Motil Cytoskeleton,* 58**,** 17-29.

BRADLEY, W. D. & KOLESKE, A. J. 2009. Regulation of cell migration and morphogenesis by Abl-family kinases: emerging mechanisms and physiological contexts. *J Cell Sci,* 122**,** 3441-54.

BRAND, A. H. & PERRIMON, N. 1994. Raf acts downstream of the EGF receptor to determine dorsoventral polarity during Drosophila oogenesis. *Genes Dev,* 8**,** 629-39.

BREITSPRECHER, D., KIESEWETTER, A. K., LINKNER, J., URBANKE, C., RESCH, G. P., SMALL, J. V. & FAIX, J. 2008. Clustering of VASP actively drives processive, WH2 domain-mediated actin filament elongation. *EMBO J,* 27**,** 2943-54.

BREITSPRECHER, D., KIESEWETTER, A. K., LINKNER, J., VINZENZ, M., STRADAL, T. E., SMALL, J. V., CURTH, U., DICKINSON, R. B. & FAIX, J. 2011. Molecular mechanism of Ena/VASP-mediated actin-filament elongation. *EMBO J,* 30**,** 456-67.

BRONNER-FRASER, M. 1994. Neural crest cell formation and migration in the developing embryo. *Faseb J,* 8**,** 699-706.

BU, W., CHOU, A. M., LIM, K. B., SUDHAHARAN, T. & AHMED, S. 2009. The Toca-1-N-WASP complex links filopodial formation to endocytosis. *J Biol Chem,* 284**,** 11622-36.

BUCCIONE, R., CALDIERI, G. & AYALA, I. 2009. Invadopodia: specialized tumor cell structures for the focal degradation of the extracellular matrix. *Cancer Metastasis Rev,* 28**,** 137-49.

BUGYI, B. & CARLIER, M. F. 2010. Control of actin filament treadmilling in cell motility. *Annu Rev Biophys,* 39**,** 449-70.

BUTT, E., ABEL, K., KRIEGER, M., PALM, D., HOPPE, V., HOPPE, J. & WALTER, U. 1994. cAMP- and cGMP-dependent protein kinase phosphorylation sites of the focal adhesion vasodilator-stimulated phosphoprotein (VASP) in vitro and in intact human platelets. *J Biol Chem,* 269**,** 14509-17.

CAI, L., MAKHOV, A. M., SCHAFER, D. A. & BEAR, J. E. 2008. Coronin 1B antagonizes cortactin and remodels Arp2/3-containing actin branches in lamellipodia. *Cell,* 134**,** 828-42.

CAI, L., MARSHALL, T. W., UETRECHT, A. C., SCHAFER, D. A. & BEAR, J. E. 2007. Coronin 1B coordinates Arp2/3 complex and cofilin activities at the leading edge. *Cell,* 128**,** 915-29.

CAMERON, L. A., GIARDINI, P. A., SOO, F. S. & THERIOT, J. A. 2000. Secrets of actin-based motility revealed by a bacterial pathogen. *Nat Rev Mol Cell Biol,* 1**,** 110-9.

CAMPBELL, R. E., TOUR, O., PALMER, A. E., STEINBACH, P. A., BAIRD, G. S., ZACHARIAS, D. A. & TSIEN, R. Y. 2002. A monomeric red fluorescent protein. *Proc Natl Acad Sci U S A,* 99**,** 7877-82.

CAMPELLONE, K. G., WEBB, N. J., ZNAMEROSKI, E. A. & WELCH, M. D. 2008. WHAMM is an Arp2/3 complex activator that binds microtubules and functions in ER to Golgi transport. *Cell,* 134**,** 148-61.

CAMPELLONE, K. G. & WELCH, M. D. 2010. A nucleator arms race: cellular control of actin assembly. *Nat Rev Mol Cell Biol,* 11**,** 237-51.

CARL, U. D., POLLMANN, M., ORR, E., GERTLERE, F. B., CHAKRABORTY, T. & WEHLAND, J. 1999. Aromatic and basic residues within the EVH1 domain of VASP specify its interaction with proline-rich ligands. *Curr Biol,* 9**,** 715-8.

CARLIER, M. F., NIOCHE, P., BROUTIN-L'HERMITE, I., BOUJEMAA, R., LE CLAINCHE, C., EGILE, C., GARBAY, C., DUCRUIX, A., SANSONETTI, P. & PANTALONI, D. 2000. GRB2 links signaling to actin assembly by enhancing interaction of neural Wiskott-Aldrich syndrome protein (N-WASp) with actin-related protein (ARP2/3) complex. *J Biol Chem,* 275**,** 21946-52.

CARNELL, M., ZECH, T., CALAMINUS, S. D., URA, S., HAGEDORN, M., JOHNSTON, S. A., MAY, R. C., SOLDATI, T., MACHESKY, L. M. & INSALL, R. H. 2011. Actin polymerization driven by WASH causes V-ATPase retrieval and vesicle neutralization before exocytosis. *J Cell Biol,* 193**,** 831-9.

CHALFIE, M., TU, Y., EUSKIRCHEN, G., WARD, W. W. & PRASHER, D. C. 1994. Green fluorescent protein as a marker for gene expression. *Science,* 263**,** 802-5.

CHEN, W. T. 1989. Proteolytic activity of specialized surface protrusions formed at rosette contact sites of transformed cells. *J Exp Zool,* 251**,** 167-85.

CHEN, Z., BOREK, D., PADRICK, S. B., GOMEZ, T. S., METLAGEL, Z., ISMAIL, A. M., UMETANI, J., BILLADEAU, D. D., OTWINOWSKI, Z. & ROSEN, M. K. 2010. Structure and control of the actin regulatory WAVE complex. *Nature,* 468**,** 533-8.

CHEREAU, D., KERFF, F., GRACEFFA, P., GRABAREK, Z., LANGSETMO, K. & DOMINGUEZ, R. 2005. Actin-bound structures of Wiskott-Aldrich syndrome protein (WASP)-homology domain 2 and the implications for filament assembly. *Proc Natl Acad Sci U S A,* 102**,** 16644-9.

CHESARONE, M. A., DUPAGE, A. G. & GOODE, B. L. 2010. Unleashing formins to remodel the actin and microtubule cytoskeletons. *Nat Rev Mol Cell Biol,* 11**,** 62-74.

CHHABRA, E. S. & HIGGS, H. N. 2007. The many faces of actin: matching assembly factors with cellular structures. *Nat Cell Biol,* 9**,** 1110-21.

CLEMENS, J. C., WORBY, C. A., SIMONSON-LEFF, N., MUDA, M., MAEHAMA, T., HEMMINGS, B. A. & DIXON, J. E. 2000. Use of double-stranded RNA interference in Drosophila cell lines to dissect signal transduction pathways. *Proc Natl Acad Sci U S A,* 97**,** 6499-503.

COMER, A. R., AHERN-DJAMALI, S. M., JUANG, J. L., JACKSON, P. D. & HOFFMANN, F. M. 1998. Phosphorylation of Enabled by the Drosophila Abelson tyrosine kinase regulates the in vivo function and protein-protein interactions of Enabled. *Mol Cell Biol,* 18**,** 152-60.

COOPER, J. A. 1987. Effects of cytochalasin and phalloidin on actin. *J Cell Biol,* 105**,** 1473-8.

CORY, G. O., CRAMER, R., BLANCHOIN, L. & RIDLEY, A. J. 2003. Phosphorylation of the WASP-VCA domain increases its affinity for the Arp2/3 complex and enhances actin polymerization by WASP. *Mol Cell,* 11**,** 1229-39.

CORY, G. O., GARG, R., CRAMER, R. & RIDLEY, A. J. 2002. Phosphorylation of tyrosine 291 enhances the ability of WASp to stimulate actin polymerization and filopodium formation. Wiskott-Aldrich Syndrome protein. *J Biol Chem,* 277**,** 45115-21.

COUTTS, A. S., MACKENZIE, E., GRIFFITH, E. & BLACK, D. M. 2003. TES is a novel focal adhesion protein with a role in cell spreading. *J Cell Sci,* 116**,** 897-906.

COUTTS, A. S., WESTON, L. & LA THANGUE, N. B. 2009. A transcription co-factor integrates cell adhesion and motility with the p53 response. *Proc Natl Acad Sci U S A,* 106**,** 19872-7.

D'AMBROSIO, M. V. & VALE, R. D. 2010. A whole genome RNAi screen of Drosophila S2 cell spreading performed using automated computational image analysis. *J Cell Biol,* 191**,** 471-8.

DAHL, J. P., WANG-DUNLOP, J., GONZALES, C., GOAD, M. E., MARK, R. J. & KWAK, S. P. 2003. Characterization of the WAVE1 knock-out mouse: implications for CNS development. *J Neurosci,* 23**,** 3343-52.

DAI, Z. & PENDERGAST, A. M. 1995. Abi-2, a novel SH3-containing protein interacts with the c-Abl tyrosine kinase and modulates c-Abl transforming activity. *Genes Dev,* 9**,** 2569-82.

DANSON, C. M., POCHA, S. M., BLOOMBERG, G. B. & CORY, G. O. 2007. Phosphorylation of WAVE2 by MAP kinases regulates persistent cell migration and polarity. *J Cell Sci,* 120**,** 4144-54.

DAYEL, M. J., HOLLERAN, E. A. & MULLINS, R. D. 2001. Arp2/3 complex requires hydrolyzable ATP for nucleation of new actin filaments. *Proc Natl Acad Sci U S A,* 98**,** 14871-6.

DE RIVOYRE, M., RUEL, L., VARJOSALO, M., LOUBAT, A., BIDET, M., THEROND, P. & MUS-VETEAU, I. 2006. Human receptors patched and smoothened partially transduce hedgehog signal when expressed in Drosophila cells. *J Biol Chem,* 281**,** 28584-95.

DEFAWE, O. D., KIM, S., CHEN, L., HUANG, D., KENAGY, R. D., RENNE, T., WALTER, U., DAUM, G. & CLOWES, A. W. 2010. VASP phosphorylation at serine239 regulates the effects of NO on smooth muscle cell invasion and contraction of collagen. *J Cell Physiol,* 222**,** 230-7.

DERIVERY, E., FINK, J., MARTIN, D., HOUDUSSE, A., PIEL, M., STRADAL, T. E., LOUVARD, D. & GAUTREAU, A. 2008. Free Brick1 is a trimeric precursor in the assembly of a functional wave complex. *PLoS ONE,* 3**,** e2462.

DERIVERY, E. & GAUTREAU, A. 2010. Generation of branched actin networks: assembly and regulation of the N-WASP and WAVE molecular machines. *Bioessays,* 32**,** 119-31.

DERIVERY, E., LOMBARD, B., LOEW, D. & GAUTREAU, A. 2009a. The Wave complex is intrinsically inactive. *Cell Motil Cytoskeleton*.

DERIVERY, E., SOUSA, C., GAUTIER, J. J., LOMBARD, B., LOEW, D. & GAUTREAU, A. 2009b. The Arp2/3 activator WASH controls the fission of endosomes through a large multiprotein complex. *Dev Cell,* 17**,** 712-23.

DISANZA, A., MANTOANI, S., HERTZOG, M., GERBOTH, S., FRITTOLI, E., STEFFEN, A., BERHOERSTER, K., KREIENKAMP, H. J., MILANESI, F., DI FIORE, P. P., CILIBERTO, A., STRADAL, T. E. & SCITA, G. 2006. Regulation of cell shape by Cdc42 is mediated by the synergic actin-bundling activity of the Eps8-IRSp53 complex. *Nat Cell Biol,* 8**,** 1337-47.

DITTRICH, M., STRASSBERGER, V., FACKLER, M., TAS, P., LEWANDROWSKI, U., SICKMANN, A., WALTER, U., DANDEKAR, T. & BIRSCHMANN, I. 2010. Characterization of a novel interaction between vasodilator-stimulated phosphoprotein and Abelson interactor 1 in human platelets: a concerted computational and experimental approach. *Arterioscler Thromb Vasc Biol,* 30**,** 843-50.

DOMINGUEZ, R. 2007. The beta-thymosin/WH2 fold: multifunctionality and structure. *Ann N Y Acad Sci,* 1112**,** 86-94.

DOMINGUEZ, R. 2009. Actin filament nucleation and elongation factors--structure-function relationships. *Crit Rev Biochem Mol Biol,* 44**,** 351-66.

DOMINGUEZ, R. & HOLMES, K. C. 2011. Actin structure and function. *Annu Rev Biophys,* 40**,** 169-86.

DOS REMEDIOS, C. G., CHHABRA, D., KEKIC, M., DEDOVA, I. V., TSUBAKIHARA, M., BERRY, D. A. & NOSWORTHY, N. J. 2003. Actin binding proteins: regulation of cytoskeletal microfilaments. *Physiol Rev,* 83**,** 433-73.

DREES, B., FRIEDERICH, E., FRADELIZI, J., LOUVARD, D., BECKERLE, M. C. & GOLSTEYN, R. M. 2000. Characterization of the interaction between zyxin and members of the Ena/vasodilator-stimulated phosphoprotein family of proteins. *J Biol Chem,* 275**,** 22503-11.

DRUSCO, A., ZANESI, N., ROLDO, C., TRAPASSO, F., FARBER, J. L., FONG, L. Y. & CROCE, C. M. 2005. Knockout mice reveal a tumor suppressor function for Testin. *Proc Natl Acad Sci U S A,* 102**,** 10947-51.

DUBIELECKA, P. M., CUI, P., XIONG, X., HOSSAIN, S., HECK, S., ANGELOV, L. & KOTULA, L. 2010. Differential regulation of macropinocytosis by Abi1/Hssh3bp1 isoforms. *PLoS One,* 5**,** e10430.

DUBIELECKA, P. M., LADWEIN, K. I., XIONG, X., MIGEOTTE, I., CHORZALSKA, A., ANDERSON, K. V., SAWICKI, J. A., ROTTNER, K.,

STRADAL, T. E. & KOTULA, L. 2011. Essential role for Abi1 in embryonic survival and WAVE2 complex integrity. *Proc Natl Acad Sci U S A,* 108**,** 7022-7.
DULEH, S. N. & WELCH, M. D. 2010. WASH and the Arp2/3 complex regulate endosome shape and trafficking. *Cytoskeleton (Hoboken),* 67**,** 193-206.
ECHARRI, A., LAI, M. J., ROBINSON, M. R. & PENDERGAST, A. M. 2004. Abl interactor 1 (Abi-1) wave-binding and SNARE domains regulate its nucleocytoplasmic shuttling, lamellipodium localization, and wave-1 levels. *Mol Cell Biol,* 24**,** 4979-93.
EDEN, S., ROHATGI, R., PODTELEJNIKOV, A. V., MANN, M. & KIRSCHNER, M. W. 2002. Mechanism of regulation of WAVE1-induced actin nucleation by Rac1 and Nck. *Nature,* 418**,** 790-3.
ERMEKOVA, K. S., ZAMBRANO, N., LINN, H., MINOPOLI, G., GERTLER, F., RUSSO, T. & SUDOL, M. 1997. The WW domain of neural protein FE65 interacts with proline-rich motifs in Mena, the mammalian homolog of Drosophila enabled. *J Biol Chem,* 272**,** 32869-77.
EVANS, I. R., RENNE, T., GERTLER, F. B. & NOBES, C. D. 2007. Ena/VASP proteins mediate repulsion from ephrin ligands. *J Cell Sci,* 120**,** 289-98.
EVANS, I. R. & WOOD, W. 2011. Drosophila embryonic hemocytes. *Curr Biol,* 21**,** R173-4.
FAIX, J. & ROTTNER, K. 2006. The making of filopodia. *Curr Opin Cell Biol,* 18**,** 18-25.
FAN, P. D., CONG, F. & GOFF, S. P. 2003. Homo- and hetero-oligomerization of the c-Abl kinase and Abelson-interactor-1. *Cancer Res,* 63**,** 873-7.
FEDOROV, A. A., FEDOROV, E., GERTLER, F. & ALMO, S. C. 1999. Structure of EVH1, a novel proline-rich ligand-binding module involved in cytoskeletal dynamics and neural function. *Nat Struct Biol,* 6**,** 661-5.
FERRON, F., REBOWSKI, G., LEE, S. H. & DOMINGUEZ, R. 2007. Structural basis for the recruitment of profilin-actin complexes during filament elongation by Ena/VASP. *EMBO J,* 26**,** 4597-606.
FORSCHER, P. & SMITH, S. J. 1988. Actions of cytochalasins on the organization of actin filaments and microtubules in a neuronal growth cone. *J Cell Biol,* 107**,** 1505-16.
FRANCO, S. J. & HUTTENLOCHER, A. 2005. Regulating cell migration: calpains make the cut. *J Cell Sci,* 118**,** 3829-38.
FRIEDL, P. 2004. Prespecification and plasticity: shifting mechanisms of cell migration. *Curr Opin Cell Biol,* 16**,** 14-23.
FRIEDL, P. & GILMOUR, D. 2009. Collective cell migration in morphogenesis, regeneration and cancer. *Nat Rev Mol Cell Biol,* 10**,** 445-57.
FRIEDL, P. & WOLF, K. 2010. Plasticity of cell migration: a multiscale tuning model. *J Cell Biol,* 188**,** 11-9.
FRIEDLAND, J. C., LEE, M. H. & BOETTIGER, D. 2009. Mechanically activated integrin switch controls alpha5beta1 function. *Science,* 323**,** 642-4.
FYRBERG, C. & FYRBERG, E. 1993. A Drosophila homologue of the Schizosaccharomyces pombe act2 gene. *Biochem Genet,* 31**,** 329-41.
GARVALOV, B. K., HIGGINS, T. E., SUTHERLAND, J. D., ZETTL, M., SCAPLEHORN, N., KOCHER, T., PIDDINI, E., GRIFFITHS, G. & WAY, M. 2003. The conformational state of Tes regulates its zyxin-dependent recruitment to focal adhesions. *J Cell Biol,* 161**,** 33-9.

GATES, J., NOWOTARSKI, S. H., YIN, H., MAHAFFEY, J. P., BRIDGES, T., HERRERA, C., HOMEM, C. C., JANODY, F., MONTELL, D. J. & PEIFER, M. 2009. Enabled and Capping protein play important roles in shaping cell behavior during Drosophila oogenesis. *Developmental biology,* 333**,** 90-107.

GAUTREAU, A., HO, H. Y., LI, J., STEEN, H., GYGI, S. P. & KIRSCHNER, M. W. 2004. Purification and architecture of the ubiquitous Wave complex. *Proc Natl Acad Sci U S A,* 101**,** 4379-83.

GEESE, M., LOUREIRO, J. J., BEAR, J. E., WEHLAND, J., GERTLER, F. B. & SECHI, A. S. 2002. Contribution of Ena/VASP proteins to intracellular motility of listeria requires phosphorylation and proline-rich core but not F-actin binding or multimerization. *Mol Biol Cell,* 13**,** 2383-96.

GERTLER, F. & CONDEELIS, J. 2011. Metastasis: tumor cells becoming MENAcing. *Trends Cell Biol,* 21**,** 81-90.

GERTLER, F. B., COMER, A. R., JUANG, J. L., AHERN, S. M., CLARK, M. J., LIEBL, E. C. & HOFFMANN, F. M. 1995. enabled, a dosage-sensitive suppressor of mutations in the Drosophila Abl tyrosine kinase, encodes an Abl substrate with SH3 domain-binding properties. *Genes Dev,* 9**,** 521-33.

GERTLER, F. B., DOCTOR, J. S. & HOFFMANN, F. M. 1990. Genetic suppression of mutations in the Drosophila abl proto-oncogene homolog. *Science,* 248**,** 857-60.

GERTLER, F. B., NIEBUHR, K., REINHARD, M., WEHLAND, J. & SORIANO, P. 1996. Mena, a relative of VASP and Drosophila Enabled, is implicated in the control of microfilament dynamics. *Cell,* 87**,** 227-39.

GLACY, S. D. 1983. Subcellular distribution of rhodamine-actin microinjected into living fibroblastic cells. *J Cell Biol,* 97**,** 1207-13.

GOH, K. L., CAI, L., CEPKO, C. L. & GERTLER, F. B. 2002. Ena/VASP proteins regulate cortical neuronal positioning. *Curr Biol,* 12**,** 565-9.

GOHL, C., BANOVIC, D., GREVELHORSTER, A. & BOGDAN, S. 2010. WAVE forms hetero- and homo-oligomeric complexes at integrin junctions in Drosophila visualized by bimolecular fluorescence complementation. *J Biol Chem,* 285**,** 40171-9.

GOLEY, E. D., RAMMOHAN, A., ZNAMEROSKI, E. A., FIRAT-KARALAR, E. N., SEPT, D. & WELCH, M. D. 2010. An actin-filament-binding interface on the Arp2/3 complex is critical for nucleation and branch stability. *Proc Natl Acad Sci U S A,* 107**,** 8159-64.

GOLEY, E. D., RODENBUSCH, S. E., MARTIN, A. C. & WELCH, M. D. 2004. Critical conformational changes in the Arp2/3 complex are induced by nucleotide and nucleation promoting factor. *Mol Cell,* 16**,** 269-79.

GOLEY, E. D. & WELCH, M. D. 2006. The ARP2/3 complex: an actin nucleator comes of age. *Nat Rev Mol Cell Biol,* 7**,** 713-26.

GOMEZ, T. S. & BILLADEAU, D. D. 2009. A FAM21-containing WASH complex regulates retromer-dependent sorting. *Dev Cell,* 17**,** 699-711.

GONCALVES-PIMENTEL, C., GOMBOS, R., MIHALY, J., SANCHEZ-SORIANO, N. & PROKOP, A. 2011. Dissecting regulatory networks of filopodia formation in a Drosophila growth cone model. *PLoS One,* 6**,** e18340.

GREVENGOED, E. E., FOX, D. T., GATES, J. & PEIFER, M. 2003. Balancing different types of actin polymerization at distinct sites: roles for Abelson kinase and Enabled. *J Cell Biol,* 163**,** 1267-79.

GRINNELL, F. 2008. Fibroblast mechanics in three-dimensional collagen matrices. *J Bodyw Mov Ther,* 12**,** 191-3.
GUO, K., SHILLCOCK, J. & LIPOWSKY, R. 2010. Treadmilling of actin filaments via Brownian dynamics simulations. *J Chem Phys,* 133**,** 155105.
HAFFNER, C., JARCHAU, T., REINHARD, M., HOPPE, J., LOHMANN, S. M. & WALTER, U. 1995. Molecular cloning, structural analysis and functional expression of the proline-rich focal adhesion and microfilament-associated protein VASP. *EMBO J,* 14**,** 19-27.
HAHNE, P., SECHI, A., BENESCH, S. & SMALL, J. V. 2001. Scar/WAVE is localised at the tips of protruding lamellipodia in living cells. *FEBS Lett,* 492**,** 215-20.
HALBRUGGE, M. & WALTER, U. 1989. Purification of a vasodilator-regulated phosphoprotein from human platelets. *Eur J Biochem,* 185**,** 41-50.
HAN, G., FAN, B., ZHANG, Y., ZHOU, X., WANG, Y., DONG, H., WEI, Y., SUN, S., HU, M., ZHANG, J. & WEI, L. 2008. Positive regulation of migration and invasion by vasodilator-stimulated phosphoprotein via Rac1 pathway in human breast cancer cells. *Oncol Rep,* 20**,** 929-39.
HANSEN, S. D. & MULLINS, R. D. 2010. VASP is a processive actin polymerase that requires monomeric actin for barbed end association. *J Cell Biol,* 191**,** 571-84.
HARBECK, B., HUTTELMAIER, S., SCHLUTER, K., JOCKUSCH, B. M. & ILLENBERGER, S. 2000. Phosphorylation of the vasodilator-stimulated phosphoprotein regulates its interaction with actin. *J Biol Chem,* 275**,** 30817-25.
HEGERFELDT, Y., TUSCH, M., BROCKER, E. B. & FRIEDL, P. 2002. Collective cell movement in primary melanoma explants: plasticity of cell-cell interaction, beta1-integrin function, and migration strategies. *Cancer Res,* 62**,** 2125-30.
HIRAO, N., SATO, S., GOTOH, T., MARUOKA, M., SUZUKI, J., MATSUDA, S., SHISHIDO, T. & TANI, K. 2006. NESH (Abi-3) is present in the Abi/WAVE complex but does not promote c-Abl-mediated phosphorylation. *FEBS Lett,* 580**,** 6464-70.
HO, H. Y., ROHATGI, R., LEBENSOHN, A. M., LE, M., LI, J., GYGI, S. P. & KIRSCHNER, M. W. 2004. Toca-1 mediates Cdc42-dependent actin nucleation by activating the N-WASP-WIP complex. *Cell,* 118**,** 203-16.
HOFFMAN, L. M., JENSEN, C. C., KLOEKER, S., WANG, C. L., YOSHIGI, M. & BECKERLE, M. C. 2006. Genetic ablation of zyxin causes Mena/VASP mislocalization, increased motility, and deficits in actin remodeling. *J Cell Biol,* 172**,** 771-82.
HOWE, A. K., HOGAN, B. P. & JULIANO, R. L. 2002. Regulation of vasodilator-stimulated phosphoprotein phosphorylation and interaction with Abl by protein kinase A and cell adhesion. *J Biol Chem,* 277**,** 38121-6.
HU, L. D., ZOU, H. F., ZHAN, S. X. & CAO, K. M. 2008. EVL (Ena/VASP-like) expression is up-regulated in human breast cancer and its relative expression level is correlated with clinical stages. *Oncol Rep,* 19**,** 1015-20.
HUANG, C. H., LIN, T. Y., PAN, R. L. & JUANG, J. L. 2007. The involvement of Abl and PTP61F in the regulation of Abi protein localization and stability and lamella formation in Drosophila S2 cells. *J Biol Chem,* 282**,** 32442-52.
HUANG, G. N., HUSO, D. L., BOUYAIN, S., TU, J., MCCORKELL, K. A., MAY, M. J., ZHU, Y., LUTZ, M., COLLINS, S., DEHOFF, M., KANG, S., WHARTENBY, K., POWELL, J., LEAHY, D. & WORLEY, P. F. 2008. NFAT

binding and regulation of T cell activation by the cytoplasmic scaffolding Homer proteins. *Science,* 319**,** 476-81.

HUTTELMAIER, S., HARBECK, B., STEFFENS, O., MESSERSCHMIDT, T., ILLENBERGER, S. & JOCKUSCH, B. M. 1999. Characterization of the actin binding properties of the vasodilator-stimulated phosphoprotein VASP. *FEBS Lett,* 451**,** 68-74.

ICHIGOTANI, Y., FUJII, K., HAMAGUCHI, M. & MATSUDA, S. 2002. In search of a function for the E3B1/Abi2/Argbp1/NESH family (Review). *Int J Mol Med,* 9**,** 591-5.

INNOCENTI, M., GERBOTH, S., ROTTNER, K., LAI, F. P., HERTZOG, M., STRADAL, T. E., FRITTOLI, E., DIDRY, D., POLO, S., DISANZA, A., BENESCH, S., DI FIORE, P. P., CARLIER, M. F. & SCITA, G. 2005. Abi1 regulates the activity of N-WASP and WAVE in distinct actin-based processes. *Nat Cell Biol,* 7**,** 969-76.

INNOCENTI, M., ZUCCONI, A., DISANZA, A., FRITTOLI, E., ARECES, L. B., STEFFEN, A., STRADAL, T. E., DI FIORE, P. P., CARLIER, M. F. & SCITA, G. 2004. Abi1 is essential for the formation and activation of a WAVE2 signalling complex. *Nat Cell Biol,* 6**,** 319-27.

INSALL, R. H. & MACHESKY, L. M. 2009. Actin dynamics at the leading edge: from simple machinery to complex networks. *Dev Cell,* 17**,** 310-22.

IROBI, E., AGUDA, A. H., LARSSON, M., GUERIN, C., YIN, H. L., BURTNICK, L. D., BLANCHOIN, L. & ROBINSON, R. C. 2004. Structural basis of actin sequestration by thymosin-beta4: implications for WH2 proteins. *EMBO J,* 23**,** 3599-608.

ISMAIL, A. M., PADRICK, S. B., CHEN, B., UMETANI, J. & ROSEN, M. K. 2009. The WAVE regulatory complex is inhibited. *Nat Struct Mol Biol*.

IWASA, J. H. & MULLINS, R. D. 2007. Spatial and temporal relationships between actin-filament nucleation, capping, and disassembly. *Curr Biol,* 17**,** 395-406.

JONCKHEERE, V., LAMBRECHTS, A., VANDEKERCKHOVE, J. & AMPE, C. 1999. Dimerization of profilin II upon binding the (GP5)3 peptide from VASP overcomes the inhibition of actin nucleation by profilin II and thymosin beta4. *FEBS Lett,* 447**,** 257-63.

JOVCEVA, E., LARSEN, M. R., WATERFIELD, M. D., BAUM, B. & TIMMS, J. F. 2007. Dynamic cofilin phosphorylation in the control of lamellipodial actin homeostasis. *J Cell Sci,* 120**,** 1888-97.

JUANG, J. L. & HOFFMANN, F. M. 1999. Drosophila abelson interacting protein (dAbi) is a positive regulator of abelson tyrosine kinase activity. *Oncogene,* 18**,** 5138-47.

KADRMAS, J. L. & BECKERLE, M. C. 2004. The LIM domain: from the cytoskeleton to the nucleus. *Nat Rev Mol Cell Biol,* 5**,** 920-31.

KELLY, A. E., KRANITZ, H., DOTSCH, V. & MULLINS, R. D. 2006. Actin binding to the central domain of WASP/Scar proteins plays a critical role in the activation of the Arp2/3 complex. *J Biol Chem,* 281**,** 10589-97.

KEREN, K., PINCUS, Z., ALLEN, G. M., BARNHART, E. L., MARRIOTT, G., MOGILNER, A. & THERIOT, J. A. 2008. Mechanism of shape determination in motile cells. *Nature,* 453**,** 475-80.

KIGER, A. A., BAUM, B., JONES, S., JONES, M. R., COULSON, A., ECHEVERRI, C. & PERRIMON, N. 2003. A functional genomic analysis of cell morphology using RNA interference. *J Biol,* 2**,** 27.

KIKUCHI, K. & TAKAHASHI, K. 2008. WAVE2- and microtubule-dependent formation of long protrusions and invasion of cancer cells cultured on three-dimensional extracellular matrices. *Cancer Sci,* 99**,** 2252-9.

KIM, A. S., KAKALIS, L. T., ABDUL-MANAN, N., LIU, G. A. & ROSEN, M. K. 2000. Autoinhibition and activation mechanisms of the Wiskott-Aldrich syndrome protein. *Nature,* 404**,** 151-8.

KIM, J. H., CHO, A., YIN, H., SCHAFER, D. A., MOUNEIMNE, G., SIMPSON, K. J., NGUYEN, K. V., BRUGGE, J. S. & MONTELL, D. J. 2011. Psidin, a conserved protein that regulates protrusion dynamics and cell migration. *Genes Dev,* 25**,** 730-41.

KLOSTERMANN, A., LUTZ, B., GERTLER, F. & BEHL, C. 2000. The orthologous human and murine semaphorin 6A-1 proteins (SEMA6A-1/Sema6A-1) bind to the enabled/vasodilator-stimulated phosphoprotein-like protein (EVL) via a novel carboxyl-terminal zyxin-like domain. *J Biol Chem,* 275**,** 39647-53.

KOBAYASHI, K., KURODA, S., FUKATA, M., NAKAMURA, T., NAGASE, T., NOMURA, N., MATSUURA, Y., YOSHIDA-KUBOMURA, N., IWAMATSU, A. & KAIBUCHI, K. 1998. p140Sra-1 (specifically Rac1-associated protein) is a novel specific target for Rac1 small GTPase. *J Biol Chem,* 273**,** 291-5.

KOESTLER, S. A., AUINGER, S., VINZENZ, M., ROTTNER, K. & SMALL, J. V. 2008. Differentially oriented populations of actin filaments generated in lamellipodia collaborate in pushing and pausing at the cell front. *Nat Cell Biol,* 10**,** 306-13.

KORN, E. D., CARLIER, M. F. & PANTALONI, D. 1987. Actin polymerization and ATP hydrolysis. *Science,* 238**,** 638-44.

KORONAKIS, V., HUME, P. J., HUMPHREYS, D., LIU, T., HORNING, O., JENSEN, O. N. & MCGHIE, E. J. 2011. WAVE regulatory complex activation by cooperating GTPases Arf and Rac1. *Proc Natl Acad Sci U S A,* 15**,** 15.

KRAUSE, M., DENT, E. W., BEAR, J. E., LOUREIRO, J. J. & GERTLER, F. B. 2003. Ena/VASP proteins: regulators of the actin cytoskeleton and cell migration. *Annu Rev Cell Dev Biol,* 19**,** 541-64.

KRAUSE, M., LESLIE, J. D., STEWART, M., LAFUENTE, E. M., VALDERRAMA, F., JAGANNATHAN, R., STRASSER, G. A., RUBINSON, D. A., LIU, H., WAY, M., YAFFE, M. B., BOUSSIOTIS, V. A. & GERTLER, F. B. 2004. Lamellipodin, an Ena/VASP ligand, is implicated in the regulation of lamellipodial dynamics. *Dev Cell,* 7**,** 571-83.

KRAUSE, M., SECHI, A. S., KONRADT, M., MONNER, D., GERTLER, F. B. & WEHLAND, J. 2000. Fyn-binding protein (Fyb)/SLP-76-associated protein (SLAP), Ena/vasodilator-stimulated phosphoprotein (VASP) proteins and the Arp2/3 complex link T cell receptor (TCR) signaling to the actin cytoskeleton. *J Cell Biol,* 149**,** 181-94.

KREISHMAN-DEITRICK, M., GOLEY, E. D., BURDINE, L., DENISON, C., EGILE, C., LI, R., MURALI, N., KODADEK, T. J., WELCH, M. D. & ROSEN, M. K. 2005. NMR analyses of the activation of the Arp2/3 complex by neuronal Wiskott-Aldrich syndrome protein. *Biochemistry,* 44**,** 15247-56.

KUNDA, P., CRAIG, G., DOMINGUEZ, V. & BAUM, B. 2003. Abi, Sra1, and Kette control the stability and localization of SCAR/WAVE to regulate the formation of actin-based protrusions. *Curr Biol,* 13**,** 1867-75.

LADWEIN, M. & ROTTNER, K. 2008. On the Rho'd: the regulation of membrane protrusions by Rho-GTPases. *FEBS Lett,* 582**,** 2066-74.

LAFUENTE, E. M., VAN PUIJENBROEK, A. A., KRAUSE, M., CARMAN, C. V., FREEMAN, G. J., BEREZOVSKAYA, A., CONSTANTINE, E., SPRINGER, T. A., GERTLER, F. B. & BOUSSIOTIS, V. A. 2004. RIAM, an Ena/VASP and Profilin ligand, interacts with Rap1-GTP and mediates Rap1-induced adhesion. *Dev Cell,* 7**,** 585-95.

LAI, F. P., SZCZODRAK, M., BLOCK, J., FAIX, J., BREITSPRECHER, D., MANNHERZ, H. G., STRADAL, T. E., DUNN, G. A., SMALL, J. V. & ROTTNER, K. 2008. Arp2/3 complex interactions and actin network turnover in lamellipodia. *EMBO J,* 27**,** 982-92.

LAI, F. P., SZCZODRAK, M., OELKERS, J. M., LADWEIN, M., ACCONCIA, F., BENESCH, S., AUINGER, S., FAIX, J., SMALL, J. V., POLO, S., STRADAL, T. E. & ROTTNER, K. 2009. Cortactin promotes migration and platelet-derived growth factor-induced actin reorganization by signaling to Rho-GTPases. *Mol Biol Cell,* 20**,** 3209-23.

LAMBRECHTS, A., KWIATKOWSKI, A. V., LANIER, L. M., BEAR, J. E., VANDEKERCKHOVE, J., AMPE, C. & GERTLER, F. B. 2000. cAMP-dependent protein kinase phosphorylation of EVL, a Mena/VASP relative, regulates its interaction with actin and SH3 domains. *J Biol Chem,* 275**,** 36143-51.

LAMMERMANN, T., BADER, B. L., MONKLEY, S. J., WORBS, T., WEDLICH-SOLDNER, R., HIRSCH, K., KELLER, M., FORSTER, R., CRITCHLEY, D. R., FASSLER, R. & SIXT, M. 2008. Rapid leukocyte migration by integrin-independent flowing and squeezing. *Nature,* 453**,** 51-5.

LANIER, L. M., GATES, M. A., WITKE, W., MENZIES, A. S., WEHMAN, A. M., MACKLIS, J. D., KWIATKOWSKI, D., SORIANO, P. & GERTLER, F. B. 1999. Mena is required for neurulation and commissure formation. *Neuron,* 22**,** 313-25.

LAUFFENBURGER, D., ARIS, R. & KELLER, K. 1982. Effects of cell motility and chemotaxis on microbial population growth. *Biophys J,* 40**,** 209-19.

LAUFFENBURGER, D. A. & HORWITZ, A. F. 1996. Cell migration: a physically integrated molecular process. *Cell,* 84**,** 359-69.

LAURENT, V., LOISEL, T. P., HARBECK, B., WEHMAN, A., GROBE, L., JOCKUSCH, B. M., WEHLAND, J., GERTLER, F. B. & CARLIER, M. F. 1999. Role of proteins of the Ena/VASP family in actin-based motility of Listeria monocytogenes. *J Cell Biol,* 144**,** 1245-58.

LE CLAINCHE, C., PANTALONI, D. & CARLIER, M. F. 2003. ATP hydrolysis on actin-related protein 2/3 complex causes debranching of dendritic actin arrays. *Proc Natl Acad Sci U S A,* 100**,** 6337-42.

LEBENSOHN, A. M. & KIRSCHNER, M. W. 2009. Activation of the WAVE complex by coincident signals controls actin assembly. *Mol Cell,* 36**,** 512-24.

LECLAIRE, L. L., 3RD, BAUMGARTNER, M., IWASA, J. H., MULLINS, R. D. & BARBER, D. L. 2008. Phosphorylation of the Arp2/3 complex is necessary to nucleate actin filaments. *J Cell Biol,* 182**,** 647-54.

LEES-MILLER, J. P., HENRY, G. & HELFMAN, D. M. 1992. Identification of act2, an essential gene in the fission yeast Schizosaccharomyces pombe that encodes a protein related to actin. *Proc Natl Acad Sci U S A,* 89**,** 80-3.

LEGG, J. A., BOMPARD, G., DAWSON, J., MORRIS, H. L., ANDREW, N., COOPER, L., JOHNSTON, S. A., TRAMOUNTANIS, G. & MACHESKY, L. M. 2007. N-WASP involvement in dorsal ruffle formation in mouse embryonic fibroblasts. *Mol Biol Cell,* 18**,** 678-87.

LENG, Y., ZHANG, J., BADOUR, K., ARPAIA, E., FREEMAN, S., CHEUNG, P., SIU, M. & SIMINOVITCH, K. 2005. Abelson-interactor-1 promotes WAVE2 membrane translocation and Abelson-mediated tyrosine phosphorylation required for WAVE2 activation. *Proc Natl Acad Sci U S A,* 102**,** 1098-103.

LI, J., KINOSHITA, T., PANDEY, S., NG, C. K., GYGI, S. P., SHIMAZAKI, K. & ASSMANN, S. M. 2002. Modulation of an RNA-binding protein by abscisic-acid-activated protein kinase. *Nature,* 418**,** 793-7.

LIEBAU, S., STEINESTEL, J., LINTA, L., KLEGER, A., STORCH, A., SCHOEN, M., STEINESTEL, K., PROEPPER, C., BOCKMANN, J., SCHMEISSER, M. J. & BOECKERS, T. M. 2011. An SK3 channel/nWASP/Abi-1 complex is involved in early neurogenesis. *PLoS One,* 6**,** e18148.

LINARDOPOULOU, E. V., PARGHI, S. S., FRIEDMAN, C., OSBORN, G. E., PARKHURST, S. M. & TRASK, B. J. 2007. Human subtelomeric WASH genes encode a new subclass of the WASP family. *PLoS Genet,* 3**,** e237.

LINDER, S., WIESNER, C. & HIMMEL, M. 2010. Degrading Devices: Invadosomes in Proteolytic Cell Invasion. *Annu Rev Cell Dev Biol,* 29**,** 29.

LINDSAY, S. L., RAMSEY, S., AITCHISON, M., RENNE, T. & EVANS, T. J. 2007. Modulation of lamellipodial structure and dynamics by NO-dependent phosphorylation of VASP Ser239. *J Cell Sci,* 120**,** 3011-21.

LINKNER, J., WITTE, G., STRADAL, T., CURTH, U. & FAIX, J. 2011. High-Resolution X-Ray Structure of the Trimeric Scar/WAVE-Complex Precursor Brk1. *PLoS One,* 6**,** e21327.

LIU, R., ABREU-BLANCO, M. T., BARRY, K. C., LINARDOPOULOU, E. V., OSBORN, G. E. & PARKHURST, S. M. 2009a. Wash functions downstream of Rho and links linear and branched actin nucleation factors. *Development,* 136**,** 2849-60.

LIU, T., SIMS, D. & BAUM, B. 2009b. Parallel RNAi screens across different cell lines identify generic and cell type-specific regulators of actin organization and cell morphology. *Genome Biol,* 10**,** R26.

LOUREIRO, J. J., RUBINSON, D. A., BEAR, J. E., BALTUS, G. A., KWIATKOWSKI, A. V. & GERTLER, F. B. 2002. Critical roles of phosphorylation and actin binding motifs, but not the central proline-rich region, for Ena/vasodilator-stimulated phosphoprotein (VASP) function during cell migration. *Mol Biol Cell,* 13**,** 2533-46.

MA, L., ROHATGI, R. & KIRSCHNER, M. W. 1998. The Arp2/3 complex mediates actin polymerization induced by the small GTP-binding protein Cdc42. *Proc Natl Acad Sci U S A,* 95**,** 15362-7.

MACHESKY, L. M., ATKINSON, S. J., AMPE, C., VANDEKERCKHOVE, J. & POLLARD, T. D. 1994. Purification of a cortical complex containing two unconventional actins from Acanthamoeba by affinity chromatography on profilin-agarose. *J Cell Biol,* 127**,** 107-15.

MACHESKY, L. M. & INSALL, R. H. 1998. Scar1 and the related Wiskott-Aldrich syndrome protein, WASP, regulate the actin cytoskeleton through the Arp2/3 complex. *Curr Biol,* 8**,** 1347-56.

MARCHAND, J. B., KAISER, D. A., POLLARD, T. D. & HIGGS, H. N. 2001. Interaction of WASP/Scar proteins with actin and vertebrate Arp2/3 complex. *Nat Cell Biol,* 3**,** 76-82.

MARTIN, A. C., WELCH, M. D. & DRUBIN, D. G. 2006. Arp2/3 ATP hydrolysis-catalysed branch dissociation is critical for endocytic force generation. *Nat Cell Biol,* 8**,** 826-33.

MARTIN, A. C., XU, X. P., ROUILLER, I., KAKSONEN, M., SUN, Y., BELMONT, L., VOLKMANN, N., HANEIN, D., WELCH, M. & DRUBIN, D. G. 2005. Effects of Arp2 and Arp3 nucleotide-binding pocket mutations on Arp2/3 complex function. *J Cell Biol,* 168**,** 315-28.

MATTILA, P. K. & LAPPALAINEN, P. 2008. Filopodia: molecular architecture and cellular functions. *Nat Rev Mol Cell Biol,* 9**,** 446-54.

MATTILA, P. K., PYKALAINEN, A., SAARIKANGAS, J., PAAVILAINEN, V. O., VIHINEN, H., JOKITALO, E. & LAPPALAINEN, P. 2007. Missing-in-metastasis and IRSp53 deform PI(4,5)P2-rich membranes by an inverse BAR domain-like mechanism. *J Cell Biol,* 176**,** 953-64.

MENDOZA, M. C., ER, E. E., ZHANG, W., BALLIF, B. A., ELLIOTT, H. L., DANUSER, G. & BLENIS, J. 2011. ERK-MAPK drives lamellipodia protrusion by activating the WAVE2 regulatory complex. *Mol Cell,* 41**,** 661-71.

MICHAEL, M., VEHLOW, A., NAVARRO, C. & KRAUSE, M. 2010. c-Abl, Lamellipodin, and Ena/VASP Proteins Cooperate in Dorsal Ruffling of Fibroblasts and Axonal Morphogenesis. *Curr Biol*.

MIKI, H., SUETSUGU, S. & TAKENAWA, T. 1998. WAVE, a novel WASP-family protein involved in actin reorganization induced by Rac. *EMBO J,* 17**,** 6932-41.

MIKI, H., YAMAGUCHI, H., SUETSUGU, S. & TAKENAWA, T. 2000. IRSp53 is an essential intermediate between Rac and WAVE in the regulation of membrane ruffling. *Nature,* 408**,** 732-5.

MIYAMOTO, Y., YAMAUCHI, J. & TANOUE, A. 2008. Cdk5 phosphorylation of WAVE2 regulates oligodendrocyte precursor cell migration through nonreceptor tyrosine kinase Fyn. *J Neurosci,* 28**,** 8326-37.

MIYAZAKI, K., MATSUDA, S., ICHIGOTANI, Y., TAKENOUCHI, Y., HAYASHI, K., FUKUDA, Y., NIMURA, Y. & HAMAGUCHI, M. 2000. Isolation and characterization of a novel human gene (NESH) which encodes a putative signaling molecule similar to e3B1 protein. *Biochim Biophys Acta,* 1493**,** 237-41.

MOGILNER, A. & OSTER, G. 2003. Force generation by actin polymerization II: the elastic ratchet and tethered filaments. *Biophys J,* 84**,** 1591-605.

MOLINA, I. J., KENNEY, D. M., ROSEN, F. S. & REMOLD-O'DONNELL, E. 1992. T cell lines characterize events in the pathogenesis of the Wiskott-Aldrich syndrome. *J Exp Med,* 176**,** 867-74.

MONTELL, D. J. 2003. Border-cell migration: the race is on. *Nat Rev Mol Cell Biol,* 4**,** 13-24.

MOREAU, V., FRISCHKNECHT, F., RECKMANN, I., VINCENTELLI, R., RABUT, G., STEWART, D. & WAY, M. 2000. A complex of N-WASP and WIP

integrates signalling cascades that lead to actin polymerization. *Nat Cell Biol,* 2**,** 441-8.

MOSELEY, J. B., SAGOT, I., MANNING, A. L., XU, Y., ECK, M. J., PELLMAN, D. & GOODE, B. L. 2004. A conserved mechanism for Bni1- and mDia1-induced actin assembly and dual regulation of Bni1 by Bud6 and profilin. *Mol Biol Cell,* 15**,** 896-907.

MUELLER, W., NUTT, C. L., EHRICH, M., RIEMENSCHNEIDER, M. J., VON DEIMLING, A., VAN DEN BOOM, D. & LOUIS, D. N. 2007. Downregulation of RUNX3 and TES by hypermethylation in glioblastoma. *Oncogene,* 26**,** 583-93.

MULLER, W. A. 2011. Mechanisms of leukocyte transendothelial migration. *Annu Rev Pathol,* 6**,** 323-44.

MULLINS, R. D., HEUSER, J. A. & POLLARD, T. D. 1998. The interaction of Arp2/3 complex with actin: nucleation, high affinity pointed end capping, and formation of branching networks of filaments. *Proc Natl Acad Sci U S A,* 95**,** 6181-6.

MYKKANEN, O. M., GRONHOLM, M., RONTY, M., LALOWSKI, M., SALMIKANGAS, P., SUILA, H. & CARPEN, O. 2001. Characterization of human palladin, a microfilament-associated protein. *Mol Biol Cell,* 12**,** 3060-73.

NARASIMHA, M. & LEPTIN, M. 2000. Cell movements during gastrulation: come in and be induced. *Trends Cell Biol,* 10**,** 169-72.

NIEBUHR, K., EBEL, F., FRANK, R., REINHARD, M., DOMANN, E., CARL, U. D., WALTER, U., GERTLER, F. B., WEHLAND, J. & CHAKRABORTY, T. 1997. A novel proline-rich motif present in ActA of Listeria monocytogenes and cytoskeletal proteins is the ligand for the EVH1 domain, a protein module present in the Ena/VASP family. *EMBO J,* 16**,** 5433-44.

NOLEN, B. J., LITTLEFIELD, R. S. & POLLARD, T. D. 2004. Crystal structures of actin-related protein 2/3 complex with bound ATP or ADP. *Proc Natl Acad Sci U S A,* 101**,** 15627-32.

NOLEN, B. J. & POLLARD, T. D. 2007. Insights into the influence of nucleotides on actin family proteins from seven structures of Arp2/3 complex. *Mol Cell,* 26**,** 449-57.

NOZUMI, M., NAKAGAWA, H., MIKI, H., TAKENAWA, T. & MIYAMOTO, S. 2003. Differential localization of WAVE isoforms in filopodia and lamellipodia of the neuronal growth cone. *J Cell Sci,* 116**,** 239-46.

OIKAWA, T., YAMAGUCHI, H., ITOH, T., KATO, M., IJUIN, T., YAMAZAKI, D., SUETSUGU, S. & TAKENAWA, T. 2004. PtdIns(3,4,5)P3 binding is necessary for WAVE2-induced formation of lamellipodia. *Nat Cell Biol,* 6**,** 420-6.

PADRICK, S. B., CHENG, H. C., ISMAIL, A. M., PANCHAL, S. C., DOOLITTLE, L. K., KIM, S., SKEHAN, B. M., UMETANI, J., BRAUTIGAM, C. A., LEONG, J. M. & ROSEN, M. K. 2008. Hierarchical regulation of WASP/WAVE proteins. *Mol Cell,* 32**,** 426-38.

PADRICK, S. B., DOOLITTLE, L. K., BRAUTIGAM, C. A., KING, D. S. & ROSEN, M. K. 2011. Arp2/3 complex is bound and activated by two WASP proteins. *Proc Natl Acad Sci U S A,* 15**,** 15.

PANCHAL, S. C., KAISER, D. A., TORRES, E., POLLARD, T. D. & ROSEN, M. K. 2003. A conserved amphipathic helix in WASP/Scar proteins is essential for activation of Arp2/3 complex. *Nat Struct Biol,* 10**,** 591-8.

PANTALONI, D., BOUJEMAA, R., DIDRY, D., GOUNON, P. & CARLIER, M. F. 2000. The Arp2/3 complex branches filament barbed ends: functional antagonism with capping proteins. *Nat Cell Biol,* 2**,** 385-91.

PANTALONI, D. & CARLIER, M. F. 1993. How profilin promotes actin filament assembly in the presence of thymosin beta 4. *Cell,* 75**,** 1007-14.

PANTALONI, D., LE CLAINCHE, C. & CARLIER, M. F. 2001. Mechanism of actin-based motility. *Science,* 292**,** 1502-6.

PASIC, L., KOTOVA, T. & SCHAFER, D. A. 2008. Ena/VASP proteins capture actin filament barbed ends. *J Biol Chem,* 283**,** 9814-9.

PAUNOLA, E., MATTILA, P. K. & LAPPALAINEN, P. 2002. WH2 domain: a small, versatile adapter for actin monomers. *FEBS Lett,* 513**,** 92-7.

PERELROIZEN, I., CARLIER, M. F. & PANTALONI, D. 1995. Binding of divalent cation and nucleotide to G-actin in the presence of profilin. *J Biol Chem,* 270**,** 1501-8.

PETERSON, F. C., DENG, Q., ZETTL, M., PREHODA, K. E., LIM, W. A., WAY, M. & VOLKMAN, B. F. 2007. Multiple WASP-interacting protein recognition motifs are required for a functional interaction with N-WASP. *J Biol Chem,* 282**,** 8446-53.

PETERSON, F. C. & VOLKMAN, B. F. 2009. Diversity of polyproline recognition by EVH1 domains. *Front Biosci,* 14**,** 833-46.

PHILIPPAR, U., ROUSSOS, E. T., OSER, M., YAMAGUCHI, H., KIM, H. D., GIAMPIERI, S., WANG, Y., GOSWAMI, S., WYCKOFF, J. B., LAUFFENBURGER, D. A., SAHAI, E., CONDEELIS, J. S. & GERTLER, F. B. 2008. A Mena invasion isoform potentiates EGF-induced carcinoma cell invasion and metastasis. *Developmental cell,* 15**,** 813-28.

PISTOR, S., CHAKRABORTY, T., WALTER, U. & WEHLAND, J. 1995. The bacterial actin nucleator protein ActA of Listeria monocytogenes contains multiple binding sites for host microfilament proteins. *Curr Biol,* 5**,** 517-25.

PLASTINO, J., OLIVIER, S. & SYKES, C. 2004. Actin filaments align into hollow comets for rapid VASP-mediated propulsion. *Curr Biol,* 14**,** 1766-71.

POCHA, S. M. & CORY, G. O. 2009. WAVE2 is regulated by multiple phosphorylation events within its VCA domain. *Cell Motil Cytoskeleton,* 66**,** 36-47.

POLLARD, T. D. 2007. Regulation of actin filament assembly by Arp2/3 complex and formins. *Annu Rev Biophys Biomol Struct,* 36**,** 451-77.

POLLARD, T. D. & BORISY, G. G. 2003. Cellular motility driven by assembly and disassembly of actin filaments. *Cell,* 112**,** 453-65.

POLLITT, A. Y. & INSALL, R. H. 2008. Abi mutants in Dictyostelium reveal specific roles for the SCAR/WAVE complex in cytokinesis. *Curr Biol,* 18**,** 203-10.

PREHODA, K. E., LEE, D. J. & LIM, W. A. 1999. Structure of the enabled/VASP homology 1 domain-peptide complex: a key component in the spatial control of actin assembly. *Cell,* 97**,** 471-80.

PREHODA, K. E., SCOTT, J. A., MULLINS, R. D. & LIM, W. A. 2000. Integration of multiple signals through cooperative regulation of the N-WASP-Arp2/3 complex. *Science,* 290**,** 801-6.

PRUYNE, D., EVANGELISTA, M., YANG, C., BI, E., ZIGMOND, S., BRETSCHER, A. & BOONE, C. 2002. Role of formins in actin assembly: nucleation and barbed-end association. *Science,* 297**,** 612-5.

QUINLAN, M. E., HEUSER, J. E., KERKHOFF, E. & MULLINS, R. D. 2005. Drosophila Spire is an actin nucleation factor. *Nature,* 433**,** 382-8.

QUINLAN, M. E., HILGERT, S., BEDROSSIAN, A., MULLINS, R. D. & KERKHOFF, E. 2007. Regulatory interactions between two actin nucleators, Spire and Cappuccino. *J Cell Biol,* 179**,** 117-28.

QUINN, C. C., PFEIL, D. S., CHEN, E., STOVALL, E. L., HARDEN, M. V., GAVIN, M. K., FORRESTER, W. C., RYDER, E. F., SOTO, M. C. & WADSWORTH, W. G. 2006. UNC-6/netrin and SLT-1/slit guidance cues orient axon outgrowth mediated by MIG-10/RIAM/lamellipodin. *Curr Biol,* 16**,** 845-53.

RAFELSKI, S. M. & THERIOT, J. A. 2004. Crawling toward a unified model of cell mobility: spatial and temporal regulation of actin dynamics. *Annu Rev Biochem,* 73**,** 209-39.

RAKIC, P. 1978. Neuronal migration and contact guidance in the primate telencephalon. *Postgrad Med J,* 54 Suppl 1**,** 25-40.

REBECCHI, M. J. & SCARLATA, S. 1998. Pleckstrin homology domains: a common fold with diverse functions. *Annu Rev Biophys Biomol Struct,* 27**,** 503-28.

RECKMANN, I., HIGLEY, S. & WAY, M. 1997. The vaccinia virus F17R protein interacts with actin. *FEBS Lett,* 409**,** 141-6.

REINHARD, M., JOUVENAL, K., TRIPIER, D. & WALTER, U. 1995. Identification, purification, and characterization of a zyxin-related protein that binds the focal adhesion and microfilament protein VASP (vasodilator-stimulated phosphoprotein). *Proc Natl Acad Sci U S A,* 92**,** 7956-60.

RENFRANZ, P. J. & BECKERLE, M. C. 2002. Doing (F/L)PPPPs: EVH1 domains and their proline-rich partners in cell polarity and migration. *Curr Opin Cell Biol,* 14**,** 88-103.

RIDLEY, A. J. 2011. Life at the Leading Edge. *Cell,* 145**,** 1012-1022.

RIDLEY, A. J., SCHWARTZ, M. A., BURRIDGE, K., FIRTEL, R. A., GINSBERG, M. H., BORISY, G., PARSONS, J. T. & HORWITZ, A. R. 2003. Cell migration: integrating signals from front to back. *Science,* 302**,** 1704-9.

RIETDORF, J., PLOUBIDOU, A., RECKMANN, I., HOLMSTROM, A., FRISCHKNECHT, F., ZETTL, M., ZIMMERMANN, T. & WAY, M. 2001. Kinesin-dependent movement on microtubules precedes actin-based motility of vaccinia virus. *Nat Cell Biol,* 3**,** 992-1000.

RIVERA, G. M., VASILESCU, D., PAPAYANNOPOULOS, V., LIM, W. A. & MAYER, B. J. 2009. A reciprocal interdependence between Nck and PI(4,5)P(2) promotes localized N-WASp-mediated actin polymerization in living cells. *Mol Cell,* 36**,** 525-35.

ROBBINS, J. R., BARTH, A. I., MARQUIS, H., DE HOSTOS, E. L., NELSON, W. J. & THERIOT, J. A. 1999. Listeria monocytogenes exploits normal host cell processes to spread from cell to cell. *J Cell Biol,* 146**,** 1333-50.

ROBINSON, R. C., TURBEDSKY, K., KAISER, D. A., MARCHAND, J. B., HIGGS, H. N., CHOE, S. & POLLARD, T. D. 2001. Crystal structure of Arp2/3 complex. *Science,* 294**,** 1679-84.

RODAL, A. A., SOKOLOVA, O., ROBINS, D. B., DAUGHERTY, K. M., HIPPENMEYER, S., RIEZMAN, H., GRIGORIEFF, N. & GOODE, B. L. 2005. Conformational changes in the Arp2/3 complex leading to actin nucleation. *Nat Struct Mol Biol,* 12**,** 26-31.

ROGERS, S. L., WIEDEMANN, U., STUURMAN, N. & VALE, R. D. 2003. Molecular requirements for actin-based lamella formation in Drosophila S2 cells. *J Cell Biol,* 162**,** 1079-88.

ROTTNER, K., HANISCH, J. & CAMPELLONE, K. G. 2010. WASH, WHAMM and JMY: regulation of Arp2/3 complex and beyond. *Trends Cell Biol,* 20**,** 650-61.

ROUILLER, I., XU, X. P., AMANN, K. J., EGILE, C., NICKELL, S., NICASTRO, D., LI, R., POLLARD, T. D., VOLKMANN, N. & HANEIN, D. 2008. The structural basis of actin filament branching by the Arp2/3 complex. *J Cell Biol,* 180**,** 887-95.

ROUSSOS, E. T., BALSAMO, M., ALFORD, S. K., WYCKOFF, J. B., GLIGORIJEVIC, B., WANG, Y., POZZUTO, M., STOBEZKI, R., GOSWAMI, S., SEGALL, J. E., LAUFFENBURGER, D. A., BRESNICK, A. R., GERTLER, F. B. & CONDEELIS, J. S. 2011. Mena invasive (MenaINV) promotes multicellular streaming motility and transendothelial migration in a mouse model of breast cancer. *J Cell Sci,* 124**,** 2120-31.

SAHAI, E. 2005. Mechanisms of cancer cell invasion. *Curr Opin Genet Dev,* 15**,** 87-96.

SAMARIN, S., ROMERO, S., KOCKS, C., DIDRY, D., PANTALONI, D. & CARLIER, M. F. 2003. How VASP enhances actin-based motility. *J Cell Biol,* 163**,** 131-42.

SAMPATH, P. & POLLARD, T. D. 1991. Effects of cytochalasin, phalloidin, and pH on the elongation of actin filaments. *Biochemistry,* 30**,** 1973-80.

SANGER, J. M., SANGER, J. W. & SOUTHWICK, F. S. 1992. Host cell actin assembly is necessary and likely to provide the propulsive force for intracellular movement of Listeria monocytogenes. *Infect Immun,* 60**,** 3609-19.

SARTI, M., SEVIGNANI, C., CALIN, G. A., AQEILAN, R., SHIMIZU, M., PENTIMALLI, F., PICCHIO, M. C., GODWIN, A., ROSENBERG, A., DRUSCO, A., NEGRINI, M. & CROCE, C. M. 2005. Adenoviral transduction of TESTIN gene into breast and uterine cancer cell lines promotes apoptosis and tumor reduction in vivo. *Clin Cancer Res,* 11**,** 806-13.

SCHIRENBECK, A., ARASADA, R., BRETSCHNEIDER, T., STRADAL, T. E., SCHLEICHER, M. & FAIX, J. 2006. The bundling activity of vasodilator-stimulated phosphoprotein is required for filopodium formation. *Proc Natl Acad Sci U S A,* 103**,** 7694-9.

SCHNEIDER, I. 1972. Cell lines derived from late embryonic stages of Drosophila melanogaster. *J Embryol Exp Morphol,* 27**,** 353-65.

SCHWOB, E. & MARTIN, R. P. 1992. New yeast actin-like gene required late in the cell cycle. *Nature,* 355**,** 179-82.

SCITA, G., NORDSTROM, J., CARBONE, R., TENCA, P., GIARDINA, G., GUTKIND, S., BJARNEGARD, M., BETSHOLTZ, C. & DI FIORE, P. P. 1999. EPS8 and E3B1 transduce signals from Ras to Rac. *Nature,* 401**,** 290-3.

SEPT, D. & MCCAMMON, J. A. 2001. Thermodynamics and kinetics of actin filament nucleation. *Biophys J,* 81**,** 667-74.

SHANER, N. C., CAMPBELL, R. E., STEINBACH, P. A., GIEPMANS, B. N., PALMER, A. E. & TSIEN, R. Y. 2004. Improved monomeric red, orange and yellow fluorescent proteins derived from Discosoma sp. red fluorescent protein. *Nat Biotechnol,* 22**,** 1567-72.

SHI, Y., ALIN, K. & GOFF, S. P. 1995. Abl-interactor-1, a novel SH3 protein binding to the carboxy-terminal portion of the Abl protein, suppresses v-abl transforming activity. *Genes Dev,* 9**,** 2583-97.

SHIKAMA, N., LEE, C. W., FRANCE, S., DELAVAINE, L., LYON, J., KRSTIC-DEMONACOS, M. & LA THANGUE, N. B. 1999. A novel cofactor for p300 that regulates the p53 response. *Mol Cell,* 4**,** 365-76.

SKOBLE, J., AUERBUCH, V., GOLEY, E. D., WELCH, M. D. & PORTNOY, D. A. 2001. Pivotal role of VASP in Arp2/3 complex-mediated actin nucleation, actin branch-formation, and Listeria monocytogenes motility. *J Cell Biol,* 155**,** 89-100.

SMALL, J. V. & CELIS, J. E. 1978. Filament arrangements in negatively stained cultured cells: the organization of actin. *Cytobiologie,* 16**,** 308-25.

SMALL, J. V., ISENBERG, G. & CELIS, J. E. 1978. Polarity of actin at the leading edge of cultured cells. *Nature,* 272**,** 638-639.

SMALL, J. V., STRADAL, T., VIGNAL, E. & ROTTNER, K. 2002. The lamellipodium: where motility begins. *Trends Cell Biol,* 12**,** 112-20.

SMITH, D. B. & JOHNSON, K. S. 1988. Single-step purification of polypeptides expressed in Escherichia coli as fusions with glutathione S-transferase. *Gene,* 67**,** 31-40.

SMITH, G. A., THERIOT, J. A. & PORTNOY, D. A. 1996. The tandem repeat domain in the Listeria monocytogenes ActA protein controls the rate of actin-based motility, the percentage of moving bacteria, and the localization of vasodilator-stimulated phosphoprotein and profilin. *J Cell Biol,* 135**,** 647-60.

SNAPPER, S. B., TAKESHIMA, F., ANTON, I., LIU, C. H., THOMAS, S. M., NGUYEN, D., DUDLEY, D., FRASER, H., PURICH, D., LOPEZ-ILASACA, M., KLEIN, C., DAVIDSON, L., BRONSON, R., MULLIGAN, R. C., SOUTHWICK, F., GEHA, R., GOLDBERG, M. B., ROSEN, F. S., HARTWIG, J. H. & ALT, F. W. 2001. N-WASP deficiency reveals distinct pathways for cell surface projections and microbial actin-based motility. *Nat Cell Biol,* 3**,** 897-904.

SODERLING, S. H., LANGEBERG, L. K., SODERLING, J. A., DAVEE, S. M., SIMERLY, R., RABER, J. & SCOTT, J. D. 2003. Loss of WAVE-1 causes sensorimotor retardation and reduced learning and memory in mice. *Proc Natl Acad Sci U S A,* 100**,** 1723-8.

SOSSEY-ALAOUI, K., LI, X. & COWELL, J. K. 2007. c-Abl-mediated phosphorylation of WAVE3 is required for lamellipodia formation and cell migration. *J Biol Chem,* 282**,** 26257-65.

STEFFEN, A., ROTTNER, K., EHINGER, J., INNOCENTI, M., SCITA, G., WEHLAND, J. & STRADAL, T. E. 2004. Sra-1 and Nap1 link Rac to actin assembly driving lamellipodia formation. *EMBO J,* 23**,** 749-59.

STOVOLD, C. F., MILLARD, T. H. & MACHESKY, L. M. 2005. Inclusion of Scar/WAVE3 in a similar complex to Scar/WAVE1 and 2. *BMC Cell Biol,* 6**,** 11.

STUART, J. R., GONZALEZ, F. H., KAWAI, H. & YUAN, Z. M. 2006. c-Abl interacts with the WAVE2 signaling complex to induce membrane ruffling and cell spreading. *J Biol Chem,* 281**,** 31290-7.

SUETSUGU, S., KURISU, S., OIKAWA, T., YAMAZAKI, D., ODA, A. & TAKENAWA, T. 2006. Optimization of WAVE2 complex-induced actin

polymerization by membrane-bound IRSp53, PIP(3), and Rac. *J Cell Biol,* 173**,** 571-85.

SUETSUGU, S., MIKI, H. & TAKENAWA, T. 1999. Identification of two human WAVE/SCAR homologues as general actin regulatory molecules which associate with the Arp2/3 complex. *Biochem Biophys Res Commun,* 260**,** 296-302.

SUETSUGU, S., YAMAZAKI, D., KURISU, S. & TAKENAWA, T. 2003. Differential roles of WAVE1 and WAVE2 in dorsal and peripheral ruffle formation for fibroblast cell migration. *Dev Cell,* 5**,** 595-609.

SVITKINA, T. M. & BORISY, G. G. 1999. Arp2/3 complex and actin depolymerizing factor/cofilin in dendritic organization and treadmilling of actin filament array in lamellipodia. *J Cell Biol,* 145**,** 1009-26.

SVITKINA, T. M., BULANOVA, E. A., CHAGA, O. Y., VIGNJEVIC, D. M., KOJIMA, S., VASILIEV, J. M. & BORISY, G. G. 2003. Mechanism of filopodia initiation by reorganization of a dendritic network. *J Cell Biol,* 160**,** 409-21.

SVITKINA, T. M., VERKHOVSKY, A. B., MCQUADE, K. M. & BORISY, G. G. 1997. Analysis of the actin-myosin II system in fish epidermal keratocytes: mechanism of cell body translocation. *J Cell Biol,* 139**,** 397-415.

SYMONS, M. H. & MITCHISON, T. J. 1991. Control of actin polymerization in live and permeabilized fibroblasts. *J Cell Biol,* 114**,** 503-13.

TAKAHASHI, K. & SUZUKI, K. 2010. WAVE2 targeting to phosphatidylinositol 3,4,5-triphosphate mediated by insulin receptor substrate p53 through a complex with WAVE2. *Cell Signal,* 22**,** 1708-16.

TAKANO, K., TOYOOKA, K. & SUETSUGU, S. 2008. EFC/F-BAR proteins and the N-WASP-WIP complex induce membrane curvature-dependent actin polymerization. *EMBO J,* 27**,** 2817-28.

TAKENAWA, T. & SUETSUGU, S. 2007. The WASP-WAVE protein network: connecting the membrane to the cytoskeleton. *Nat Rev Mol Cell Biol,* 8**,** 37-48.

TANI, K., SATO, S., SUKEZANE, T., KOJIMA, H., HIROSE, H., HANAFUSA, H. & SHISHIDO, T. 2003. Abl interactor 1 promotes tyrosine 296 phosphorylation of mammalian enabled (Mena) by c-Abl kinase. *J Biol Chem,* 278**,** 21685-92.

TATARELLI, C., LINNENBACH, A., MIMORI, K. & CROCE, C. M. 2000. Characterization of the human TESTIN gene localized in the FRA7G region at 7q31.2. *Genomics,* 68**,** 1-12.

TAYLER, T. D. & GARRITY, P. A. 2003. Axon targeting in the Drosophila visual system. *Curr Opin Neurobiol,* 13**,** 90-5.

THERIOT, J. A. & MITCHISON, T. J. 1991. Actin microfilament dynamics in locomoting cells. *Nature,* 352**,** 126-31.

THERIOT, J. A., MITCHISON, T. J., TILNEY, L. G. & PORTNOY, D. A. 1992. The rate of actin-based motility of intracellular Listeria monocytogenes equals the rate of actin polymerization. *Nature,* 357**,** 257-60.

TI, S. C., JURGENSON, C. T., NOLEN, B. J. & POLLARD, T. D. 2011. Structural and biochemical characterization of two binding sites for nucleation-promoting factor WASp-VCA on Arp2/3 complex. *Proc Natl Acad Sci U S A,* 108**,** E463-71.

TILNEY, L. G. & PORTNOY, D. A. 1989. Actin filaments and the growth, movement, and spread of the intracellular bacterial parasite, Listeria monocytogenes. *J Cell Biol,* 109**,** 1597-608.

TOBIAS, E. S., HURLSTONE, A. F., MACKENZIE, E., MCFARLANE, R. & BLACK, D. M. 2001. The TES gene at 7q31.1 is methylated in tumours and encodes a novel growth-suppressing LIM domain protein. *Oncogene,* 20**,** 2844-53.

TOMASEVIC, N., JIA, Z., RUSSELL, A., FUJII, T., HARTMAN, J. J., CLANCY, S., WANG, M., BERAUD, C., WOOD, K. W. & SAKOWICZ, R. 2007. Differential regulation of WASP and N-WASP by Cdc42, Rac1, Nck, and PI(4,5)P2. *Biochemistry,* 46**,** 3494-502.

TORRES, E. & ROSEN, M. K. 2006. Protein-tyrosine kinase and GTPase signals cooperate to phosphorylate and activate Wiskott-Aldrich syndrome protein (WASP)/neuronal WASP. *J Biol Chem,* 281**,** 3513-20.

TSUJITA, K., SUETSUGU, S., SASAKI, N., FURUTANI, M., OIKAWA, T. & TAKENAWA, T. 2006. Coordination between the actin cytoskeleton and membrane deformation by a novel membrane tubulation domain of PCH proteins is involved in endocytosis. *J Cell Biol,* 172**,** 269-79.

TUCKER, P. K., EVANS, I. R. & WOOD, W. 2011. Ena drives invasive macrophage migration in Drosophila embryos. *Dis Model Mech,* 4**,** 126-34.

TUCKER, R. P. 2004. Neural crest cells: a model for invasive behavior. *Int J Biochem Cell Biol,* 36**,** 173-7.

URBAN, E., JACOB, S., NEMETHOVA, M., RESCH, G. P. & SMALL, J. V. 2010. Electron tomography reveals unbranched networks of actin filaments in lamellipodia. *Nat Cell Biol,* 12**,** 429-35.

VELTMAN, D. M. & INSALL, R. H. 2010. WASP family proteins: their evolution and its physiological implications. *Mol Biol Cell,* 21**,** 2880-93.

VERKHOVSKY, A. B., SVITKINA, T. M. & BORISY, G. G. 1999. Self-polarization and directional motility of cytoplasm. *Curr Biol,* 9**,** 11-20.

VINSON, V. K., DE LA CRUZ, E. M., HIGGS, H. N. & POLLARD, T. D. 1998. Interactions of Acanthamoeba profilin with actin and nucleotides bound to actin. *Biochemistry,* 37**,** 10871-80.

VOLKMAN, B. F., PREHODA, K. E., SCOTT, J. A., PETERSON, F. C. & LIM, W. A. 2002. Structure of the N-WASP EVH1 domain-WIP complex: insight into the molecular basis of Wiskott-Aldrich Syndrome. *Cell,* 111**,** 565-76.

WALDERS-HARBECK, B., KHAITLINA, S. Y., HINSSEN, H., JOCKUSCH, B. M. & ILLENBERGER, S. 2002. The vasodilator-stimulated phosphoprotein promotes actin polymerisation through direct binding to monomeric actin. *FEBS Lett,* 529**,** 275-80.

WALDMANN, R., NIEBERDING, M. & WALTER, U. 1987. Vasodilator-stimulated protein phosphorylation in platelets is mediated by cAMP- and cGMP-dependent protein kinases. *Eur J Biochem,* 167**,** 441-8.

WANG, W., GOSWAMI, S., LAPIDUS, K., WELLS, A. L., WYCKOFF, J. B., SAHAI, E., SINGER, R. H., SEGALL, J. E. & CONDEELIS, J. S. 2004. Identification and testing of a gene expression signature of invasive carcinoma cells within primary mammary tumors. *Cancer Res,* 64**,** 8585-94.

WANG, W., WYCKOFF, J. B., GOSWAMI, S., WANG, Y., SIDANI, M., SEGALL, J. E. & CONDEELIS, J. S. 2007. Coordinated regulation of pathways for

enhanced cell motility and chemotaxis is conserved in rat and mouse mammary tumors. *Cancer Res,* 67**,** 3505-11.

WANG, Y. L. 1985. Exchange of actin subunits at the leading edge of living fibroblasts: possible role of treadmilling. *J Cell Biol,* 101**,** 597-602.

WATERMAN-STORER, C. M., DESAI, A., BULINSKI, J. C. & SALMON, E. D. 1998. Fluorescent speckle microscopy, a method to visualize the dynamics of protein assemblies in living cells. *Curr Biol,* 8**,** 1227-30.

WAY, M., POPE, B., GOOCH, J., HAWKINS, M. & WEEDS, A. G. 1990. Identification of a region in segment 1 of gelsolin critical for actin binding. *EMBO J,* 9**,** 4103-9.

WEAVER, A. M., HEUSER, J. E., KARGINOV, A. V., LEE, W. L., PARSONS, J. T. & COOPER, J. A. 2002. Interaction of cortactin and N-WASp with Arp2/3 complex. *Curr Biol,* 12**,** 1270-8.

WEGNER, A. & ISENBERG, G. 1983. 12-fold difference between the critical monomer concentrations of the two ends of actin filaments in physiological salt conditions. *Proc Natl Acad Sci U S A,* 80**,** 4922-5.

WEIJER, C. J. 2009. Collective cell migration in development. *J Cell Sci,* 122**,** 3215-23.

WEINER, O. D., RENTEL, M. C., OTT, A., BROWN, G. E., JEDRYCHOWSKI, M., YAFFE, M. B., GYGI, S. P., CANTLEY, L. C., BOURNE, H. R. & KIRSCHNER, M. W. 2006. Hem-1 complexes are essential for Rac activation, actin polymerization, and myosin regulation during neutrophil chemotaxis. *PLoS Biol,* 4**,** e38.

WEISSWANGE, I., NEWSOME, T. P., SCHLEICH, S. & WAY, M. 2009. The rate of N-WASP exchange limits the extent of ARP2/3-complex-dependent actin-based motility. *Nature,* 458**,** 87-91.

WELCH, M. D., IWAMATSU, A. & MITCHISON, T. J. 1997. Actin polymerization is induced by Arp2/3 protein complex at the surface of Listeria monocytogenes. *Nature,* 385**,** 265-9.

WELCH, M. D., ROSENBLATT, J., SKOBLE, J., PORTNOY, D. A. & MITCHISON, T. J. 1998. Interaction of human Arp2/3 complex and the Listeria monocytogenes ActA protein in actin filament nucleation. *Science,* 281**,** 105-8.

WINTER, D., PODTELEJNIKOV, A. V., MANN, M. & LI, R. 1997. The complex containing actin-related proteins Arp2 and Arp3 is required for the motility and integrity of yeast actin patches. *Curr Biol,* 7**,** 519-29.

WOLF, K., MAZO, I., LEUNG, H., ENGELKE, K., VON ANDRIAN, U. H., DERYUGINA, E. I., STRONGIN, A. Y., BROCKER, E. B. & FRIEDL, P. 2003. Compensation mechanism in tumor cell migration: mesenchymal-amoeboid transition after blocking of pericellular proteolysis. *J Cell Biol,* 160**,** 267-77.

WOLF, K., WU, Y. I., LIU, Y., GEIGER, J., TAM, E., OVERALL, C., STACK, M. S. & FRIEDL, P. 2007. Multi-step pericellular proteolysis controls the transition from individual to collective cancer cell invasion. *Nat Cell Biol,* 9**,** 893-904.

XU, Y., MOSELEY, J. B., SAGOT, I., POY, F., PELLMAN, D., GOODE, B. L. & ECK, M. J. 2004. Crystal structures of a Formin Homology-2 domain reveal a tethered dimer architecture. *Cell,* 116**,** 711-23.

YAMAMOTO, A., SUZUKI, T. & SAKAKI, Y. 2001. Isolation of hNap1BP which interacts with human Nap1 (NCKAP1) whose expression is down-regulated in Alzheimer's disease. *Gene,* 271**,** 159-69.

YAMAZAKI, D., FUJIWARA, T., SUETSUGU, S. & TAKENAWA, T. 2005. A novel function of WAVE in lamellipodia: WAVE1 is required for stabilization of lamellipodial protrusions during cell spreading. *Genes Cells,* 10**,** 381-92.

YAMAZAKI, D., SUETSUGU, S., MIKI, H., KATAOKA, Y., NISHIKAWA, S., FUJIWARA, T., YOSHIDA, N. & TAKENAWA, T. 2003. WAVE2 is required for directed cell migration and cardiovascular development. *Nature,* 424**,** 452-6.

YAN, C., MARTINEZ-QUILES, N., EDEN, S., SHIBATA, T., TAKESHIMA, F., SHINKURA, R., FUJIWARA, Y., BRONSON, R., SNAPPER, S. B., KIRSCHNER, M. W., GEHA, R., ROSEN, F. S. & ALT, F. W. 2003. WAVE2 deficiency reveals distinct roles in embryogenesis and Rac-mediated actin-based motility. *EMBO J,* 22**,** 3602-12.

YANAGAWA, S., LEE, J. S. & ISHIMOTO, A. 1998. Identification and characterization of a novel line of Drosophila Schneider S2 cells that respond to wingless signaling. *J Biol Chem,* 273**,** 32353-9.

YOSHIDA, K. & SOLDATI, T. 2006. Dissection of amoeboid movement into two mechanically distinct modes. *J Cell Sci,* 119**,** 3833-44.

ZALEVSKY, J., GRIGOROVA, I. & MULLINS, R. D. 2001a. Activation of the Arp2/3 complex by the Listeria acta protein. Acta binds two actin monomers and three subunits of the Arp2/3 complex. *J Biol Chem,* 276**,** 3468-75.

ZALEVSKY, J., LEMPERT, L., KRANITZ, H. & MULLINS, R. D. 2001b. Different WASP family proteins stimulate different Arp2/3 complex-dependent actin-nucleating activities. *Curr Biol,* 11**,** 1903-13.

ZARRINPAR, A., BHATTACHARYYA, R. P. & LIM, W. A. 2003. The structure and function of proline recognition domains. *Sci STKE,* 2003**,** RE8.

ZETTL, M. & WAY, M. 2002. The WH1 and EVH1 domains of WASP and Ena/VASP family members bind distinct sequence motifs. *Curr Biol,* 12**,** 1617-22.

ZHENG, J. Q., WAN, J. J. & POO, M. M. 1996. Essential role of filopodia in chemotropic turning of nerve growth cone induced by a glutamate gradient. *J Neurosci,* 16**,** 1140-9.

ZIMMERMANN, J., LABUDDE, D., JARCHAU, T., WALTER, U., OSCHKINAT, H. & BALL, L. J. 2002. Relaxation, equilibrium oligomerization, and molecular symmetry of the VASP (336-380) EVH2 tetramer. *Biochemistry,* 41**,** 11143-51.

ZUCHERO, J. B., COUTTS, A. S., QUINLAN, M. E., THANGUE, N. B. & MULLINS, R. D. 2009. p53-cofactor JMY is a multifunctional actin nucleation factor. *Nat Cell Biol,* 11**,** 451-9.

ZUZGA, D. S., PELTA-HELLER, J., LI, P., BOMBONATI, A., WALDMAN, S. A. & PITARI, G. M. 2011. Phosphorylation of vasodilator-stimulated phosphoprotein ser239 suppresses filopodia and invadopodia in colon cancer. *Int J Cancer*.